An investigation into the spatio-temporal patterns of SO_2, NO_x and surface O_3 across the Highveld Priority Area, South Africa

Sarah Roffe 678816

University of the Witwatersrand

School of Geography, Archaeology and Environmental Studies

Supervisors: Dr. Raeesa Moolla and Prof. Fethi Ahmed

A thesis submitted to the Faculty of Science, University of the Witwatersrand, in fulfillment of the requirements for the degree of Master of Science

Declaration

I hereby declare that this dissertation is my own, original work, except where otherwise acknowledged. It is being submitted for the degree MSc to the University of the Witwatersrand, Johannesburg. I have not submitted it previously, for the purpose of obtaining any degree, qualification or otherwise at this, or any other, university.

Sarah Roffe

Signed on this day 25th of May 2017

Abstract

The Highveld is identified as an air pollution 'hotspot' area where pollutant concentrations are elevated due to the high density of industrial and non-industrial air pollution sources. To enhance air quality across the Highveld, it was declared a priority area to manage and monitor pollutants to reduce their negative impact on the environment and society. Hence, the aim of this study was to investigate ambient air pollution across the Highveld Priority Area (HPA), using ground-level SO_2, NO_x and surface O_3 concentrations, meteorological parameters and Moderate resolution imaging spectroradiometer (MODIS) atmosphere products, for January to December 2011, to develop new modelling techniques to aid in the management of air pollution.

Results show the annual mean trace gas concentrations of SO_2, NO_x and surface O_3 were 12.14, 14.75 and 28.77 ppb, respectively. SO_2 and NO_x concentrations were highest during winter at an average of 17.56 and 20.96 ppb, where surface O_3 concentrations were highest during spring at an average of 32.82 ppb. Diurnal patterns of SO_2 and surface O_3 were similar, where a midday peak occurred. NO_x concentrations instead showed peaks during traffic hours. Ambient air temperature, solar radiation, relative humidity, wind speed and rainfall levels peaked during summer. Atmospheric pressure was relatively stable throughout the year. Winds typically ranged from N to E up to April and from S to NW from May. Very little variation in SO_2 and NO_x concentrations was explainable by meteorology, 4 to 29 % and 5 to 23 %, while the influence of meteorology on surface O_3 concentrations was more significant, 23 to 53 %. Spatial multiple regression statistical models using a cross validation approach for model validation were made over a number of temporal scales. The model fitting and validation processes indicated that the models were not a good fit as only up to 69, 74 and 58 % of SO_2, NO_x and surface O_3 concentrations with high root means square error (RMSE) values of up to 22.10, 15.56 and 18.59 ppb, respectively, could be explained by the models. This process revealed the potential to model pollutants across the HPA, and as a pilot study future work can be based on this study. It is clear that spatial modelling for pollution estimation and management is necessary as seen by the frequent exceedances of the national and international ambient air quality standards.

Acknowledgments

I would like to thank and acknowledge the following people and organisations for their assistance and contribution to this study:

- To my supervisors, Dr. Raeesa Moolla and Prof. Fethi Ahmed, for all your guidance, support and assistance throughout this study.
- To my family and friends for your constant support.
- To the National Research Foundation for the NRF Free-standing Masters Scholarship award for 2016, reference number SFH150626121295.
- To the University of the Witwatersrand for their financial support through the award of the Postgraduate Merit Award for 2016.
- To the South African Weather Services for the provision of air quality and meteorological monitoring data.

Table of Contents

List of figures

List of tables

correlation coefficient greater than 0.7 highlighted by a double asterisk; no data is represented by -.

Table 5.6: Strength of the relationship between Surface O_3 and atmospheric pressure. Statistically significant correlations are indicated by an asterisk.

Table 5.7: The relationship of SO_2 to meteorology. A statistically significant correlation is indicated by an asterisk.

Table 5.8: The relationship of NO_x to meteorology. A statistically significant correlation is indicated by an asterisk.

Table 5.9: The relationship of surface O_3 to meteorology. A statistically significant correlation is indicated by an asterisk. A relationship with a correlation coefficient greater than 0.7 highlighted by a double asterisk.

Table 5.10: The relationship of SO_2 to level 2 and level 3 (daily, 8-day and monthly) satellite-derived AOD and meteorology. A statistically significant correlation is indicated by an asterisk. A relationship with a correlation coefficient greater than 0.7 highlighted by a double asterisk.

Table 5.11: Details of the RMSE and R^2 for the SO_2 level 2 and level 3 (daily, 8-day and monthly) model validation. A statistically significant correlation is indicated by an asterisk.

Table 5.12: The relationship of NO_x to level 2 and level 3 (daily, 8-day and monthly) satellite-derived AOD and meteorology. A statistically significant correlation is indicated by an asterisk. A relationship with a correlation coefficient greater than 0.7 highlighted by a double asterisk.

Table 5.13: Details of the RMSE and R^2 for the NO_x level 2 and level 3 (daily, 8-day and monthly) model validation. A relationship with a correlation coefficient greater than 0.7 highlighted by a double asterisk.

Table 5.14: The relationship of surface O_3 to level 2 and level 3 (daily, 8-day and monthly) satellite-derived Ozone and meteorology. A statistically significant correlation is indicated by an asterisk. A relationship with a correlation coefficient greater than 0.7 highlighted by a double asterisk.

Table 5.15: Details of the RMSE and R^2 for the surface O_3 level 2 and level 3 (daily, 8-day and monthly) model validation. A statistically significant correlation is indicated by an asterisk. A relationship with a correlation coefficient greater than 0.7 highlighted by a double asterisk.

Table 5.16: Frequency of exceedance SO_2 using the SANAAQS and the WHOAQG.

Table 5.17: Probability of exceedance of the SANAAQS SO_2 1 hour 134 ppb, 24 hour 48 ppb and WHOAQG SO_2 24 hour 8 ppb standards.

Table 5.18: Frequency of exceedance NO_2 using the SANAAQS and the WHOAQG.

Table 5.19: Probability of exceedance of the SANAAQS 1 hour NO_2 106 ppb standard.

Table 5.20: Frequency of exceedance Surface O_3 using the SANAAQS and the WHOAQG.

List of acronyms, abbreviations

AOD	Aerosol optical depth
AOT	Aerosol optical thickness
AQMP	Air quality management plan
AQS	Air quality standards
AQG	Air quality guideline
CH_4	Methane
CO	Carbon monoxide
GHG	Greenhouse gas
GWR	Geographic weighted regression
HPA	Highveld priority area
MAIAC	Multi-Angle Implementation of Atmospheric Correction
m.a.s.l.	Meters above mean sea level
MODIS	Moderate resolution imaging spectroradiometer
MPE	Mean predicted error
NAAQS	National ambient air quality standards
NEMAQA	National Environmental Management: Air Quality Act
NMHC's	Non-methane hydrocarbons
NO	Nitric oxide
NO_2	Nitrogen dioxide
NO_x	Oxides of nitrogen
O	Atomic oxygen
O_2	Molecular oxygen
O_3	Ozone
OH^-	Hydroxide
OMI	Ozone mapping instrument
PM	Particulate matter
$PM_{2.5/10}$	Particulate matter 2.5/10 micrometers or less in diameter
Ppb	Parts per billion
RMSE	Root means square error

SAAQIS	South African air quality information system
SAWS	South African Weather Services
SO_2	Sulphur dioxide
Surface O_3	Surface ozone
VOC's	Volatile organic compounds

Chapter 1: Introduction

(Source: Crompton, 2016)

1.1. Background

Clean air is considered a basic human right and a requirement for human health and well-being (WHO, 2005). Increasing levels of air pollutants across the world have become an issue for human and environmental health (WHO, 2005; Josipovic *et al.*, 2010). Expanding industrial and urban areas, especially in developing countries where populations are growing quickly such as South Africa, are largely responsible for increasing air pollution levels (Josipovic *et al.*, 2010; Gaur *et al.*, 2014). South Africa has been identified as a significant air pollution source (Josipovic *et al.*, 2010). Across the country seven criteria air pollutant species are frequently emitted, C_6H_6, CO, NO_2, O_3, PB, PM_{10}, SO_2 (DEA, 2009). Within South Africa there are a number of air pollution 'hotspot' areas, namely the Highveld Priority Area (HPA), the Vaal Triangle Air-shed Priority Area and the Waterberg Bojanala Priority Area. These are areas where ambient air quality standards for criteria air pollutants are or may be exceeded or any other situation exists which is causing or may cause a significant negative impact on air quality in the area (DEA, 2017).

Among the different pollutants emitted across the HPA, SO_2, NO_x and surface O_3 are particularly common where they can cause or exacerbate a number of respiratory problems, cardiovascular and lung disease, and other damaging effects on human health (WHO, 2005; Vallero, 2008; DEA, 2011). Major pollution sources across the HPA include domestic fossil fuel burning, mining, power generation, transport, petrochemical sectors and other industrial sectors (DEA, 2011). Each of these major pollutant sources are responsible for emissions of the pollutants SO_2 and NO_x, while in situ photochemical oxidation of carbon linked compounds (i.e. CO, CH_4 and VOC's), emitted, in the presence of NO_x are responsible for the production of the surface O_3 (DEA, 2011; Gaur *et al.*, 2014).

To effectively manage and monitor pollutant concentrations, it is crucial to determine pollutant levels, their variations and their relationship to regional meteorological patterns, which is typically done using ground-based monitoring networks (Gupta and Christopher, 2009a; Gupta and Christopher, 2009b; Hu *et al.*, 2014a; Hu *et al.*, 2014b; Sotoudeheian and Arhami, 2014; You *et al.*, 2015). Across the HPA, the South African air quality information (SAAQIS) monitoring network is used for this purpose. Although ground-level measurements are considered accurate, these measurements are inadequate as they only cover a small area (Hu *et al.*, 2014a). Consequently studies incorporating these measurements are narrow

due to the limited coverage and irregular distribution of monitoring stations (Hu *et al.*, 2014a; Hu *et al.*, 2014b; Sotoudeheian and Arhami, 2014). To achieve complete coverage of an area using ground-based monitoring networks is costly and as a result studies into more efficient monitoring techniques to attain comprehensive measurements of pollutants is necessary (Sotoudeheian and Arhami, 2014; You *et al.*, 2015). In recent decades, innovations in remote sensing techniques have encouraged measuring air pollutants using satellite imagery from a number of sensors, such as MODIS on Terra and Aqua satellites among others (Sotoudeheian and Arhami, 2014; Hu *et al.*, 2014a; Hu *et al.*, 2014b; You *et al.*, 2015). Hence, remote sensing techniques using derived measurements have been applied for the purpose of modelling pollutants to gain a full spatial coverage of pollutants across an area (Hu *et al.*, 2014a; Hu *et al.*, 2014b; You *et al.*, 2015). Using derived measurements of trace gases and aerosols obtained from satellite imagery to estimate ground-level pollutant concentrations is a necessary but challenging task to manage and monitor pollutants across an area (Gupta and Christopher, 2009a; Gupta and Christopher, 2009b; Sotoudeheian and Arhami, 2014; Hu *et al.*, 2014a; Hu *et al.*, 2014b; You *et al.*, 2015). To date no investigation into air pollution modelling across the HPA using satellite imagery has been undertaken. As a result, in the following sections of this study, the spatio-temporal patterns of SO_2, NO_x and surface O_3 across the HPA are investigated using satellite imagery.

1.2. Rationale

The National Environmental Management: Air Quality Act (No. 39 of 2004) (NEMAQA) illustrates that the constitutional right of an environment is that it is kept healthy, and nothing harmful to the environments health and wellbeing should be done (DEA, 2004). The Highveld has for long now been an area associated with poor air quality (DEA, 2011; Balashov *et al.*, 2014). Hence, the HPA was named in November 2007 as it is an area in need of air pollution control and governance as indicated by the frequent and potential exceedances of air quality standards (DEA, 2011). Thus, the HPA is an air pollution 'hotspot' whereby the roots of air pollution problems are to be identified and addressed in an Air Quality Management Plan (AQMP) (DEA, 2011). AQMP's do not follow all avenues to address air quality problems as they are just guidelines. As a result this study will introduce new techniques into modelling pollutants which can be used to identify and address air quality problems using information on the relationship of air pollutants to meteorology and

for air quality to satellite-derived measurements, meteorology and other potential factors, which is a recent study endeavor never performed across any area in South Africa.

1.3. Contribution to existing knowledge

To comprehensively monitor pollutants it is necessary to measure the variation of pollutant concentrations over numerous temporal scales (Zunckel *et al.*, 2004; Pudasainee *et al.*, 2006; Laakso *et al.*, 2008; Elampari and Chithambarathanu, 2011; Gaur *et al.*, 2014). Across the country studies have investigated the temporal variation of many aerosols and trace gases (Zunckel *et al.*, 2004; Laakso *et al.*, 2008; Collett *et al.*, 2010; Abiodun *et al.*, 2014; Balashov *et al.*, 2014). Few studies have focused on the temporal variation of pollutant species over Highveld area (Collett *et al.*, 2010; Balashov *et al.*, 2014). As a result, this study will add to the body of knowledge on the temporal variation of pollutants SO_2, NO_x and surface O_3 concentrations across the Highveld.

In addition, it is important to understand how meteorological parameters influence the concentrations of pollutants (Dueñas *et al.*, 2002; Elminir, 2005; Elampari and Chithambarathanu, 2011). There are few studies across the world (Dueñas *et al.*, 2002; Elminir, 2005; Elampari and Chithambarathanu, 2011), and none across the Highveld. Hence, this study will add to the body of knowledge on the relationship of SO_2, NO_x and surface O_3 to regional meteorology and of this subject across the Highveld area.

Many studies have used simple linear regression modelling to relate ground-level concentrations of trace gases and aerosols to satellite-derived measurements (Chu *et al.*, 2003; Wang and Christopher *et al.*, 2003; Engel-Cox *et al*., 2004; Engel-Cox *et al.*, 2006; Hutchinson *et al.*, 2006; Fishman *et al.*, 2010). More recently, multiple regression and non-linear modelling has been used for the purpose of relating the two by including other factors that influence ground-level trace gas and aerosol concentrations (Gupta and Christopher, 2009a; Gupta and Christopher, 2009b; Sotoudeheian and Arhami, 2014; Hu *et al.*, 2014a; Hu *et al.*, 2014b; You *et al.*, 2015). This study will add to this body of knowledge by using multiple regression modelling incorporating some of the many factors that influence trace gas concentrations, in a new location being the Highveld and for SO_2, NO_x and surface O_3 over numerous temporal scales.

Many air quality monitoring studies measure the frequency of exceedance of air quality standards for trace gases and aerosols (Josipovic *et al.*, 2010; Venter *et al.*, 2012). This study will add to the body of knowledge of the frequency of exceedance of SO_2, NO_x and surface O_3 across the HPA. New ways to identify a pollution 'hotspot' will be explored using the probability of exceedance.

This study may be used as guideline for modelling pollutants to develop methods whereby pollutants across an area may be accurately modelled using satellite and ground-level data.

1.4. Aim and objectives

This study aims to investigate ambient air pollution, using ground-level SO_2, NO_x and surface O_3 concentrations, meteorological parameters and MODIS atmosphere products, across the HPA, a pollution 'hotspot' area in South Africa.

The main objectives are:

1. To determine the seasonal, monthly and diurnal variation of ground-level SO_2, NO_x and surface O_3 concentrations,
2. To investigate how regional meteorological conditions influence SO_2, NO_x and surface O_3 concentrations,
3. To investigate the relationship between ground-level SO_2, NO_x and surface O_3 concentrations, meteorological conditions and MODIS atmosphere products and,
4. To investigate if SO_2, NO_x and surface O_3 levels exceed national and international air quality guidelines and the human and environmental health implications thereof.

1.5. Structure of thesis

The work presented herein is divided into six chapters. **Chapter 1** provides an introduction to this study. **Chapter 2** discusses the associated literature. **Chapter 3** provides an overview of the study area. **Chapter 4** explains the data and methodological approaches utilised. The results are presented and discussed in **Chapter 5**. In **Chapter 6** the key findings are summarised with recommendations.

Chapter 2: Literature review

(Eskom, 2017b)

2.1. Primary and secondary pollutants

SO_2, NO_x and surface O_3 are common air pollutants in South Africa's ambient air and across the HPA (DEA, 2004). These air pollutants can be considered in two main categories, primary and secondary air pollutants. SO_2 and NO_x are primary pollutants emitted directly from sources into the atmosphere (Vallero, 2008; Harrison *et al.*, 2014). Surface O_3 is a secondary air pollutant manufactured in air when primary pollutants (i.e. precursor gases) under the influence of sunshine react with and in the presence of one another (Vallero, 2008; Harrison *et al.*, 2014).

2.2. What is SO_2

SO_2 belongs to a group of air pollutants known as oxides of Sulphur (SO_x) (Datta *et al.*, 2010). SO_2 is a non-flammable, strong smelling gas phase pollutant (Chen *et al.*, 2001; Datta *et al.*, 2010). It is one of the most commonly released sulphur compounds in the atmosphere (Chen *et al.*, 2001). It is predominantly a primary pollutant, but when dimethylsulphide from the ocean is oxidised by OH radicals, SO_2 is formed as a secondary pollutant (Chen *et al.*, 2001; Jourdain and Legrand, 2001; Fisshea *et al.*, 2006; Datta *et al.*, 2010). SO_2 may also be oxidised to produce secondary aerosols and cause acid rain (Lin *et al.*, 2008).

SO_2 is emitted from a number of natural and anthropogenic sources (Table 2.1). Anthropogenic emissions of SO_2 from combustion processes, for example coal burning for power generation, are the most common and they occur at high enough concentrations for SO_2 to be considered a major atmospheric pollutant (Datta *et al.*, 2010; Lu *et al.*, 2010). The majority of SO_2 emissions, particularly across the HPA, are from the combustion of sulphur containing fuels at point sources (Chen *et al.*, 2001; Datta *et al.*, 2010; DEA, 2011; Harrison et al., 2014). SO_2 sources are generally unevenly distributed across an area and as a result SO_2 concentrations vary spatially, especially across the HPA where the majority of SO_2 sources are across the eastern side (Datta *et al.*, 2010; DEA, 2011). Additionally, SO_2 has an uneven temporal distribution as a result of its short atmospheric lifetime of about 2 to 3 days (Zunckel, 1999; Stehr *et al.*, 2000; Chen *et al.*, 2001).

Table 2.1: Common sources of SO_2 (Stehr *et al.*, 2000; Chen *et al.*, 2001; Datta *et al.*, 2010; DEA, 2011; Gaur *et al.*, 2014; Harrison *et al.*, 2014).

Pollutant	**Sources of SO_2**
SO_2	• Petrochemical plants – petroleum production • Fossil fuel burning – biomass, domestic (household), vehicle exhaust emissions and power generation • Mining (coal) • Gas extraction • Emissions from soil microbial processes • Agricultural activities – land clearing • Geothermal – Volcanoes and hot springs

SO_2 is highly reactive and soluble and as a result it is easily removed from the atmosphere through wet and dry depositional processes (Fisshea *et al.*, 2006). According to Zunckel *et al.* (1996) the rate of dry deposition of SO_2 over the Highveld largely exceeds the rate of wet deposition, mainly due to the low levels of precipitation experienced. Dry deposition occurs throughout the year when pollutants settle on land, water, building and vegetation surfaces (Zunckel *et al.*, 1996; Zunckel, 1999). During the summer months the Highveld experiences the majority of its rain, and during this time SO_2 is removed through wet deposition processes, namely precipitation or scavenging (within clouds as cloud condensation nuclei) (Zunckel *et al.*, 1996; Zunckel, 1999).

2.2.1. Why does SO_2 matter

SO_2 is an important pollutant to consider as exposure may influence both human and environmental health as well as climate (Vallero, 2008; Harrison *et al.*, 2014). In a developing country such as South Africa, high SO_2 levels as a result of coal combustion persist (Lourens *et al.*, 2011; Harrison *et al.*, 2014). The resulting SO_2 concentrations build up to dangerous levels under certain meteorological conditions and in particular terrains which limit dispersion (Datta *et al.*, 2010; Gaur *et al.*, 2014; Harrison *et al.*, 2014).

SO_2 exposure influences human health immensely. Brief exposure to SO_2 for as short as 10 minutes, may begin to affect pulmonary function in individuals (WHO, 2005). Mortality as a result of long term exposure to SO_2 may occur (WHO, 2005; Harrison *et al.*, 2014). In humans, SO_2 typically affects the respiratory system by constricting bronchi through mucus secretion, worsening asthmatic symptoms making breathing difficult or bringing about

asthma, promoting chronic bronchitis and causing coughing (Vallero, 2008; Harrison *et al.*, 2014). Exposure to SO_2 may also act as an irritant to eyes, nose and throat (Vallero, 2008; Harrison *et al.*, 2014).

In vegetation, SO_2 may cause severe stress through: inhibition of growth; physical destruction namely leaf blemishes; disturbance of internal processes namely metabolic function; and deterioration of health increasing plant susceptibility to other stressors namely disease and/or insect attack (Vallero, 2008; Harrison *et al.*, 2014). The outcome of the influence of SO_2 on vegetation may have economic and aesthetic effects (Vallero, 2008; Harrison *et al.*, 2014). In ecologically sensitive areas particularly SO_2 exposure may lead an overall decline in biodiversity through loss of sensitive species (Vallero, 2008; Harrison *et al.*, 2014).

SO_2 in the atmosphere is commonly converted to SO_4^{2-} through oxidation reactions (Chen *et al.*, 2001). The resulting SO_4^{2-} particles actively scatter solar radiation promoting surface and atmospheric cooling (Datta *et al.*, 2010; Harrison *et al.*, 2014). These particles also act a cloud condensation nuclei and as a result cloud albedo levels are increased which leads to an increase in cloud droplet numbers, a decrease in cloud sizes reducing the precipitation ability of clouds increasing their lifetime effectively enhancing the reflection of solar radiation to space (Harrison *et al.*, 2014).

2.2.2. Seasonal variation of SO_2

SO_2 has an obvious seasonal variation. During rainy seasons, namely summer across the HPA, SO_2 concentrations are lowest as SO_2 is easily removed from the atmosphere through wet depositional processes (Laakso *et al.*, 2008; Meng *et al.*, 2009; Datta *et al.*, 2010; Gaur *et al.*, 2014). Additionally, SO_2 may be photochemically reduced through heat and sunlight (Meng *et al.*, 2009). Hence, during summer months SO_2 concentrations are typically lowest due to removal by precipitation, more rapid photochemical reactions and vertical and horizontal mixing in an unstable atmosphere (Laakso et al., 2008; Meng et al., 2009; Data et al., 2010; Gaur et al., 2014).

Stable winter atmospheric conditions from high pressure cells promote subsidence and more frequent temperature inversions prohibiting any vertical mixing of SO_2 concentrations

(Laakso et al., 2008; Meng et al., 2009; Data et al., 2010; Gaur et al., 2014). As a result, SO_2 concentrations peak during winter (Lyubovtseva *et al.*, 2005; Laakso et al., 2008; Meng et al., 2009; Data et al., 2010; Gaur et al., 2014). Higher SO_2 concentrations in South Africa's winter months according to Venter *et al.* (2012) may partially be as a result of regional recirculation of pollutants.

In South Africa and particularly over the Highveld where the majority of the country's power stations reside, winter SO_2 concentrations are high not only due to the conditions of the atmosphere, but because more electricity and domestic burning is used for space heating (Lourens *et al.*, 2011). Furthermore, the seasonal variation of SO_2 is more pronounced where pollutant sources are strongest or more concentrated (Meng *et al.*, 2009; Datta *et al.*, 2010; Venter *et al.*, 2012; Gaur *et al.*, 2014).

2.2.3. Monthly variation of SO_2

During winter, June, July and August for the Southern hemisphere, SO_2 concentrations peak and then during summer, December, January and February, these concentrations are at their lowest as discussed in the previous section. Pollutant concentrations are also known to vary monthly due to changing meteorological conditions, source strength characteristics among others (Vallero, 2008). Hence, during one season SO_2 concentrations may not vary or they may vary substantially from month to month.

In Washington, United States, Chen *et al.* (2001) found that from 1999 to 2000 SO_2 concentrations were lowest during August and during December concentrations were particularly high. Similarly, Gaur *et al.* (2014) in Northern India and Meng *et al.* (2009) in Northern China identified peak SO_2 concentrations during December and during August the concentrations of SO_2 were lowest. In Hyytiälä, Finland Lyubovtseva *et al.* (2005) investigated SO_2 concentrations in a boreal forest and found that August concentrations were lowest while during February, concentrations of SO_2 were highest. From September 2004 to May 2005 Saliba *et al.* (2006) investigated SO_2 concentrations across Beirut, Lebanon and identified a December peak. Summer concentrations were not measured but during September, the beginning of autumn, SO_2 concentrations were at their lowest for the sampling campaign (Saliba *et al.*, 2006).

In South Africa across the Highveld Lourens *et al.* (2011) investigated SO_2 concentrations during 2007 and 2008 and found that SO_2 concentrations peaked during July and during November they were lowest. Near Mafikeng in the North-West, South Africa Laakso *et al.* (2008) showed that during 2006 and 2007 the concentrations of SO_2 peaked during July and during January they were lowest.

2.2.4. Diurnal variation of SO_2

SO_2 has a complex diurnal variation, which is more distinct during winter (Laakso *et al.*, 2008; Datta *et al.*, 2010; Gaur *et al.*, 2014). It has two diurnal variations resulting from diurnal changes of the mixing layer and from the type of source for SO_2 (Stehr *et al.*, 2000; Chen *et al.*, 2001).

One diurnal variation which is characteristic of rural and semi-rural areas shows a mid-day SO_2 peak around 12h00 and 13h00 (Zunckel *et al.*, 1999; Stehr *et al.*, 2000; Chen *et al.*, 2001; Lyubovtseva *et al.*, 2005; Laakso *et al.*, 2008; Lin *et al.*, 2008; Meng *et al.*, 2009; Collett *et al.*, 2010). This is as a result of a shallow mixing layer forcing SO_2 concentrations to subside and mix at the surface (Zunckel *et al.*, 1999; Stehr *et al.*, 2000; Chen *et al.*, 2001 Meng *et al.*, 2009; Collett *et al.*, 2010). SO_2 concentrations in this case generally decrease at night as a result of dry deposition (Zunckel *et al.*, 1999; Laakso *et al.*, 2008).

Another SO_2 variation occurs as a result of source strength and temperature inversion layers during the morning and evening (Data *et al.*, 2010; Gaur *et al.*, 2014). A morning and evening peak are as a result of peak time traffic emissions, power use and domestic fossil fuel use (Datta *et al.*, 2010; Gaur *et al.*, 2014). Additionally the evening peak is exacerbated by the onset of an inversion layer (induced by low surface temperature from nocturnal radiative cooling) that prohibits vertical mixing and the morning peak is exacerbated once the nocturnal inversion layer has broken up and a mixing layer has developed (Datta *et al.*, 2010; Venter *et al.*, 2012; Gaur *et al.*, 2014). During winter the morning and evening peaks are more pronounced as a result of source strength and more persistent and pronounced temperature inversion layers (Venter *et al.*, 2012).

2.3. What is NO_x

Oxides of Nitrogen (NO_x = NO + NO_2) are a group of highly reactive gases which contain nitrogen and oxygen atoms (Pandey *et al.*, 2008). NO_x are mainly generated from fossil fuel combustion (Table 2.2) (Harrison *et al.*, 2014). NO is a colourless, insoluble, odourless gas emitted directly to the atmosphere and is photochemically oxidised to form the NO_2, a brown odorous gas (Lal *et al.*, 2000; Harrison *et al.*, 2014). Oxidation of NO_x may produce secondary aerosols and cause acid rain (Lin *et al.*, 2008). NO_x for this study is a primary pollutant.

Table 2.2: Common sources of NO_x (Abdul-Wahab and Bouhamra, 2004; David and Nair, 2011; DEA, 2011; Gaur *et al.*, 2014; Harrison *et al.*, 2014).

Pollutant	Sources of NO_x
NO_x	• Fossil fuel burning – biomass, domestic, vehicle exhaust emissions and industrial • Mining • Wild fires • Lightning strikes • Soil microbial activity • Agricultural activities – land clearing, agricultural waste combustion

The majority of NO_x are emitted from combustion processes in vehicles (Harrison *et al.*, 2014). NO emissions levels are dependent on source density (i.e. traffic density) (Abdul-Wahab and Bouhamra, 2004). NO_x sources are unevenly distributed and concentrated, as a result NO_x concentrations exhibit a large spatial variation (Ahammed *et al.*, 2006; Pandey *et al.*, 2008; Meng *et al.*, 2009; Gaur *et al.*, 2014). NO_x has an atmospheric lifetime, shorter than SO_2, of a couple of hours to a day (Gaur *et al.*, 2014).

A major sink for NO_x is the photochemical reaction producing surface O_3 (Ahammed *et al.*, 2006; Pandey *et al.*, 2008; Meng *et al.*, 2009; Gaur *et al.*, 2014). NO_x are removed through dry deposition processes. NO may easily be removed to form NO_2 (Lal *et al.*, 2000; Jain *et al.*, 2005; Pandey *et al.*, 2008; Harrison *et al.*, 2014). NO_2, a gas soluble in liquids, may easily be removed through cloud scavenging and precipitation as well as through dry deposition (Jain *et al.*, 2005; Gaur *et al.*, 2014). Over the Highveld, as is the case for SO_2 removal, dry deposition and photochemical reactions are the most common removal paths for the soluble NO_x as there is little precipitation (Collett *et al.*, 2010).

2.3.1. Why does NO_x matter

NO_x are an important group of pollutants that may both directly and indirectly negatively influence both human and environmental health (Harrison *et al.*, 2014). NO_x levels may build up under particular meteorological conditions which limit dispersion (Harrison *et al.*, 2014). NO_x also acts as a catalyst during surface O_3 formation (Harrison *et al.*, 2014).

At extremely high levels NO_x exposure can cause death, while at low levels NO_x mainly targets the respiratory system affecting the structure of lung tissue (Harrison *et al.*, 2014). NO_x can also disturb the blood's ability to transport oxygen throughout the body leading to headaches, fatigue and dizziness (Harrison *et al.*, 2014). NO_2 is toxic to both humans and animals. High levels of NO_2 can permanently damage the respiratory tract and lungs, increasing vulnerability to asthma (WHO, 2005; Harrison *et al.*, 2014). Exposure to NO can cause unconsciousness, vomiting, mental confusion and damage to teeth (Harrison *et al.*, 2014). NO_x also acts as an irritant to the eyes, nose, throat and lungs (Harrison *et al.*, 2014). It also causes shortness of breath, fatigue and nausea (Harrison *et al.*, 2014).

NO_x is toxic and may both indirectly and directly damage vegetation (Harrison *et al.*, 2014). Physically NO_x may reduce plant growth rates, bleach plant tissue, promote leaf blemishes, and cause leaf fall (Harrison *et al.*, 2014). NO_x indirectly damages plants through wet and dry deposition, when deposited NO_x enters the soil increasing soil mineral nutrients to levels too high for vegetation (Harrison *et al.*, 2014).

NO_x is a catalyst during the production of surface O_3 (Harrison *et al.*, 2014). This is important as surface O_3 is a Greenhouse gas (GHG), as a result NO_x indirectly warms the Earth's surface (Harrison *et al.*, 2014). During the production of surface O_3, NO_x initiates the production of the OH^- radical which removes some GHG's, namely CO, CH_4 and HCFC's, essentially acting as a cooling agent (Ahrens, 2009; The Royal Society, 2008). NO_2 is oxidised to form nitrate particles which directly and indirectly cause a negative surface forcing resulting in net cooling (Ahrens, 2009).

2.3.2. Seasonal variation of NO_x

NO_x demonstrates a clear seasonal variation. The seasonal variation of atmospheric conditions plays a major role in the variation of NO_x concentrations (Abiodun *et al.*, 2014). In

areas where NO_x sources are strongest, for example urban city centres, there is a more distinct seasonal variation (Hassan *et al.*, 2013; Abiodun *et al.*, 2014), while Gaur *et al.* (2014) found no seasonal variation in rural areas with no significant NO_x sources.

In winter, across the Highveld, NO_x concentrations are allowed to accumulate as a result of increased emissions from widespread biomass burning, power generation and domestic fossil fuel burning and slower removal from less efficient photochemical removal (Piketh *et al.*, 1999; Collett *et al.*, 2010). High NO_x concentrations during winter are also promoted by subsidence and more frequent and persistent temperature inversion layers from high pressure systems (Collett *et al.*, 2010).

According to David and Nair (2011) a decrease in NO_x concentrations coincides with an increase in surface O_3 concentrations. In spring and summer as photochemical activity increases NO_x concentrations decrease (Lyubovtseva *et al.*, 2005; Beig *et al.*, 2007; Pandey *et al.*, 2008; Meng *et al.*, 2009; Collett *et al.*, 2010). However, in addition frequent precipitation results in minimum NO_x concentrations during summer months (Lyubovtseva *et al.*, 2005; Beig *et al.*, 2007; Pandey *et al.*, 2008; Meng *et al.*, 2009; Collett *et al.*, 2010).

2.3.3. Monthly variation of NO_X

During winter, June, July and August for the Southern hemisphere, NO_x concentrations are highest while during summer, December, January and February NO_x concentrations are at their lowest as discussed in the previous section. NO_x concentrations may or may not during a particular season vary from month to month.

Across India there have been many investigations into the levels of NO_x. Beig *et al.* (2007) sampled during 2003 and 2004 and found that during December NO_x concentrations peaked while during July and August NO_x concentrations were lowest. Similarly Gaur *et al.* (2014) sampled from 2009 to 2013 and found that during December NO_x concentrations were highest while during July they were at their lowest. David and Nair (2011) also found December NO_x concentrations to be highest during 2007 to 2009 at Trivandrum, India while during June they were lowest. During 2001 to 2003 at Anantapur, India Ahammed *et al.* (2006) found that during January NO_x concentrations peaked and during October they were lowest.

During 2003 to 2006 Meng *et al.* (2009) measured NO_x across Northern China and found that December NO_x concentrations were highest and during July these concentrations were substantially lower. Abdul-Wahab and Bouhamra (2002) measured NO_x concentrations during 1997 in Kuwait and found that concentrations during August were noticeably low while concentrations during January were relatively higher. In Jeddah City, Saudi Arabia Hassan *et al.* (2013) found that concentrations of NO_x measured from December 2011 to December 2012 were highest during March and during July they were lowest. In Hyytiälä, Finland from 1997 to 2003 concentrations of NO_x displayed a peak during March and during August they were lowest (Lyubovtsev *et al.*, 2005).

In South Africa, NO_x concentrations measured by Abiodun *et al.* (2014) in Cape Town during 2001 to 2008 were highest during June and during January they were particularly low. NO_x concentrations measured by Laakso *et al.* (2008) near Mafikeng, North-West during 2006 and 2007 were found to peak during June and during March they were lowest.

2.3.4. Diurnal variation of NO_x

In most rural areas, during summer, during strong wind episodes diluting NO_x concentrations and during high rainfall periods NO_x concentrations generally do not display any diurnal variation (Pandey *et al.*, 2008; Collett *et al.*, 2010; Gaur *et al.*, 2014). During winter and in areas with major NO_x sources, NO_x concentrations show a distinct diurnal variation (Abdul-Wahab and Bouhamra, 2004; Lyubovtseva *et al.*, 2005; Abiodun *et al.*, 2010). The boundary layer remains lower for longer during winter promoting a distinct diurnal variation (Beig *et al.*, 2007).

A typical diurnal variation for NO_x concentrations can be described by a morning peak when traffic densities are high, surface winds are slow and the nocturnal temperature inversion layers break up, followed by a minimum during the day when NO_x is removed by photochemical processes, diluted from strong winds and expansion of the mixing layer, and a distinct evening peak (greater than the morning peak) when traffic densities are high and temperature inversions onset (Lal *et al.*, 2000; Abdul-Wahab and Bouhamra, 2004; Lyubovtseva *et al.*, 2005 Ahammed *et al.*, 2006; Beig *et al.*, 2007; Lin *et al.*, 2008; Pandey *et al.*, 2008; Meng *et al.*, 2009; Collett *et al.*, 2010; David and Nair, 2011; Reddy *et al.*, 2012; Abiodun *et al.*, 2014; Gaur *et al.*, 2014).

2.4. What is O_3

O_3 is an almost colourless gaseous component of the atmosphere occurring in both the stratosphere and troposphere layers (Figure 2.1) (Xu *et al.*, 2008; Ahrens, 2009). About 90% of O_3 is present in the stratosphere. Here O_3 is produced following the photolysis of molecular oxygen (Xu *et al.*, 2008; Ahrens, 2009). This creates the 'ozone layer', which acts as a protective layer filtering out dangerous UV radiation (Xu *et al.*, 2008; Ahrens, 2009). In the troposphere, O_3 is present when it is transported from the stratosphere through stratospheric intrusions from westerly waves (Balashov *et al.*, 2014), and on the surface tropospheric O_3 is additionally produced photochemically and is a principal component of smog (Vingarzan, 2004; Ahammed *et al.*, 2006; Xu *et al.*, 2008; Ahrens, 2009). Here, O_3 is a GHG that absorbs terrestrial radiation and particularly at ground-level, photochemical O_3 is a hazardous air pollutant (Xu *et al.*, 2008; Ahrens, 2009). O_3 within the troposphere is a toxic substance with an unpleasant smell (Ahrens, 2009).

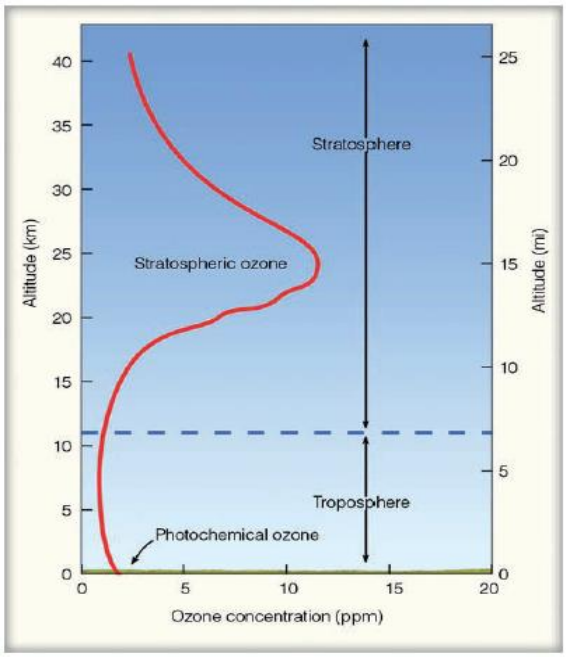

Figure 2.1: A schematic diagram of O_3 in the stratosphere and in the troposphere – showing ground-level photochemical O_3 (Ahrens, 2009).

2.4.1. O_3 as a surface air pollutant

O_3 is a common air pollutant in South Africa's ambient air (DEA, 2004). Surface O_3 is an air pollutant in the troposphere especially within the surface boundary layer. Combustion of fossil fuels is one of the principal processes that release the gaseous precursor pollutants

that react form surface O_3 (Table 2.3) (Gaur *et al.*, 2014). Along with the presence of the precursor gases, many meteorological conditions promote the formation of surface O_3 (Gaur *et al.*, 2014). The formation, transport, chemical destruction, deposition and atmospheric lifetime of surface O_3 will determine its concentration in any given area (Vingarzan, 2014). The lifetime of surface O_3 to about 2 days (Fishman *et al.*, 1991). The lifetime of tropospheric ozone is approximately 90 days (Fishman *et al.*, 1991).

Table 2.3: Common sources of the precursors that form O_3 (Abdul-Wahab and Bouhamra, 2004; Vingarzan, 2004; Ahammed *et al.*, 2006; David and Nair, 2011; DEA, 2011; Gaur *et al.*, 2014; Harrison *et al.*, 2014).

Pollutant	**Sources of O_3 precursors**
O_3	• Fossil fuel burning – biomass, domestic, vehicle exhaust emissions, power generation and industrial • Mining • Land changes – deforestation • Wild fires • Lightning strikes • Soil microbial activity • Agricultural activities – land clearing, agricultural waste combustion

Surface O_3 in particular is produced from the reaction between the precursor gases, namely VOC's (NMHC and CH_4) as well as CO in the presence of sunlight, and the OH (hydroxyl radical) and NO_x catalysts in the boundary layer (Figure 2.2) (Dueñas *et al.*, 2002; Zunckel *et al.*, 2004; Ahammed *et al.*, 2006; Lin *et al.*, 2008; The Royal Society, 2008; Xu *et al.*, 2008; Ahrens, 2009; David and Nair, 2011; Abiodun et al., 2014; Balashov *et al.*, 2014; Gaur *et al.*, 2014; Harrison *et al.*, 2014). The photochemistry of O_3 is a complex series of chemical reactions that is dependent on the availability of O_3 precursor gases (Crutzen *et al.*, 1999) (Figure 2.2).

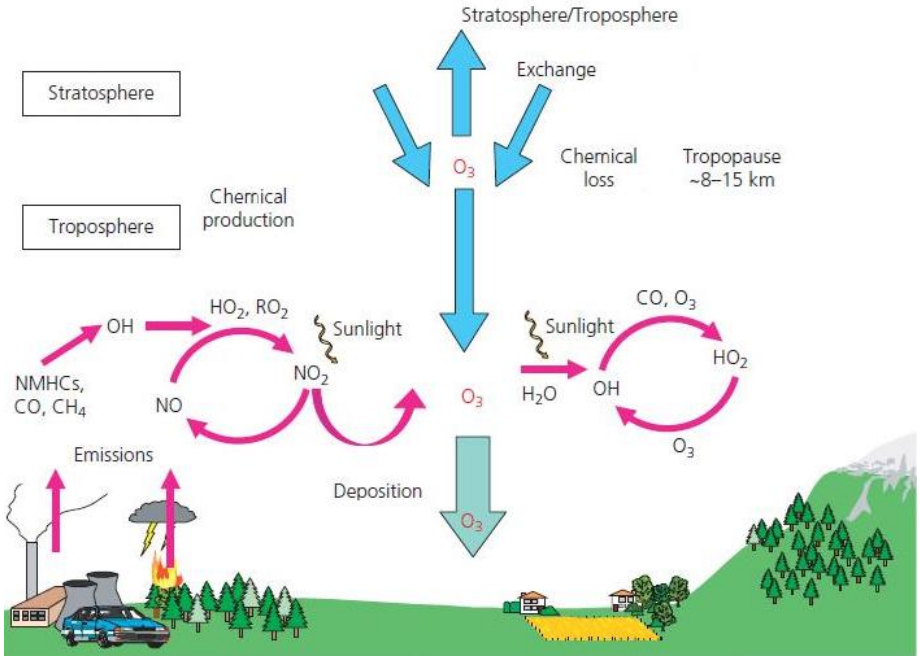

Figure 2.2: A schematic representation of O_3 in the stratosphere and the production and destruction of O_3 in the boundary layer of the Troposphere (After: The Royal Society, 2008).

The first reaction is the photolysis of O_3 which is a destruction process (reaction 1) (The Royal Society, 2008; Ahrens, 2009; Harrison *et al.*, 2014). This reaction occurs when solar radiation (hν) at wavelengths (λ) less than about 320 nm penetrates the atmosphere to reach the boundary layer (The Royal Society, 2008; Ahrens, 2009; Harrison *et al.*, 2014). O_3 photolysis generates excited (single state) oxygen atoms, $O(^1D)$, which easily react with water vapour (H_2O) to form hydroxyl radicals, OH^- (reaction 2) (The Royal Society, 2008; Ahrens, 2009; Harrison *et al.*, 2014). This is an important reaction as OH^- is responsible for most chemical change within the atmosphere (The Royal Society, 2008; Harrison *et al.*, 2014). In this way OH^- determines the oxidising capacity of the atmosphere and the atmospheric lifetime of O_3 (Crutzen *et al.*, 1999; Staehelin *et al.*, 2001). When OH^- reacts with CO and VOC's (CH_4 and NMHC's), O_3 is easily produced or removed (Crutzen *et al.*, 1999; Staehelin *et al.*, 2001).

$$O_3 + h\nu \rightarrow O(^1D) + O_2 \; \lambda < 320 \text{ nm (reaction 1)}$$

$$O(^1D) + H_2O \rightarrow 2OH^- \text{ (reaction 2)}$$

O_3 is formed naturally when O and O_2 react in the presence of solar radiation (Crutzen *et al.*, 1999; Staehelin *et al.*, 2001; The Royal Society, 2008; Harrison *et al.*, 2014). Some of the $O(^1D)$ atoms formed in reaction 1 are deactivated to ground state, where O_3 and M is produced (reaction 3) (Crutzen *et al.*, 1999; Staehelin *et al.*, 2001; The Royal Society, 2008; Harrison *et al.*, 2014). M is a third body that absorbs the energy released during the reaction (The Royal Society, 2008).

$$O + O_2 \rightarrow O_3 + M (\text{reaction } 3)$$

O_3 may be removed or produced when OH^- reacts with the precursor gases in the presence of NO_x and sunlight (Crutzen *et al.*, 1999; Staehelin *et al.*, 2001; The Royal Society, 2008; Harrison *et al.*, 2014). The net production of O_3 is very dependent on the concentration of NO_x in the atmosphere (Crutzen *et al.*, 1999; Dueñas *et al.*, 2002).

An example of the photochemical production of O_3, when CO is oxidised by OH^- O_3 is readily formed through the following reactions (Crutzen *et al.*, 1999; Staehelin *et al.*, 2001; The Royal Society, 2008; Harrison *et al.*, 2014):

$$CO + OH^- \rightarrow CO_2 + H (\text{reaction } 4)$$

Here, H reacts with O_2 to produce the peroxyl radical, HO_2 (reaction 5), which may react with NO to produce OH^- and NO_2 (reaction 6) (Crutzen *et al.*, 1999; Staehelin *et al.*, 2001; The Royal Society, 2008; Harrison *et al.*, 2014). When solar radiation penetrates through the atmosphere to ground-level and is less than 420 nm, any NO_2 present will produce NO and O (reaction 7) (Crutzen *et al.*, 1999; Staehelin *et al.*, 2001; The Royal Society, 2008; Harrison *et al.*, 2014). This reaction occurs most commonly when air is highly polluted (The Royal Society, 2008; Ahrens, 2009). Following this reaction 3 occurs to produce O_3, where the net reaction of this process is reaction 8 (Crutzen *et al.*, 1999; Staehelin *et al.*, 2001; The Royal Society, 2008; Harrison *et al.*, 2014).

$$H + O_2 + M \rightarrow HO_2 + M (\text{reaction } 5)$$

$$HO_2 + NO \rightarrow OH^- + NO_2 \text{ (reaction } 6)$$

$$NO_2 + h\nu \rightarrow NO + O \; \lambda < 420\, nm \text{ (reaction } 7)$$

$$CO + 2O_2 \rightarrow CO_2 + O_3 (\text{reaction } 8)$$

O_3 can easily be destroyed when it combines with NO (reaction 9) (Ahrens, 2009; Harrison *et al.*, 2014). O_3 can also be easily destroyed when it combines with HO_2 (reaction 10) (The Royal Society, 2008). According to David and Nair (2011), the amount of surface O_3 lost due to photochemical loss mechanisms is greater than the loss due to dry deposition. The net result of the destruction of O_3 with CO shown by reaction 11 (Crutzen *et al.*, 1999; Staehelin *et al.*, 2001; The Royal Society, 2008; Harrison *et al.*, 2014).

$$O_3 + NO \rightarrow NO_2 + O_2 \text{(reaction 9)}$$

$$O_3 + HO_2 \rightarrow OH^- + 2O_2 \text{(reaction 10)}$$

$$CO + O_3 \rightarrow CO_2 + O_2 \text{(reaction 11)}$$

O_3 is a soluble compound easily removed during precipitation episodes (Balashov *et al.*, 2014; Gaur *et al.*, 2014). O_3 may also easily settle on vegetation, water and land surfaces (Ahammed *et al.*, 2006; David and Nair, 2011; Harrisson *et al.*, 2014). According to Zunckel *et al.* (2004) the removal of O_3 through dry deposition over the Highveld is far greater than through wet deposition.

2.4.2. Why does surface O_3 matter

Surface O_3 is an important pollutant as it exerts a negative influence on both human and environmental health as well as climate in the boundary layer (The Royal Society, 2008; Ahrens, 2009; Elampari and Chithambarathanu, 2011). Even at low concentrations surface O_3 adversely impacts human and environmental health (Ahrens, 2009). Surface O_3 has a harmful impact on the biosphere, human health, animal populations, manufactured goods and agricultural productivity (Lal *et al.*, 2000; Dueñas *et al.*, 2002; Zunckel *et al.*, 2004; Jain *et al.*, 2005; Lin *et al.*, 2008; Xu *et al.*, 2008; Khoder, 2009; David and Nair, 2011; Hassan *et al.*, 2013).

In humans, surface O_3 predominantly targets the respiratory system (Kouvarakis *et al.*, 2000; The Royal Society, 2008; Ahrens, 2009; Elampari and Chithambarathanu, 2011; Gvozdić *et al.*, 2011; Reddy *et al.*, 2012; Balashov *et al.*, 2014). For extreme cases, from long term exposure, mortality (usually respiratory related) from surface O_3 is possible (Beig *et al.*, 2011; Ahrens, 2009). Most other cases reveal that surface O_3 exposure brings about

respiratory problems, irritation of eyes, nausea and headaches (Kouvarakis *et al.*, 2000; The Royal Society, 2008; Ahrens, 2009; Elampari and Chithambarathanu, 2011; Gvozdić *et al.*, 2011; Reddy *et al.*, 2012; Balashov *et al.*, 2014). The main concern in humans is respiratory damage as this may decrease lung function, exacerbate asthma in asthmatic subjects or even bring about asthma, cause pulmonary inflammation, chest pain, coughing, pulmonary congestion and an overall decline in lung capacity (Kouvarakis *et al.*, 2000; The Royal Society, 2008; Ahrens, 2009; Elampari and Chithambarathanu, 2011; Gvozdić *et al.*, 2011; Reddy *et al.*, 2012; Balashov *et al.*, 2014).

In natural vegetation and agricultural crops, surface O_3 may cause severe stress, produce visible injuries and negatively influence their growth ability and overall health by increasing their susceptibility to disease (Pochanart *et al.*, 1999; Satsangi *et al.*, 2004; Avnery *et al.*, 2011; Lourens *et al.*, 2011). The resulting influence of surface O_3 on crops and plants may be detrimental to economies and food security (Wang and Mauzerall, 2004; Avnery *et al.*, 2011). For agricultural crops, crop yields as well as quality are reduced (Avnery *et al.*, 2011; Elampari and Chithambarathanu, 2011). Exposure may also influence natural vegetation and agricultural crops abilities to produce as well as store food and it may cause changes in morphology and physiology (Avnery *et al.*, 2011; Elampari and Chithambarathanu, 2011).

Surface O_3 also influences climate. It is a GHG that can alter the surface energy balance, by absorbing outgoing terrestrial radiation (infrared radiation) in the atmospheric window ($\lambda \sim 9.6$ µm) (IPCC, 2001; Betts *et al.*, 2002; Yamanji *et al.*, 2006; Ahrens, 2009). It is the third most important GHG after CO_2 and CH_4 (IPCC, 2001; Betts *et al.*, 2002; Ahrens, 2009).

2.4.3. Seasonal variation of surface O_3

Seasonally surface O_3 concentrations display a clear variation. During the wet season, in summer, cloud cover and precipitation reduce the amount of solar radiation reaching the surface and in turn it reduces the amount of surface O_3 being formed by promoting the removal of surface O_3 and its precursors through wet deposition (Zunckel *et al.*, 2004; Jain *et al.*, 2005; Ahammed *et al.*, 2006; Meng *et al.*, 2009; Reddy *et al.*, 2012; Hassan *et al.*, 2013; Gaur *et al.*, 2014).

Surface O_3 concentrations have a broad peak during the dry season (August to November) when skies are clear and temperatures are warm, as solar radiation easily reaches the surface promoting a large amount of photochemical generation of surface O_3 (Zunckel *et al.*, 2004; Jain *et al.*, 2005; Ahammed *et al.*, 2006; Meng *et al.*, 2009; Reddy *et al.*, 2012; Hassan *et al.*, 2013; Gaur *et al.*, 2014). Over the Highveld surface O_3 concentrations show a strong seasonal variation, where the surface O_3 peak, during the dry season, is supported by widespread NO_x (a precursor of Surface O_3) generation from fossil fuel and biomass burning (Zunckel *et al.*, 2004).

During late summer and early autumn, surface O_3 concentrations in South Africa are at a minimum (Zunckel *et al.*, 2004). In other parts of South Africa, in the Southern African Savannah environment, the seasonal variation of surface O_3 may be particularly weak (Laakso *et al.*, 2008).

2.4.4. Monthly variation of surface O_3

During spring, September, October and November for the Southern hemisphere, surface O_3 concentrations peak and then during autumn, March, April and May, these concentrations are lowest as discussed in the previous section. During one season surface O_3 concentrations may not vary or they may vary substantially from month to month.

Across India many studies have investigated the monthly variation of surface O_3, their findings follow: Khemani *et al.* (1995) found that during 1991 and 1992 surface O_3 levels across Pune were highest during April and lowest during August; across Ahmedabad City from 1991 to 1995, Lal *et al.* (2000) found a maximum during April and during August concentrations were at their lowest; Naja *et al.* (2003) worked in Mt Abu from 1993 to 2000 and found maximum surface O_3 levels during May and minimum levels during August; Satsangi *et al.* (2004) worked in Agra from 2000 to 2002 and found that during April surface O_3 levels peaked while August levels were at a minimum; across New Delhi from 1997 to 2003 Jain *et al.* (2005) found concentrations peaked during April and during August they were lowest; across Anantapur from 2001 to 2003 Ahammed *et al.* (2006) found that during March surface O_3 levels peaked and during August these levels were at a minimum for the sampling period; similarly to Khemani *et al.*(1995), Beig *et al.* (2007) found that surface O_3 levels across Pune during 2003 and 2004 peaked during April and during August they were

at a minimum; across Trivandrum from 2007 to 2009 surface O_3 levels measured by David and Nair (2011) were maximum during December while during June they were lowest; Reddy *et al.* (2012) also measured surface O_3 levels across Anantapur but did not find the same results as Ahammed *et al.* (2006) and instead found that during 2010 the surface O_3 levels peaked during April and during September they were lowest; Sharma *et al.* (2013) sampled surface O_3 levels across the North Western Himalayan region during 2010 and found that during May these levels were highest while during October they were lowest; lastly Gaur *et al.* (2014) sampled surface O_3 levels from 2009 to 2013 across Kanapur and found that levels were highest during May and lowest during August.

Across China many studies have investigated the monthly variation of surface O_3, their findings follow: Tu *et al.* (2007) worked in Nanjing City from 2000 to 2003 and found that surface O_3 levels peaked during May and during December they were lowest; Lin *et al*. (2008) worked across Northern China from 2004 to 2006 and found that during May surface O_3 levels peaked while during November they were lowest; across Eastern China during 2004 Shan *et al.* (2008) found that surface O_3 levels peaked during April and during December they were lowest; during 1994 and 1995 and then during 2005 and 2006 Xu *et al.* (2008) found that surface O_3 peaked during May and were lowest during December; Similarly to Lin *et al.* (2008), Meng *et al.* (2009) worked across Northern China but instead found that during April surface O_3 levels were highest while during November they were lowest; across the Pearl River Delta during 2006 and 2007 Zheng *et al.* (2010) found that surface O_3 levels peaked during May and during December they were lowest.

Across Eastern Asia Wang and Mauserall (2004) found that during May surface O_3 levels from 1999 to 2000 peaked and during December they were lowest. Similarly Yamaji *et al.* (2006) also worked across Eastern Asia and found that during 1995 surface O_3 levels peaked during May and during December they were lowest.

Across the rest of the world there have been fewer studies. From 1997 to 2003 Lyubovtseva *et al.* (2005) found that in Hyytiälä, Finland surface O_3 levels peaked during April while during October they were lowest. Jaffe and Ray (2007) used surface O_3 measurements from 1987 to 2004 from North and Western United States and Alaska and found that concentrations were highest during May and lowest during August. Across Cairo, Egypt

during 2004 and 2005 Khoder (2009) found that surface O_3 levels peaked during July and during January they were lowest. Across the Jeddah City, Saudi Arabia from 2011 to 2012 Hassan *et al.* (2013) measured surface O_3 and found that levels peaked during August and during February they were at their lowest. During July across Kuwait, Iraq, Abdul-Wahab and Bouhamra (2002) and across Northern Spain, Garcia *et al.* (2005) found surface O_3 concentrations to be highest and during December these concentrations were found to be lowest.

In South Africa, Balashov *et al.* (2014) using data recorded across the Highveld found that surface O_3 concentrations peaked during October and during May they were lowest for the period of 1990 to 2007. Across the Highveld during 2006 and 2007 Lourens *et al.* (2011) identified an October peak in surface O_3 concentrations and during May the concentrations were lowest. Near Mafikeng, North-West, South Africa, Laakso *et al.* (2008) during a 2006 to 2007 sampling campaign found that surface O_3 concentrations were highest during September while during July they were lowest. Across Southern Africa, Zunckel *et al.* (2004) identified that during 1999 to 2001 October concentrations of surface O_3 were highest while February concentrations were lowest.

2.4.5. Diurnal variation of surface O_3

Surface O_3 concentrations exhibit a clear diurnal variation. South African surface O_3 concentrations are high during the day and low at night throughout all the seasons (Zunckel *et al.*, 2004). During the dry season the diurnal variation is more pronounced than for the rest of the year (Zunckel *et al.*, 2004).

Surface O_3 concentrations are lowest at night and drop to a minimum around sunrise as sources of surface O_3 precursor gases emit very little at night and photochemical reactions cannot occur in the absence of sunlight and photochemical loss mechanisms dominate under the nocturnal inversion layer (Zunckel *et al.*, 2004; Jain *et al.*, 2005; Lyubovtseva *et al.*, 2005; Ahammed *et al.*, 2006; Meng *et al.*, 2009; David and Nair, 2011; Reddy *et al.*, 2012; Hassan *et al.*, 2013; Gaur *et al.*, 2014).

Once the nocturnal inversion layer is broken up by sunlight, air aloft is allowed to mix downward allowing upper tropospheric O_3 to mix in with boundary layer surface O_3, and the

surface O_3 precursors are allowed to mix and photochemically react bringing about a gradual rise in surface O_3 concentrations (Zunckel *et al.*, 2004; Jain *et al.*, 2005; Ahammed *et al.*, 2006; Meng *et al.*, 2009; David and Nair, 2011; Reddy *et al.*, 2012; Hassan *et al.*, 2013; Gaur *et al.*, 2014). Throughout the day temperatures gradually increase as the sunlight intensity increases promoting surface O_3 formation (Zunckel *et al.*, 2004). From midday to the late afternoon surface O_3 concentrations peak, and following that concentrations gradually decrease as sunlight intensity and temperatures decrease (Zunckel *et al.*, 2004).

2.5. Transportation of air pollutants over South Africa

Meteorology plays a central role in ambient air quality levels. The overall temporal variation and spatial distribution of air pollutants are explained by source characteristics, emission rates, atmospheric lifetimes, vertical and horizontal transport and local terrain (Cosijn and Tyson, 1996; Gartsang *et al.*, 1996; Tyson *et al.*, 1996b; Dueñas *et al.*, 2002). Meteorology influences the emission and removal, transport and mixing, and photochemical reactions (Dueñas *et al.*, 2002; Tu *et al.*, 2007; David and Nair, 2011). The lifetime of pollutants will also play an important role in their transportation across an area; pollutants with longer atmospheric lifetimes will be transported over further distances (Fishman *et al.*, 1991; Krishnamurti *et al.*, 1993).

The concentration of air pollutants in a given area is not only dependent on their regional production but also on the meteorology across the region, dispersion into and out of an area and the accumulation of pollutants (Tyson *et al.*, 1996b). The dispersion and accumulation of pollutants in a given area is a function of transportation of air throughout the atmosphere (Gartsang *et al.*, 1996; Tyson *et al.*, 1996b). Air pollutant transportation is dependent on the state of the atmosphere, namely whether the atmosphere is stable or unstable (Gartsang *et al.*, 1996; Tyson *et al.*, 1996b). Air transport over southern Africa is highly controlled (Tyson *et al.*, 1996b). The transportation of air pollutants over southern Africa is driven by planetary and synoptic scale circulation features of the general circulation patterns for the Southern hemisphere (Gartsang *et al.*, 1996). These general circulation features control vertical and horizontal transport and patterns for pollutants (Cosijn and Tyson, 1996; Gartsang *et al.*, 1996; Tyson *et al.*, 1996b; Tyson *et al.*, 1997).

Five major general circulation types with different frequencies throughout the year dominate over Southern Africa explaining the dispersion and accumulation of pollutants (Figure 2.3) (Tyson *et al.*, 1996b). The first, the *semi-permanent subtropical anticyclones* mostly present during winter months, with a frequency exceeding 70%, are characteristic of the subsidence limbs of the Southern hemisphere general circulation Hadley and Ferrell cells (Figure 2.3) (Tyson *et al.*, 1996b). The *transient mid-latitude ridging anticyclones* occur throughout the year with a frequency of 10% (Figure 2.3). Together both anticyclones have a frequency of 80% during July (Figure 2.3). During this time pollutants have restricted vertical motion and recirculation will typically occur (Tyson *et al.*, 1996a). The *westerly baroclinic disturbances*, namely the cut-off low, occur with a frequency of 20-30% throughout the year (Figure 2.3). The *barotropic quasi-stationary tropical easterly waves* are primarily a summer phenomenon and occur at a frequency of 50 – 60% in January (Figure 2.3).

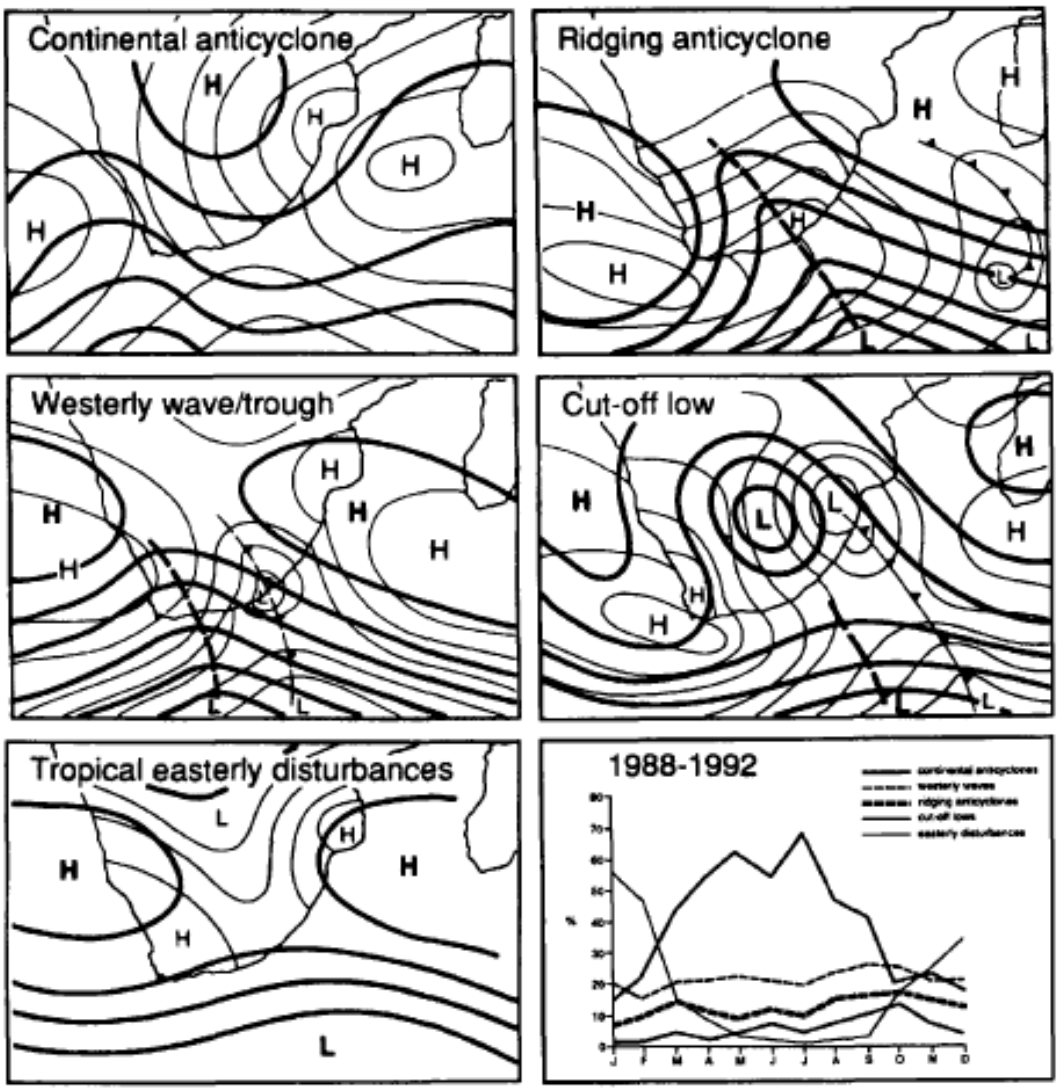

Figure 2.3: Major circulation types affecting southern Africa and their monthly occurrence frequencies from 1988-1992. For the graph legend, the thick black line represents the continental anticyclone, the thin dashed line represents the westerly wave, the thick dashed line represents the ridging anticyclone, the second thickest black line represents the cut-off low and the thinnest black line represents the easterly disturbances. Thick lines represent conditions at 500hPa and light lines represent conditions at 850hPa (Tyson *et al.*, 1996b).

2.5.1. Vertical transport

Southern Africa and its adjacent oceans are positioned for wide-spread subsidence as they are located under the subsidence limbs of both the Hadley and Ferrell cells (Gartsang *et al.*, 1996). The result is large scale stability over South Africa. In a stable atmosphere easterly disturbances and cut-off lows may occur encouraging instability for unstable conditions to

persist which promotes vertical movement and transport of air and its constituents (Cosijn and Tyson, 1996; Tyson *et al.*, 1996b).

Given South Africa's position and the high level of stability, absolutely stable layers i.e. stable discontinuities, where the lapse rate of temperature is less than the saturated adiabatic lapse rate, are known to occur (Cosijn and Tyson, 1996; Gartsang *et al.*, 1996; Tyson *et al.*, 1996a). Absolutely stable layers regulate and control vertical mixing and as a result of these layers horizontal mixing is promoted over vertical mixing (Cosijn and Tyson, 1996; Gartsang *et al.*, 1996; Tyson *et al.*, 1996a; Kirkman *et al.*, 2000). Pollutants are typically trapped between these layers and trapped pollutants may readily photochemically react or may accumulate or be transported horizontally from their sources (Kirkman *et al.*, 2000). Very little vertical mixing of pollutants occurs over South Africa (Cosijn and Tyson, 1996; Gartsang *et al.*, 1996; Tyson *et al.*, 1996a).

The semi-permanent absolutely stable layers occur on most no-rain days at 700 hPa, 500 hPa and 300 hPa throughout the country and at coastal areas an additional stable layer is present at 850 hPa (Figure 2.4) (Cosijn and Tyson, 1996; Gartsang *et al.*, 1996). The 700 hPa stable layer is present on top of the mixing layer at a height of 1.5 km above the interior plateau, it lasts for about 7 days and it is easily broken by the westerly wave (Figure 2.4) (Cosijn and Tyson, 1996; Gartsang *et al.*, 1996; Tyson and Gatebe, 2001). The main stable layer, situated at 500 hPa, is spatially abundant and temporally persistent and it is about 3 km above the interior plateau (Figure 2.4) (Cosijn and Tyson, 1996; Gartsang *et al.*, 1996). This stable layer can withstand westerly disturbances to last for up to 40 days at a time (Gartsang *et al.*, 1996). The 300 hPa layer is located about 8 km above the interior plateau and just under the troposphere and lasts for about 2 days (Figure 2.4) (Cosijn and Tyson, 1996; Gartsang *et al.*, 1996).

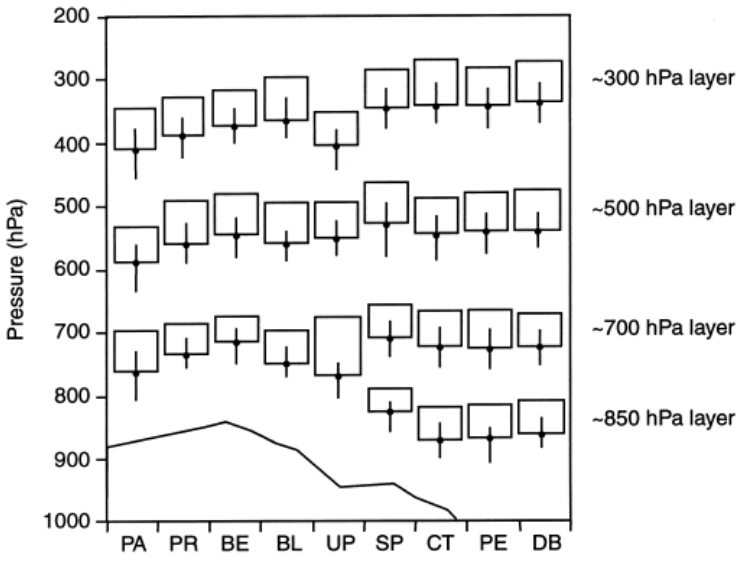

Figure 2.4: Mean annual location of the absolutely stable layers over southern Africa. The depth of the layers is indicated by the vertical extent of the shaded boxes; vertical lines give the standard deviation of the base height. PI denotes Pietersburg, PR Pretoria, BE Bethlehem, BL Bloemfontein, UP Upington, SP Springbok, CT Cape Town, PE Port Elizabeth and DB Durban (Cosijn and Tyson, 1996).

These layers are all stable enough to inhibit vertical transport of pollutants, and thus pollutants may easily accumulate under these layers creating stratification within the atmosphere (Tyson *et al.*, 1996b; Tyson and Gatebe, 2001). Once broken up and destabilised by well-developed low pressure troughs and cut-off lows, the stable layers release trapped pollutants and at this time vertical mixing occurs (Cosijn and Tyson, 1996; Gartsang *et al.*, 1996; Tyson *et al.*, 1996b; Tyson and Gatebe, 2001).

Additionally, inversion layers, where temperature increases with height, in the boundary layer promotes the horizontal dispersion and accumulation of pollutants as vertical motion is inhibited (Tyson *et al.*, 1988). Two types of inversion layers are typical over southern Africa, namely, the temperature inversion and the elevated inversion layer (Tyson *et al.*, 1988).

2.5.2. Horizontal transport

In South Africa's typically stable atmosphere air is more likely to disperse horizontally than vertically (Cosijn and Tyson, 1996). There are five basic modes of horizontal air transport over southern Africa (Figure 2.5). These modes of air transport are as a result of the five major circulation types affecting southern Africa (Gartsang *et al.*, 1996). These modes of

transport are shown in Figure 2.5. Each synoptic circulation type produces different transport fields (Tyson *et al.*, 1996b).

Dominating these modes of transport is the anticyclone mode, the continental and ridging anticyclone (Figure 2.5) (Gartsang *et al.*, 1996; Tyson *et al.*, 1996b). This mode of transport results in frequent recirculation at spatial scales that vary from tens to thousands of kilometers (Gartsang *et al.*, 1996).

Two modes of direct transport can be expected from anticyclonic systems (Figure 2.5) (Tyson *et al.*, 1996b). Air exiting the sub-continent and into the Atlantic Ocean is known as the Angolan plume (Figure 2.5) (Tyson *et al.*, 1996b). While, air exiting the sub-continent and into the Indian Ocean is known as the Natal plume (Figure 2.5) (Tyson *et al.*, 1996b). About 75% of all air exiting the sub-continent exits via the Natal plume for the continental cyclone (Tyson *et al.*, 1996b). The Angolan plume is favoured by the ridging anticyclone (Tyson *et al.*, 1996b).

The continental high is also associated with recirculation of air and its constituents over tens to thousands of kilometers for about 2 to 3 days up to almost three weeks (Figure 2.5) (Tyson *et al.*, 1996a; Tyson *et al.*, 1996b; Tyson and Abreton, 1998). About 44% of air transport is through recirculation during no-rain days, this generally takes place between the surface and 500 hPa (Figure 2.5) (Tyson *et al.*, 1996a; Tyson and Gatebe, 2001). Recirculated pollutants may be carried by local to macro scale winds that generally return to their sources (Tyson and Abreton, 1998).

The westerly wave general circulation pattern quickly transports air towards the Indian Ocean, whereas the Easterly wave produces as fast air transport field towards the Atlantic Ocean (Figure 2.5) (Tyson *et al.*, 1996b).

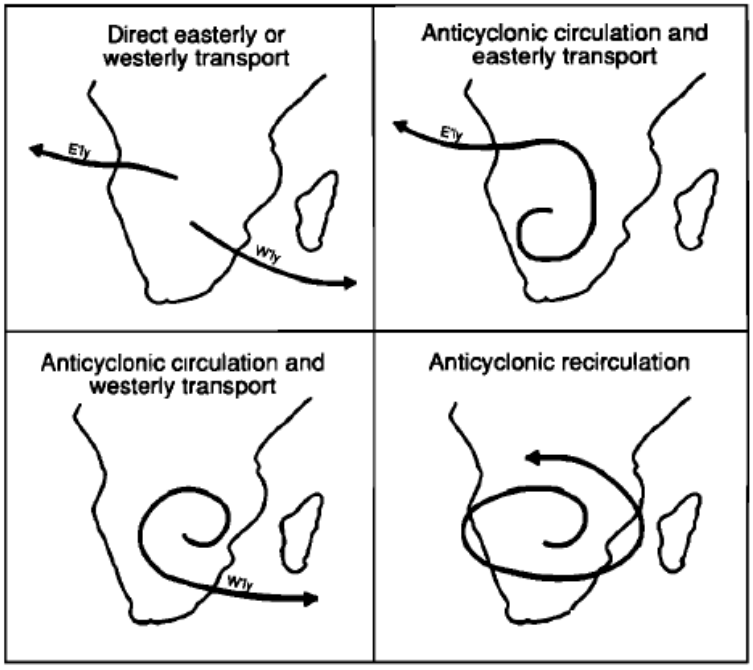

Figure 2.5: Schematic representation of major low-level air transport modes over South Africa (Gartsang *et al.*, 1996).

2.5.3. Transport of pollutants into and out of the Highveld

The Highveld region is one of the largest anthropogenic emission sources in the Southern hemisphere. Understanding the nature of the transport of pollutants into and out of the industrial Highveld is a crucial starting point toward an understanding of the nature of the atmospheric chemistry and air transport over southern Africa (Frieman and Piketh, 2002). Air transported into and out of the Highveld affects pollutant concentrations over the Highveld and the pollutant concentrations over other regions in southern Africa, even as far as Cape Town (Frieman and Piketh, 2002; Abiodun *et al.*, 2014).

Four air transport pathways towards the Highveld occur between 700 and 850 hPa (Frieman and Piketh, 2002). Air is transported towards the Highveld from the Atlantic Ocean, the Indian Ocean, the African continent and the sub-continent (Figure 2.6). The majority of air transported to the Highveld is from the Atlantic Ocean, this air is generally emission free (Frieman and Piketh, 2002). When Atlantic air flow is associated with pronounced ridging behind a cold front recirculation of trace gases and aerosols may occur (Frieman and Piketh, 2002). African transport, most prominent during winter, of air may bring trace gases and aerosols from central-Africa to the Highveld; this air frequently carries pollutants (Figure

2.6) (Frieman and Piketh, 2002). Recirculated air flow, sub-continental flow (Figure 2.6), is typically filled with pollutants and takes up to 2 to 3 days to reach the Highveld (Frieman and Piketh, 2002). Recirculation of air typically occurs during autumn and winter (Frieman and Piketh, 2002). Indian Ocean airflow is typically associated with high moisture levels from the ocean and ocean aerosols (Frieman and Piketh, 2002).

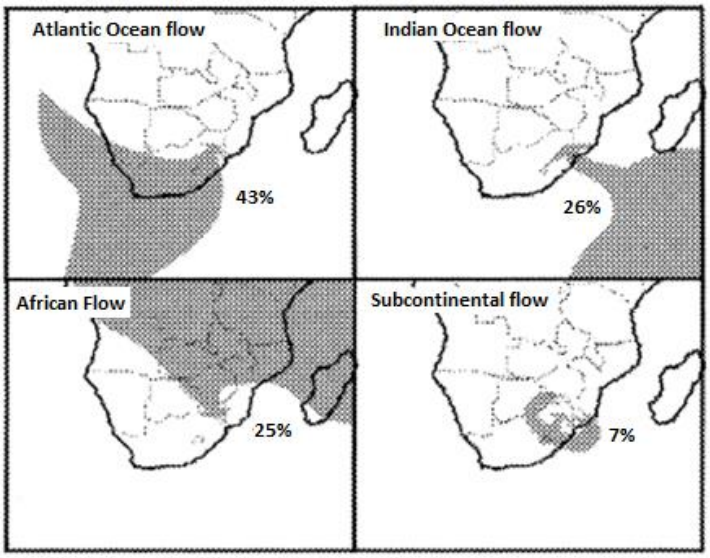

Figure 2.6: Air transport pathways into the Highveld region and their percentage frequency occurrence (After: Frieman and Piketh, 2002).

There are two main modes of air transport out of the Highveld (Frieman and Piketh, 2002). The first is direct transport where air is transported to Equatorial Africa, the Atlantic Ocean, the Indian Ocean and the South Indian Ocean (Figure 2.7) (Frieman and Piketh, 2002). The second mode is recirculated transport, whereby air and its constituents recirculate towards their point of origin over regional to sub-continental scales (Figure 2.7) (Frieman and Piketh, 2002). The main transport routes are towards the Indian Ocean (39%) and recirculation (33%) (Figure 2.8) (Frieman and Piketh, 2002).

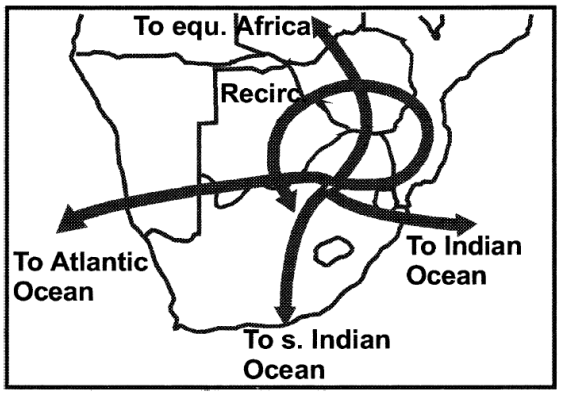

Figure 2.7: The main transport pathways out of the Highveld region (Frieman and Piketh, 2002).

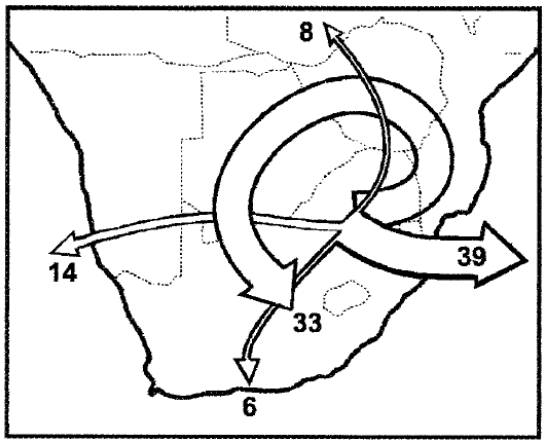

Figure 2.8: The percentage frequency of the main transport pathways out of the Highveld region (Frieman and Piketh, 2002).

2.6. Meteorological controls on the levels of primary pollutants, SO_2 and NO_x

Meteorology along with emissions, atmospheric chemistry and topography are well known contributors to air pollution episodes (Akpinar *et al.*, 2008). Hence, the effect of meteorological conditions on pollutant concentrations has been readily analysed. For primary pollutants meteorological factors, in particular, wind speed, wind direction, atmospheric pressure, relative humidity and temperature are known to influence the behavior of pollutants (For example: Cuhadaroglu and Demirci, 1997; Demirci and Cuhadaroglu, 2000; Latini *et al.*, 2002; Elminir, 2005; Turalioğlu *et al.*, 2005; Akpinar *et al.*, 2008; Giri *et al.*, 2008; Ilten and Selici, 2008; Lin *et al.*, 2008; Luvsan *et al.*, 2012). High pollution levels are often a result of unfavorable meteorological conditions, which reduce the atmospheres ability to disperse and transport pollutants (Latini *et al.*, 2002; Xu *et al.*,

2011). Moreover, regional and local scale meteorology influences pollutants in different ways (Xu *et al.*, 2011).

NO_x and SO_2 are both to an extent easily influenced by meteorological conditions. Chio *et al.* (2013) found that primary pollutant concentrations are, in addition to regional meteorology, particularly dependent on emission rates from sources and land cover/use patterns. The majority of studies have found that primary pollutants are not significantly related to any particular meteorological parameter and they are typically insignificantly related to the combined action of all the meteorological factors in a particular area (For example: Cuhadaroglu and Demirci, 1997; Demirci and Cuhadaroglu, 2000; Latini *et al.*, 2002; Elminir, 2005; Turalioğlu *et al.*, 2005; Akpinar *et al.*, 2008; Giri *et al.*, 2008; Ilten and Selici, 2008; Lin *et al.*, 2008; Luvsan *et al.*, 2012).

The majority of studies have identified that primary pollutant concentrations are negatively correlated to wind speed, rainfall, temperature and solar radiation, and are positively correlated to relative humidity and atmospheric pressure (Cuhadaroglu and Demirci, 1997; Demirci and Cuhadaroglu, 2000; Latini *et al.*, 2002; Elminir, 2005; Turalioğlu *et al.*, 2005; Akpinar *et al.*, 2008; Giri *et al.*, 2008; Ilten and Selici, 2008; Laurinavičienė, 2008; Lin *et al.*, 2008; Luvsan *et al.*, 2012). Luvsan *et al.* (2012) used multiple regression analysis and found that 87.4% of daily SO_2 concentrations accumulated due to lower temperatures, lower wind speeds, lower precipitation, higher relative humidity, higher atmospheric pressure and lower levels of solar radiation. They also identified that these concentrations were dependent on the topographic and geographic setting of Ulaanbaatar, Mongolia. Turalioğlu *et al.* (2005) similarly found that high SO_2 concentrations are related to colder temperatures, lower wind speeds, high atmospheric pressure, lower precipitation and higher relative humidity in Erzurum, Turkey.

Lin *et al.* (2008) found that NO_x concentrations are negatively related to wind speeds and temperatures and are positively related to relative humidity in Beijing, China. In addition, Laurinavičienė (2008) found that NO_x are negatively related to wind speed and rainfall and are positively related to temperature in Kaunas city, Lithuania. Akpinar *et al.* (2008) found that primary pollutant concentrations had a moderate to weak relationship with the meteorological parameters that characterise Elaziğ city, Turkey and that along with the

source emission rates and topographic setting, the pollutant concentration patterns could be explained. Hence, it is evident that pollutant levels are dependent on meteorological parameters, but in addition to this they are influenced by source emissions, land use/cover and atmospheric lifetime (previous day concentrations) among other factors (Latini *et al.*, 2002; Turalioğlu *et al.*, 2005). As a result, there are no clear linear relationships between meteorology and pollutant concentrations (Xu *et al.*, 2011).

2.7. Meteorological controls on the levels of secondary pollutants, surface O_3

The chemical reactions responsible for secondary air pollutants depend on ambient air pollutants, thus there is ample evidence throughout the literature indicating surface O_3 not only relies on its precursor gases but also the meteorological conditions that prevail in the boundary layer (For example: Adul-Wahab and Bouhamra, 2002; Dueñas *et al.*, 2002; Elminir *et al.*, 2005; Pudasianee *et al.*, 2006; Tu *et al.*, 2007; David and Nair, 2011; Balashov *et al.*, 2014). To better understand the influence of surface O_3 on humans and the environment, studies have incorporated analyses of regional meteorological conditions and their relationship to surface O_3 to characterise the spatial and temporal distribution of surface O_3 (Elminir, 2005).

Considerable variations in meteorological conditions over diurnal and monthly scales can exert an impact on surface O_3 levels (Dueñas *et al.*, 2002; Elminir, 2005; Balashov *et al.*, 2014). Ambient air temperature is typically cited as one of the closest direct associates with surface O_3, but Flaum *et al.* (1996) identified that ambient air temperature alone cannot adequately explain the variation in surface O_3. Thus, consideration of the relationship between surface O_3 and multiple meteorological variables is more viable, as surface O_3 being a secondary pollutant is dependent on meteorology in complex ways (Flaum *et al.*, 1996; Thompson *et al.*, 2001; Dueñas *et al.*, 2002; Elminir, 2005; Balashov *et al.*, 2014). Hence, the meteorological conditions that are known to influence surface O_3 in the boundary layer are solar radiation, ambient air temperature, wind speed and direction, atmospheric pressure, humidity, cloud cover and precipitation (Dueñas *et al.*, 2002; Elminir, 2005; Tu *et al.*, 2007; Balashov *et al.*, 2014).

Surface O_3 has been found to show a clear trend with ambient air temperature in a number of locations, South Africa (Balashov *et al.*, 2014), India (David and Nair, 2011), Egypt (Elminir, 2005), Kuwait (Abdul-Wahab and Bouhamra, 2002), Spain (Dueñas *et al.*, 2002), USA (Rasmussen *et al.*, 2012) and China (Tu *et al.*, 2007). Typically a rise in ambient air temperature increases photochemical reaction rate gradually increasing surface O_3 concentration, therefore surface O_3 is positively related to ambient air temperature (Abdul-Wahab and Bouhamra, 2002; Dueñas *et al.*, 2002; Elminir, 2005; Tu *et al.*, 2007; Adame *et al.*, 2008; David and Nair, 2011; Rasmussen *et al.*, 2012; Balashov *et al.*, 2014).

Elampari and Chithambarathanu (2011) found that O_3 peaked when ambient air temperatures peaked for the day. Ambient air temperature is essentially a reflection of the amount of solar radiation received at the surface, which is a necessary component for the photochemical reactions forming surface O_3 (Balashov *et al.*, 2014). Solar radiation is positively correlated to surface O_3 (Dueñas *et al.*, 2002; Elminir, 2005; Elampari and Chithambarathanu, 2011). Interestingly, Abdul-Wahab and Al-Alwai (2002) found that temperature plays an important role on surface O_3 concentrations, while solar radiation had a lesser effect than expected.

Winds play a role in transporting O_3 and its precursor gases, controlling the spatial distribution of O_3 and its precursor gases (Abdul-Wahab and Bouhamra, 2002; Dueñas *et al.*, 2002; Elminir, 2005; David and Nair, 2011; Elampari and Chithambarathanu, 2011). Pollutants generally accumulate when wind speeds are not strong enough for dilution (Elminir, 2005). Most studies have identified that surface O_3 accumulates during calm, low wind speed conditions with a constant wind direction (Elminir, 2005; Balashov *et al.*, 2014). In contrast to this Abdul-Wahab and Bouhamra (2002), found that the average O_3 concentrations showed a progressively higher concentrations during stronger winds, than during calm winds. They concluded that this might be related to the fact that vertical transfer of air becomes active with the development of turbulence and mixing and this might have brought O_3 from the upper levels of the atmosphere, the stratosphere, down to the lower levels, the troposphere. The result of this was an increase in O_3 levels in addition to the photochemically produced O_3 at the surface. While Tu *et al.* (2007) found that average surface O_3 concentrations increased steadily with wind speeds from 1 – 4 $m.s^{-1}$ and

then dropped once wind speeds exceeded 4 $m.s^{-1}$, when stability in the boundary layer reduced.

Relative humidity is an indicator of the moisture content in the air (Dueñas *et al.*, 2002; Elminir, 2005; Tu *et al.*, 2007; Balashov *et al.*, 2014). The moisture content of air may easily alter the concentration of OH^- which resultantly promotes the growth or decay of surface O_3 (Dueñas *et al.*, 2002; Elminir, 2005; Tu *et al.*, 2007; Balashov *et al.*, 2014). Dueñas *et al.* (2002), found the highest average surface O_3 concentrations occur at a humidity less than or equal to 40%. High relative humidity may indicate wet and cloudy conditions which tends to remove surface O_3 and its precursor gases through wet deposition, and scattering and reflecting solar radiation thereby reducing photochemical processes (Dueñas *et al.*, 2002; Elminir, 2005; Elampari and Chithambarathanu, 2011; Balashov *et al.*, 2014).

Studies have indicated that surface O_3 is positively and significantly influenced by ambient air temperature and solar radiation, significantly and negatively influenced by relative humidity and negatively influenced by wind speed, wind direction and rainfall (For example: Dueñas *et al.*, 2002; Elminir, 2005; Elampari and Chithambarathanu, 2011; Balashov *et al.*, 2014).

2.8. Satellite observations for air quality modelling: relating satellite-derived measurements and ground-based measurements

The most direct way to obtain air quality measurements is from ground-level pollutant measurements, routinely collected from surface monitoring stations (Al-Saadi *et al.*, 2005). However, there are many gaps in surface monitoring networks (Al-Saadi *et al.*, 2005). Observations from satellites can help overcome the limitations associated with point surface monitoring by spatially enhancing the surface network (Al-Saadi *et al.*, 2005). Since 1995, instruments measuring trace gases, among others, O_3, PM's, NO, NO_2 and SO_2, in the troposphere and stratosphere have been put into orbit (Hoff and Christopher, 2009). Remote sensing of trace gases and aerosols has developed rapidly since the 1990's and MODIS in particular is one of the instruments that effectively provide derived measurements that can assist air quality modelling.

Advances in remote sensing has opened the way for measuring and modelling atmospheric pollution across continental and global scales (Edwards, 2006). A challenge for remote sensing missions is to directly assess local and regional scale air quality to provide important information for public health, policy development and application, etc. (Edwards, 2006). One such way that remote sensing has been used to aid air quality modelling is by relating satellite-derived measurements to ground-level measurements (Al-Saadi *et al.*, 2005; Edwards, 2006). Using satellite imagery to retrieve full atmospheric column measurements is a simple task. To get a measure of the ground-level concentration of trace gases and aerosols is a more complex task as a relationship between satellite-derived measurements and ground-level concentrations needs to be established. Many studies have opted to identify a simple linear relationship between satellite-derived measurements and ground-level concentrations, while more recent studies have incorporated meteorology and surface information (For example: Land use/cover, elevation etc.) to refine this relationship using, for example multiple regression modelling, Geographic weighted regression (GWR) and multivariate non-linear modelling (Table 2.4) (Hoff and Christopher, 2009).

Table 2.4: Some literature on the relationship of MODIS satellite imagery to trace gases and aerosols across the world. [a]Slope and Intercept converted. [m]Multiple regression.

Reference	Pollutant(s)	Sensor	Location	Number of ground monitors	Regression (linear or multiple)	R value
Chu *et al.*, 2003	PM_{10}	MODIS	Northern Italy	1	PM_{10} = 54.7 AOD + 8.0	0.82
Wang and Christopher, 2003[a]	$PM_{2.5}$	MODIS (Terra)	Jefferson Country, USA	7	$PM_{2.5}$ = 77.0 AOT – 0.23	0.67
		MODIS (Aqua)			$PM_{2.5}$ = 68.6 AOT + 1.93	0.76
		Average of MODIS Terra and Aqua			$PM_{2.5}$ = 72.3 AOT + 0.85	0.98
Engel-Cox *et al.*, 2004	$PM_{2.5}$	MODIS	USA	1338	$PM_{2.5}$ (Daily) = 18.66 AOD + 7.54	0.428
					$PM_{2.5}$ (Hourly) = 22.55 AOD + 7.5	0.4
Li *et al.*, 2005	PM_{10}	MODIS	Hong Kong, China	14	PM_{10} (1 km resolution AOD) = 327.87 AOD – 69.55	0.695
					PM_{10} (10 km resolution AOD) = 263.83 AOD – 24.93	0.419
Engel-Cox *et al.*, 2006	$PM_{2.5}$	MODIS	Baltimore, USA	4	$PM_{2.5}$ = 31.1 AOD + 5.2	0.65

Gupta *et al.*, 2006[a]	$PM_{2.5}$	MODIS	Hong Kong, China; Sydney, Australia; Switzerland, Europe; Delhi, India; New York, USA	5	$PM_{2.5}$ (Average) = 166.67 AOT – 24.83	0.96
Hutchinson *et al.*, 2006[a]	$PM_{2.5}$	MODIS	Texas, US	28	$PM_{2.5}$ (August) = 68.8 AOD – 39.9	0.47
					$PM_{2.5}$ (September) = 59.7 AOD – 17.2	0.98
Koelemeijer *et al.*, 2006	PM_{10}	MODIS	Europe	88	PM_{10} = 214 AOD – 42.3	0.58
van Donkelaar *et al.*, 2006[a]	$PM_{2.5}$	MODIS	USA and Canada	Not given	$PM_{2.5}$ = 1.22 AOD – 4.61	0.69
An *et al.*, 2007[a]	PM	MODIS	Beijing, China	6	$PM_{2.5}$ = 21.7 AOD + 6.1	0.92
					PM_{10} = 31.1 AOD + 5.1	0.92
Gupta and Christopher, 2008	$PM_{2.5}$	MODIS	Southeastern USA	38	$PM_{2.5}$ = 29.4 AOD + 8.8	0.62
					$PM_{2.5}$ = 27.5 AOD + 15.81	0.52
Schaap *et al.*, 2009	$PM_{2.5}$	MODIS	Cabauw, Netherlands	1	$PM_{2.5}$ = 120 AOD + 5.1	0.72
Zhang *et al.*, 2009	$PM_{2.5}$	MODIS	USA	521	$PM_{2.5}$ (Average) = 0.8113 AOD + 3.2672	0.90
Nicolantonio *et al.*, 2009[a]	$PM_{2.5}$	MODIS (Terra)	Northern Italy	25	$PM_{2.5}$ = 1.18 AOD – 1.71	0.68
		MODIS (Aqua)			$PM_{2.5}$ = 1.23 AOD – 1.79	0.59
Barnaba *et al.*, 2010[a]	PM_{10}	MODIS	Po Valley, Italy	3	PM_{10} = - 526.32 AOT + 131.58	0.18
van Donkelaar *et al.*, 2010[a]	$PM_{2.5}$	MODIS	USA	Not given	$PM_{2.5}$ = 0.93 AOD + 1.64	0.77
Lee *et al.*, 2011	$PM_{2.5}$	MODIS	Northeastern USA	26	$PM_{2.5}$ = 0.96 AOD + 0.44	0.97
Li *et al.*, 2011[a]	PM_{10}	MODIS	China and Northern Thailand	200	PM_{10} = 2.58 AOT – 166.85	0.62
Chen *et al.*, 2013	$PM_{2.5}$	MODIS	Northern Tien-Shan Central Asia	2	$PM_{2.5}$ = 58.3 AOD + 8.9	0.74
Hu *et al.*, 2014a[m]	$PM_{2.5}$	MAIAC	Southeastern USA	166	$PM_{2.5}$ = 13.75 +12.67 AOD – 0.65 Wind speed + 0.0003 Elevation + 0.0005 Major roads – 2.06 Forest cover + 0.01 Point emissions	0.91
Ma *et al.*, 2014	$PM_{2.5}$	MODIS	China	113	$PM_{2.5}$ = 0.61 AOD + 24.85	0.80
Xin *et al.*, 2014	$PM_{2.5}$	MODIS	Northern China	1	$PM_{2.5}$ (Average) = 89.72 AOD + 28.46	0.81
Chu *et al.*, 2015[a]	$PM_{2.5}$	MODIS	Baltimore Washington corridor, USA	1	$PM_{2.5}$ = 1.82 AOD – 15.96	0.75
Lin *et al.*, 2015[a]	$PM_{2.5}$	MODIS	China	565	$PM_{2.5}$ (Annual) = 1.23 AOD – 7.19	0.90
					$PM_{2.5}$ (Monthly) = 1.35 AOD – 18.35	0.76
Nguyen *et al.*, 2015[a]	$PM_{2.5}$	MODIS	Vietnam	274	$PM_{2.5}$ = 1.66 AOD – 15.73	0.76

Sinha *et al.*, 2015	$PM_{2.5}$	MODIS	Hyderabad, India	Not given	$PM_{2.5}$ (Average) = 30.913 AOD + 29.295	0.57

Relating trace gases and aerosols to satellite imagery for the purpose of modelling pollutants is still a discipline in its developing stages. Researchers have identified that satellite-derived measurements of Aerosol Optical Depth (AOD) and O_3, among others, are related to ground-level trace gas and aerosol concentration and can be empirically converted to give measurements of aerosol and trace gas concentrations (You *et al.*, 2015). A clear majority of studies have focused on $PM_{2.5}$ and PM_{10} in particular to develop models to estimate ground-level concentrations from satellite-derived AOD products (Table 2.4). No studies have focused on other trace gases and aerosols which this study has been based on.

Early exploration into this topic, Chu *et al.* (2003) found that MODIS aerosol retrievals provide useful information for global air pollution as a high correlation of 0.82 between PM_{10} and AOD for a single site in Northern Italy was identified. Wang and Christopher (2003) found a higher correlation of 0.98 between $PM_{2.5}$ and AOD across a number of sites in the US by using both Aqua and Terra daily data and concluded that MODIS Aerosol Optical Thickness (AOT) products may provide useful for air quality modelling across USA. Engel-Cox *et al.* (2004) examined the linear relationship between $PM_{2.5}$ and AOD across the entire USA and found a low correlation of 0.4 between them. They identified a better correlation in the eastern and Midwest portion of the country, while patchy data left them with poor correlations across the western parts of the country (Engel-Cox *et al.*, 2004). They concluded that the correlation was location dependent (Engel-Cox *et al.*, 2004).

Application of the 1-km MODIS AOD by Li *et al.* (2005) proved useful to characterise PM_{10} and evaluate the spatial variability of surface PM_{10} across Hong Kong, but it was noted that further improvements on the relationship are necessary to accurately monitor pollutants. Hutchinson *et al.* (2006) worked in Texas, USA and found that the relationship between $PM_{2.5}$ and MODIS AOD was time specific and during September the correlation (0.98) was stronger than during August (0.47). Gupta *et al.* (2006) measured the relationship of $PM_{2.5}$ to AOT at a number of locations across the world and concluded that derived AOT is a good proxy for monitoring PM air quality but a stronger relationship will come from the inclusion of meteorological parameters in the relationship. van Donkelaar *et al.* (2006) found a

significant, 0.69, relationship between AOD and $PM_{2.5}$ and concluded that satellite AOD measurements have the potential to provide a unique synopsis of ground-based $PM_{2.5}$ provided other information influencing $PM_{2.5}$ concentration is coupled into the relationship. Koelemeijer *et al.* (2006) found that using information about the boundary layer to develop a relationship between AOD and PM_{10} improved the significance of the relationship to 0.58 and further meteorological and land use information added to the relationship may improve the significance.

Across Beijing An *et al.* (2007) found that both $PM_{2.5}$ and PM_{10} are significantly relatable to AOD. Gupta and Christopher (2008) found that mean hourly $PM_{2.5}$ was more significantly related to AOD, with a correlation of 0.62, than $PM_{2.5}$ hourly, which had a correlation of 0.52, and concluded that the relationship strength may increase with addition of other factors, for example meteorology and land use, to the relationship. Gupta and Christopher (2009a and 2009b) looked at how to effectively monitor $PM_{2.5}$ to examine whether the use of meteorological parameters would improve the relationship of $PM_{2.5}$ and AOT. They found a 20 – 50 % improvement of the model RMSE when adding in temperature and boundary layer height to the relationship (Gupta and Christopher, 2009a; Gupta and Christopher, 2009b). They also found that multiple regression modelling with these meteorological parameters improved the R value of the model from 0.60 to 0.68 (Gupta and Christopher, 2009a; Gupta and Christopher, 2009b).

Schaap *et al.* (2009) explored the relationship between AOD and $PM_{2.5}$ at Cabauw, Netherlands and found an R value of 0.70 but further identified that the methodology used needs to be investigated to develop the use of satellite imagery for air pollution monitoring purposes. Zhang *et al.* (2009) measured the relationship of AOD to $PM_{2.5}$ across the USA and confirmed that this relationship was location specific as throughout the USA there were different correlations and across the southeastern part of the country this relationship was highest at 0.6 and an average relationship across the country was high at 0.9. Nicolantonio *et al.* (2009) worked in Northern Italy and found a significant correlation of 0.80 between $PM_{2.5}$ and AOD through the combined used of AOD, meteorological simulations and ground-level measurements on a monthly basis. The relationship incorporated assumptions about the influence of meteorology on $PM_{2.5}$, without incorporating actual meteorological data (Nicolantonio *et al.*, 2009).

Up until 2010 it was clear that further investigation into this relationship of satellite-derived measurements and pollutants was necessary. More work on incorporating meteorology and land use/cover was essential, but further investigation in different locations was necessary and more importantly an investigation into higher spatial resolution imagery and more than just AOD/AOT derived products relating to other trace gases and aerosols was necessary.

During and following 2010, more studies incorporated satellite-derived images and ground-level pollutant concentrations into their study. Studies also incorporated other factors known to influence pollutant concentrations to develop multiple regression relationships. van Donkelaar *et al.* (2010) used AOD measurements to estimate $PM_{2.5}$ concentrations across the USA for use in health impact studies and found a correlation of 0.77 between the two, but recommended that further investigation be done to incorporate other factors that influence pollutant concentrations. Using two years of ground-level PM_{10} data and satellite-derived AOD in the Po Mountain Valley, Barnaba *et al.* (2010) were not able to identify a strong relationship and attributed that to the absence of measurements of other factors influencing the concentration of PM_{10}. They also expressed that further investigation into this relationship was necessary to estimate the frequency of exceedance of pollutants (Barnaba *et al.*, 2010).

Lee *et al.* (2011) investigated a method to reduce the bias of only a few monitoring stations in epidemiological studies by incorporating satellite-derived AOD. They expressed the great potential remote sensing technologies have to expand on ground-based monitoring networks but identified the need for further study into this topic especially by incorporating meteorological and other parameters that influence ground-level pollutant concentrations (Lee *et al.*, 2011). Li *et al.* (2011) correlated AOT and PM_{10} and found that the correlation demonstrated substantial seasonal and regional difference, likely to be as a result of atmospheric conditions, particularly relative humidity, among other factors. They concluded that the inclusion of these factors into regression models may lead to more accurate assessment of PM_{10} from space borne observations (Li *et al.*, 2011). Emili *et al.* (2011) found that the correlation between PM_{10} and AOD is location specific and in flatter sites the accuracy of this relationship was higher than in alpine valleys and elevated sites. They concluded that satellite-derived PM_{10} maps are too inaccurate and more work on the relationship between the two is needed (Emili *et al.*, 2011).

Tsai *et al.* (2011) correlated $PM_{2.5}$ and AOD across Taiwan and found that addition of boundary layer heights in this relationship increased the R value from about 0.80 up to about 0.90 but validation of this relationship generated poor results. Chen *et al.* (2013) found that the linear regression results between $PM_{2.5}$ and AOD showed that $PM_{2.5}$ can be estimated from AOD measurements, but there is still need to improve this relationship as the validation results obtained were poor. Toth *et al.* (2014) investigated the relationship between $PM_{2.5}$ and AOD and concluded that for a stronger relationship, improvements in the spatial scale of satellite-derived MODIS 10 km^2 AOD are necessary. Xin *et al.* (2014) investigated the linear regression between AOD and $PM_{2.5}$ across Northern China and found a strong correlation of 0.76 for the full year but during each season the slope and intercept found were completely different from one another. Additionally, the validation results obtained were found to be poor (Xin *et al.*, 2014).

Ma *et al.* (2014) investigated the correlation between $PM_{2.5}$ and AOD in China and found a strong correlation of 0.78 with a strong cross validation result of 0.8, but the RMSE result was high resulting in a Mean predicted error (MPE) of 8.28 $\mu g/m^3$. Their results confirmed the need for satellite-derived AOD to be used in conjunction with land use and meteorological parameters for correlation with $PM_{2.5}$ (Ma *et al.*, 2014). Hu *et al.* (2014a) identified that the coarse resolution of satellite-derived AOD makes it difficult to estimate $PM_{2.5}$. To better test this relationship they incorporated Multi-angle implementation of atmospheric correction (MAIAC) 1km^2 satellite-derived AOD, meteorological and land use parameters and found a strong correlation for 2003 using multiple regression analysis (Hu *et al.*, 2014a). They were less concerned with the correlation results and more so with the validation results which was high at 0.91 with a high prediction error of 2.73 $\mu g/m^3$ (Hu *et al.*, 2014a). They concluded that the higher spatial resolution satellite imagery improved their correlation as local pollution episodes were easily identifiable (Hu *et al.*, 2014a).

Most monitoring stations are situated in urban areas, Hu *et al.* 2014b concluded that the relationship between satellite-derived AOD, $PM_{2.5}$, meteorological and land use parameters can reduce the bias introduced from the position of monitoring stations. They found a strong correlation of 0.85, a MPE of 1.73 $\mu g/m^3$ and a validation of 0.88 for the 10 year analysis (Hu *et al.*, 2014b). Soutoudeheian and Arhami (2014) found that multiple regression models outperformed the linear regression models incorporating land use and

meteorological parameters over Tehran, Iran. Overall they found that the models did not completely reflect the spatial variation of PM_{10} and that further investigation using other statistical models is necessary (Soutoudeheian and Arhami, 2014).

Chu *et al.* (2015) acknowledged the relationship between AOD and $PM_{2.5}$ but their validation results were poor and this was attributed to the coarse resolution satellite imagery, and the lack of land use/cover and meteorological parameters known to influence ground $PM_{2.5}$ concentrations. Lin *et al.* (2015) found a good agreement between satellite-derived AOD and $PM_{2.5}$ across China. They found the linear regression method to be well applicable as a simulation based method would bring in many model uncertainties when predicting $PM_{2.5}$ (Lin *et al.*, 2015). Their result suggest that this approach may effectively estimate $PM_{2.5}$ concentrations but the relationship needs further investigation as the results were poor. Nguyen *et al.* (2015) results highlighted the potential use of MODIS AOD at a regional scale across Vietnam. However, the coarse resolution of the 10 km^2 AOD and the model limitation in over/under estimating maximum and/or minimum $PM_{2.5}$ concentrations needs further investigation by incorporating higher spatial resolution satellite imagery, atmospheric conditions and physical aspects known to influence ground-level $PM_{2.5}$ concentrations.

Sinha *et al.* (2015) found, during their investigation of ground-level $PM_{2.5}$ along with meteorological parameters and satellite-derived AOD, that changes in local emissions and boundary layer dynamics are major concerns in the accurate estimation of $PM_{2.5}$ from MODIS AOD, while the uneven spatial distribution of $PM_{2.5}$ in the urban environment made estimating $PM_{2.5}$ using the correlation of meteorology, ground-level $PM_{2.5}$ and AOD a considerable challenge across Hyderabad, India. You *et al.* (2015) found a low correlation between $PM_{2.5}$ and AOD. Later correlations using meteorological and land use parameters yielded better results improving model performance to 0.88 (You *et al.*, 2015). They concluded that these results and the results from all studies incorporating meteorology and land use parameters may be useful to develop models incorporating satellite-derived measurements for the purpose of estimating local and regional trace gas and aerosol concentrations (You *et al.*, 2015).

It is still clear that further investigation into the relationship between satellite-derived measurements and ground-level pollutant concentrations is necessary. More work on

incorporating meteorology and land use parameters has been done but still not enough work has been done as results are still poor and other aerosols and trace gases besides PM have rarely been investigated. Other trace gases and aerosols need to be considered and other parts of the world, especially South Africa – the focus area of this study, need to be studied. The resolution of satellite-derived AOD and other satellite-derived products needs to be improved as pollution episodes may be smaller than the current resolution of imagery. Other satellite-derived products have been developed, for example satellite-derived ozone, and their usefulness needs to be investigated further.

Few studies have used MODIS AOD to identify a relationship with pollutants besides $PM_{10/2.5}$. An *et al.* (2007) found that SO_2 concentrations were relatable to AOD with a significant relationship of 0.7 across Beijing. Lamasal *et al.* (2008) used Ozone mapping instrument (OMI) to infer ground-level NO_2 concentrations for part of the study across the USA. They found a relationship of 0.67 between OMI and ground-level NO_2 concentrations and concluded that the temporal and spatial correlation between OMI derived and ground-level NO_2 was even higher than previously found for $PM_{2.5}$ over North America (Lamasal *et al.*, 2008). Fishman *et al.* (2010) investigated the relationship of Total ozone mapping spectrometer derived measurements and surface O_3 across Midwest USA and found this relationship to be significant at 0.75 and that satellite data may be useful to assess the impact of surface O_3 on crop yields. Before the relationship may be utilised fully, other factors influencing surface O_3 concentration are to be included in the investigation of this relationship (Fishman *et al.*, 2010). Focusing on other traces gases and aerosols will be beneficial for future study on the relationship of satellite-derived measurements and concentrations of air pollutants. Additionally, this discipline will benefit from higher spatial resolution satellite imagery to pick up on local scale pollution events.

2.9. Ambient air quality guidelines for SO_2, NO_x and Surface O_3 and the associated health risks if these guidelines are exceeded

To protect the public health of South African citizens particular air quality standards have been set by the South African government (DEA, 2009). Air quality standards are fundamental to effective air quality management and exceedances of these standards indicate potential health risks and impacts (DEA, 2011; CSIR, 2012). By comparing monitored

ambient air quality data against air quality standards the exposure to pollution may be captured (CSIR, 2012). When these standards are exceeded in populated areas, the risks to human health may be significant (DEA, 2011). Hence, it is important to monitor the frequency of exceedance of the air standards using legislation guidelines.

Previously ambient air pollution across South Africa was controlled by the Air Pollution Prevention Act (No. 45 of 1965) which regulated the release of harmful gases primarily from industrial sources. More recently the NEMAQA (No. 39 of 2004) has been implemented.

Through the implementation of the NEMAQA, National Ambient Air Quality Standards (NAAQS) have been developed specifically for South Africa (Table 2.5). As a result, the Department of Environmental Affairs and municipalities have key responsibilities to ensure the development and implementation of air quality management policies, local guidelines and standards of emissions and ambient concentrations, air quality database, licensing provisions, public awareness campaigns and a framework to enforce legal compliance (DEA, 2004). These responsibilities are necessary to ensure effective air quality management (DEA, 2009).

Table 2.5: Ambient AQG's for SO_2, NO_2 and O_3 (Australian Government, 2002; WHO, 2005; DEA, 2009; European Commission, 2015; EPA, 2016).

Pollutant	**South African National Ambient Air Quality Standards (µg/m³)**	**World Health Organisation Air Quality Guidelines (µg/m³)**	**United States Environmental Protection Agency National Air Quality Standards**	**Australian National Environmental Protection Council National Ambient Air Quality Standards (ppm)**	**European Commission Air Quality Standards (µg/m³)**
SO_2	500 (191 ppb) (10-minutes mean)	20 (8 ppb) (24-hour mean)	75 ppb (1-hour mean)	0.20 (1-hour mean)	350 (1-hour mean)
	350 (134 ppb) (1-hour mean)			0.08 (1-day mean)	
	125 (48 ppb) (24-hour mean)	500 (191 ppb) (10-minute mean)	0.5 ppm (3-hour mean)	0.02 (1-year mean)	125 (24-hour mean)
	50 (19 ppb) (annual mean)				
NO_2	200 (106 ppb) (1-hour mean)	200 (106 ppb) (1-hour mean)	100 ppb (1-hour mean)	0.12 (1-hour mean)	200 (1-hour mean)
	40 (21 ppb)	40 (21 ppb)	53 ppb (annual	0.03 (1-yar mean)	40 (1-year

	(annual mean)	(annual mean)	mean)		mean)
O_3	120 (61 ppb) (8-hour mean)	100 (50 ppb) (8-hour mean)	0.070 ppm (8-hour mean)	0.10 (1-hour mean)	120 (8-hour mean)
				0.08 (4-hour man)	

Ambient Air Quality Standards (AQS) are designed as a guideline to protect public health and to reduce the impact of air pollution (Colls, 1997; WHO, 2005). Each standard is an exposure level over a specific time period and is based on an extensive body of scientific evidence relating to air pollution and its health consequences (WHO, 2005; Vallero, 2008). The ambient AQS provides the acceptable maximum concentration of criteria air pollutants in the atmosphere without threatening human health. These guidelines cannot fully protect human health, especially for sensitive individuals who may experience potential health issues at levels below these guidelines (Colls, 1997; WHO, 2005; Vallero, 2008). Each standard describes the concentrations of pollutants that cannot be legally exceeded during a specific time period within an area, hence they need to be complied with (Vallero, 2008; DEA, 2009). In South Africa, source specific control measures have been developed and put in place for a number of sources, mainly industrial sources, to maintain that the AQS's are not exceeded to allow for effective air quality management across the country (DEA, 2011).

Setting AQS is fundamental for effective air quality management (DEA, 2009; WHO, 2005). Ambient air quality guidelines are regulated throughout most of the world (Table 2.5). Although the guidelines have gaps and uncertainties, they offer a strong foundation for the recommended guidelines and they are constantly being worked on to improve the information base of these guidelines (WHO, 2005). The WHO guidelines, in particular, provide scientific guidance on setting AQS for all countries (WHO, 2005). National standards are generally based on a particular approach adopted for balancing health risks, technological feasibility, economic considerations and various other political and social factors, which in turn will depend on among other things the level of development and national capability in air quality management (WHO, 2005).

Unfortunately South Africa is limited by human, financial and technological resources. Thus, a priority area approach was adopted to focus available resources in areas that are considered to have very poor air quality and are in need of immediate attention. In keeping

with the requirements of NEMAQA, the HPA has been developed and is in the process of implementing the AQMP for the Highveld (DEA, 2011).

These three pollutants may be associated with adverse health effects as mentioned earlier on and as listed in Table 2.6. Inhalation or absorption of SO_2, NO_x and Surface O_3 may generally exacerbate pre-existing disease states in Table 2.6 (Vallero, 2008). In particular, O_3 is associated with damage to crops and vegetation and potential adverse health effects, while NO_x and SO_2 may have potential longer-term human health effects (Lourens *et al.*, 2011). Furthermore, these adverse health effects will most likely occur when the pollutant concentrations reach/exceed the ambient AQG's in Table 2.5. Moreover, the effects of air pollution are assumed to be greater in developing countries, such as South Africa, than in developed countries due to difference in the levels of exposure and co-exposure to a mixture of pollutants, the population structure, nutritional status, lifestyle and socioeconomic status (Romieu and Herndandez-Avila, 2002).

Table 2.6: Some of the adverse human health effects associated with SO_2, NO_x and Surface O_3 (Vallero, 2008).

Pollutant	**Associated adverse human health effects**
SO_2	Respiratory (bronchial inflammation, bronchitis, lung edema) Irritant (eyes, nose, throat, respiratory tract) Increasing chance of asthma
NO_x	Rapid death (at extremely high concentrations) Respiratory (bronchial inflammation, bronchitis) Irritant (nose, throat) Haematological (impairs normal blood transport)
Surface O_3	Respiratory (severe pulmonary edema, bronchial inflammation) Irritant (eyes, throat, chest – asthma and discomfort, respiratory tract) Fatigue, lack of coordination Headache Haematological (decrease in blood pressure, weakens pulse)

Ambient air quality modelling forms an important part of the monitoring plan for the HPA. A well-developed air quality monitoring network which is built up by a number of aspects, for example ground-based monitoring stations and satellite imagery among others, helps the HPA work towards achieving the air quality management objectives set out by the HPA air

quality management plan by allowing the government to identify temporal and spatial trends in air pollution which is essential for effective air quality management (DEA, 2011).

2.10. Synthesis of the literature review

Typically SO_2 and NO_x concentrations peak during winter, while surface O_3 peaks during spring. On a smaller spatial scale site specificity often occurs, for example SO_2 concentrations may exhibit one of two diurnal variations related generally to meteorology and source characteristics. Meteorology in particular is a factor that governs pollutant concentrations over annual to diurnal time scales and over numerous spatial scales. Moreover, meteorology and anthropogenic influences play a particularly important role in the formation, transport and destruction of pollutants.

Modelling pollutant concentrations for the purpose of concentration estimation is a complex task which relies heavily on the factors that influence pollutant concentrations. Satellite imagery has made it possible to view pollutants over numerous spatial scales and as a result satellite-derived measurements are invaluable pieces of data for these models. Spatio-temporal statistical pollutant estimation models are site specific and for this reason models need to be speicified to an area by considering the factors that influence pollutants concentrations in that specific area. In order to develop this relationship for adequate ground-level measurements of pollutants, meteorology, land use/cover and satellite imagery on spatial scales comparable to local scale pollution are necessary. Such a model would become useful for civil society and therefore complex statistical models should be avoided. Simple statistical models, for example GWR and multiple regression etc., will benefit society and aid in improving air quality and essentially human and environmental health. Furthermore, with studies of spatial modeling for estimation of pollutant concentrations using statistical models to estimate pollutants being absent in South Africa, this study should further contribute to the knowledge gap and possibly promote future studies of this kind across the country.

Chapter 3: Study site

(Eskom, 2017a)

This study primarily focuses on the Highveld to investigate air pollution. Air pollution has for long now been recognised as a major issue for the Highveld (Balashov *et al.*, 2014). The Highveld is South Africa's most populated area and the largest industrial hub with over 75% of the country's industrial infrastructure (Freiman and Piketh, 2002; Balashov *et al.*, 2014). As a result the Highveld accounts for the majority of South Africa's ambient air pollutants (Freiman and Piketh, 2002). Understanding the nature of gaseous air pollutants across the Highveld is essential to an understanding of air pollution over South Africa. Therefore, it is important that this study takes place within Highveld and in particular within the HPA.

3.1. Basic geography of the Highveld

The Free State, Mpumalanga and Gauteng provinces of South Africa make up the Highveld area. The Highveld area occupies 25° - 27°S and 28° - 30°E (Frieman and Piketh, 2002; Esau *et al.*, 2012). This area is a high lying plateau about 1700 meters above sea level with an approximate area of 300 000 km^2 (Tyson *et al.*, 1988; Frieman and Piketh, 2002; Esau *et al.*, 2012; Balashov *et al.*, 2014). The Highveld is a plateau which is generally flat with some surface undulation (Esau *et al.*, 2012). The Highveld landscape has been modified by urbanisation, industrialisation, mining, forestry and agriculture and as a result little natural grassland remains (Tyson *et al.*, 1988; DEA, 2011; Esau *et al.*, 2012; Balashov *et al.*, 2014).

3.2. Basic climatology of the Highveld

The Highveld is at a high altitude and as a result its climate is generally cooler than other places at similar latitudes (Esau *et al.*, 2012). South Africa resides at the descending limb of the Hadley cell (Frieman and Piketh, 2002; Esau *et al.*, 2012). Consequently, the Highveld area experiences general anti-cyclonic conditions promoting clear skies and an average air pressure of about 800 hPa throughout the year (Tyson *et al.*, 1988; Frieman and Piketh, 2002; Esau *et al.*, 2012). Winds over the Highveld are generally variable (Esau *et al.*, 2012).

Winters (June to August) are generally dry and mild with average day time temperatures of about 15 – 19 °C, but at night temperatures can drop below freezing (Tyson *et al.*, 1988; Esau *et al.*, 2012). During winter, surface inversions that last from the evening till just before sunrise are common as a result of stable and clear conditions (Tyson *et al.*, 1988; Esau *et al.*,

2012). Winter precipitation is uncommon, but vertical uplift from the development of cold fronts may bring about winter precipitation (Esau *et al.*, 2012).

During summer (December to February) the average day time temperatures are high ranging from 25 – 32 °C (Tyson *et al.*, 1988; Esau *et al.*, 2012). Solar radiation absorption at the surface facilitates the development of unstable low pressure troughs which promotes precipitation (Tyson *et al.*, 1988; Esau *et al.*, 2012). Precipitation over the Highveld ranges from 600 to 800mm per annum and mainly occurs during the summer time (Esau *et al.*, 2012). During summer surface inversion layers are less common (Esau *et al.*, 2012).

Hence, the Highveld has high atmospheric stability, clear skies, low winds speeds and persistent temperature inversions which are highly adverse climatic conditions for the dispersion of atmospheric pollutants (Tyson *et al.*, 1988). Moist unstable conditions during the summer period offer for the dispersion and deposition of atmospheric pollutants, whereas during winter dry and stable conditions promote the accumulation of atmospheric pollutants (Tyson *et al.*, 1988).

3.3. The HPA

This area covers about 31 106 km^2 in parts of the Mpumalanga and Gauteng provinces (Figure 3.1) (DEA, 2011). It consists of the Ekurhuleni, Lesedi, Dipaleseng, Delmas, Goven Mbeki, Emalahleni, Steve Tshwete, Lekwa, Muskaligwa and Pixley ka Seme local municipalities (DEA, 2011).

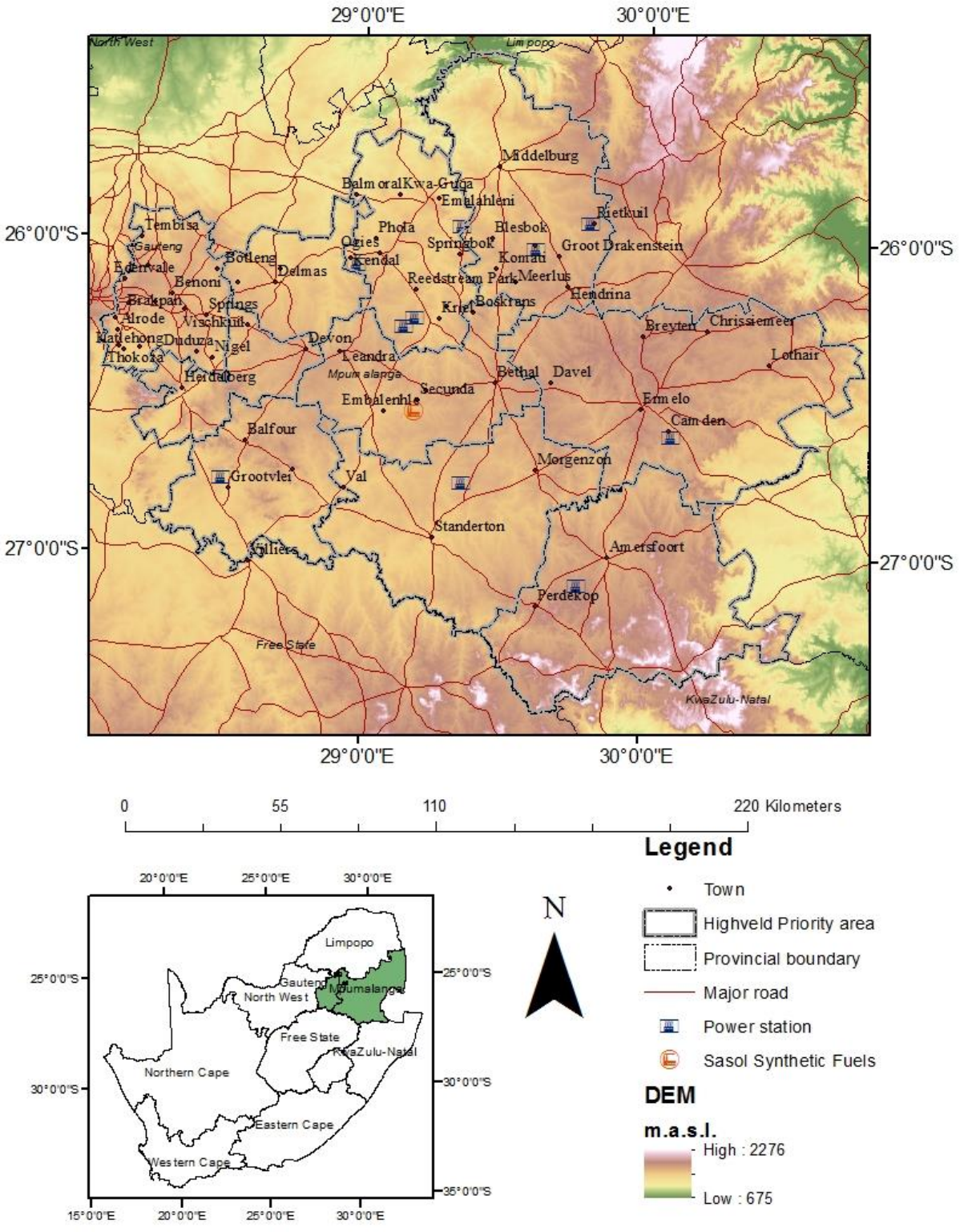

Figure 3.1: Map of the study area including elevation, major towns, roads and some major pollution sources using a SRTM DEM and NGI topographic layers (Author: S Roffe).

The HPA is known for its diverse range of anthropogenic activities, which promote elevated levels of pollutants, namely agriculture, coal-fired power generation, industry, mining, coal dumps, transportation (namely air and motor vehicle transportation), clay brick manufacturing, waste treatment and disposal, household activities (For example: fuel burning) and petrochemical operations (Figure 3.2) (Tyson *et al.*, 1988; Lourens *et al.*, 2011; DEA, 2011; Balashov *et al.*, 2014). As a result the HPA is an air pollution 'hotspot' area that accounts for over 90% of the country's emissions of gaseous air pollutants (Collett *et al.*, 2010).

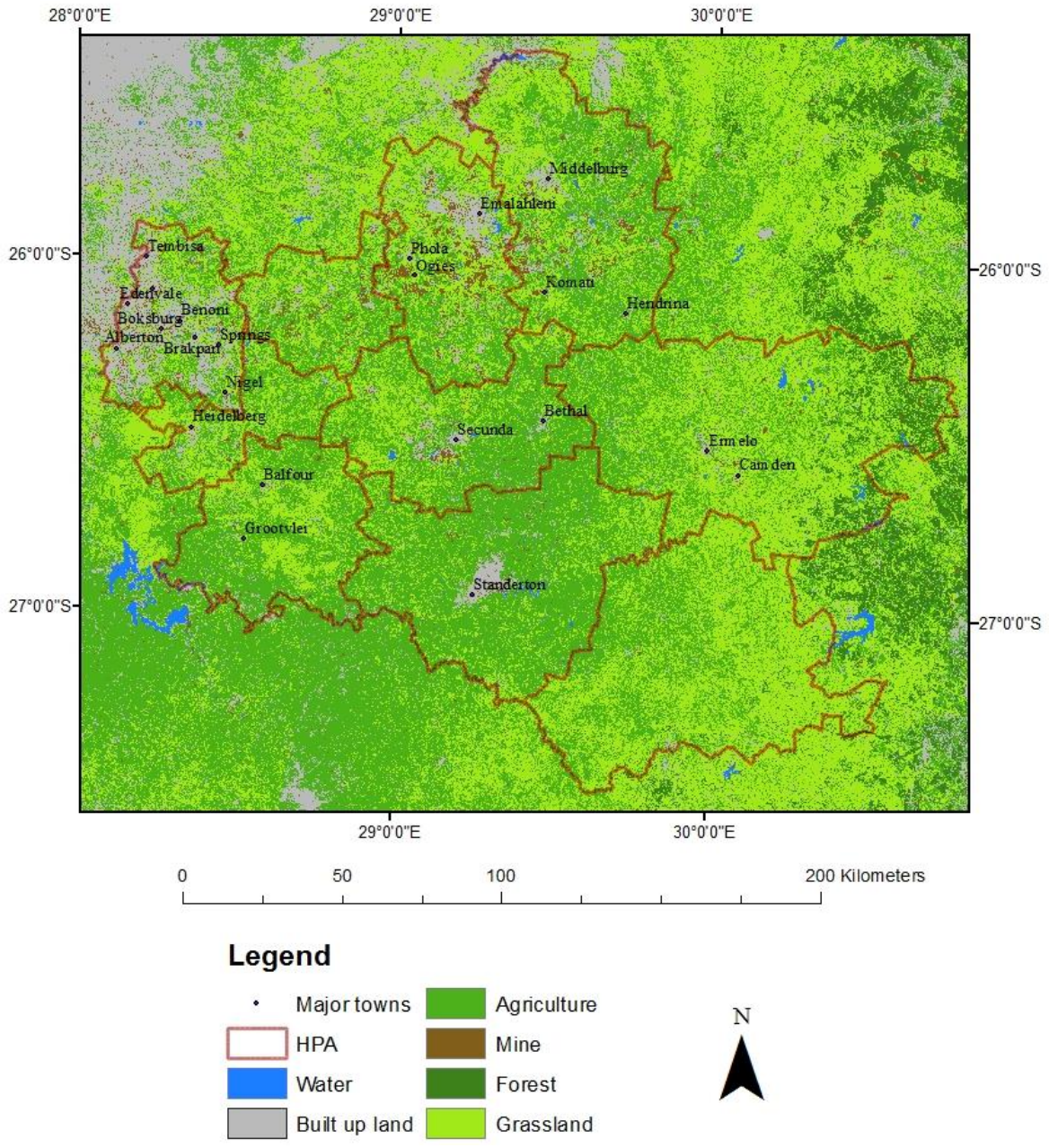

Figure 3.2: Land use/cover across the HPA (Author: S Roffe).

3.4. Population distribution across the HPA

This HPA houses about 3.6 million individuals (Figure 3.3) (DEA, 2011; Lourens *et al.*, 2011). Gauteng houses the bulk of individuals and within Gauteng Ekurhuleni hosts the majority persons. Within Mpumalanga Lesedi, Goven Mbeki and Emalahleni have the greatest population densities.

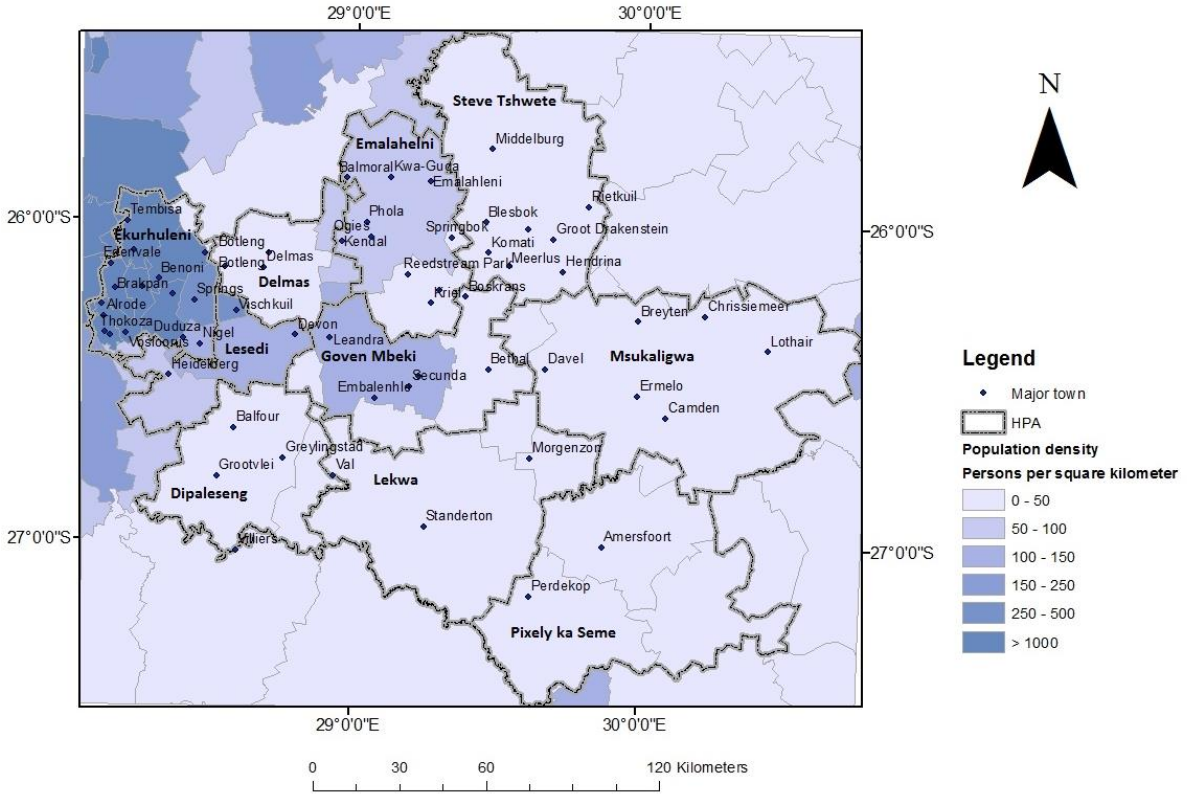

Figure 3.3: Population distribution across the HPA using 2011 census figures (Author: S Roffe).

Chapter 4: Data and Methodology

(Outdoorphoto, 2007)

4.1. Data

Three main sources of data have been used in this study. These are: pollutant concentrations, meteorological parameters and MODIS atmosphere products.

4.1.1. Pollutant concentrations

Pollution monitoring relies heavily on networks of ground-level monitors measuring ambient air pollutant concentrations within the boundary layer (Emili *et al.*, 2011). The pollutants of interest for this study were SO_2, NO_x and surface O_3. These are criteria air pollutants commonly found over the HPA with known human and environmental health implications (Lourens *et al.*, 2011).

Ground-based measurements are the representative data for pollutants with the boundary layer (Alston *et al.*, 2012). This study is concerned with pollutants within this layer, as in this layer pollutants directly influence human and environmental health. The SAAQIS network of monitoring stations provides measurements of pollutant concentrations within the boundary over numerous temporal scales. Across the HPA there are 24 monitoring stations situated within areas of high population density. The SAWS was contacted in order to obtain measurements from these monitoring stations.

Twenty four datasets, for the period of 2010 to 2015, were provided. For a station to have been included in this study, a full dataset was required. A full dataset is one with at least one full week of readings for each month throughout a year. As a result, many stations had to be excluded from this study due to missing data. Only one full year of data was deemed necessary for this study, as there was a limited amount of full datasets.

For SO_2, in 2010 only 5 full datasets were present, while there was 13 for 2011, 10 for 2012, and 6 for 2013, 2014 and 2015. For NO_x, in 2010 only 6 full datasets were present, while there were 8 in 2011, 8 for 2012, 4 for 2013 and 5 for 2014 and 2015. For surface O_3, in 2010 only 6 full datasets were present, while there was 9 for 2011, 8 for 2012, 7 for 2013 and 2014, and 5 for 2015. With the lack of full datasets, only 2011 was selected for this study on the basis of there being the majority of data available. No temporal interpolation was performed on this data.

Only monitoring stations with data for each month during 2011 for the HPA have been used (Table 4.1). Data regarding the concentrations of SO_2, NO_x and surface O_3 were at hourly intervals in *Microsoft excel* spreadsheets. Each monitoring station continuously samples, and therefore each hourly measurement obtained is the concentration in *ppb* measured at that particular time and not an hourly average. Additionally, each monitoring station has detection limits, representing the lowest measurable concentration of pollutants (DNP, 2012). The detection limits are: <0.4 ppb for SO_2, <0.4 ppb for NO_x and <1 ppb for surface O_3 (DNP, 2012). Figure 4.1 shows the spatial distribution of the monitoring stations throughout the study area.

Table 4.1: Details of the monitoring stations.

Station	**Pollutant(s)**	**Longitude**	**Latitude**	**Site classification (emissions measured)**	**Altitude (m.a.s.l.)**
Balfour	SO_2, NO_x and surface O_3	28.59	-26.66	Residential (domestic fuel burning) and industrial	1572
Camden	SO_2, NO_x and surface O_3	30.11	-26.62	Industrial (power generation and mining)	1637
Elandsfontein	SO_2, surface O_3	29.42	-26.25	Rural (agriculture) and Industrial (power generation, mining and petro chemical)	1746
Ermelo	SO_2, surface O_3	29.97	-26.49	Residential (domestic fuel burning) and industrial (coal transportation and power generation)	1767
Grootvlei	SO_2, NO_x and surface O_3	28.48	-26.77	Industrial (petro chemical and power generation)	1517
Hendrina	SO_2, NO_x and surface O_3	29.73	-26.13	Residential (domestic fuel burning) and industrial	1768
Komati	SO_2	29.45	-26.1	Rural and industrial (power generation)	1620
Leandra	SO_2 and NO_x	28.48	-26.37	Rural (farming) and industrial (power generation, petro chemical and mining)	1687
Middleburg	SO_2 and NO_x	29.46	-25.8	Residential (domestic fuel burning) and industrial (mining)	1508
Phola	SO_2 and NO_x	29.04	-26	Rural (farming) and industrial (power generation, petro chemical and	1534

				mining)	
Secunda	SO_2, surface O_3	29.08	-26.55	Industrial (petro chemical) and residential (domestic fuel burning)	1620
Standerton	surface O_3	29.22	-26.97	Residential (domestic fuel bringing)	1569
Wattville	SO_2	28.3	-26.23	Residential and industrial	1650
Witbank	SO_2, NO_x and surface O_3	29.19	-25.88	Residential (domestic fuel burning and transportation) and industrial (mining)	1600

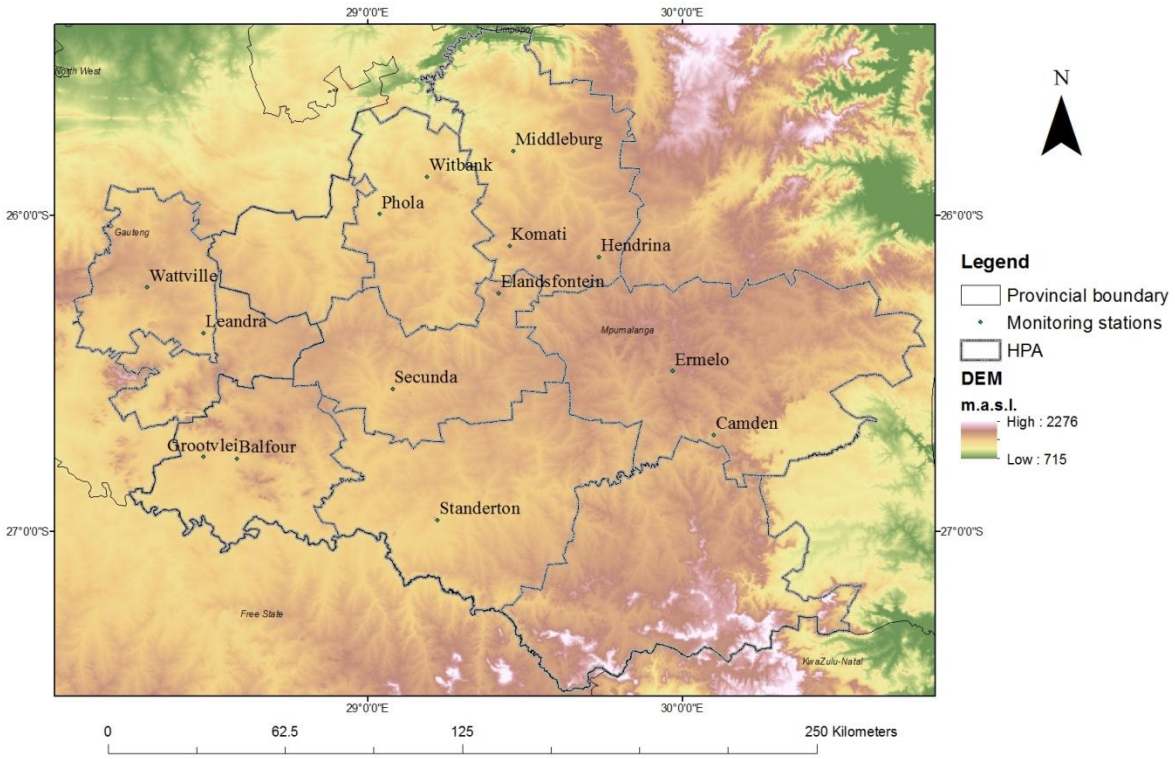

Figure 4.1: Location of the monitoring stations in the study area (Author: S. Roffe).

4.1.2. Meteorological parameters

To monitor pollutants an understanding of their behaviour is essential (Dueñas *et al.*, 2002). Hence, an understanding of the meteorological conditions that govern their behaviour is necessary (Dueñas *et al.*, 2002). SO_2 and NO_x are primary pollutants and are influenced by meteorology, for their transportation and destruction, as soon as they are emitted from sources (Elminir, 2005). Surface O_3 as a secondary pollutant is reliant on meteorology during its formation, transportation and destruction processes (Dueñas *et al.*, 2002; Elmini, 2005; Balashov *et al.*, 2014).

Most monitoring stations from the SAAQIS network have co-located meteorological monitoring stations. The meteorological data collected by these stations was used for this study (Table 4.2). Only stations with a full year of data were used. Ten monitoring stations had full year datasets for 2011. No stations had atmospheric pressure measurements. Atmospheric pressure plays an important role in the behavior of pollutants (Vallero, 2008). Consequently, additional stand-alone meteorological data for the HPA was obtained from the SAWS. Two extra stations were provided (Table 4.2). Twelve meteorological stations to describe the regional meteorological conditions for the HPA were used (Figure 4.2; Table 4.2).

Both sets of datasets were obtained as *Microsoft excel spreadsheets*. Data from the 10 meteorological stations was continuously collected data at hourly intervals. The following meteorological variables were obtained from these stations: relative humidity (%); ambient air temperature (°C); solar radiation ($W.m^{-2}$), rainfall (mm), wind speed ($m.s^{-1}$) and wind direction (°). Data from the two stand-alone meteorological stations were daily averages. The following meteorological variables were obtained: atmospheric pressure (hPa) and rainfall (mm). Table 4.3 shows the meteorological parameters measured by each monitoring station. No temporal interpolation was performed.

Table 4.2: Details for the meteorological monitoring stations.

Station	Latitude	Longitude	Altitude (m.a.s.l.)	Stand-alone/co-located
Balfour	28.586	-26.663	1572	Co-located
Camden	30.106	-26.6226	1637	Co-located
Elandsfontein	29.417522	-26.245517	1746	Co-located
Ermelo_1	29.969002	-26.49348	1767	Co-located
Ermelo_2	29.983	-26.497	1774	Stand-alone
Grootvlei	28.48	-26.7647	1517	Co-located
Komati	29.4507	-26.097	1620	Co-located
Leandra	28.480089	-26.372	1687	Co-located
Middleburg	29.4636	-25.796061	1508	Co-located
Phola	29.038164	-25.99567	1534	Co-located
Secunda	-26.497	29.186	1657	Stand-alone
Standerton	29.2228	-26.965	1569	Co-located

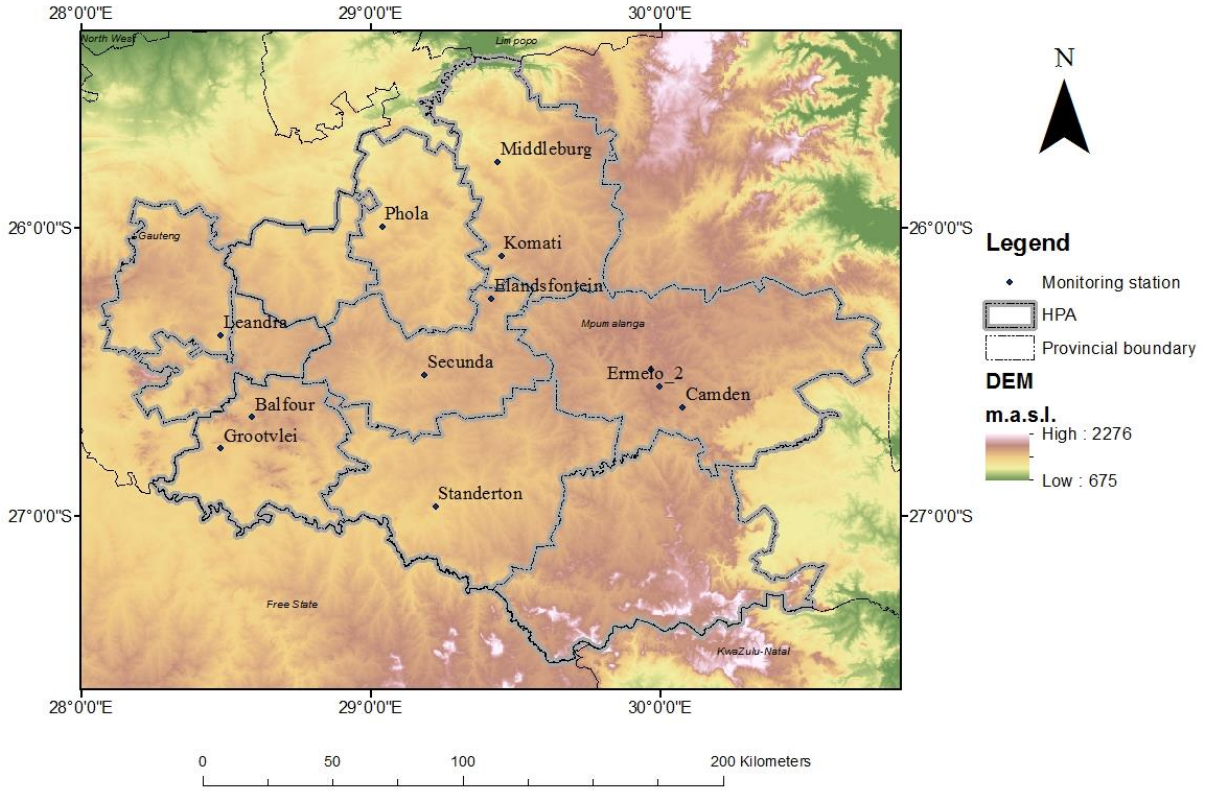

Figure 4.2: Meteorological monitoring stations in the study area (Author: S Roffe).

Table 4.3: Details of the meteorological variables for each monitoring station.

	Meteorological variable						
Station	Temperature (°C)	Solar radiation ($W.m^{-2}$)	Relative humidity (%)	Wind speed ($m.s^{-1}$)	Wind direction (°)	Rainfall (mm)	Atmospheric pressure (hPa)
Balfour	Yes	No	Yes	Yes	Yes	Yes	No
Camden	Yes	No	Yes	Yes	Yes	Yes	No
Elandsfontein	Yes	No	No	Yes	Yes	Yes	No
Ermelo_1	Yes	Yes	Yes	No	No	No	No
Ermelo_2	No	No	No	No	No	Yes	Yes
Grootvlei	Yes	No	No	Yes	Yes	No	No
Komati	Yes	No	Yes	Yes	Yes	No	No
Leandra	Yes	Yes	Yes	Yes	Yes	Yes	No
Middleburg	Yes	Yes	Yes	No	No	No	No
Phola	Yes	No	No	Yes	Yes	No	No
Secunda	No	No	No	No	No	Yes	Yes
Standerton	Yes	No	Yes	Yes	Yes	Yes	No

4.1.3. MODIS data

Satellite imagery has a large spatial and a good temporal coverage of landscapes (Prasad and Singh, 2007). Satellite remote sensing of air pollutants in the boundary layer has evolved dramatically. Satellite observations successfully provide estimates of trace gases and aerosols in regions where ground-level measurements are unavailable. Satellite observations are available for a range of pollutant aerosol and trace gas species (Martin, 2008). Passive sampling satellites flying in near-polar, sun-synchronous, low Earth orbits with an altitude of 705 km will yield information on lower tropospheric constituents (Martin, 2008).

The MODIS instrument, on board the Terra (launched 18 December 1999) and Aqua (launched 4 May 2002) platforms is a passive sampler at an altitude of 705 km with a near polar, sun-synchronous, low Earth orbit, is uniquely designed with a wide spectral range (0.4 to 14.4 $\mu g/m^3$) of 36 band channels which provide an abundance of information of atmospheric, terrestrial and oceanic phenomenon (Seeman *et al.*, 2006; Martin, 2008; NASA, 2016). MODIS has a wide viewing swath of 2330 km (cross track) by 10 km (along track at nadir) with a 55° scanning pattern (NASA, 2016). It provides a wide spectral coverage of the visible, near infrared and infrared regions of the electromagnetic spectrum, thus providing a large amount of information on phenomena (Seeman *et al.*, 2006; NASA, 2016). It provides a medium spatial resolution of 250 – 1000 m, where band channels 1 – 2 are at 250 m, band channels 3 – 7 are at 500 m and band channels 8 – 36 are at 1000 m (Seeman *et al.*, 2006; NASA, 2016). It provides a near daily global coverage across most of the world and two equator crossings per day at 10:30 AM in a descending direction (Terra) and at 13:30 PM in an ascending direction (Aqua) (Martin, 2008; NASA, 2016). The near-daily coverage, wide spectral range and medium spatial resolution MODIS provides, enables it to observe the Earth's atmosphere to continuously monitor change (Seeman *et al.*, 2006). Hence, the MODIS instrument can provide information on the evolution and extent of air pollution, addressing air quality on a daily basis.

The MODIS instrument has a full set of on-board calibrators to provide radiometric, spectral and spatial calibration to aid in offering an unprecedented look at phenomena (NASA, 2016). This means that the Terra and Aqua instruments have a stable spectral and spatial

performance and no pre-processing for radiometric and geometric corrections will be necessary (NASA, 2016).

MODIS has 3 levels of data (NASA, 2016). Level 1 products are daily scenes, while level 2 and 3 data are specifically derived atmosphere, land, ocean and cryosphere products (NASA, 2016). Level 2 and level 3 imagery, from the Terra platform, from the Goddard Space Flight Centre NASA LAADS free of charge have been used for this study (Appended table 8.1).

4.1.3.1. Level 2

Two level 2 MODIS imagery products have been used for this study. The first is the MOD04_L2 which has a resolution of 10 x 10 km at nadir (NASA, 2016). The AOD (no units) was obtained at 550 nm with a data range of -0.05 to 5.0 (NASA, 2016). This product monitors the ambient aerosol optical thickness over oceans and land masses and has been used for the analyses of SO_2 and NO_x (NASA, 2016). AOD is related to the loadings of fine particles in an atmospheric column and it measures light extinction by aerosol scattering and absorption in an atmospheric column (Hu *et al.*, 2014a). The second product used, MOD07_L2, has a resolution of 5 x 5 km at nadir and a data range of 0 to 500 DU (NASA, 2016). The total-ozone burden product used from this collection of products is an estimate from band channel 30 (9.580 – 9.880 µm) of the total-column stratospheric and tropospheric ozone content over a 5 km^2 atmospheric column and has been used for the analyses of surface O_3 (NASA, 2016).

4.1.3.2. Level 3

The three Level-3 MODIS products are global gridded MODIS Atmosphere products (NASA, 2016). Each level-3 products contain statistics generated from the corresponding level-2 products (NASA, 2016). Among other statistics calculated are simple (mean, minimum, maximum, standard deviation) statistics and histograms of the quantity measurement and confidence of the quantity measurement (NASA, 2016). These statistics are summarized and interpolated over a 1x1° global grid for daily (*MOD08_D3*), eight-day (*MOD08_E3*) and monthly (*MOD08_M3*) temporal periods (NASA, 2016). Each temporal resolution has been used for this study.

The first product, total column ozone derived is an estimate of O_3 measured in Dobson units (*Du*) where 1 unit *ppb* of tropospheric O_3 = 0.65 *Du* and the data range is 0 to 500 DU (IPPC, 2001; NASA, 2016). This total column ozone measurement is derived from band 30 (9.580 – 9.880 μm) and was developed to monitor the potential harm caused by the anthropogenic depletion of stratospheric O_3 as well as the anthropogenic formation of tropospheric O_3 (NASA, 2016). Whereas, the AOD derived is an estimate of the aerosol optical depth for a column of air which can range from -0.05 to 5.0 (NASA, 2016). This AOD measurement was developed to monitor the effect of aerosols on climate (NASA, 2016). The AOD images have been used for the analysis of SO_2 and NO_x, while the total column ozone has been used for the analysis of surface O_3.

4.1.4. Data limitations: Pollutant concentrations and meteorological parameters

A ground-based monitoring station accurately measures pollutant levels and meteorological parameters within the boundary layer. These networks have a limited geographic coverage, and in particular for the networks across the HPA monitoring stations are only located in high population density areas. Hence, pollutant concentrations and meteorological patterns of a limited geographic coverage are available. A comprehensive ground-based monitoring network is difficult to obtain due to the high maintenance, calibration and establishment costs associated. This and missing data limits the quality of data obtained from ground-level monitoring networks. Datasets are not always checked before archiving and as a result many outliers and errors are present in these datasets.

Initially, there were many gaps in each dataset. Removal of errors and outliers, as per section *4.2.1.*, resulted in additional gaps. Where data were missing and removed, these remain as omitted data, rather than being filled by interpolated values as the results generated show misleading trends. As a result, the large number of current data gaps within the SAWS datasets reduce the reliability of these ground-level datasets. Hence, satellite imagery was used to improve these datasets. Coupled with satellite-derived measurements, the ground-level data readings of pollutant concentrations and meteorology may bring out the advantages of each dataset and potentially be more reliable to monitor and model SO_2, NO_x and surface O_3 levels across the HPA. This reiterates the purpose of this study.

4.1.5. Data limitations: Satellite imagery

Satellite remote sensing can step in to monitor regional air quality where ground monitors are not available, not reliable or sparsely distributed (Gupta and Christopher, 2009a; Emili *et al.*, 2011; Hu *et al.*, 2014a). Satellite imagery does however have limitations. MODIS data products in particular are limited: by their coarse spatial resolution, temporally with only one or two sunlit overpasses of a region per day, and to clear sky pixels among other factors (Emili *et al.*, 2011; Alston *et al.*, 2012). These factors may lead to misleading data in a pixel, especially as data values are interpolated over large spatial resolutions. Therefore, combining ground-level and satellite data potentially exploits the advantages of both measuring methods (Emili *et al.*, 2011).

4.2. Methodology

The following methodology is an investigation into the spatio-temporal patterns of SO_2, NO_x and surface O_3 concentrations. These concentrations were first investigated on diurnal to seasonal time scales. They were then investigated with regard to the regional HPA meteorology. Next, the pollutants were modelled on the time scales of the MODIS atmospheric products. Lastly, the pollutants were investigated with regard to national and international ambient air quality standards.

4.2.1. Initial data analysis

A critical first step for this data analysis required an understanding of the mean and the distribution of this data, i.e. the 'five number summary'. The 'five number summary' is the minimum and maximum values, middle (median), upper and lower quartile values (Underhill and Bradfield, 2009). The mean and summary of the observations of SO_2, NO_x and surface O_3 concentrations and meteorological variables have been used to identify outliers in each dataset and for later sections.

The arithmetic mean value provides a measure of central tendency and was calculated using the following equation:

Arithmetic mean: $\bar{x} = \frac{1}{N}\sum_{i=1}^{N} x_i$ (Underhill and Bradfield, 2009) {Equation 1}.

The median, represents the middle ranked value of the dataset. The following equation was used:

Median: $Q2 = \frac{n+1}{2}$ (Underhill and Bradfield, 2009) {Equation 2}.

The upper and lower quartiles are the numbers ranked halfway between the median and the upper and lower fences. The following equations were used:

Lower quartile: $Q1 = \frac{Q2+1}{2}$; Upper quartile: $Q3 = n - Q1 + 1$ (Underhill and Bradfield, 2009) {Equations 3.1 and 3.2}

The upper and lower fences represent the upper and lower extremes of the datasets. Any values outside of these may be outliers. The follow equations were used:

Upper fence: $U = Q3 + 1.5IQR$; Lower fence: $L = Q1 - 1.5IQR$; Interquartile range: $IQR = Q3 - Q1$(van Emden, 2008; Underhill and Bradfield, 2009) {Equations 4.1, 4.2 and 4.3}.

Outliers are values that are significantly different to the bulk of the dataset. These values may be genuine observations, namely extremes, or machine failures. All negative values have been taken as errors as a negative concentration value is impossible. All non-reading values 999 have been removed. Most of the outliers identified have been taken as correct readings and all readings which were significantly different from surrounding data values were removed.

4.2.2. Analysis for variation

Pollutant concentrations vary indefinitely over various time scales. This variability is characterised by the time variability of source strengths, transport and dispersion processes, deposition mechanisms, chemical conversion mechanisms and pollutant atmospheric lifetimes (Vallero, 2008). Meteorology is considered to be one of the strongest factors influencing pollutant concentrations over temporal scales (Dueñas *et al.*, 2002; Vallero, 2008; Hassan *et al.*, 2013; Gaur *et al.*, 2014). The meteorology across the South African Highveld varies temporally over diurnal to seasonal scales (Frieman and Piketh, 2002; Esau *et al.*, 2012). The source characteristics also vary over diurnal to seasonal scales (Vallero,

2008). To determine the seasonal, monthly and diurnal variation of SO_2, NO_x and surface O_3 time series plotting has been used in the form of graphs and maps.

4.2.2.1. Analysis for seasonal variation

In South Africa, and particularly across the Highveld, meteorological conditions are subject to strong seasonal variability (Laasko *et al.*, 2012). As a result of this and regional HPA source characteristics, pollutant concentrations vary seasonally across the Highveld (Laakso *et al.*, 2012). Changes in source strength throughout a year may also bring about a marked seasonal variation of pollutant concentrations, for example during South African winters more coal is burned to fuel the growing energy demands increasing the pollutant concentrations emitted from power stations. In South Africa there are four seasons (Table 4.4). The seasonal variation is then based on the fluctuation of pollutant concentrations at a seasonal scale over a particular 2011.

Table 4.4: Duration of each season for South Africa (SAWS, 2016).

Season	**Summer**	**Autumn**	**Winter**	**Spring**
Duration	1 December to 28/29 February	1 March to 31 May	1 June to 31 August	1 September to 30 November

The seasonal mean concentrations for SO_2, NO_x and surface O_3 have been calculated using equation 1 and graphed for each monitoring station (Zunckel *et al.*, 2004; Ahammed *et al.*, 2006; Abdul-Wahab and Bouhamra, 2007; David and Nair, 2011; Reddy *et al.*, 2012). Each mean has an error bar which represents the standard deviation, which demonstrates how much the bulk concentrations differ from the mean (Underhill and Bradfield, 2009). The following equation was used to calculate the standard deviation:

$$\sigma = \sqrt{\frac{\sum(x-\bar{x})^2}{n-1}}$$ (Underhill and Bradfield, 2009) {Equation 5}.

4.2.2.2. Analysis for monthly variation

The monthly variation of pollutants is very similar to the seasonal variation, but it is calculated over the twelve months of the year: January, February, March, April, May, June, July, August, September, October, November and December.

The monthly cycle of SO_2, NO_x and surface O_3 has been determined using the five number summary for each month of each monitoring station (Dueñas *et al.*, 2002; Zunckel *et al.*, 2004; Laakso *et al.*, 2008; Gaur *et al.*, 2014). The 'five number summary' shows the spread of concentrations for each month and the mean monthly concentrations for each monitoring station (Dueñas *et al.*, 2002; Zunckel *et al.*, 2004; Laakso *et al.*, 2008; Gaur *et al.*, 2014). These values were calculated using the equations 1 to 4.3. These were plotted as box-and-whisker plots. Each box has 3 lines, the bottom being the lower quartile, the middle being the median and the top being the upper quartile. The lines extending out from the box represent the lower (from the lower quartile) and upper (from the upper quartile) fences, i.e. the extremes in each dataset.

4.2.2.3. Analysis for diurnal variation

Pollutant concentrations typically vary over a 24 hour period. A typical diurnal variation for each pollutant at each monitoring station for each season has been graphed (Zunckel *et al.*, 2004; Ahammed *et al.*, 2006; Fisshea *et al.*, 2006; Adame *et al.*, 2008; Laakso *et al.*, 2008; Gaur *et al.*, 2014). A single day with no missing data was chosen at random to plot graphs of the typical diurnal variations of SO_2, NO_x and surface O_3 for each monitoring station.

4.2.3. Regional meteorological patterns

Meteorological conditions govern the behaviour of pollutants (Elminir, 2005). In order to understand the behaviour of SO_2, NO_x and surface O_3, it is essential to gain an understanding of the meteorological influences on these pollutants. Before this can be done, it is essential to first gain an understanding of the prevailing meteorological conditions. The regional meteorological patterns have been identified through time series plotting. Considerable variations in pollutants concentrations as a result of synoptic meteorology occur over monthly and diurnal scales (Dueñas *et al.*, 2002; Elminir, 2005; David and Nair, 2011). Therefore, each meteorological condition was plotted over a monthly

and diurnal scale using the same methods as for section *4.2.2*. Over a monthly scale, relatively longer term trends were identified, whereas over a diurnal scale shorter term anomalies were identified (Dueñas *et al.*, 2002). The SAWS stand-alone stations have daily average measurements, therefore diurnal time series plotting was only possible for the SAWS co-located stations. Rainfall has been analysed as monthly totals (Dueñas *et al.*, 2002; Elminir, 2005; Laakso *et al.*, 2008). Wind directions per station have been graphed monthly as a frequency distribution chart as per the methodology of Laakso *et al.* (2008), showing the frequency of the 8 cardinal directions per month (Table 4.5).

Table 4.5: Details of the 8 cardinal wind directions.

Degree range (°)	Direction
$0 \leq x < 45$	N
$45 \leq x < 90$	NE
$90 \leq x < 135$	E
$135 \leq x < 180$	SE
$180 \leq x < 225$	S
$225 \leq x < 270$	SW
$270 \leq x < 315$	W
$315 \leq x < 360$	NW

4.2.4. The linear relationship of meteorology and SO_2, NO_x and surface O_3 levels

To determine if there is a relationship between regional synoptic meteorological patterns and SO_2, NO_x and surface O_3 across the HPA, correlation analysis has been undertaken (Dueñas *et al.*, 2002; Elminir, 2005; Underhill and Bradfield, 2009). Correlation analysis determines whether a relationship between a dependent (*y*) and an independent (*x*) variable is present (Underhill and Bradfield, 2009). To determine if synoptic meteorology influences these pollutants, meteorology was the independent (*x*) variable and the pollutant concentrations were the dependent (*y*) variable (Dueñas *et al.*, 2002; Elminir, 2005). To identify if a relationship exists, the correlation coefficient *r* has been calculated. The correlation coefficient (*r*) will always lie between -1 and +1 and the closer *r* is to +/- 1, the stronger the relationship is between the two variables (Underhill and Bradfield, 2009). The *r* value will indicate the strength and direction of the correlation, where a negative value will indicate a decrease in one variable when the other increases and a positive value will

indicate an increase in one variable as the other increases (Underhill and Bradfield, 2009). A value close to +/- 1 will indicate a consistent change in the SO_2, NO_x and surface O_3 concentrations (x) from a change in the independent meteorological variables (y) (Dueñas *et al.*, 2002; Elminir, 2005; Underhill and Bradfield, 2009). The Pearson correlation coefficient for the strength of the relationship between SO_2, NO_x and surface O_3 concentrations and each meteorological variable has been calculated using the statistical package *IBM SPSS Statistics 23*, using the following equation:

$$|r| = \left| \frac{\sum(x_i - \bar{x})(y_i - \bar{y})}{\sqrt{\sum(x_i - \bar{x})^2 (y_i - \bar{y})^2}} \right|$$ (Underhill and Bradfield, 2009) {Equation 6}.

Once the strength of the relationship has been calculated, it is necessary to determine the statistical significance of this relationship. The statistical significance, *p value*, is a measure of the probability that the results obtained are representative of the population or just as a result of a coincidence of the random sampling (Underhill and Bradfield, 2009). This value ranges from 0 to 1. The closer p is to 0, the smaller this value, the greater the chance that the result obtained is a true indicator of the behaviour of the data over the study period (Underhill and Bradfield, 2009). The *p value* obtained tests the null hypothesis (H_0: $p = 0$) that there is no relationship between SO_2, NO_x and surface O_3 concentrations and synoptic meteorology, the dependent and independent variables (Underhill and Bradfield, 2009). The *p values* were calculated using *SPSS*.

When associating dependent variables such as SO_2, NO_x and surface O_3 concentrations with independent variables such as synoptic meteorological conditions among others, it is important to calculate the proportion of the total variability of the dependent variable as a result of the changes observed in the independent variable (Underhill and Bradfield, 2009). This is calculated using the coefficient of determination (R^2) (Underhill and Bradfield, 2009). The result is an R^2 value between 0 and 1 (Underhill and Bradfield, 2009). A value closer to 1 suggests that a greater proportion of variability in the dependent variable is explained by variation in the independent variable (Underhill and Bradfield, 2009). The R^2 value was calculated in *SPSS* using the following equation:

$$R^2 = \frac{b\left(\sum xy - \frac{\sum x \sum y}{n}\right)}{\sum y^2 - \frac{(\sum y)^2}{n}}$$ (Underhill and Bradfield, 2009) {Equation 7}.

Synoptic meteorological conditions are known to influence pollutants over monthly scales (For example: Comrie, 1990; Comrie and Yarnal, 1992; Comrie, 1994; Eder *et al.*, 1994; Cuhadaroglu and Demirci, 1997; Demirci and Cuhadaroglu, 2000; Dueñas *et al.*, 2002; Latini *et al.*, 2002; Elminir, 2005; Lin *et al.*, 2011; Luvsan *et al.*, 2012; Balashov *et al.*, 2014). As a result the correlation and regression analysis will be done over a monthly scale for each monitoring station as demonstrated by Elmini (2005). Temperature, solar radiation, relative humidity, rainfall, atmospheric pressure, wind speed and wind direction have been correlated to SO_2, NO_x and surface O_3 over a monthly scale.

For the monthly scale correlation and regression analysis, the SO_2, NO_x and surface O_3 and meteorological data were grouped per month to determine the pearson correlation coefficient and the significance of the relationship between SO_2, NO_x and surface O_3 and each meteorological parameter (Dueñas *et al.*, 2002; Elminir, 2005; Elampari and Chithambarathanu, 2011). Each monitoring station does not have co-located meteorological stations. This analysis was only performed using monitoring stations with co-located meteorological stations and only between the meteorological variables measured by the meteorological station. The monthly average atmospheric pressure for Ermelo_2 and Secunda were correlated with the monthly average SO_2, NO_x and surface O_3 stations for the Ermelo and Secunda monitoring stations, as this is the only scale available for atmospheric pressure. Ermelo and Secunda do not have NO_x data. To obtain a general understanding of the influence of atmospheric pressure on NO_x, Camden and Balfour NO_x concentrations were used.

4.2.4.1. Statistical limitations

The primary limitation of statistical analyses arises from gaps in the dataset. Missing data are inevitable and as a result the *n value* is reduced for statistical analyses. The *p value* determines the probability that the calculated trends and relationships may still hold in a fuller dataset (Underhill and Bradfield, 2009). There is concern regarding the possibility that the missing values may potentially change the *p value* of the linear correlations. Hence, the effect of a reduced *n value* resulting from the omission of missing data ensures that the *p value* reported is a true probability result and not one created by chance when interpolating

missing values (Underhill and Bradfield, 2009). The resulting *p value* may still be limited by missing values which may dilute or strengthen correlations (Underhill and Bradfield, 2009).

4.2.5. Multiple regression analysis of meteorology and SO_2, NO_x and surface O_3 levels

The influence of each meteorological variable has now been studied alone. It is unlikely that only one meteorological variable will explain the behaviour of SO_2, NO_x and surface O_3. Rather a combination of the meteorological variables that occur simultaneously will explain their behaviour (Dueñas *et al.*, 2002; Elminir, 2005; Balashov *et al.*, 2014). Each meteorological variable has been used for the multiple regression analysis over a monthly scale (Dueñas *et al.*, 2002; Balashov *et al.*, 2014). Each multiple regression model will demonstrate the relationship between SO_2, NO_x and surface O_3 and the independent meteorological variables for each monitoring station as Akpinar *et al.* (2009) demonstrated.

Each model was calculated using *SPSS* using the following equation:

$$y = \beta_0 + \beta_1 x_1 + \beta_2 x_2 + \cdots + \beta_k x_k + \epsilon$$ (Underhill and Bradfield, 2009) {Equation 8}.

The strength of each model has been determined by the coefficient of variation (R^2) equation 7 (Underhill and Bradfield, 2009). The strength depends on the degree to which the combination of independent meteorological variables can explain the changes in the behaviour of SO_2, NO_x and surface O_3 (Underhill and Bradfield, 2009).

The accuracy of each multiple regression model is necessary to calculate as some independent variables included may in fact be surplus factors and they may not necessarily influence the behaviour of the dependent variable (Underhill and Bradfield, 2009). Surplus factors do not influence the strength of the model, but they do reduce the accuracy of a model (Underhill and Bradfield, 2009). The accuracy of the model is determined by the root-mean-square error (RMSE) on *SPSS*:

$$\sigma_{est} = RMSE = \sqrt{\frac{\sum(y - y_{est})^2}{N}}$$ (Underhill and Bradfield, 2009) {Equation 9}.

4.2.5.1. Multiple regression model limitations and recommendations

The multiple regression models created for this section are limited by the meteorological data obtained from the SAAQIS network. These datasets do not provide measurements for each meteorological parameter at each station nor does each station have meteorological measurements. To improve these models more data and reliable data are necessary. Additionally, missing data may dilute or strengthen the significance of each variable within the multiple regression, thereby influencing the significance of each model.

4.2.6. Satellite derived measurements

Each raw image has been processed using the MODIS conversion toolkit (MCTK), a plugin on ENVI, as per the MCTK user guide (White *et al.*, 2016). The MCTK processes each MODIS product by converting the digital numbers to extract/retrieve AOD at 550 nm (You *et al.*, 2015) or Ozone (Du) values at 9.580 – 9.880 µm (NASA, 2016). In this process the map projection can be specified and it has been specified to the datum WGS84.

4.2.7. Exploring the relationship between ground-level pollutant concentrations, meteorological parameters and satellite-derived measurements across the HPA

Ground based measurements of trace gas and aerosol concentrations are the most accurate measurements of pollutant levels within the boundary layer (Hu *et al.*, 2014a). The ground-based monitoring network across the HPA is associated with many limitations as discussed previously. Satellite derived measurements of total atmospheric column have the potential to enhance the SAAQIS monitoring network measurements to provide pollutant exposure measurements. The MODIS satellite products have medium spatial resolutions which limit their ability to alone estimate pollutant concentrations but coupled with ground-level measurements improves their estimation ability.

Many previous studies have used linear regression methods to establish a relationship between satellite-derived measurements and ground-level trace gases and aerosols (Table 3.4). Most of these studies concluded that a linear relationship between satellite-derived measurements and ground-level measurements is not suitable to estimate surface level pollutants.

Ground level pollutant concentrations across the HPA are influenced by meteorology and land use (For example: elevation, emission sources and land cover, etc.) among other factors. Simple linear regression models between satellite-derived measurements and ground-level pollutant concentrations will not be suitable to describe pollutants across the HPA. Instead models incorporating meteorology and land use should be developed.

Multiple regression models incorporating meteorology and satellite-derived measurements have been created to estimate ground-level pollutant concentrations (Figure 4.3) (Gupta and Christopher, 2009; Hu *et al.*, 2014a; Hu *et al.*, 2014b; Sotoudeheian and Arhami, 2014; You *et al.*, 2015). Incorporating measurements of land use has been left for future work. Using meteorological measurements of: temperature (°C); relative humidity (%); solar radiation (W/m^2); rainfall (mm); wind speed ($m.s^{-1}$); wind direction (°) and atmospheric pressure (hPa) and satellite-derived AOD or total column O_3, multiple regression models have been created. Each model was calculated using *SPSS* using equation 8. An R^2 value, which identifies how well the model fits the data, was calculated using *SPSS* for each model using the equation 7.

Twelve models, four per pollutant, were made using the level 2, level 3: daily, 8-day and level 3 monthly MODIS satellite imagery, pollutant concentrations data and meteorological data. The model building process is indicated in Figure 4.3. All data were averaged over the temporal scale matching the satellite imagery.

Each model incorporates data from the peak and trough months of each pollutants variation to create the model. SO_2 and NO_x concentration peaks were generally during June and they were generally at their lowest during January. An average of 7h00 and 8h00 on the 15th of January and June were used for the level 2 model, the average of the 15th of January and June were used for the level 3 daily model, the average of the 12th to the 15th of January and June were used for the level 3 8-day model and the average of January and June were used for the level 3 monthly model. Surface O_3 generally peaked during September and is lowest generally during April. An average of 8h00 and 9h00 on the 15th of April and September were used for the level 2 model, the average of the 15th of April and September were used for the level 3 daily model, the average of the 12th to the 15th of April and September were

used for the level 3 8-day model and the average of April and September were used for the level 3 monthly model.

The meteorological data for each model were averaged over the same scales as the pollutant data. Meteorological data were interpolated using the closest two stations for those stations without meteorological data or without data of a meteorological parameter. Atmospheric pressure data for the level 2 models were the atmospheric levels for the daily models; this was done to include atmospheric pressure as it was shown to significantly influence each pollutant and thus it is important to include in each model.

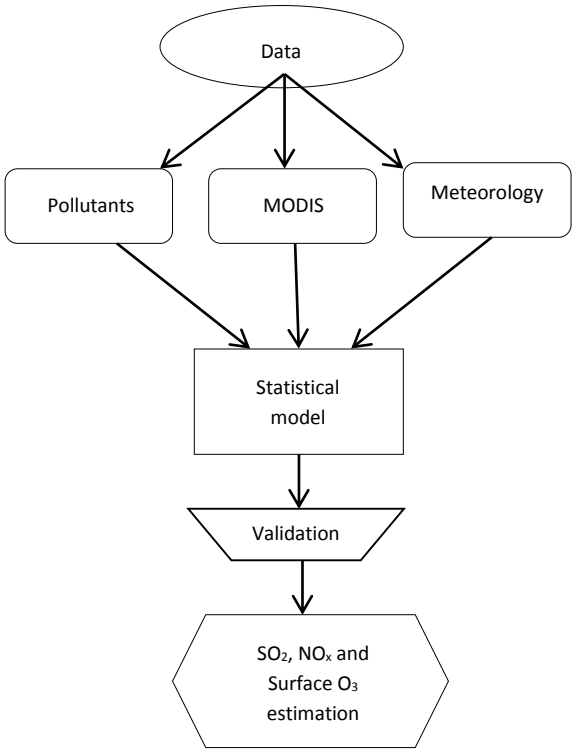

Figure 4.3: An outline of the model building steps (adapted from Gupta and Christopher, 2009a).

4.2.7.1. Validation of the relationship between ground-level pollutant concentrations and satellite-derived measurements

Before the models may be used for application purposes, an assessment of validity is essential. This will determine if the models will be able to function successfully for their purpose and which scale model may be best applicable. Validation of each model involves testing each models predictive performance using a cross validation method (Gupta and

Christopher, 2009; Montgomery *et al.*, 2012; Chen *et al.*, 2013; Hu *et al.*, 2014a; Hu *et al.*, 2014b; Sotoudeheian and Arhami, 2014; You *et al.*, 2015).

This validation method used 2011 data for the month of August, i.e. data not included in the model building process (Montgomery *et al.*, 2012; Burt *et al.*, 2009). Satellite-derived values and meteorological data for the month of August during 2011 were used in the multiple regression models to determine a predicted (model) value of pollutant concentration at each monitoring stations for each model. This value was then compared to the measured (observed) values using the following RMSE equation:

$$RMSE = \sqrt{\frac{\sum_{i=1}^{n}(Y_i - X_i)^2}{n}}$$ (Burt *et al.*, 2009) {Equation 10}.

Y_i is the observed value, X_i is the model value and n is the sample size (Burt *et al.*, 2009). This value represents the offset of the models predicted data compared to the observed data.

The next step involved calculating the coefficient of determination, R^2, value between the predicted and observed values for each model. An R^2 value greater than 0.75 indicates that the model fits the data well, and that model may be applicable across the HPA (Burt *et al.*, 2009). The R^2 value was calculated in *SPSS* using equation 7 previously mentioned.

4.2.7.2. Model limitations

Each model has many limitations associated with the quality of data used. Firstly, each model is limited by the lack of meteorological data and the interpolation of this meteorological data. To create a model it was necessary to interpolate the data. Interpolation may introduce trends that do not exist in the datasets. Each model was limited by the amount of monitoring stations as more monitoring stations would have captured more of the spatio-temporal patterns that exist.

The MODIS satellite imagery have medium to poor spatial scales, of 5 km^2, 10 km^2 and $1°^2$. Each of these pixels contains interpolated statistics. Pollutant hotspots may be as small as a couple of meters (Vallero *et al.*, 2008). Hence, any spatial variability in pollutant species smaller than the pixel size is lost.

Pollutant concentrations are influenced by land use patterns among other factors (Vallero *et al.*, 2008; Hu *et al.*, 2014a; Hu *et al.*, 2014b). All influential factors were not included in the model building process. This may significantly influence the applicability and accuracy of each model of each model (Montgomery *et al.*, 2010).

4.2.8. Frequency of exceedance of international and national ambient air quality standards for SO_2, NO_x and surface O_3 across the HPA

For the purpose of this study, some of the international WHO air quality guidelines (WHOAQG) and the South African National Ambient Air Quality Standards (SANAAQS) have been used (Table 4.6). The South African standards are a benchmark against which the measurements from this study should be compared while the WHO standards are referenced in order to contextualise the values internationally. The frequency of exceedance of these standards for SO_2, NO_x and surface O_3 has been measured by averaging the hourly pollutant concentrations over the respective averaging periods in Table 4.6 (DEA, 2009). Once averaged, the data were compared to the standards to determine the frequency of exceedance for each pollutant at each monitoring station (DEA, 2009).

Table 4.6: Ambient AQG's for SO_2, NO_2 and O_3 (WHO, 2005; DEA, 2009).

Pollutant	**South African National Ambient Air Quality Standards (µg/m³)**			**World Health Organisation Air Quality Guidelines (µg/m³)**	
SO_2	350 (134 ppb) (1-hour averaging period) (88 exceedances allowed per year)	125 (48 ppb) (24-hour averaging period) (4 exceedances allowed per year)	50 (19 ppb) (annual averaging period) (No exceedance allowed)	20 (8 ppb) (24-hour averaging period)	
NO_2	200 (106 ppb) (1-hour averaging period) (88 exceedances allowed per year)	40 (21 ppb) (annual averaging period) (No exceedance allowed)		200 (106 ppb) (1-hour averaging period)	40 (21 ppb) (annual averaging period)
O_3	120 (61 ppb) (8-hour averaging period) (11 exceedances allowed per year)			100 (50 ppb) (8-hour averaging period)	

When the ambient air quality standards at a particular monitoring station are or may be exceeded, this monitoring station is identified as a pollution 'hotspot' (DEA, 2011). Using data from each monitoring station allows one to identify some pollution 'hotspot' areas across the HPA, while interpolation surfaces can allow one to spatially visualise pollutant exceedances over a raster surface. The IDW interpolation technique has been used to view the frequency of exceedances as a raster surface across the entire HPA. IDW is a simple

spatial interpolator which estimates grid points based on a weighted average of measured values surrounding the unmeasured location (Wong *et al.*, 2004; Emili *et al.*, 2011). It was chosen on the basis that it makes the assumption that things closer to one another are more alike than those further apart and to predict a value for an unmeasured location the cells closer to the prediction location will have a greater influence on the cells value than those farther away (Wong *et al.*, 2004; Emili *et al.*, 2011). The advantage of using IDW is that it does not form assumptions about the statistical model that forms the basis of the data (Wong *et al.*, 2004; Emili *et al.*, 2011). There are drawbacks to using IDW: a) no information about the error of the predicted values is provided as it is for kriging, and b) maximum and minimum of the field always corresponds to the position of the measurements which may typically not be a physical quantity of the dataset (Wong *et al.*, 2004; Emili *et al.*, 2011).

4.2.9. Probability of exceedance of international and national ambient air quality standards for SO_2, NO_x and surface O_3 across the HPA

Probability is an estimate of the likelihood of a particular event occurring (Burt *et al.*, 2009; Mendenhall, 2009). This value ranges between 0 and 1, where a value closer to 1 indicates a higher confidence of an event occurring (Burt *et al.*, 2009; Mendenhall, 2009). Identifying the probability of exceeding an ambient air quality standard may be a potential way to identify a pollution 'hotspot'. Both the WHOAQG and SANAAQS were used (Table 4.6).

The data for 2011 for each monitoring station is assumed to follow the normal distribution. The probability question has been identified as *P (X > ambient air quality standard)*. *X* represents the pollutant concentrations averaged over the averaging period for a particular ambient air quality standard. To determine the probability of *X* exceeding a particular ambient air quality standard, the area under the probability density function curve above *X* is calculated by standardizing *X* to a *z score* using the following equation:

$$z = \frac{X-\mu}{\sigma}$$ (Mendenhall, 2009) {Equation 11}.

Where, *X* is a normally distributed variable with a mean, μ and a standard deviation, σ. The standardized value z has a standard normal distribution (Mendenhall, 2009). Once *X* has been standardized the probability question becomes $P\left(Z > \frac{X-\mu}{\sigma}\right)$ (Mendenhall, 2009). To calculate the respective area under the curve for the probability of exceedance of each

standard, the *p value*, corresponding to the *z value* for *X* in the *z table* was obtained (Mendenhall, 2009). This value represents the area under the curve to the left of the *z value* (Mendenhall, 2009). To determine the area to the right of the *z value* for *X* the following formula was used (Mendenhall, 2009):

$$P\ (X > \text{ambient air quality standard}) = P\left(Z > \frac{X-\mu}{\sigma}\right) = 1 - P\left(Z > \frac{X-\mu}{\sigma}\right) \quad \{\text{Equation 12}\}.$$

4.2.10. Frequency and probability of exceedance limitations and recommendations

The missing data from the SAAQIS network limits both of these sections largely as the measure and probability of exceedances may be greater if a full dataset was available. The spatial coverage of the monitoring stations over the HPA is limited and thus the spatial coverage of the exceedances is in turn limited, especially to identify pollution 'hotspot' areas. Improvements in satellite imagery used for air quality, especially improvements in spatial resolution, will be beneficial as areas without ground-level monitoring stations may be analysed to identify pollution 'hotspots'.

4.2.11. Summary of the methodological procedure

A step by step flow diagram of the methodological procedure is presented below in Figure 4.4.

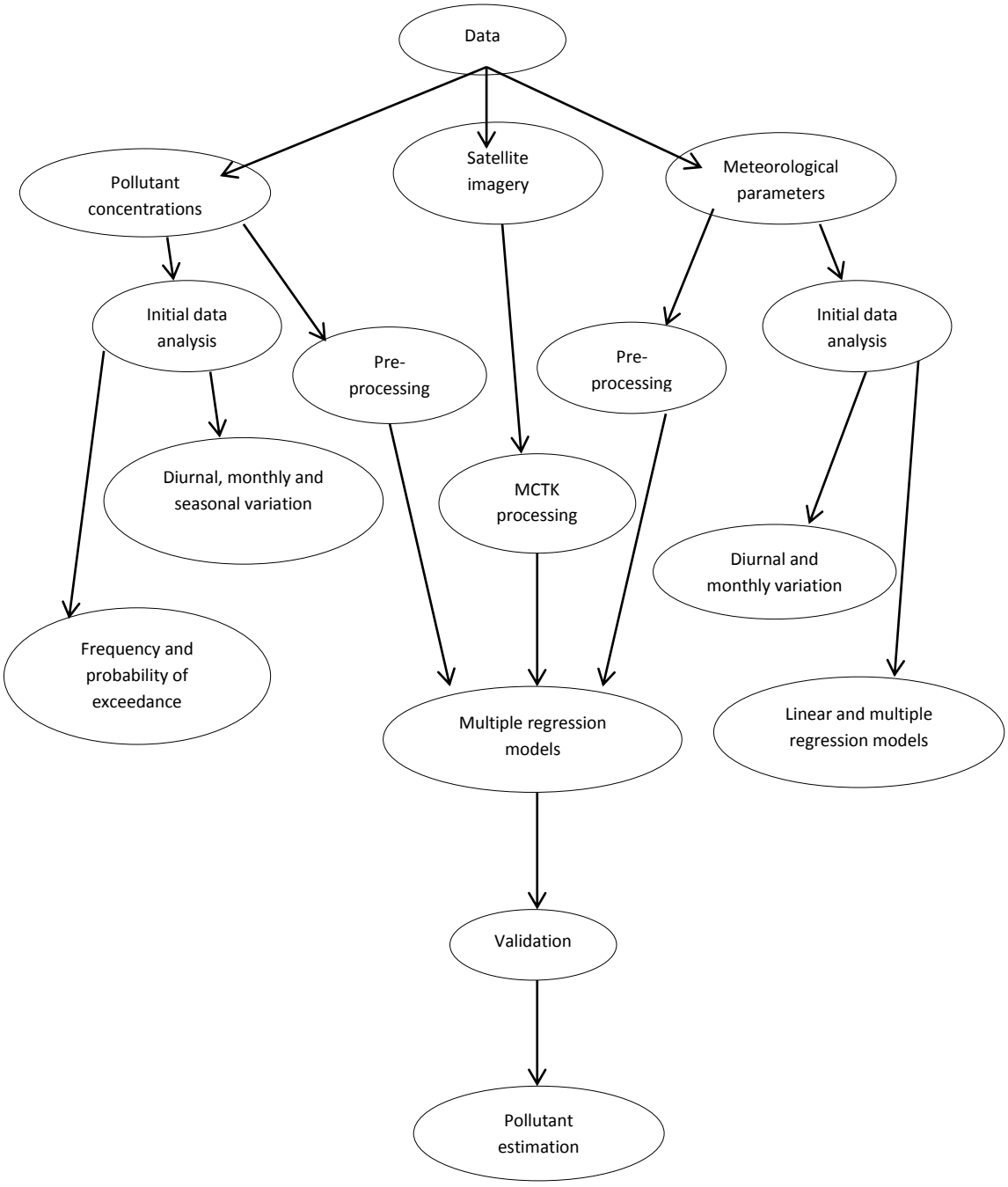

Figure 4.4: Flow diagram of the methodological procedure for this study.

Chapter 5: Results and Discussion

(Steyn, 2013)

The primary aim of this study was to investigate ambient air pollution during 2011, using ground-level SO_2, NO_x and surface O_3 concentrations, meteorological parameters and MODIS atmosphere products, across the HPA, a pollution 'hotspot' area in South Africa. In doing so, this study contributes to the existing body of scientific knowledge on: the temporal variability of pollutants; the influence meteorology has on pollutants; estimating ground-level pollutants using satellite imagery; pollution 'hotspots'.

The results for 2011 are discussed throughout this chapter. This discussion aims to address the objectives of this study by critically analysing the results obtained throughout this study in comparison to results from other studies.

5.1. Temporal variation of pollutants

Pollutant concentrations vary over numerous temporal scales that may range across annual to diurnal time scales (Vallero, 2008). Pollution monitoring is an essential task required for the management of pollutants. An understanding of the variation in pollutant concentrations over time is a key component to the monitoring process. Therefore, in the sections following, the results seasonal, monthly and diurnal variations of SO_2, NO_x and surface O_3 are analysed for the eventual aim of managing these pollutants across the HPA.

5.1.1. Variation of SO_2

The annual average concentration of SO_2 was 12.14±5.0 ppb. The highest SO_2 concentration recorded was 474.3 ppb (at the Komati monitoring station) and the lowest concentration recorded was 0.4 ppb (at the Camden monitoring station). The annual average obtained in this study was typically higher than for most studies across the world and across South Africa (For example: Carmichael *et al.*, 2003; Laakso *et al.*, 2008; Pandey *et al.*, 2008; Meng *et al.*, 2009; Lourens *et al.*, 2011; Venter *et al.*, 2012; Gaur *et al.*, 2014; Harrison *et al.*, 2014). Higher SO_2 levels were observed across the HPA may be directly attributed to a relatively high population density, a high density of pollution sources, i.e. coal fired power stations, fossil fuel emissions from industrial sources, biomass burning, domestic fuel use, transportation and agricultural land clearing for food production among other sources, poor emission controls and poor implementation of legislation (DEA, 2011).

Seasonal average SO_2 concentrations ranged between 5 and 30 ppb, where winter concentrations are at an average of 17.56 ppb were usually higher and summer concentrations at an average of 9.73 ppb were generally lower similar to other studies (Appended figure 8.1; Figure 5.1) (For example: Lyubovtseva *et al.*, 2005; Laakso *et al.*, 2008; Lourens *et al.*, 2011; Venter *et al.*, 2012). Variation from this seasonal pattern occurred (Figure 5.1; Appended figure 8.1). During winter Secunda had extremely high SO_2 concentrations possibly due to a higher demand on the petrochemical plant located in Secunda and domestic fuel use (Figure 3.1) (Table 4.1). In Grootvlei and Balfour a slight summer maximum occurred with little variation during the rest of the year possibly due to an increased demand for power generation, from the Grootvlei power station, and residential emissions during this time (Figure 3.1) (Table 4.1). In Leandra a spring maximum occurred with little variation during the rest of the year possibly due to an increase in the rural and industrial emissions across Leandra (Figure 3.1) (Table 4.1).

Across the Highveld during winter high pressure cells are persistent and they bring about atmospheric stability, stagnant air, low mixing heights, the formation and persistence of inversion layers, vertically stable layers and little to no rainfall (Cosijn and Tyson, 1996; Lourens *et al.*, 2011; Venter *et al.*, 2012). Along with air transport into the Highveld, these factors all contribute to high SO_2 levels across the HPA.

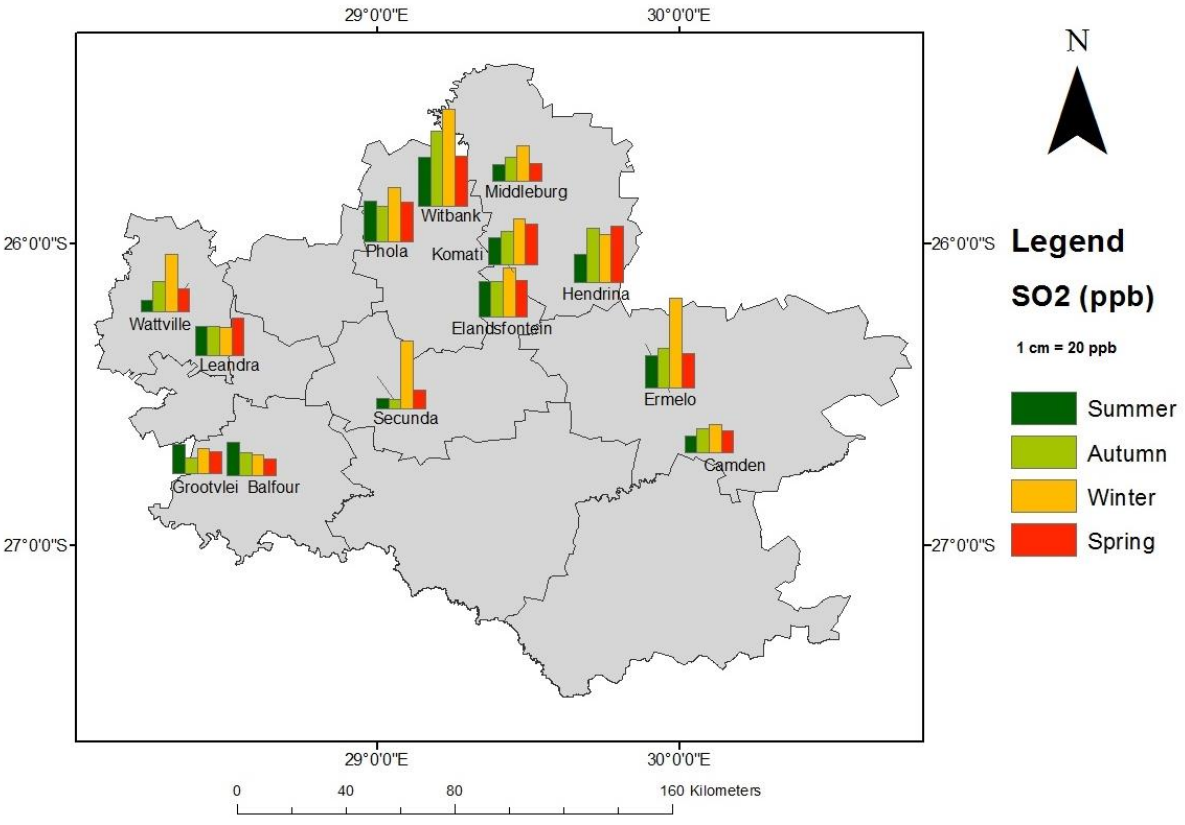

Figure 5.1: Map showing the seasonal variation of SO_2.

Anthropogenic heating during winter resulting in SO_2 within the ambient atmosphere would have promoted the winter maximum (Meng *et al.*, 2009; DEA, 2011). Summer air was normally cleaner due to high mixing heights and few inversion layers from low pressure cells which are able to push through to the HPA (Tyson and Preston-Whyte, 2000). SO_2 was found to be lower during summer and this may be directly attributed to wet depositional processes removing SO_2 at high rates (Zunckel *et al.*, 2000).

The monthly variation in SO_2 concentrations was similar to the seasonal variation, where concentrations of SO_2 peaked during winter and during summer they were at their lowest similar to other studies (Figure 5.2; Appended figure 8.2) (For example: Lyubovtseva *et al.*, 2005; Laakso *et al.*, 2008; Meng *et al.*, 2009; Datta *et al.*, 2011; Lourens *et al.*, 2011; Venter *et al.*, 2012; Gaur *et al.*, 2014). It is clear that concentrations generally peaked during June at an average of 20.08 ppb and during January concentrations were at a minimum with an average of 9.40 ppb (Appended figure 8.2).

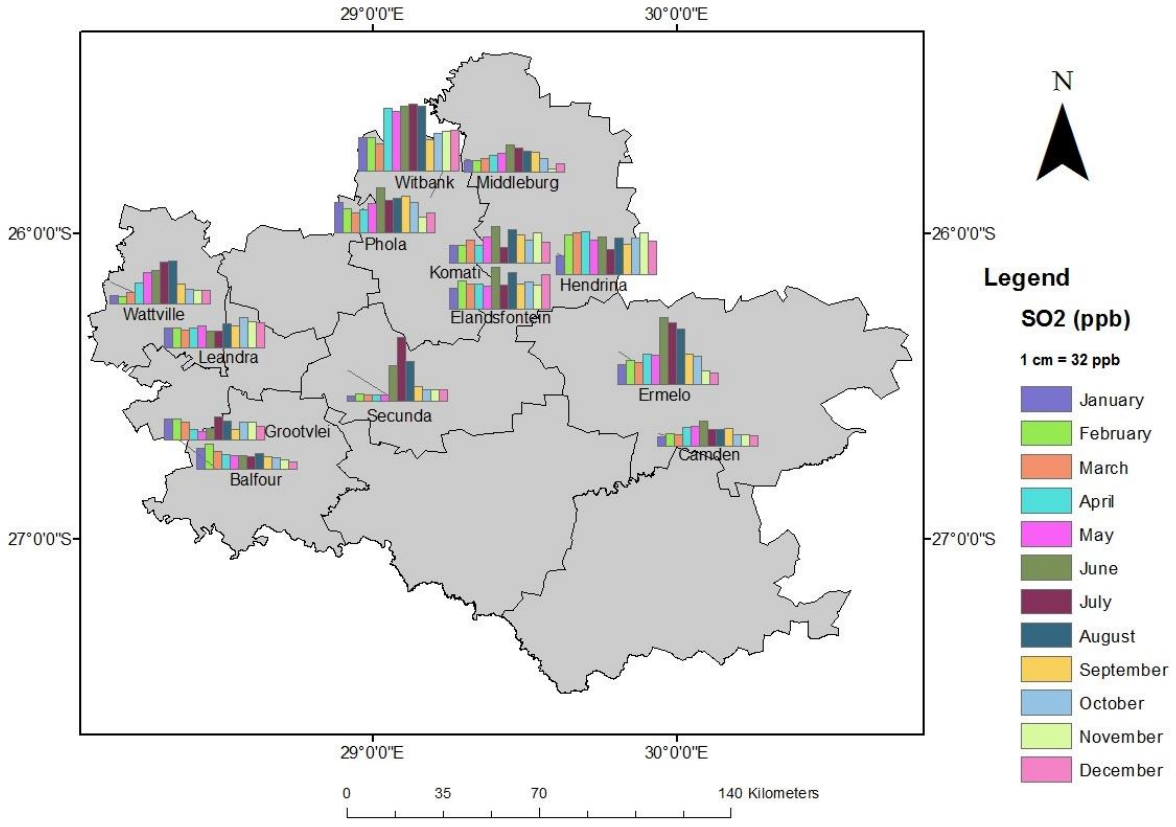

Figure 5.2: Map showing the monthly variation of SO_2.

As previously mentioned SO_2 can have two diurnal variation patterns. SO_2 concentrations displayed a distinct and clear variation during each season (Figures 5.3). The diurnal

variations at each monitoring station were typically similar and peaked during the midday, between 8h00 and 15h00 similar to other studies (Saliba *et al.*, 2006; Lin *et al.*, 2008; Laakso *et al.*, 2008; Meng *et al.*, 2009; Gvozdić *et al.*, 2011; Venter *et al.*, 2012).

The variation at each monitoring station was more pronounced during winter, due to less effective mixing which reduces the dilution of SO_2, much the same as other studies (For example: Saliba *et al.*, 2006; Laakso *et al.*, 2008; Meng *et al.*, 2009; Venter *et al.*, 2012). This diurnal variation pattern is typically associated with semi-rural and rural areas whereby inversion layers play a large role in the diurnal variation (Venter *et al.*, 2012).

The SO_2 diurnal variation patterns across the HPA were not associated with cooking and space-heating practices which would produce SO_2 peaks during the morning between 6h00 and 8h00 and during the evening between 18h00 and 20h00 (Venter *et al.*, 2012). Instead this single peak during the midday correlated with the breakup of inversion layers (Venter *et al.*, 2012). When the strong inversions layers, which formed during the night persisting until sunrise, break up SO_2 is released into the boundary layer where the levels gradually increased to peak around midday between 12h00 and 15h00 (Figure 5.3) (Venter *et al.*, 2012). Higher level stack emissions, from for example power stations, would have accumulated between inversion layers resulting in high SO_2 levels able to subside to the boundary layer once the inversion layers broke up promoting SO_2 accumulation during the day (Figure 5.3) (Venter *et al.*, 2012). During winter these inversion layers would have been more pronounced and strong due to the presence of high pressure cells promoting a more distinct variation (Figure 5.3) (Laakso *et al.*, 2008; Venter *et al.*, 2012). SO_2 concentrations were low at night and decreased as a result of dry deposition throughout the day (Figure 5.3) (Zunckel *et al.*, 1999; Laakso *et al.*, 2008).

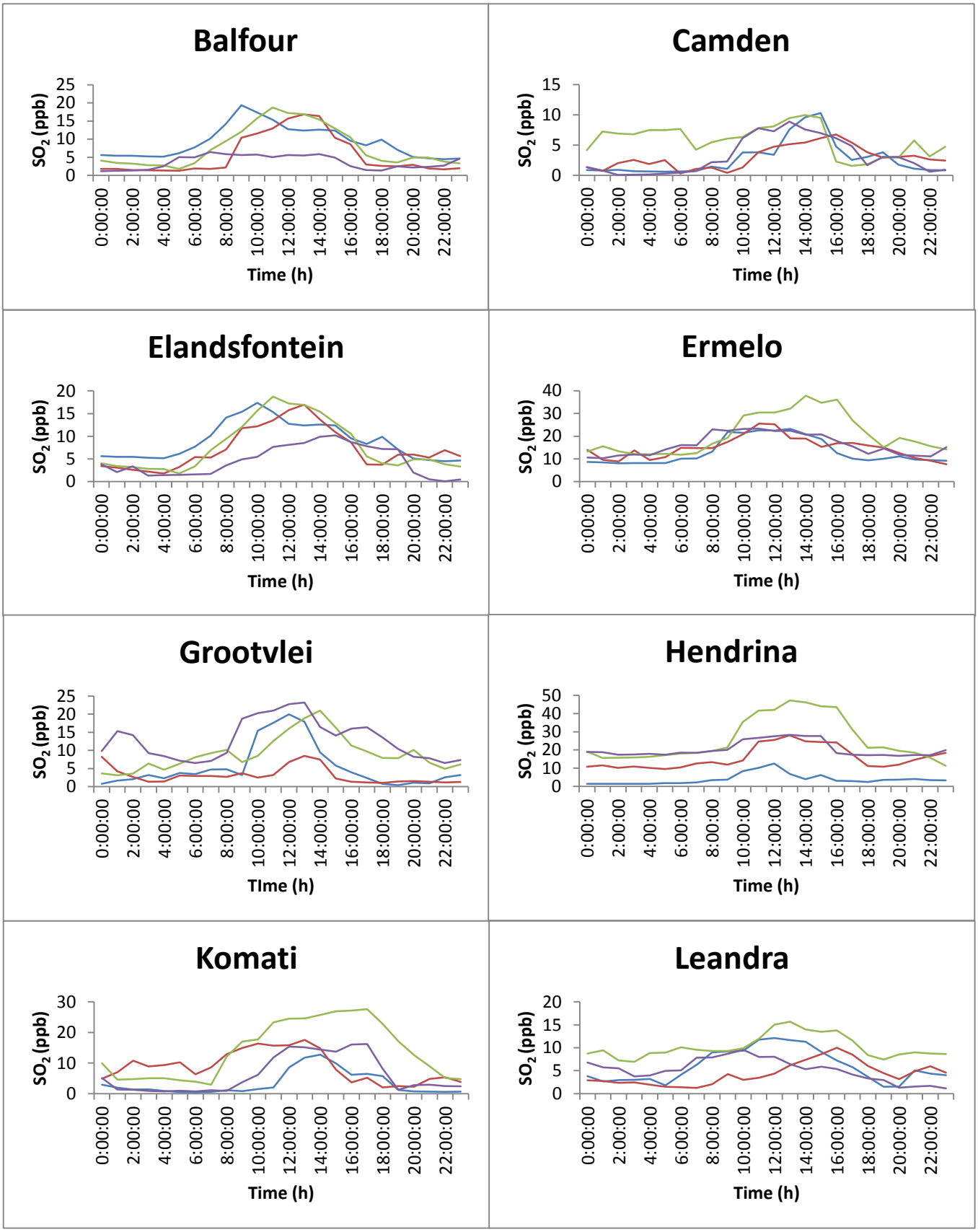

Figure 5.3: Diurnal variation of SO_2. Each line represents a season. Blue – Summer; Red – Autumn; Green – Winter; Purple – Spring.

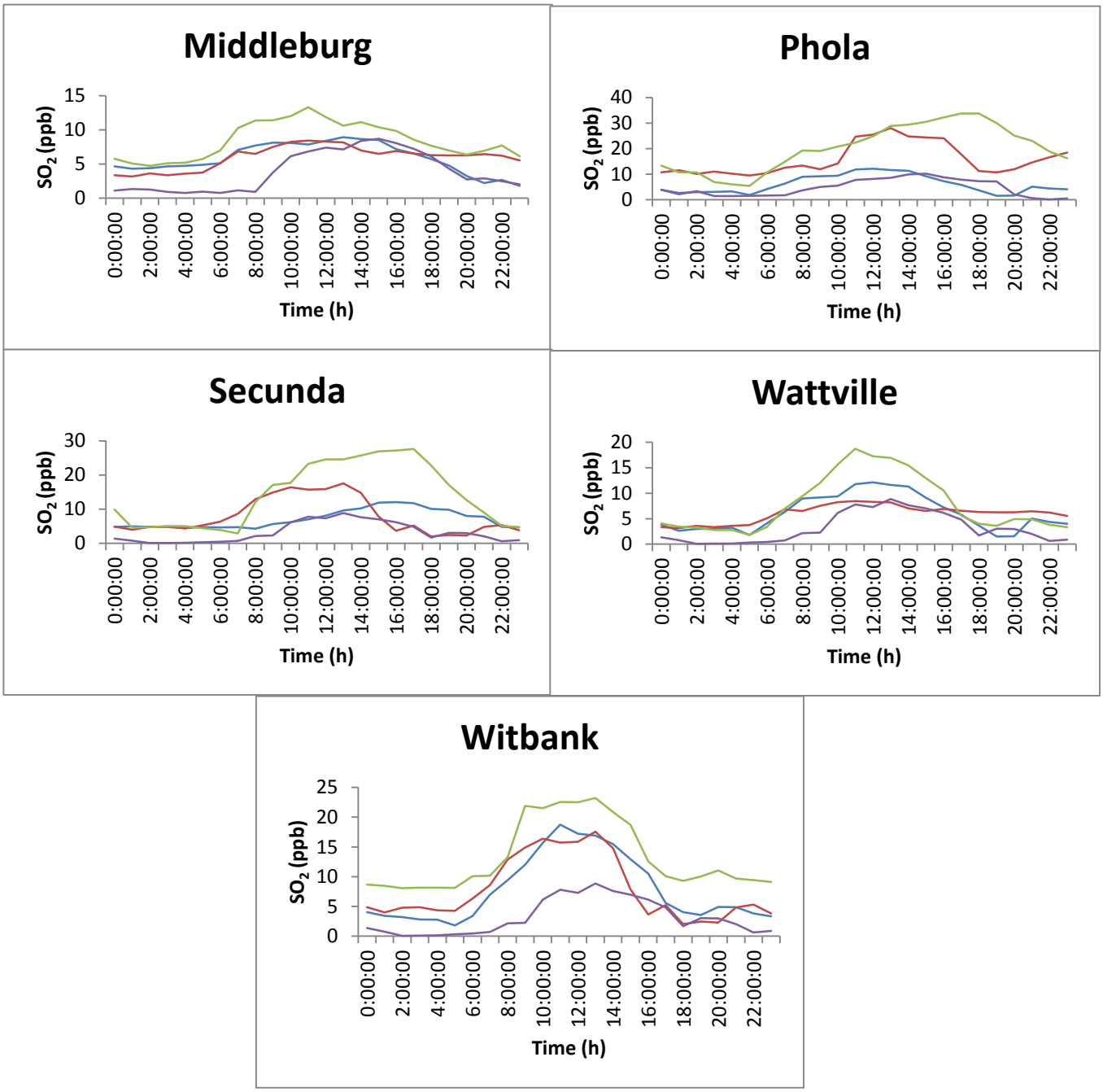

Figure 5.3 continued: Diurnal variation of SO_2. Each line represents a season. Blue – Summer; Red – Autumn; Green – Winter; Purple – Spring.

5.1.2. Variation of NO_x

The annual average concentration of NO_x was 14.75±5.17 ppb. The highest NO_x concentration recorded was 261.8 ppb (at the Phola monitoring station) and the lowest concentration recorded was 0.4 ppb (at the Leandra monitoring station). The annual average obtained in this study was typically higher than most studies across the world and

across South Africa (For example: Naja and Lal, 2002; Naja *et al.*, 2003; Ahammed *et al.*, 2006; Beig *et al.*, 2007; Laakso *et al.*, 2008; Debaje and Kakade, 2009; Meng *et al.*, 2009; Nishanth *et al.*, 2012; Reddy *et al.*, 2012; Gaur *et al.*, 2014). Higher NO_x concentrations across the HPA may be attributed to the relatively high population density across the HPA as well as the extremely high density of pollution sources across the HPA, i.e. fossil fuel emission sources – especially vehicles, industrial sources and agricultural land clearing for food production among other sources and poor emission controls (DEA, 2011).

There are a number of studies with NO_x annual averages higher than for this study, for example: Abdul-Wahab and Bouhamra (2002) found an annual average of 60.8 ppb; Pandey *et al.* (2008) found an annual average of 180 ppb and 67.1 ppb; Hassan *et al.* (2013) found an annual average of 37.9 ppb. These studiers strategically placed their monitoring sites at road side locations (Abdul-Wahab and Bouhamra, 2002; Pandey *et al.*, 2008; Hassan *et al.*, 2013). The majority of NO_x are emitted from combustion processes in vehicles which was why these studies had such high concentrations of NO_x (Ahammed *et al.*, 2006; Laakso *et al.*, 2010; Harrisson *et al.*, 2014).

Seasonal average NO_x concentrations ranged between 5 and 35 ppb, where the winter average at 20.90 ppb was the maximum and the summer average of 9.68 ppb was the minimum similar to other studies (Appended figure 8.3; Figure 5.4) (For example: Naja and Lal, 2002; Abdul-Wahab and Bouhamra, 2002; Naja *et al.*, 2003; Ahammed *et al.*, 2006; Beig *et al.*, 2007; Laakso *et al.*, 2008; Pandey *et al.*, 2008; Debaje and Kakade, 2009; Meng *et al.*, 2009; Nishanth *et al.*, 2012; Reddy *et al.*, 2012; Hassan *et al.*, 2013; Gaur *et al.*, 2014). Variation from this seasonal pattern occurred at the Middleburg monitoring station (Figure 5.4; Appended figure 8.3). During spring maximum NO_x concentration levels occurred while there was little variation during the rest of the year possibly due to an increased demand in the surrounding industrial areas, increased vehicle emissions and increased domestic burning during spring.

Higher NO_x levels during winter are attributable to: a lack of wet deposition removal due to rainfall; the prevailing circulation type, being typically high pressure cells promoting stagnant air parcels, prohibiting vertical and turbulent mixing due to a low mixing height and a high presence and persistence of inversion layers; increased anthropogenic emissions

namely for heating purposes, reduced photochemical reduction of NO_x to form surface O_3; local surface wind processes; and stronger horizontal regional wind processes promoting transboundary transport of NO_x and air flow into the HPA (Naja and Lal, 2002; Abdul-Wahab and Bouhamra, 2002; Naja *et al.*, 2003; Ahammed *et al.*, 2006; Beig *et al.*, 2007; Laakso *et al.*, 2008; Pandey *et al.*, 2008; Debaje and Kakade, 2009; Meng *et al.*, 2009; Nishanth *et al.*, 2012; Reddy *et al.*, 2012; Hassan *et al.*, 2013; Gaur *et al.*, 2014).

Lower NO_x levels during summer were attributable to: a higher level of dry deposition during summer; the persistence of low pressure cells promoting higher rainfall and essentially wet deposition, less inversion layers and vertical mixing due to a higher mixing height; and high levels of solar radiation promoting day time reduction of NO_x through photochemical reduction processes to form surface O_3 (Naja and Lal, 2002; Abdul-Wahab and Bouhamra, 2002; Naja *et al.*, 2003; Ahammed *et al.*, 2006; Beig *et al.*, 2007; Laakso *et al.*, 2008; Pandey *et al.*, 2008; Debaje and Kakade, 2009; Meng *et al.*, 2009; Nishanth *et al.*, 2012; Reddy *et al.*, 2012; Hassan *et al.*, 2013; Gaur *et al.*, 2014).

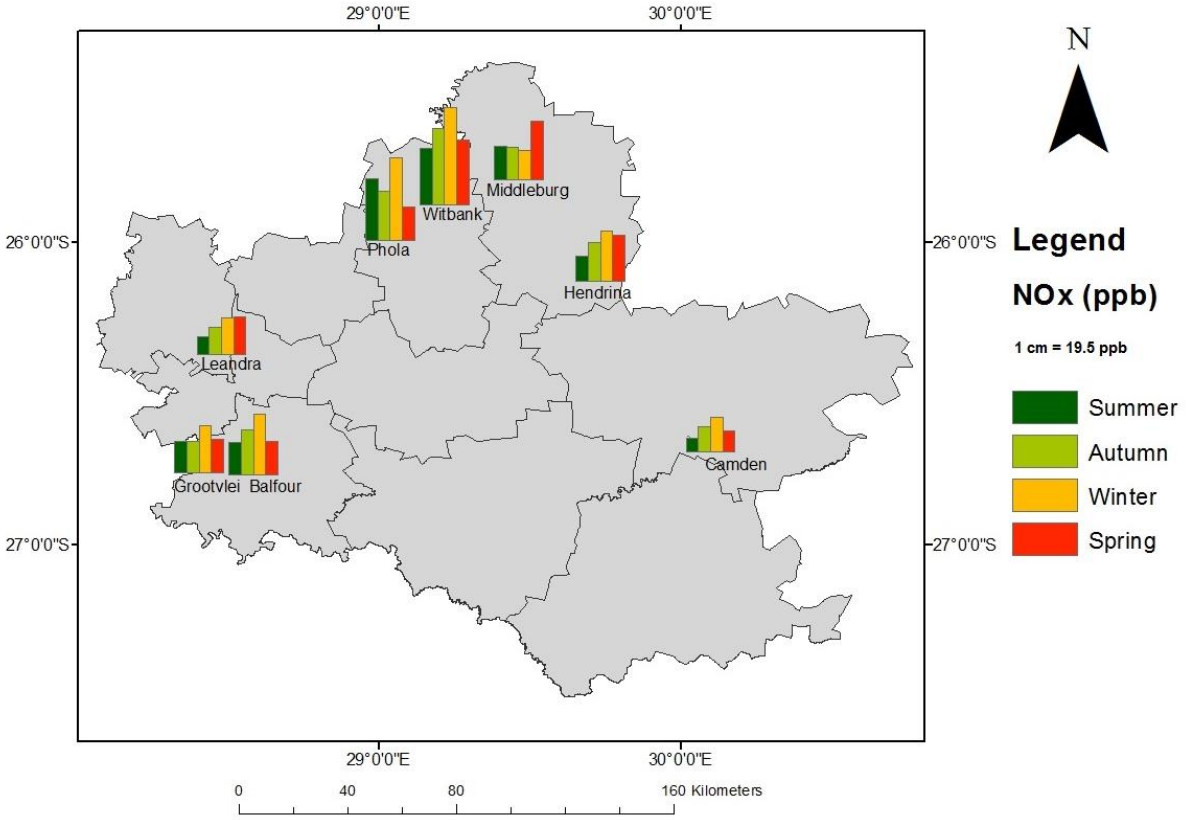

Figure 5.4: Map showing the seasonal variation of NO_x.

The monthly variation of NO_x concentrations was similar to the seasonal variation where the winter months demonstrated peak NO_x concentrations, while the summer displayed NO_x minima similar to many other studies (Figure 5.5; Appended figure 8.4) (For example: Naja and Lal, 2002; Abdul-Wahab and Bouhamra, 2002; Naja *et al.*, 2003; Ahammed *et al.*, 2006; Beig *et al.*, 2007; Laakso *et al.*, 2008; Pandey *et al.*, 2008; Debaje and Kakade, 2009; Meng *et al.*, 2009; Nishanth *et al.*, 2012; Reddy *et al.*, 2012; Hassan *et al.*, 2013; Gaur *et al.*, 2014). June concentrations were generally the highest with an average of 22.61 ppb, while January concentrations were lowest with an average of 12.34 ppb (Appended figure 8.4). Typically there was no variation in the monthly concentrations of NO_x during one season, while there was a variation in the monthly concentrations between the different seasons.

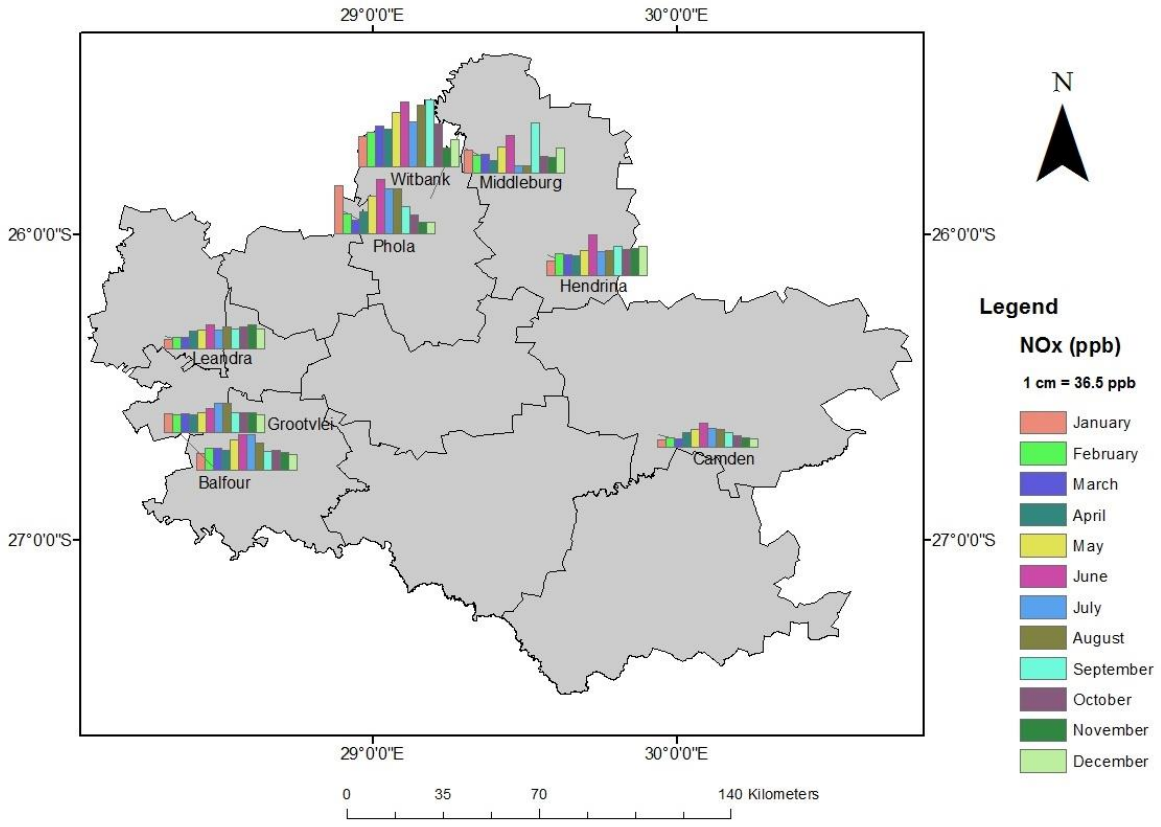

Figure 5.5: Map showing the monthly variation of NO_x.

The typical diurnal variation found had two peaks, during the morning and evening hours (Figure 5.6). High NO_x levels persisted from the evening to the late morning and then during the day, especially when surface O_3 levels peak, NO_x levels were particularly low; this was similar to many studies around the world (For example: Naja and Lal, 2002; Abdul-Wahab and Bouhamra, 2002; Naja *et al.*, 2003; Ahammed *et al.*, 2006; Beig *et al.*, 2007; Laakso *et*

al., 2008; Pandey *et al.*, 2008; Debaje and Kakade, 2009; Meng *et al.*, 2009; Nishanth *et al.*, 2012; Reddy *et al.*, 2012; Hassan *et al.*, 2013; Gaur *et al.*, 2014). The two peaks were associated with peak traffic hours when vehicle emissions were highest (Naja *et al.*, 2003; Ahammed *et al.*, 2006; Beig *et al.*, 2007; Pandey *et al.*, 2008; Debaje and Kakade, 2009; Meng *et al.*, 2009; Zheng *et al.*, 2010; Reddy *et al.*, 2012; Hassan *et al.*, 2013; Gaur *et al.*, 2014).

Persisting NO_x concentrations from the early evening to the late morning hours were attributed to the presence of nocturnal inversion layers which persisted throughout this time (Figure 5.6) (Naja *et al.*, 2003; Ahammed *et al.*, 2006; Beig *et al.*, 2007; Pandey *et al.*, 2008; Debaje and Kakade, 2009; Meng *et al.*, 2009; Zheng *et al.*, 2010; Reddy *et al.*, 2012; Hassan *et al.*, 2013; Gaur *et al.*, 2014). These nocturnal inversion layers trapped NO_x across the surface; they were prominent during winter leading to a more distinct diurnal variation of NO_x during this time (Figure 5.6) (Naja *et al.*, 2003; Ahammed *et al.*, 2006; Beig *et al.*, 2007; Pandey *et al.*, 2008; Debaje and Kakade, 2009; Meng *et al.*, 2009; Zheng *et al.*, 2010; Reddy *et al.*, 2012; Hassan *et al.*, 2013; Gaur *et al.*, 2014).

A dip in NO_x concentrations during the daytime hours was attributed to photochemical reduction processes of NO_x, a surface O_3 precursor, to form surface O_3 (Naja *et al.*, 2003; Ahammed *et al.*, 2006; Beig *et al.*, 2007; Pandey *et al.*, 2008; Debaje and Kakade, 2009; Meng *et al.*, 2009; Zheng *et al.*, 2010; Reddy *et al.*, 2012; Hassan *et al.*, 2013; Gaur *et al.*, 2014). NO_x levels were generally at a minimum when surface O_3 levels peaked for the day, similar to the rest of the world (Figures 5.6) (For example: Naja *et al.*, 2003; Ahammed *et al.*, 2006; Beig *et al.*, 2007; Pandey *et al.*, 2008; Debaje and Kakade, 2009; Meng *et al.*, 2009; Zheng *et al.*, 2010; Reddy *et al.*, 2012; Hassan *et al.*, 2013; Gaur *et al.*, 2014). Dilution of pollutants due to mixing promoted by the formation of the boundary layer may have also been a reason why NO_x concentrations were lower during the daytime (Figure 5.6) (Ahammed *et al.*, 2006).

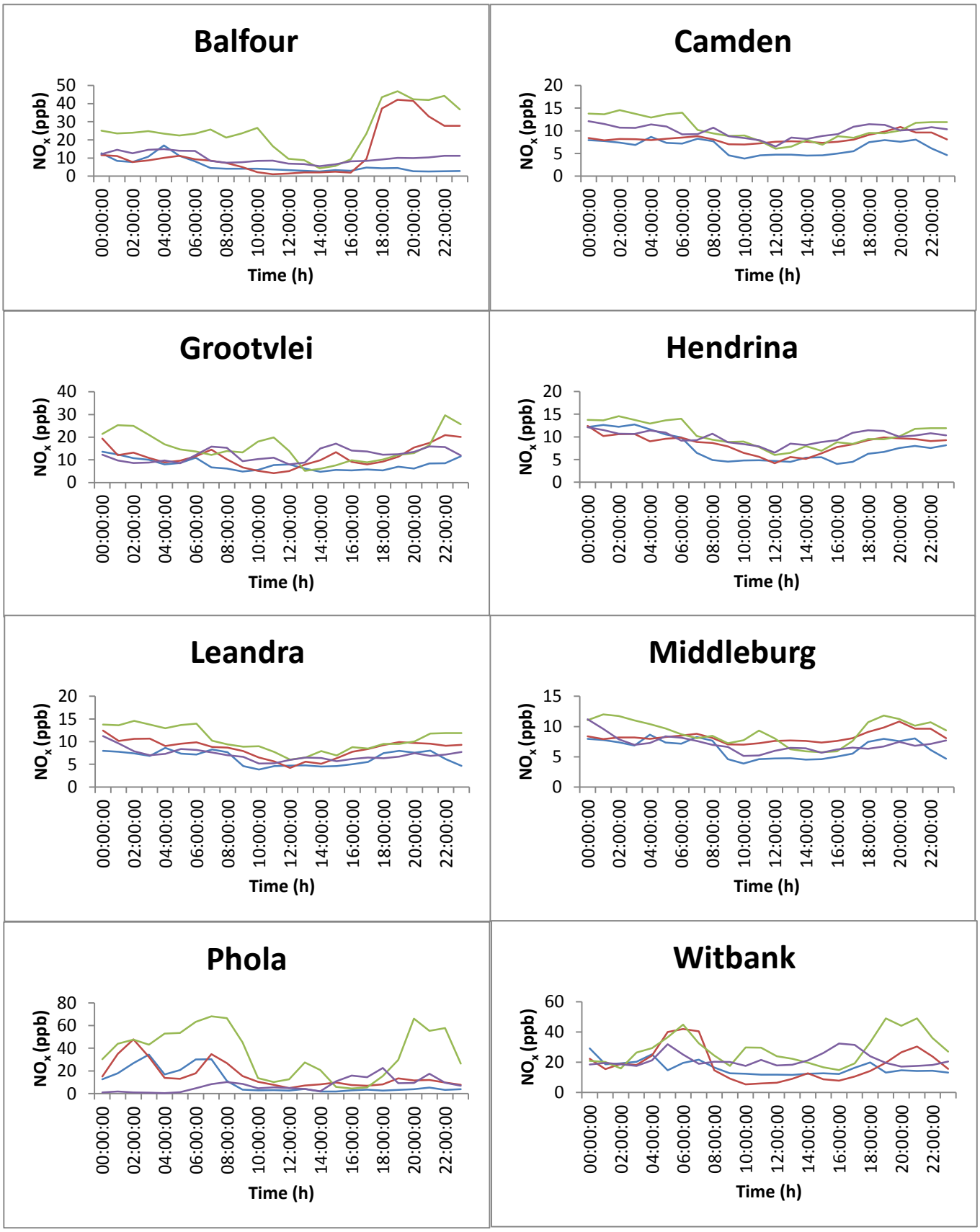

Figure 5.6: Diurnal variation of NO_x. Each line represents a season. Blue – Summer; Red – Autumn; Green – Winter; Purple – Spring.

5.1.3. Variation of surface O_3

The annual average concentration of surface O_3 was 28.77±9.09 ppb. The highest surface O_3 concentration recorded was 495.5 ppb (at the Camden monitoring station) and the lowest concentration recorded was 1 ppb (at the Ermelo monitoring station). The annual average obtained in this study is typically similar to most of the studies across the world (For example: Guicherit and Roemer, 2000; Naja and Lal, 2002; Carmichael *et al.*, 2003; Naja *et al.*, 2003; Satsangi *et al.*, 2004; Zunckel *et al.*, 2004; Ahammed *et al.*, 2006; Meng *et al.*, 2009; Pudasainee *et al.*, 2006; Sahu and Lal, 2006; Beig *et al.*, 2007; Tu *et al.*, 2007; Adame *et al.*, 2008; Laakso *et al.*, 2008; Tiwari *et al.*, 2008; Debaje and Kakade, 2009; Elampari and Chithambarathanu, 2011; Lourens *et al.*, 2011; Kumar *et al.*, 2012; Laakso *et al.*, 2012; David and Nair, 2011; Chelani, 2012; Nirshanth *et al.*, 2012; Reddy *et al.*, 2013; Balashov *et al.*, 2014; Gaur *et al.*, 2014; Harisson *et al.*, 2014). Higher surface O_3 concentrations were found particularly for rural sites. This was also clear across the HPA as surface O_3 is easily dispersed and high concentrations are generally further away from pollutant sources in rural areas (Lourens *et al.*, 2011). In general high levels of surface O_3 exist across the HPA.

Seasonal average surface O_3 concentrations ranged between 10 and 80 ppb, where late winter and spring concentrations were generally higher and end of summer and autumn concentrations were generally lower (Figure 5.7; Appended figure 8.5). Average spring and autumn concentrations across the HPA were 32.82 and 23.88 ppb respectively. Variation from this seasonal pattern of surface O_3 occurred at the Balfour, Secunda and Witbank monitoring stations (Figure 5.1; Appended figure 8.1). A summer maximum in surface O_3 concentrations and little variation during the rest of the year occurred at the Balfour monitoring station, while an autumn maximum and little variation during the rest of the year occurred at Secunda and in Witbank a winter maximum with little variation during the rest of the year. The variation of these seasonal patterns were possibly all due to a higher occurrence of the conditions to form surface O_3 as well as a higher level of surface O_3 precursor gases during the time when maximum levels occurred.

Across the HPA the late winter to early spring maxima may be attributed to prevailing semi-permanent high pressure cells promoting inversion layers which allows very little mixing of air resulting in trapping of O_3 precursor gases emitted during winter from biomass burning and other fossil fuel burning processes, recirculation of air especially air trapped between or

under inversion layers i.e. absolute stable layers; air flow into the Highveld; clear skies, low relative humidity levels, little to no rainfall, high solar radiation levels, high temperatures and stagnant air with low wind speeds which is similar to other studies (For example: Khemani *et al.*, 1995; Pochanart *et al.*, 2001; Abdul-Wahab and Bouhamra, 2002; Dueñas *et al.*, 2002; Naja *et al.*, 2003; Zunckel *et al.*, 2004; Garcia *et al.*, 2005; Jain *et al.*, 2005; Ahammed *et al.*, 2006; Beig *et al.*, 2007; Adame *et al.*, 2008; Khoder *et al.*, 2009; Meng *et al.*, 2009; Laakso *et al.*, 2010; Zheng *et al.*, 2010; David and Nair, 2011; Elampari and Chithambarathanu, 2011; Reddy *et al.*, 2012; Venter *et al.*, 2012; Hassan *et al.*, 2013; Balashov *et al.*, 2014; Gaur *et al.*, 2014). Higher surface O_3 levels during this time may have also been as a result of stratosphere-troposphere O_3 exchange mechanisms being higher during the end of winter and during early spring (Khemani *et al.*, 1995; Varotsos *et al.*, 2001; Garcia *et al.*, 2005; Ahammed *et al.*, 2006).

The end of summer and autumn minimum may then be attributed to prevailing low pressure systems displacing high pressure systems to influence the HPA (Zunckel *et al.*, 2004). During this time the conditions promoted are lower levels of solar radiation, lower temperatures, higher relative humidity levels promoting higher cloud cover as well as rainfall and essentially wet deposition, higher wind speeds and more effective vertical mixing similar to other studies (For example: Khemani *et al.*, 1995; Pochanart *et al.*, 2001; Abdul-Wahab and Bouhamra, 2002; Dueñas *et al.*, 2002; Naja *et al.*, 2003; Zunckel *et al.*, 2004; Garcia *et al.*, 2005; Jain *et al.*, 2005; Ahammed *et al.*, 2006; Beig *et al.*, 2007; Adame *et al.*, 2008; Khoder *et al.*, 2009; Meng *et al.*, 2009; Laakso *et al.*, 2010; Zheng *et al.*, 2010; David and Nair, 2011; Elampari and Chithambarathanu, 2011; Reddy *et al.*, 2012; Venter *et al.*, 2012; Hassan *et al.*, 2013; Balashov *et al.*, 2014; Gaur *et al.*, 2014).

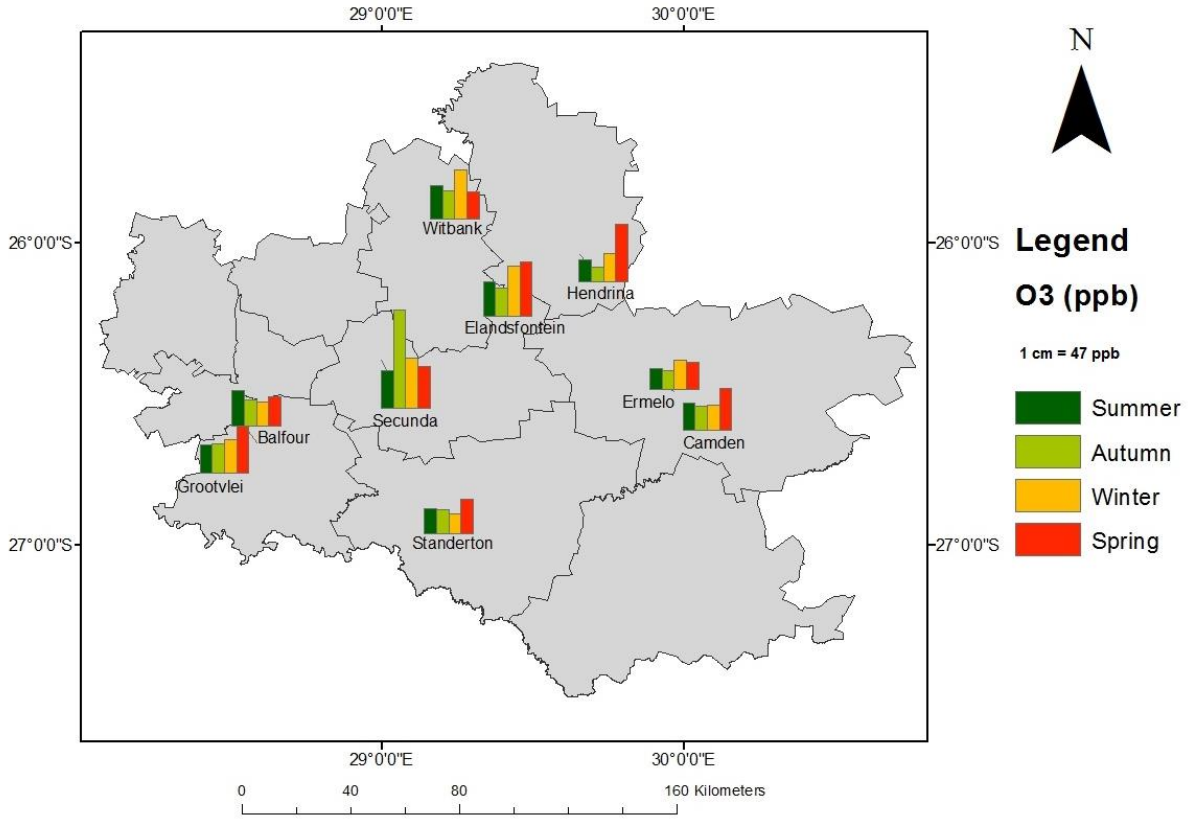

Figure 5.7: Map showing the seasonal variation of surface O_3.

The monthly variation of surface O_3 concentrations typically peaked during the spring months and they dropped to a minimum during the autumn months similar to many other studies (Figure 5.7; Appended figure 8.6) (For example: Khemani *et al.*, 1995; Pochanart *et al.*, 2001; Abdul-Wahab and Bouhamra, 2002; Dueñas *et al.*, 2002; Naja *et al.*, 2003; Zunckel *et al.*, 2004; Garcia *et al.*, 2005; Jain *et al.*, 2005; Ahammed *et al.*, 2006; Beig *et al.*, 2007; Adame *et al.*, 2008; Khoder *et al.*, 2009; Meng *et al.*, 2009; Laakso *et al.*, 2010; Zheng *et al.*, 2010; David and Nair, 2011; Elampari and Chithambarathanu, 2011; Reddy *et al.*, 2012; Venter *et al.*, 2012; Hassan *et al.*, 2013; Balashov *et al.*, 2014; Gaur *et al.*, 2014). September concentrations were generally highest with an average of 38.54 ppb, while April concentrations were generally lowest with an average of 22.21 ppb (Appended figure 8.6). Typically there was no variation in the monthly concentrations of surface O_3 during one season, while there was a variation in the monthly concentrations between the different seasons.

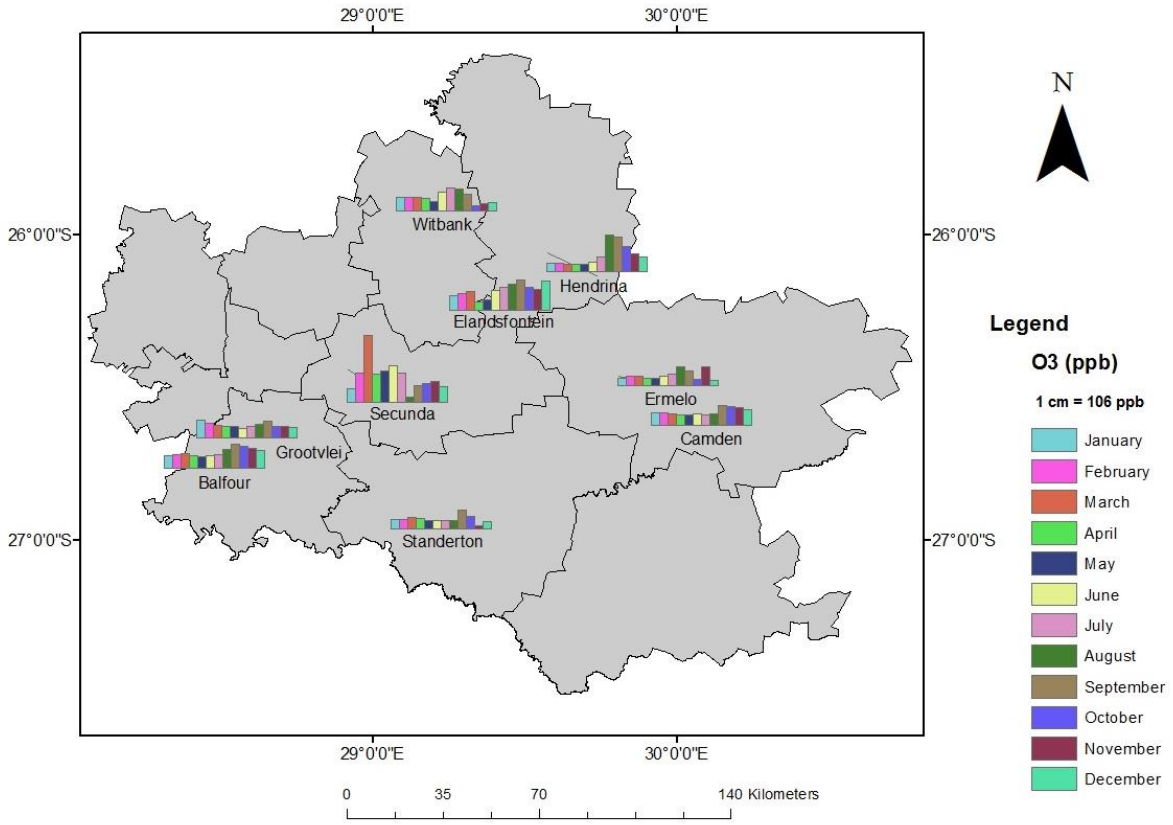

Figure 5.8: Map showing the seasonal variation of surface O_3.

The diurnal cycle of surface O_3 was characterised by a gradual increase after sunrise, followed by a maximum O_3 concentration during the afternoon hours (12h00 to 16h00), a decline after the maximum, steady night time levels and a minimum O_3 concentration during the early morning hours (6h00 to 8h00) (Figure 5.9), much like the diurnal variation of surface O_3 across the world (For example: Khemani *et al.*, 1995; Lal *et al.*, 2000; Dueñas *et al.*, 2002; Pudasainee *et al.*, 2003; Zunckel *et al.*, 2004; Garcia *et al.*, 2005; Jain *et al.*, 2005; Ahammed *et al.*, 2006; Beig *et al.*, 2007; Tu *et al.*. 2007; Adame *et al.*, 2008; Lin *et al.*, 2008; Shan *et al.*, 2008; Xu *et al.*, 2008; Khoder *et al.*, 2009; Meng *et al.*, 2009; Zheng *et al.*, 2010; David and Nair, 2011; Elampari and Chithambarathanu, 2011; Reddy *et al.*, 2012; Hassan *et al.*, 2013; Sharma *et al.*, 2013; Gaur *et al.*, 2014).

The diurnal variation of surface O_3 was strongly influenced by the level of surface O_3 precursors and meteorological conditions (Khoder *et al.*, 2009). The typical diurnal variation of surface O_3 coincided with the intensity of solar radiation and temperature throughout the day (Figure 5.9) (Elampari and Chithambarathanu, 2011).

The surface O_3 cycle started with a morning minimum which was attributed to NO titration of surface O_3 via reaction 9 in *section 2.4.1.* (Abdul-Wahab and Bouhamra, 2002; Garcia *et al.*, 2005; Beig *et al.*, 2007; Tu *et al.*, 2007; Adame *et al.*, 2008; Shan *et al.*, 2008; Zheng *et al.*, 2010; Reddy *et al.*, 2012; Sharma *et al.*, 2013). From 6h00 to 8h00 peak levels of surface O_3 precursors were present (Figure 5.9). The formation of surface O_3 is strongly dependent on the amount of precursor gases present and once the nocturnal inversion layer breaks up after sunrise, the presence of these precursor gases along with increasing solar radiation levels, increasing temperatures, an increase in the boundary layer i.e. mixing layer height, low relative humidity levels and low wind speeds all promote the gradual formation of surface O_3 (Khemani *et al.*, 1995; Lal *et al.*, 2000; Abdul-Wahab and Bouhamra, 2002; Dueñas *et al.*, 2002; Garcia *et al.*, 2005; Beig *et al.*, 2007; Tu *et al.*, 2007; Adame *et al.*, 2008; Shan *et al.*, 2008; Khoder *et al.*, 2009; Zheng *et al.*, 2010; Elampari and Chithambarathanu, 2011; Reddy *et al.*, 2012; Sharma *et al.*, 2013). Solar radiation activates the photochemical production of surface O_3 as well as the mixing of parcels in upper tropospheric O_3 rich air with lower tropospheric air promoting the formation of surface O_3 (Dueñas *et al.*, 2002).

Between 12h00 and 15h00 maximum solar radiation and temperatures push the mixing layer to a maximum height from convective heating (Figure 5.9) (Khemani *et al.*, 1995; Lal *et al.*, 2000; Abdul-Wahab and Bouhamra, 2002; Dueñas *et al.*, 2002; Garcia *et al.*, 2005; Beig *et al.*, 2007; Tu *et al.*, 2007; Adame *et al.*, 2008; Shan *et al.*, 2008; Khoder *et al.*, 2009; Zheng *et al.*, 2010; Elampari and Chithambarathanu, 2011; Reddy *et al.*, 2012; Sharma *et al.*, 2013). At this time surface O_3 levels were at their maximum as photochemical reactions were maximised and the process of O_3 rich air from the upper troposphere mixing with the lower troposphere was maximised (Figure 5.9) (Khemani *et al.*, 1995; Lal *et al.*, 2000; Abdul-Wahab and Bouhamra, 2002; Dueñas *et al.*, 2002; Garcia *et al.*, 2005; Beig *et al.*, 2007; Tu *et al.*, 2007; Adame *et al.*, 2008; Shan *et al.*, 2008; Khoder *et al.*, 2009; Zheng *et al.*, 2010; Elampari and Chithambarathanu, 2011; Reddy *et al.*, 2012; Sharma *et al.*, 2013). When surface O_3 levels reached a maximum the levels of the precursor gas, NO_x, were at a minimum (Figure 5.6; Figure 5.9) (Elampari and Chithambarathanu, 2011). Recirculation of surface O_3 was also more likely to occur when the mixing height was highest (Adame *et al.*, 2008).

After a maximum was reached solar radiation levels and ambient air temperatures started decreasing and surface O_3 levels gradually declined to low and steady night time levels (Figure 5.9) (Khemani *et al.*, 1995; Lal *et al.*, 2000; Abdul-Wahab and Bouhamra, 2002; Dueñas *et al.*, 2002; Garcia *et al.*, 2005; Beig *et al.*, 2007; Tu *et al.*, 2007; Adame *et al.*, 2008; Shan *et al.*, 2008; Khoder *et al.*, 2009; Zheng *et al.*, 2010; Elampari and Chithambarathanu, 2011; Reddy *et al.*, 2012; Sharma *et al.*, 2013). During this time NO titration and dry deposition removal mechanisms acted to reduce the surface O_3 concentrations (Khemani *et al.*, 1995; Lal *et al.*, 2000; Abdul-Wahab and Bouhamra, 2002; Dueñas *et al.*, 2002; Garcia *et al.*, 2005; Beig *et al.*, 2007; Tu *et al.*, 2007; Adame *et al.*, 2008; Shan *et al.*, 2008; Khoder *et al.*, 2009; Zheng *et al.*, 2010; Elampari and Chithambarathanu, 2011; Reddy *et al.*, 2012; harma *et al.*, 2013). The removal processes would have occurred throughout the day but a decline in surface O_3 was only noted after sunrise as photochemical reactions slow down when solar radiation and temperatures decrease (Khemani *et al.*, 1995; Lal *et al.*, 2000; Abdul-Wahab and Bouhamra, 2002; Dueñas *et al.*, 2002; Garcia *et al.*, 2005; Beig *et al.*, 2007; Tu *et al.*, 2007; Adame *et al.*, 2008; Shan *et al.*, 2008; Khoder *et al.*, 2009; Zheng *et al.*, 2010; Elampari and Chithambarathanu, 2011; Reddy *et al.*, 2012; Sharma *et al.*, 2013).

After sunset nocturnal inversion layers persist and during this time residual surface O_3 concentrations would have remained steady in the stable night time atmosphere and the presence of nocturnal inversion layers traps surface O_3 inhibiting any mixing (Khemani *et al.*, 1995; Lal *et al.*, 2000; Abdul-Wahab and Bouhamra, 2002; Dueñas *et al.*, 2002; Garcia *et al.*, 2005; Beig *et al.*, 2007; Tu *et al.*, 2007; Adame *et al.*, 2008; Shan *et al.*, 2008; Khoder *et al.*, 2009; Zheng *et al.*, 2010; Elampari and Chithambarathanu, 2011; Reddy *et al.*, 2012; Sharma *et al.*, 2013).

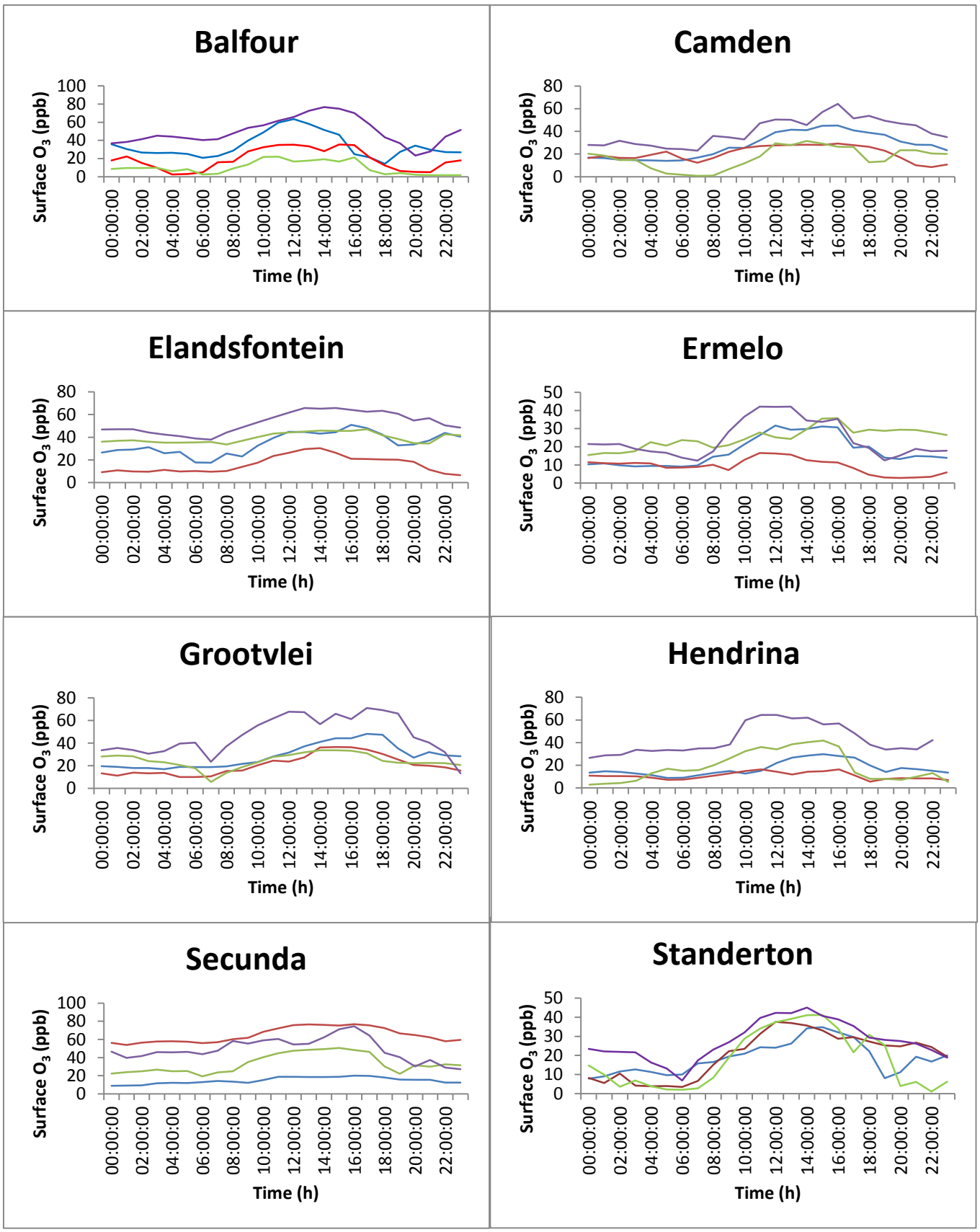

Figure 5.9: Diurnal variation of surface O_3 at each monitoring station. Each line represents a season. Blue – Summer; Red – Autumn; Green – Winter; Purple – Spring.

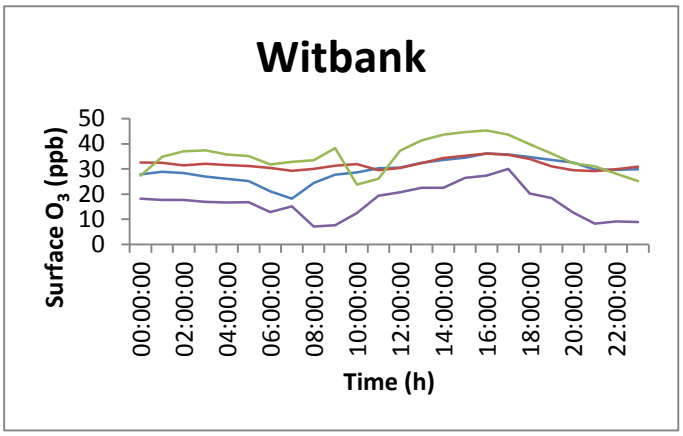

Figure 5.9 continued: Diurnal variation of surface O_3. Each line represents a season. Blue – Summer; Red – Autumn; Green – Winter; Purple – Spring.

5.2. Regional meteorological patterns across the HPA

Above the HPA the atmospheric circulation is dominated by anticyclonic systems during most of the year with frequent easterly disturbances during summer. The regional meteorological patterns discussed below confirm this.

5.2.1. Temperature

Temperatures across the HPA were warmer during summer and cooler during winter (Figure 5.10; Appended figure 8.7). Mean monthly temperatures were about 20 °C during summer and during winter they dropped to an average of 10 °C. Temperatures often dropped below 0 °C during winter particularly during the evening and early morning hours, between 20h00 and 7h00 (Figure 5.10; Figure 5.11; Appended figure 8.7). During the rest of the year, minimum temperatures ranged between 0 and 15 °C. The lowest recorded temperature was – 9.47 °C during July. Winter maximum temperatures ranged between 20 and 25 °C between 12h00 and 16h00 (Figure 5.10; Figure 5.11; Appended figure 8.7). During summer the maximum temperatures typically ranged between 30 and 35 °C and occasionally exceeded 35 °C (Figure 5.10; Figure 5.11; Appended figure 8.7). During the rest of the year, maximum temperatures ranged between 20 and 30 °C. The highest recorded temperature was 38.08 °C recorded during December.

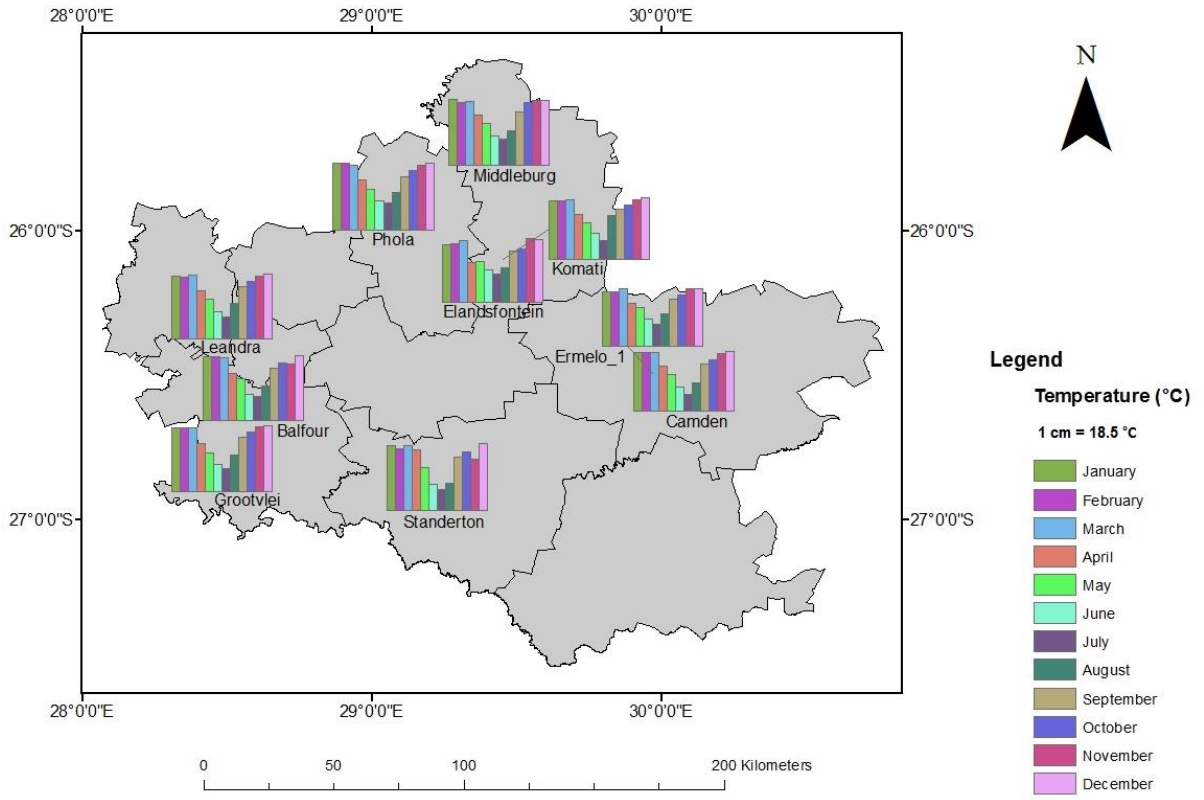

Figure 5.10: Map showing the monthly variation of temperature.

The diurnal variation of temperature during a typical day was low and steady during the evening and morning hours just before sunrise, between 5h00 and 6h00, as persisting nocturnal inversion layers would have inhibited temperature variations (Figure 5.11). Thereafter convective warming of the surface increased ambient air temperatures gradually until they reached a maximum between 12h00 and 16h00 depending on the season (Figure 5.11). Following this temperatures start to gradually decline until sunset between 18h00 and 19h00 (Figure 5.11).

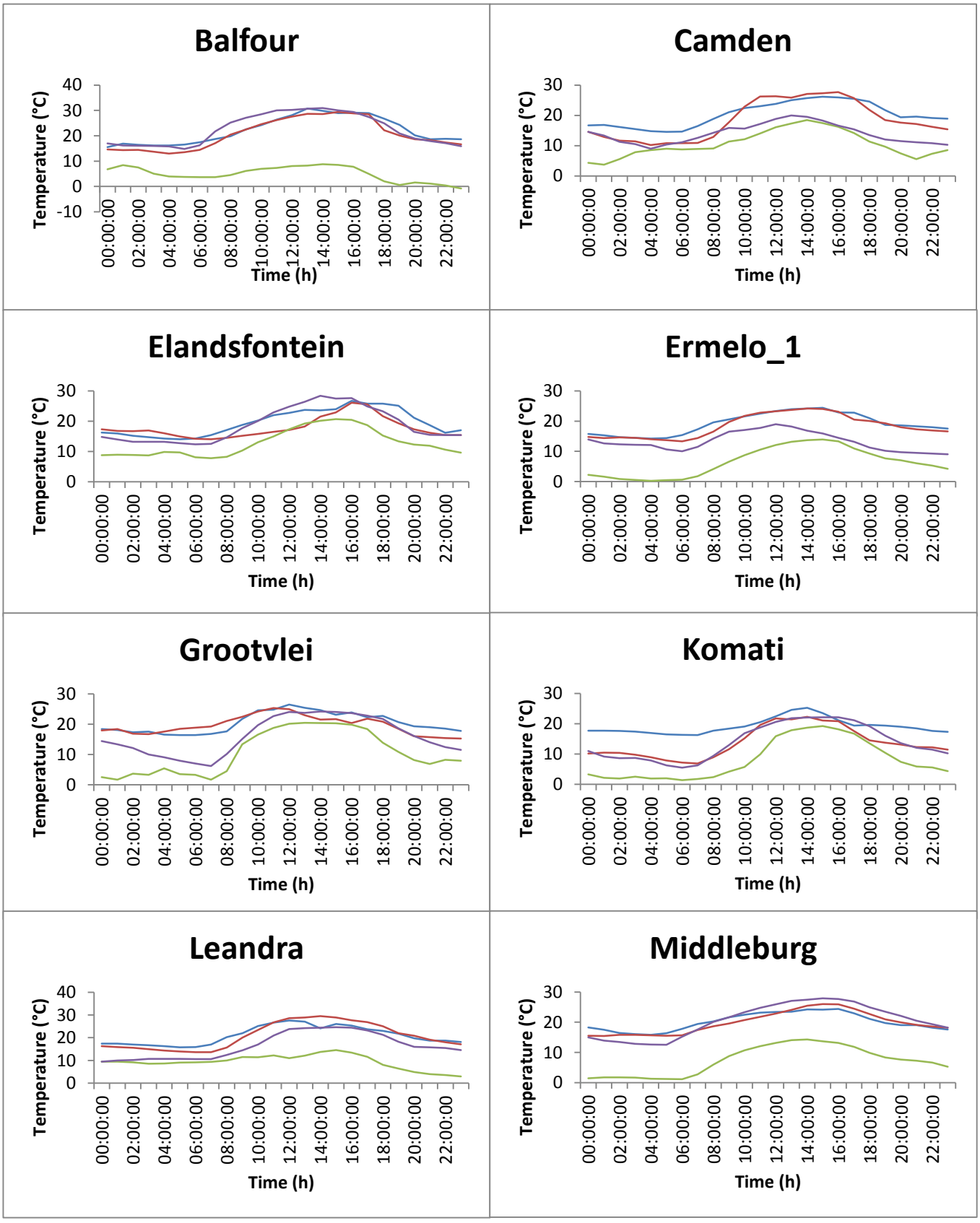

Figure 5.11: Diurnal variation of temperature. Each line represents a season. Blue – Summer; Red – Autumn; Green – Winter; Purple – Spring.

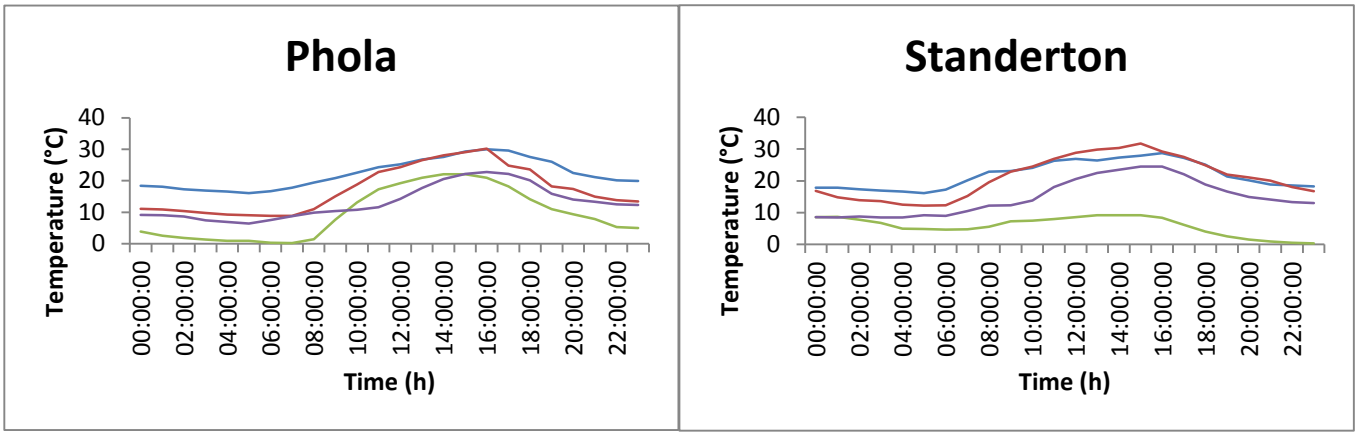

Figure 5.11 continued: Diurnal variation of temperature. Each line represents a season. Blue – Summer; Red – Autumn; Green – Winter; Purple – Spring.

5.2.2. Solar radiation

Solar radiation levels ranged between 0 and 1000 W.m^{-2} (Figure 5.12; Appended figure 8.8). During winter the maximum ranged between 400 and 740 W.m^{-2} (Figure 5.12; Appended figure 8.8). During summer the solar radiation levels were typically higher ranging between 800 and 1000 W.m^{-2}, where the maximum solar radiation recorded was 1100 W.m^{-2} during January (Appended figure 8.8). Average solar radiation values ranged between 130 and 500 W.m^{-2} (Appended figure 8.8), where the summer average was about 400 W.m^{-2} and the winter average was about 200 W.m^{-2} (Appended figure 8.8).

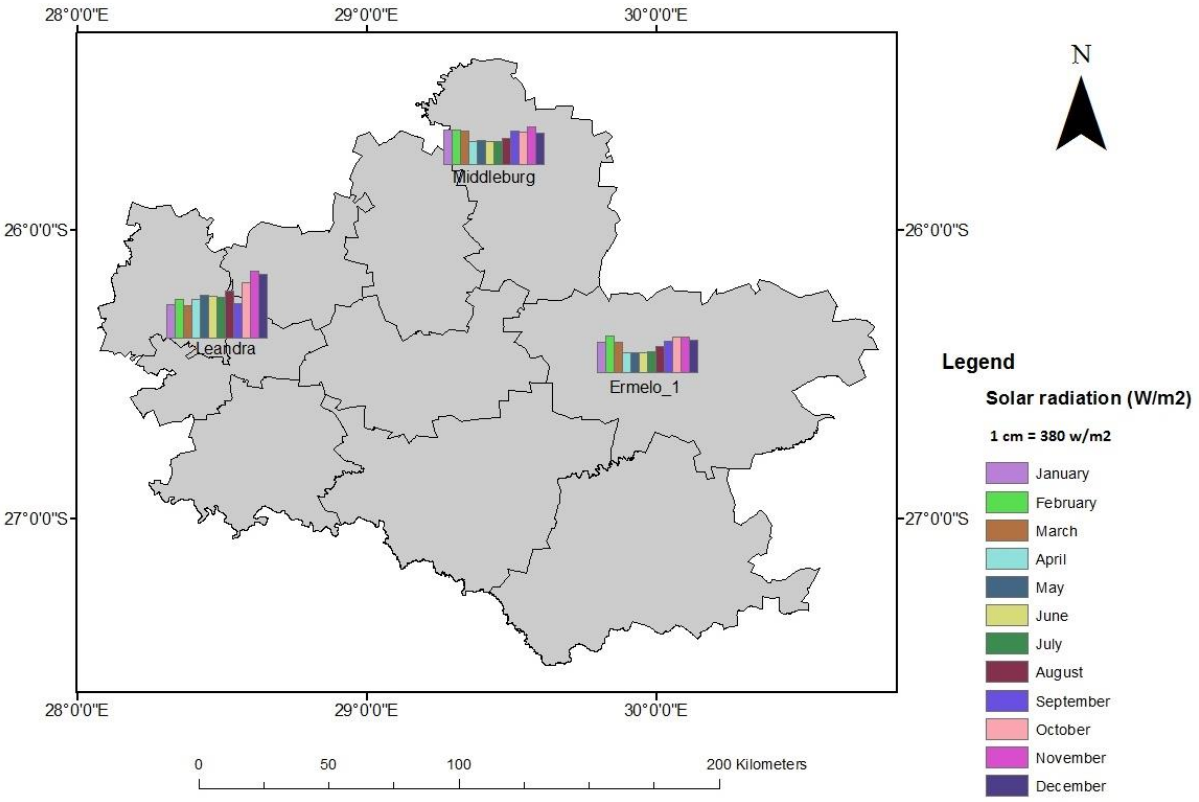

Figure 5.12: Map showing the monthly variation of solar radiation.

The diurnal variation of solar radiation was clear with no solar radiation before sunrise and after sunset (Figure 5.13). After sunrise, ~6h00, solar radiation levels gradually started rising to reach maximum levels around ~12h00 and 13h00 (Figure 5.13). Thereafter solar radiation levels started to gradually decline to 0 $W.m^{-2}$ by ~19h00 (Figure 5.13).

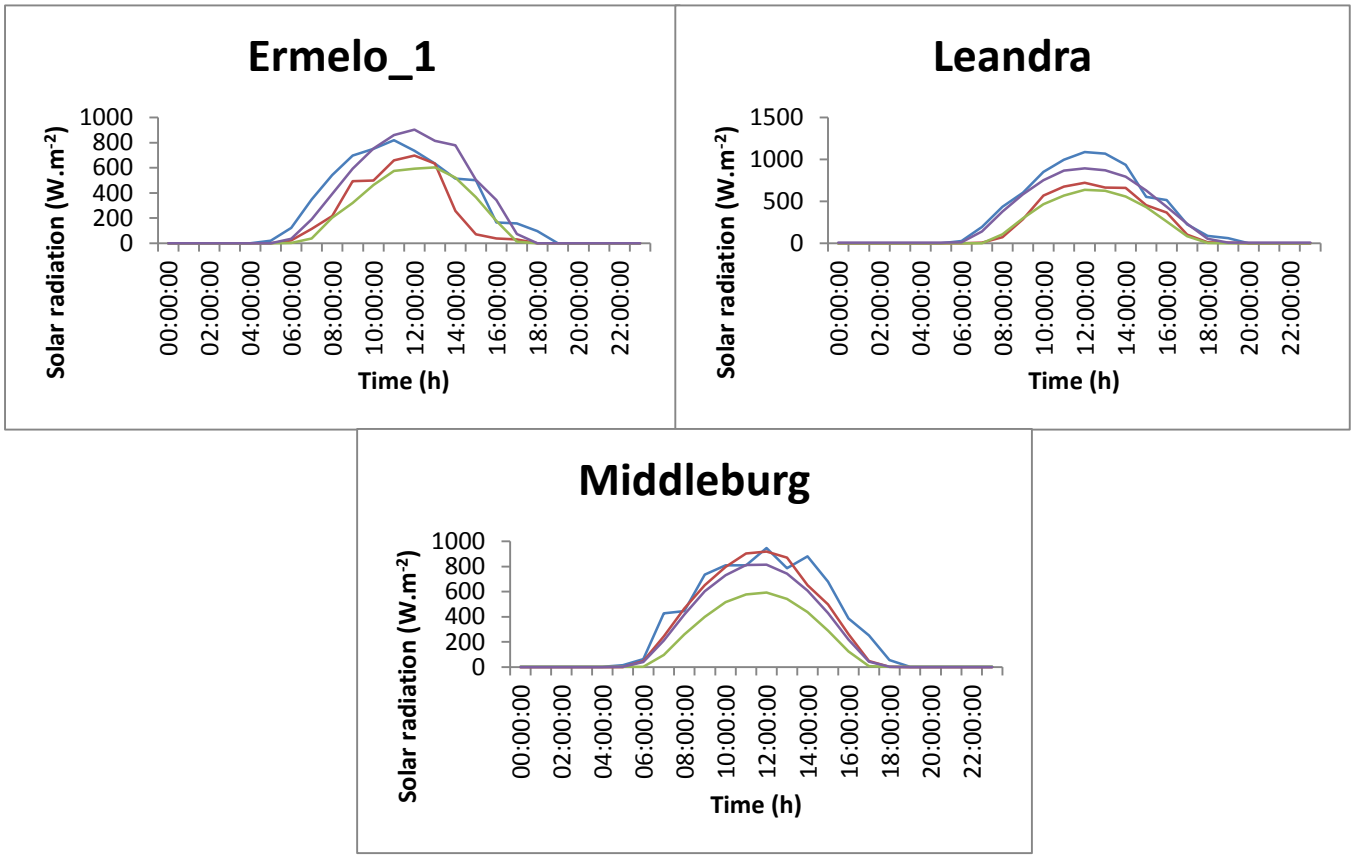

Figure 5.13: Diurnal variation of solar radiation. Each line represents a season. Blue – Summer; Red – Autumn; Green – Winter; Purple – Spring.

5.2.3. Relative Humidity

Relative humidity levels were higher during summer and lower during winter, and for Komati they showed a smaller variation with higher levels during winter and spring instead (Figure 5.14). During summer relative humidity levels were as high as 80 %, while during winter they dropped to around 50 % (Figure 5.14; Appended figure 8.9). During summer, higher relative humidity levels would have promoted cloud formation due to the frequent occurrence of easterly lows whereas during winter semi-permanent high pressure cells

would have promoted low relative humidity levels and almost no cloud cover across the HPA.

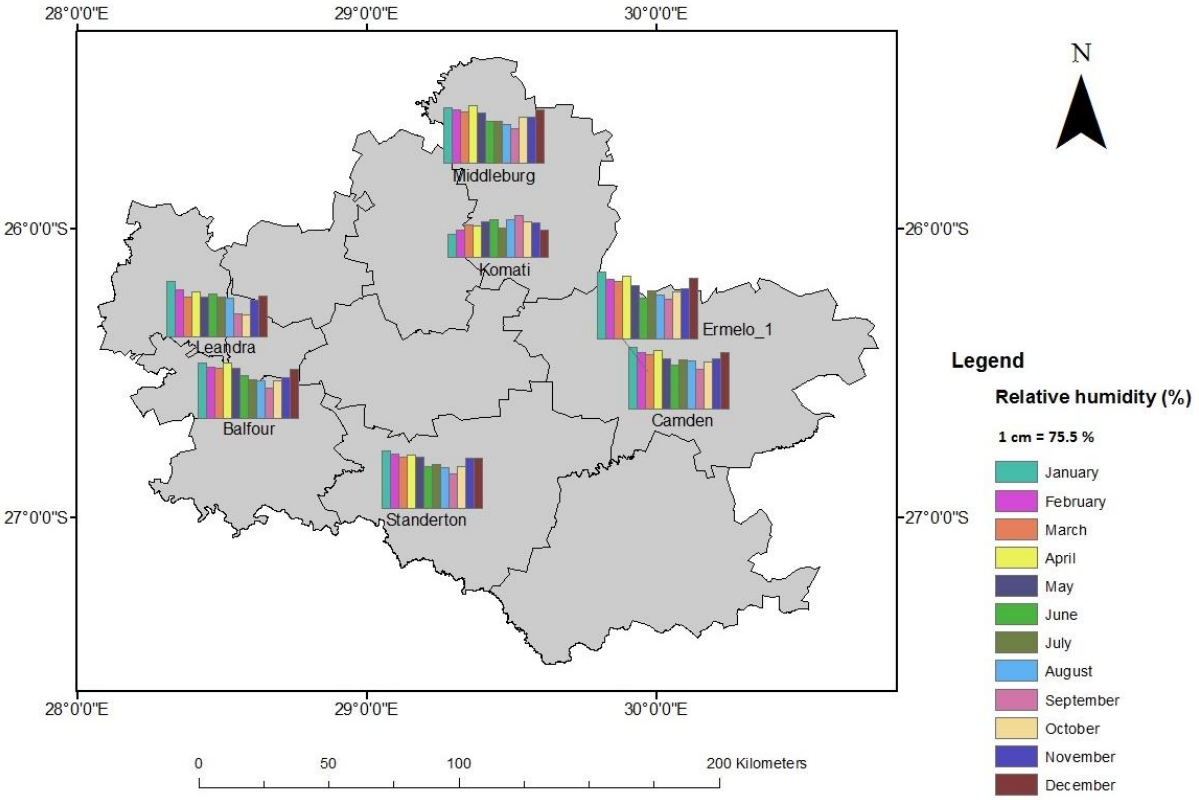

Figure 5.14: Map showing the monthly variation of relative humidity.

Relative humidity levels were high and steady during the night and early morning hours due to persistent nocturnal inversion layers (Figure 5.15). After sunrise, ~6h00, relative humidity levels began to gradually decline until minimum levels of about ~40 % were reached (Figure 5.15). Thereafter relative humidity levels started to gradually rise until sunset, ~19h00 (Figure 5.15).

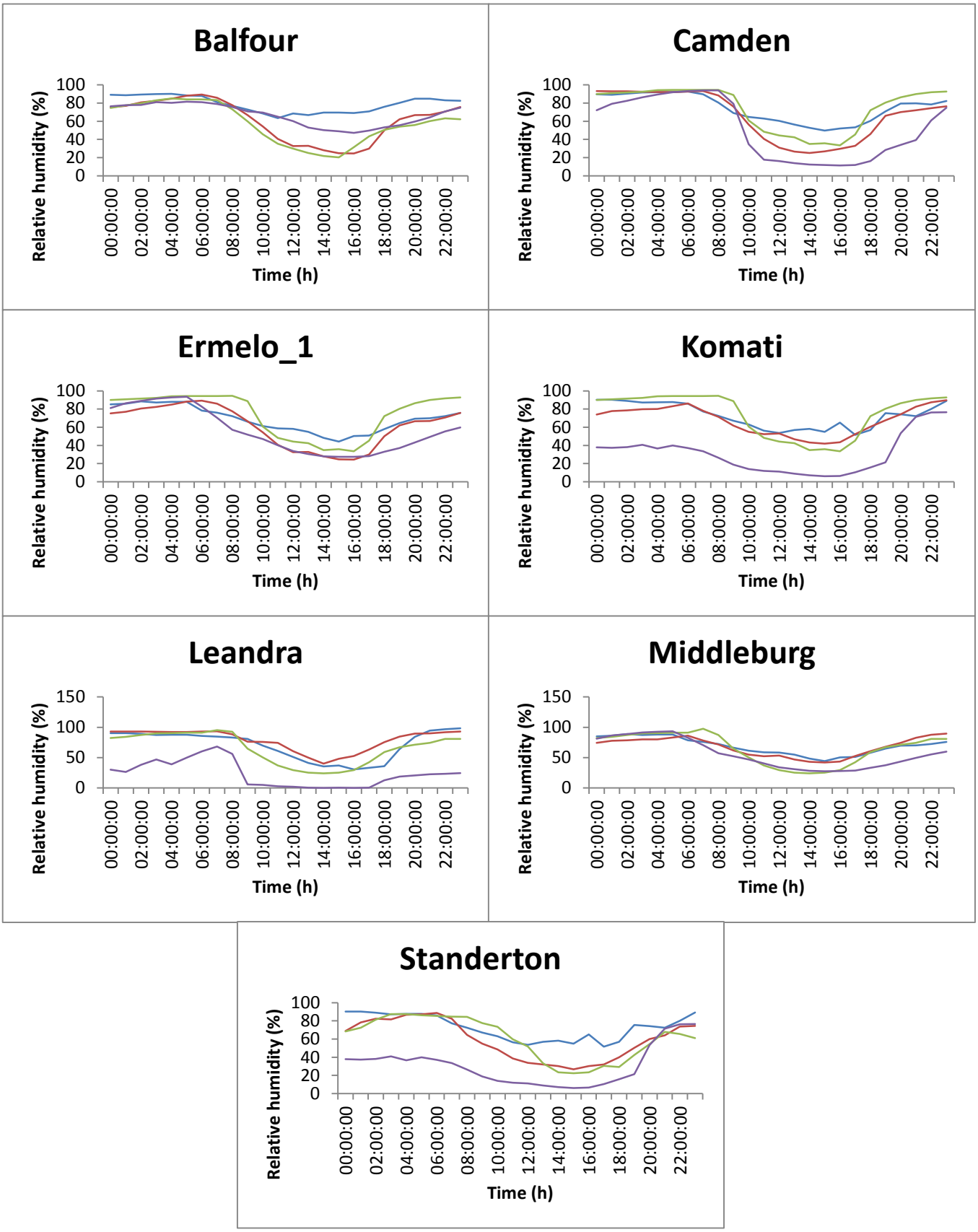

Figure 5.15: Diurnal variation of relative humidity. Each line represents a season. Blue – Summer; Red – Autumn; Green – Winter; Purple – Spring.

5.2.4. Rainfall

Rainfall fell mainly during summer, particularly from October through to March, when easterly waves persisted (Figure 5.16; Appended figure 8.10) (Tyson and Preston-Whyte, 2000). During winter rainfall rarely fell (Figure 5.16; Appended figure 8.10). Rainfall levels ranged between 10 and 230 mm per month during October to March rainfall season and during the rest of the year they ranged between 0 and 60 mm per month (Appended figure 8.10).

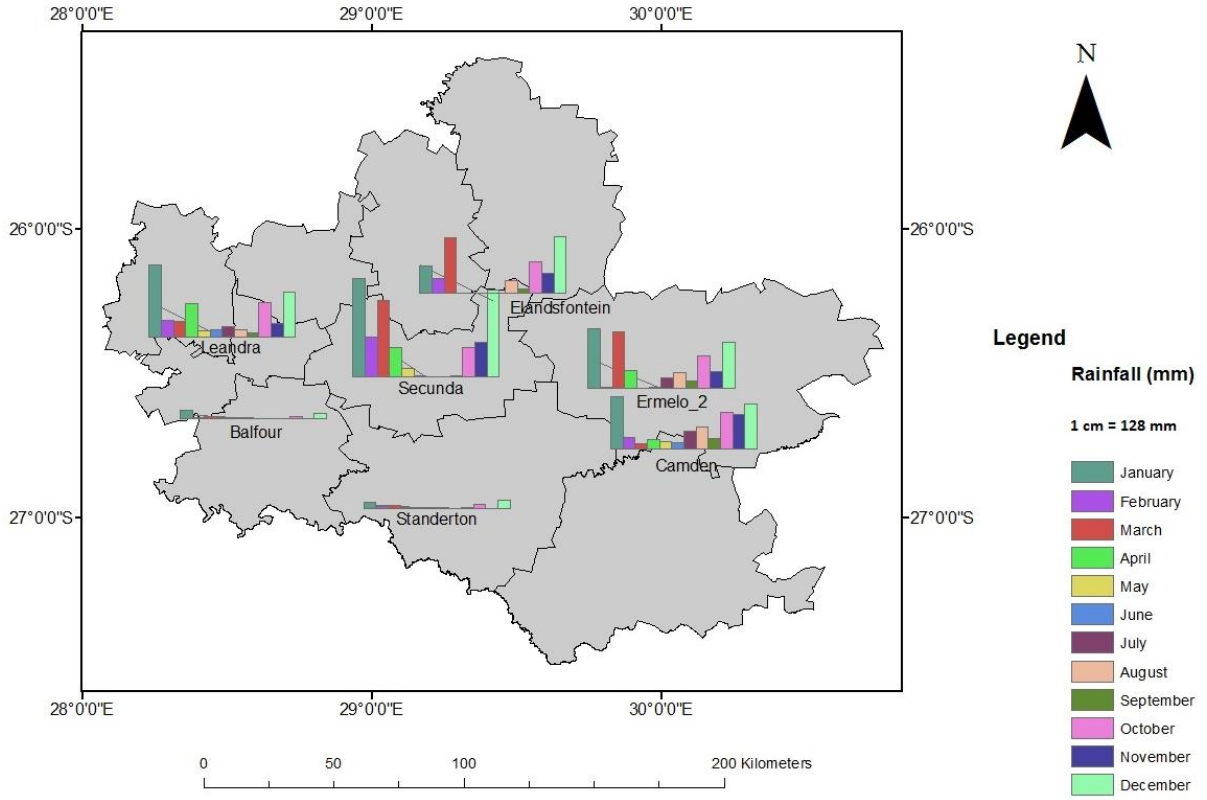

Figure 5.16: Map showing the monthly level of rainfall.

5.2.5. Wind speed

Wind speeds were similar throughout the year (Figure 5.17; Appended figure 8.12). Average wind speeds ranged between 1.7 and 16 $m.s^{-1}$ (Figure 5.17; Appended figure 8.12). Minimum wind speeds were as low as 0 $m.s^{-1}$ and ranged between 0 and 1.5 $m.s^{-1}$ (Figure 5.17; Appended figure 8.12). The maximum wind speeds recorded ranged between 5 and 16 $m.s^{-1}$, where the highest recorded wind speed was 15.88 $m.s^{-1}$ (Figure 5.17; Appended figure 8.12).

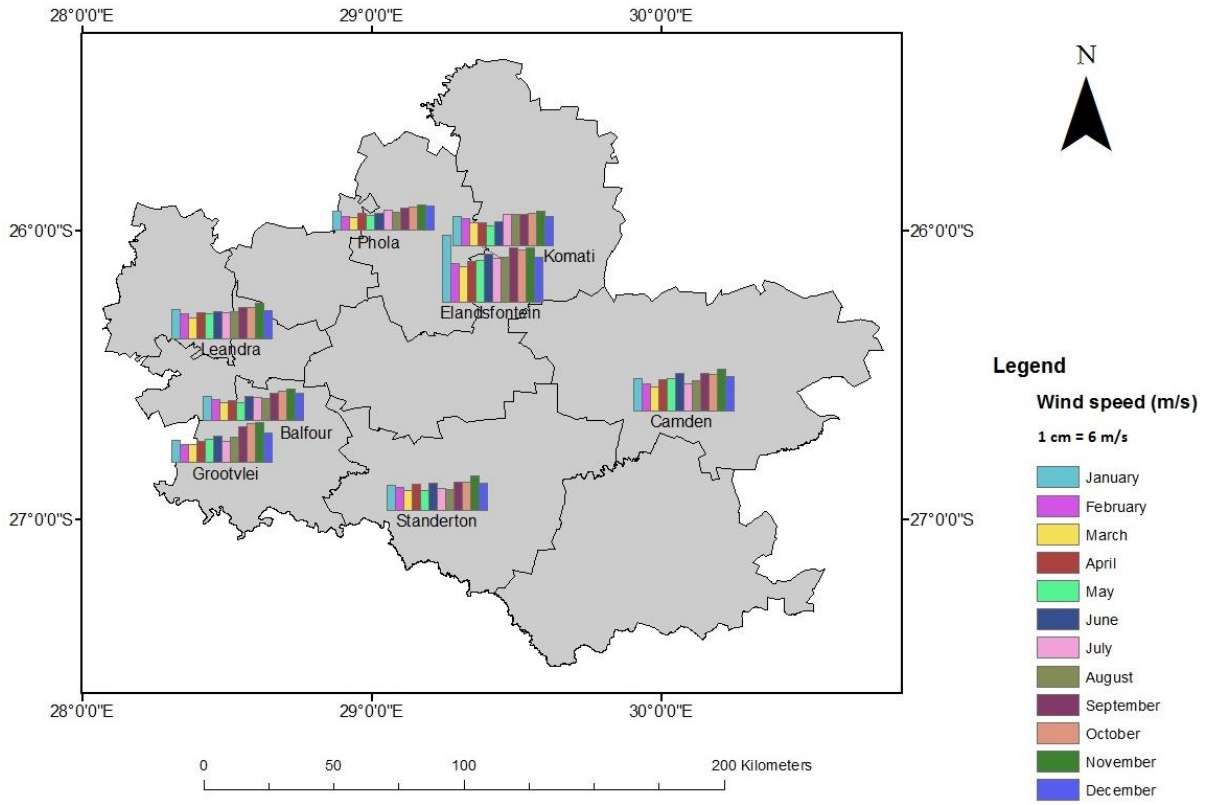

Figure 5.17: Map showing the monthly variation of wind speed.

Between ~18h00 and 6h00 nocturnal inversion layers persist (Tyson and Preston-Whyte, 2000). During this time meteorological variables are typically stable and wind speeds during this time were no different (Figure 5.18). After 6h00 wind speeds started to gradually rise until a maximum was reached between 12h00 and 15h00 (Figure 5.18). Thereafter wind speeds started to gradually decline (Figure 5.18).

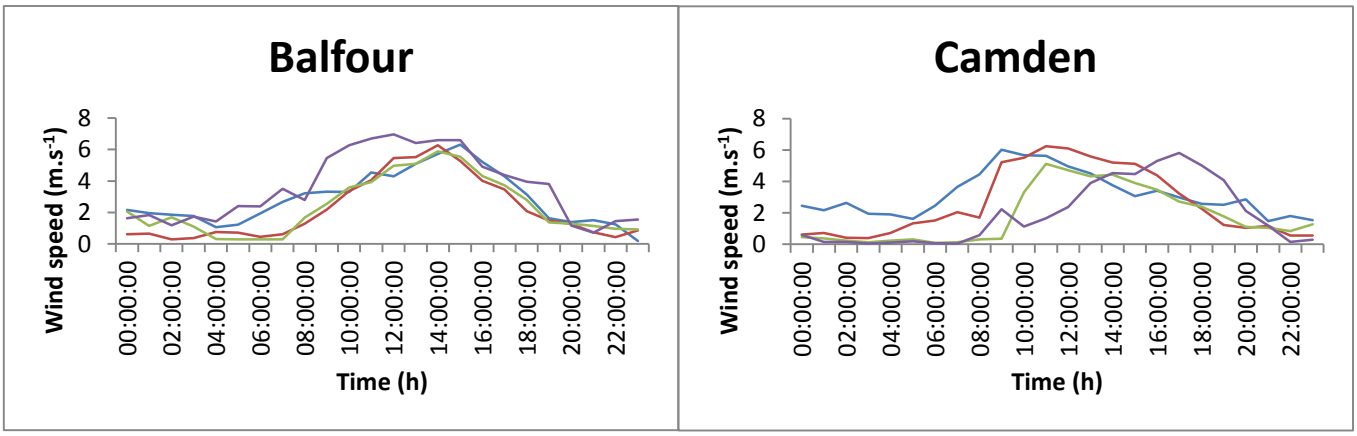

Figure 5.18: Diurnal variation of wind speed. Each line represents a season. Blue – Summer; Red – Autumn; Green – Winter; Purple – Spring.

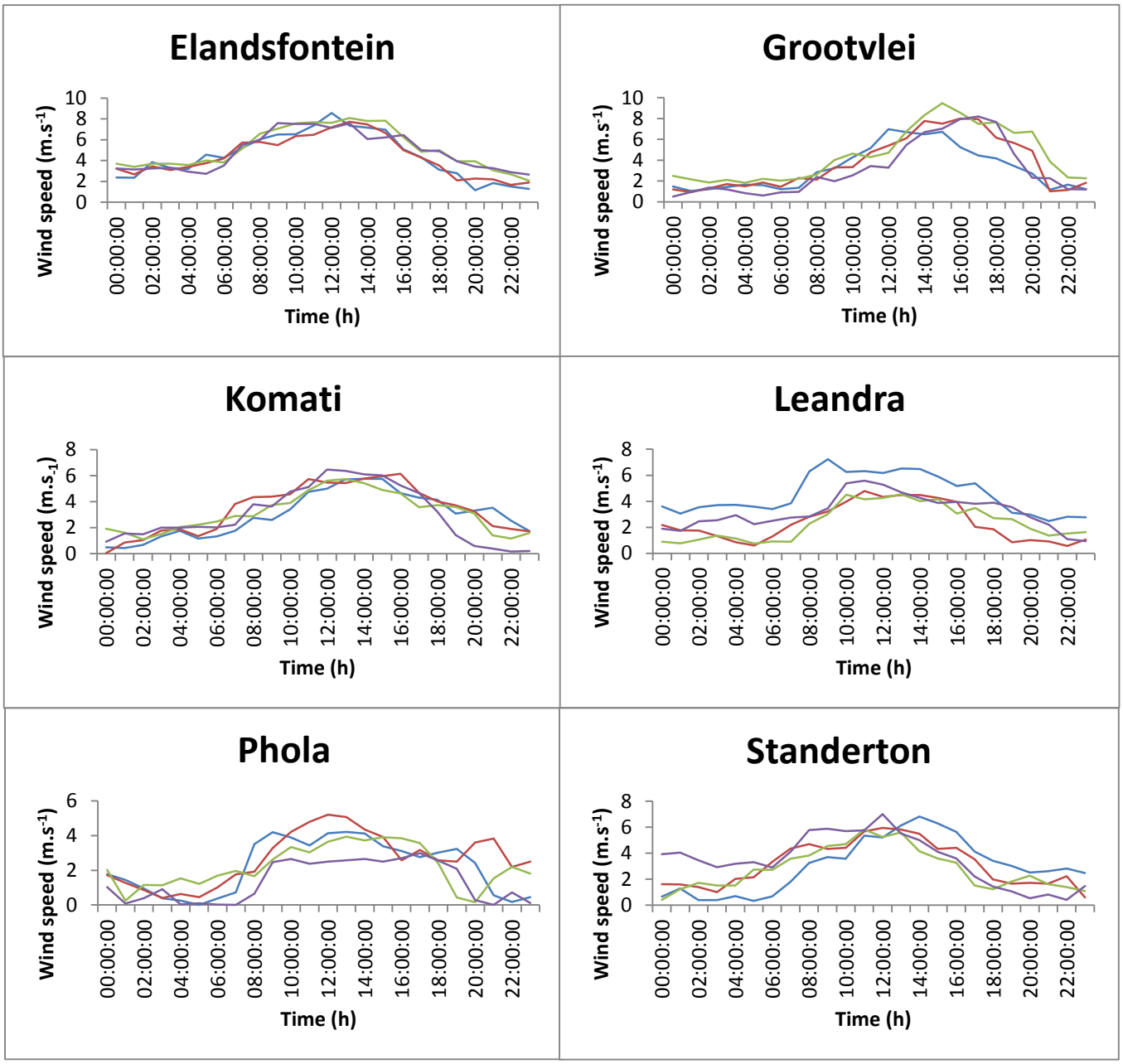

Figure 5.18 continued: Diurnal variation of wind speed. Each line represents a season. Blue – Summer; Red – Autumn; Green – Winter; Purple – Spring.

5.2.6. Wind direction

Monthly wind directions ranged from N to E during January to April, summer and autumn (Figure 5.19). From May to December they ranged between S and NW (Figure 5.19).

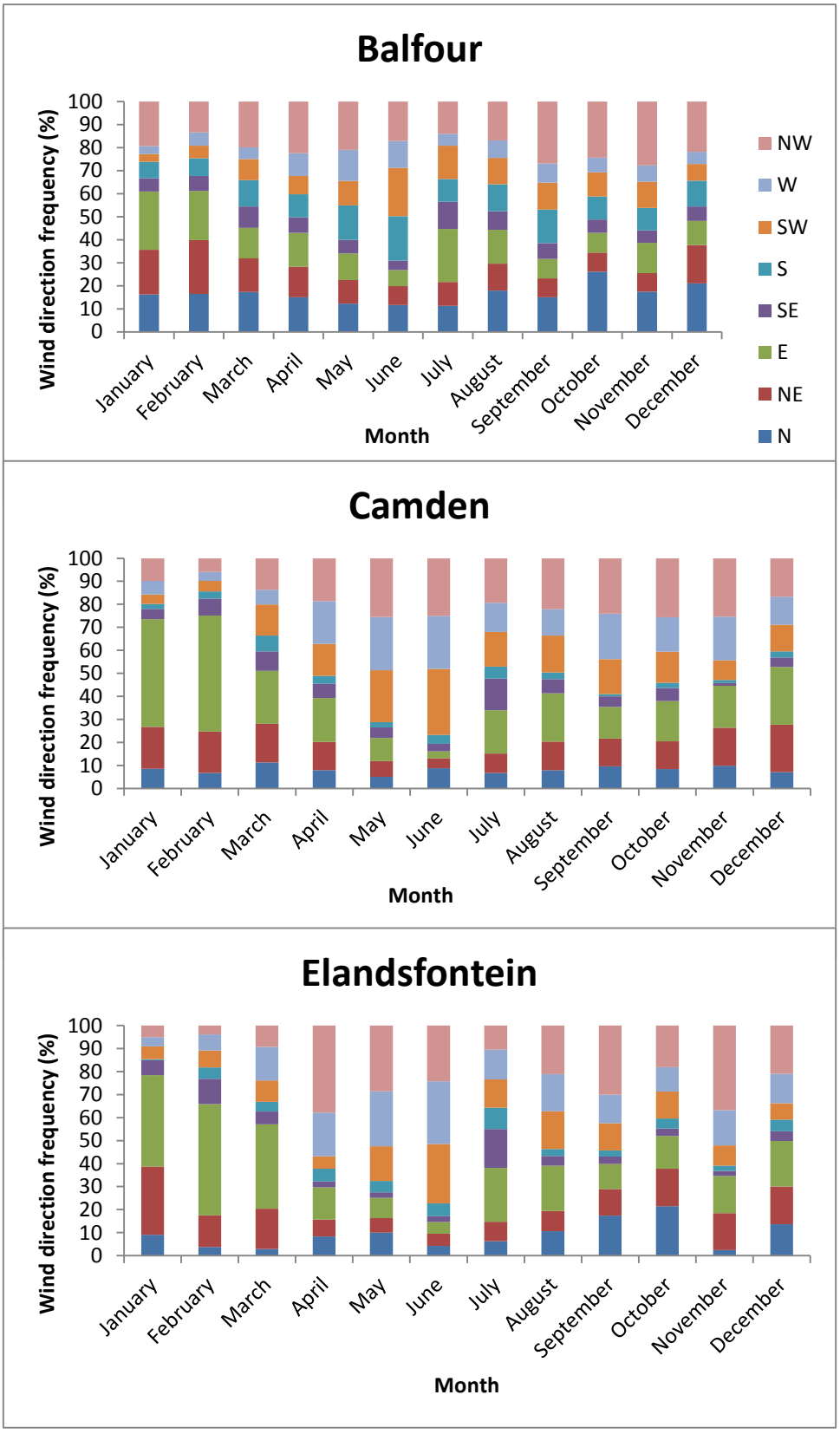

Figure 5.19: Monthly variation of wind direction.

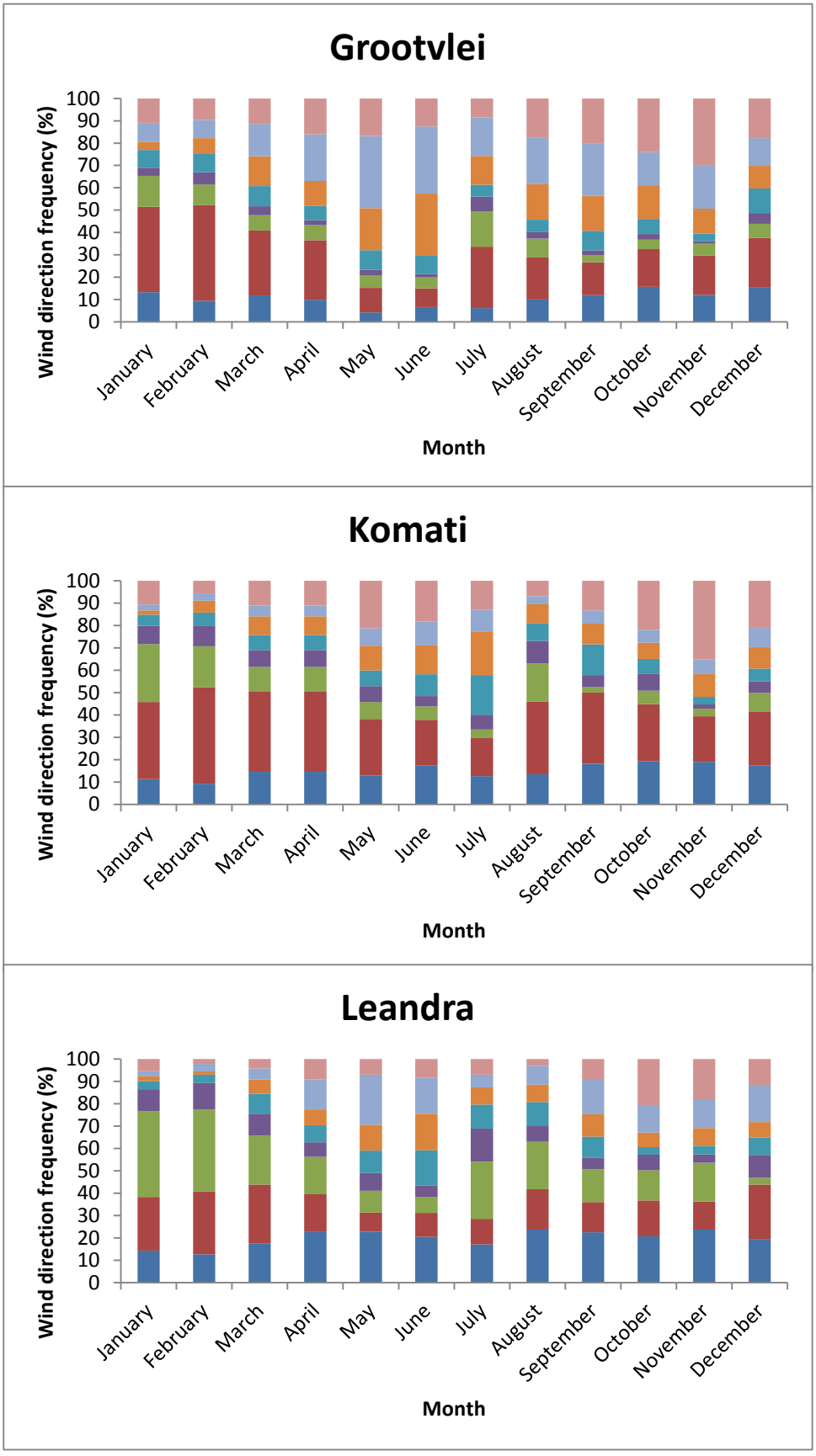

Figure 5.19 continued: Monthly variation of wind direction.

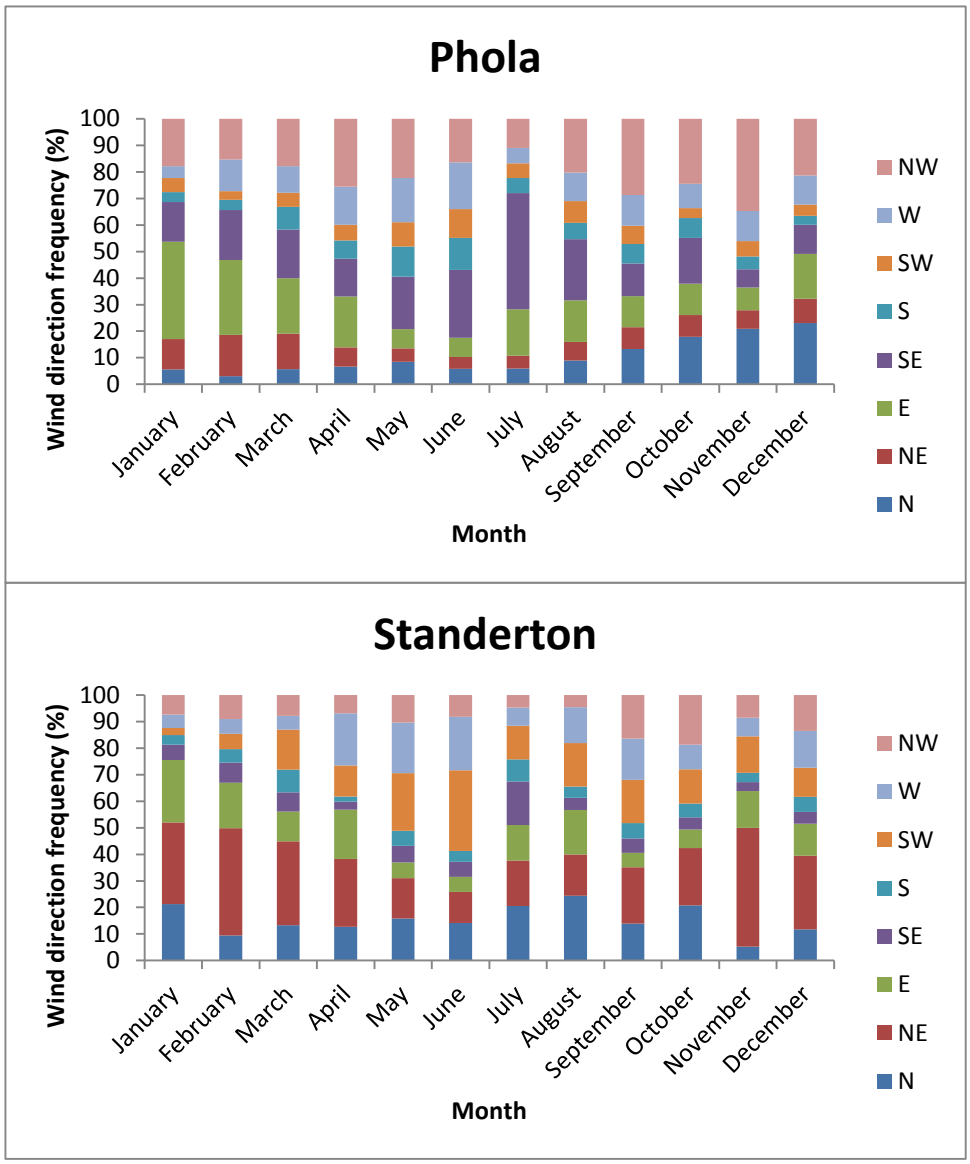

Figure 5.19 continued: Monthly variation of wind direction.

5.2.7. Atmospheric pressure

Anticyclonic semi-permanent high pressure systems dominate throughout the year (Tyson and Preston-Whyte, 2000). During summer easterly wave disturbances occur lowering the average monthly atmospheric pressure values (Appended figure 8.11). The atmospheric pressure was stable ranging between 800 and 840 hPa throughout the year (Figure 5.20; Appended figure 8.11).

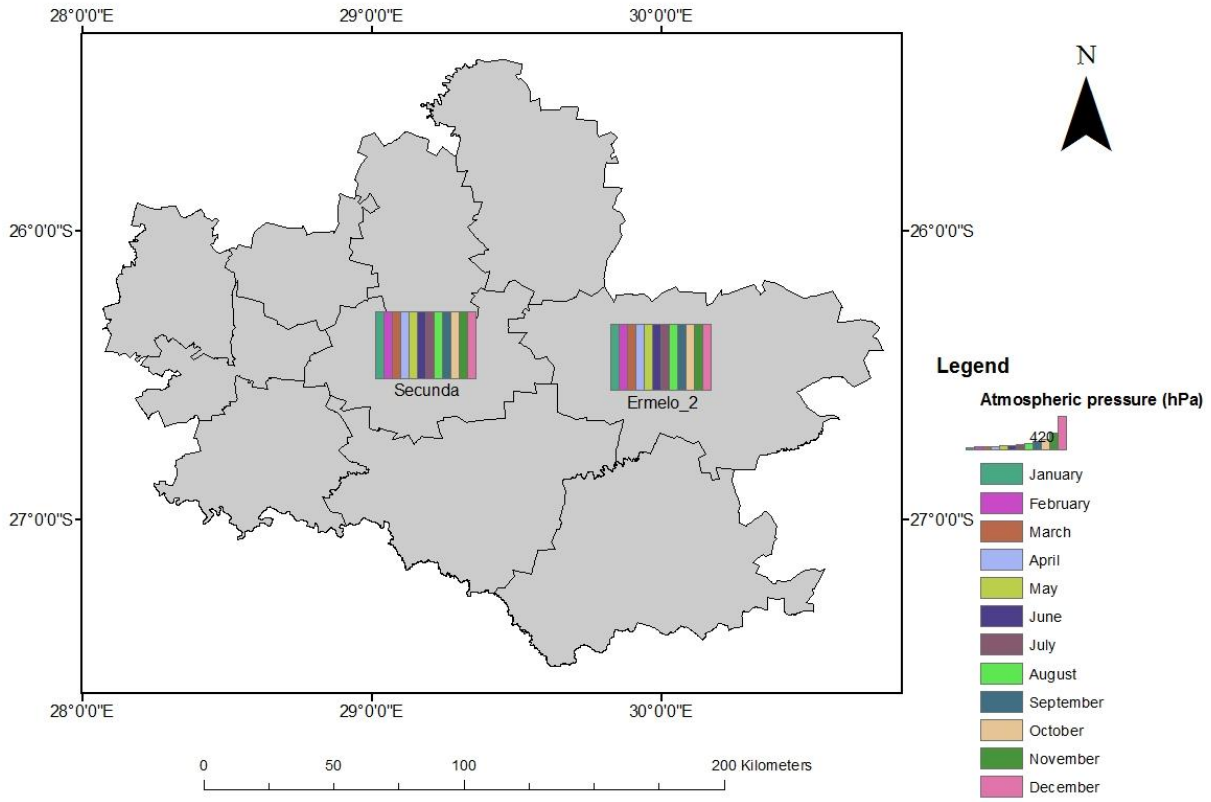

Figure 5.20: Map showing the monthly variation of atmospheric pressure.

5.3. The relationship of meteorology and pollutants across the HPA

Air quality is influenced by prevailing meteorology. Meteorology plays an important role in the formation, accumulation, transportation and destruction of both primary and secondary pollutants. As a result the relationship between some meteorological parameters and SO_2, NO_x and surface O_3 has been analysed across the HPA.

5.3.1. SO_2

SO_2 typically displayed a weak significant or insignificant relationship to most meteorological parameters similar to other studies (Table 5.1) (For example: Kartal and Özer, 1998; Cuhadaroglu and Dermici, 1997; Elminir, 2005; Turalioğlu *et al.*, 2005; Akpinar *et al.*, 2008; Ilten and Selici, 2008; Akpinar *et al.*, 2009; Lin *et al.*, 2011). Few relationships were found to be significant (Table 5.1). The relationship of SO_2 to temperature and solar radiation was positive similar to other studies (For example: Cuhadaroglu and Dermici, 1997; Kartal and Özer, 1998). Temperature was shown to be negatively related similar to a few studies (Table 5.1) (For example: Elminir, 2005; Turalioğlu *et al.*, 2005; Akpinar *et al.*, 2008; Ilten and Selici,

2008; Akpinar *et al.*, 2009; Lin *et al.*, 2011). Akpinar *et al.* (2008) found a negative relationship between SO_2 and solar radiation. Relative humidity, wind speed, wind direction and rainfall were found to be negative and insignificantly related to meteorology (Table 5.1) similar to most studies (For example: Cuhadaroglu and Dermici, 1997; Akpinar *et al.*, 2005; Elminir, 2005; Turalioğlu *et al.*, 2005; Ilten and Selici, 2008; Akpinar *et al.*, 2009; Lin *et al.*, 2011).

Table 5.1: Strength of the relationship between SO_2 and each meteorological variable. Statistically significant correlations are indicated by an asterisk; no data is represented by -.

Pollutant: SO_2										
		Monitoring station strength of relationship (r)								
Month	**Meteorological variable**	**Balfour**	**Camden**	**Elandsfontein**	**Ermelo**	**Grootvlei**	**Komati**	**Leandra**	**Middleburg**	**Phola**
January	Temperature (°C)	0.20	0.22	*0.31	0.28	0.14	*0.38	0.27	0.24	0.22
	Solar radiation ($W.m^{-2}$)	-	-	-	0.28	-	-	0.23	0.20	-
	Relative humidity (%)	-0.25	-0.29	-	-0.26	-	-0.03	-0.05	-0.28	-
	Wind speed ($m.s^{-1}$)	-0.06	-0.23	-0.27	-	-0.02	-0.09	-0.03	-	-0.10
	Wind direction (°)	-0.17	-0.29	-0.25	-	-0.11	-0.08	-0.18	-	-0.07
	Rainfall (mm)	-0.04	-0.04	-0.08	-	-	-	-0.0004	-	-
February	Temperature (°C)	*0.36	0.31	0.27	*0.34	*0.31	0.26	0.26	*0.58	*0.34
	Solar radiation ($W.m^{-2}$)	-	-	-	*0.31	-	-	*0.33	*0.37	-
	Relative humidity (%)	*-0.38	-0.28	-	*-0.35	-	-0.0002	-0.11	*-0.53	-
	Wind speed ($m.s^{-1}$)	-0.09	-0.05	-0.27	-	-0.02	-0.11	-0.01	-	-0.09
	Wind direction (°)	-0.14	-0.23	*-0.40	-	-0.15	-0.07	-0.17	-	-0.05
	Rainfall (mm)	-0.04	-0.02	-0.01	-	-	-	-0.06	-	-
March	Temperature (°C)	*0.39	*0.39	0.28	*0.36	*0.40	*0.41	*0.36	*0.38	0.28
	Solar radiation ($W.m^{-2}$)	-	-	-	0.29	-	-	*0.34	*0.36	-
	Relative humidity (%)	*-0.40	-0.28	-	*-0.35	-	-0.03	-0.28	*-0.32	-
	Wind speed ($m.s^{-1}$)	-0.20	-0.14	-0.15	-	-0.06	-0.18	-0.06	-	-0.11
	Wind direction (°)	-0.05	-0.18	-0.33	-	-0.10	-0.04	-0.02	-	-0.05
	Rainfall (mm)	-0.01	-0.01	-0.004	-	-	-	-0.06	-	-
April	Temperature (°C)	0.21	*0.32	*0.51	0.18	0.28	*0.47	0.10	*0.30	0.23
	Solar radiation ($W.m^{-2}$)	-	-	-	0.22	-	-	0.20	*0.41	-
	Relative humidity (%)	-0.22	*-0.37	-	-0.23	-	-0.14	-0.02	*-0.46	-
	Wind speed ($m.s^{-1}$)	-0.06	*-0.35	-0.14	-	-0.06	-0.26	-0.09	-	-0.25
	Wind direction (°)	-0.13	-0.24	-0.16	-	-0.16	-0.04	-0.08	-	-0.08
	Rainfall (mm)	-0.01	-0.02	-0.03	-	-	-	-0.07	-	-
May	Temperature (°C)	0.20	*0.37	0.23	*0.39	0.21	0.25	0.08	0.18	-0.01
	Solar radiation ($W.m^{-2}$)	-	-	-	0.21	-	-	0.05	*0.31	-
	Relative humidity (%)	-0.24	*-0.46	-	*-0.42	-	-0.06	-0.02	*-0.36	-
	Wind speed ($m.s^{-1}$)	-0.19	*-0.31	-0.16	-	-0.03	-0.22	-0.06	-	-0.14
	Wind direction (°)	-0.03	-0.18	-0.09	-	-0.15	-0.07	-0.15	-	-0.19
	Rainfall (mm)	-0.04	-0.005	-0.02	-	-	-	-0.06	-	-

June	Temperature (°C)	0.28	*0.40	0.25	0.27	0.22	0.16	0.21	*0.31	0.07
	Solar radiation ($W.m^{-2}$)	-	-	-	0.07	-	-	0.20	*0.35	-
	Relative humidity (%)	-0.19	*-0.34	-	*-0.40	-	-0.10	-0.21	*-0.37	-
	Wind speed ($m.s^{-1}$)	-0.17	*-0.32	-0.04	-	-0.03	-0.06	-0.02	-	-0.005
	Wind direction (°)	-0.08	-0.16	-0.23	-	-0.07	-0.06	-0.12	-	-0.12
	Rainfall (mm)	-0.03	-0.03	-0.06	-	-	-	-0.05	-	-
July	Temperature (°C)	*0.30	*0.36	*0.38	*0.34	0.12	0.29	*0.35	0.25	0.10
	Solar radiation ($W.m^{-2}$)	-	-	-	0.09	-	-	0.29	*0.35	-
	Relative humidity (%)	-0.29	*-0.43	-	*-0.49	-	-0.11	-0.17	*-0.35	-
	Wind speed ($m.s^{-1}$)	-0.03	*-0.32	-0.05	-	-0.02	-0.26	-0.04	-	-0.08
	Wind direction (°)	-0.03	-0.21	*-0.36	-	-0.19	-0.02	-0.06	-	-0.27
	Rainfall (mm)	-0.03	-0.05	-0.05	-	-	-	-0.02	-	-
August	Temperature (°C)	0.20	*0.39	0.22	0.25	0.02	0.27	0.36	*0.42	0.10
	Solar radiation ($W.m^{-2}$)	-	-	-	0.10	-	-	0.26	*0.40	-
	Relative humidity (%)	-0.20	*-0.40	-	*-0.38	-	-0.08	-0.28	*-0.39	-
	Wind speed ($m.s^{-1}$)	-0.04	-0.13	-0.13	-	-0.04	-0.11	-0.01	-	-0.06
	Wind direction (°)	-0.01	-0.25	*-0.31	-	-0.19	-0.20	-0.08	-	-0.24
	Rainfall (mm)	-0.0002	-0.04	-0.05	-	-	-	-0.01	-	-
September	Temperature (°C)	0.10	*0.44	*0.38	*0.36	0.07	*0.38	*0.53	0.25	-0.07
	Solar radiation ($W.m^{-2}$)	-	-	-	0.16	-	-	*0.41	*0.32	-
	Relative humidity (%)	-0.03	*-0.40	-	*-0.43	-	-0.10	*-0.31	*-0.33	-
	Wind speed ($m.s^{-1}$)	-0.03	-0.25	-0.05	-	-0.02	-0.28	-0.04	-	-0.13
	Wind direction (°)	-0.06	-0.23	-0.20	-	-0.10	-0.04	0.02	-	-0.19
	Rainfall (mm)	-0.03	-0.02	-0.02	-	-	-	-0.01	-	-
October	Temperature (°C)	0.12	*0.42	0.28	*0.35	0.14	*0.34	*0.45	*0.30	-0.12
	Solar radiation ($W.m^{-2}$)	-	-	-	0.13	-	-	*0.46	*-0.30	-
	Relative humidity (%)	-0.22	*-0.38	-	*-0.31	-	-0.13	-0.15	-0.17	-
	Wind speed ($m.s^{-1}$)	-0.07	-0.20	-0.18	-	-0.20	-0.16	-0.01	-	-0.21
	Wind direction (°)	-0.01	-0.23	-0.19	-	-0.16	-0.16	-0.01	-	*-0.37
	Rainfall (mm)	-0.06	-0.01	-0.07	-	-	-	-0.13	-	-
November	Temperature (°C)	0.11	*0.42	0.11	0.09	0.04	0.26	*0.32	0.15	-0.25
	Solar radiation ($W.m^{-2}$)	-	-	-	0.20	-	-	*0.30	0.11	-
	Relative humidity (%)	-0.01	*-0.39	-	-0.18	-	-0.03	-0.03	-0.18	-
	Wind speed ($m.s^{-1}$)	-0.10	-0.18	-0.13	-	-0.04	-0.13	-0.04	-	-0.28
	Wind direction (°)	-0.10	*-0.32	-0.12	-	-0.16	-0.01	-0.07	-	-0.23
	Rainfall (mm)	-0.002	-0.04	-0.03	-	-	-	-0.06	-	-
December	Temperature (°C)	0.09	*0.41	*0.35	0.09	0.14	*0.38	0.19	*0.34	0.09
	Solar radiation ($W.m^{-2}$)	-	-	-	0.11	-	-	0.29	0.11	-
	Relative humidity (%)	-0.10	*-0.40	-	-0.17	-	-0.11	-0.13	-0.21	-
	Wind speed ($m.s^{-1}$)	-0.10	-0.16	-0.24	-	-0.003	-0.21	-0.18	-	-0.03
	Wind direction (°)	-0.12	*-0.41	-0.18	-	-0.05	-0.02	-0.08	-	-0.11
	Rainfall (mm)	-0.01	-0.07	-0.07	-	-	-	-0.06	-	-

Atmospheric pressure was significantly and positively related to SO_2 across the HPA, similar to many studies (For example: Turalioğlu *et al.*, 2005; Akpinar *et al.*, 2009) (Table 5.8). Hence, across the HPA increasing atmospheric pressure generally resulted in an increase in SO_2 concentrations during 2011.

Table 5.2: Strength of the relationship between SO_2 and atmospheric pressure. Statistically significant correlations are indicated by an asterisk; relationships with a correlation coefficient greater than 0.7 highlighted by a double asterisk.

Monitoring station	Strength of relationship (r)
Ermelo	*0.44
Secunda	**0.72

Meteorological governance of SO_2 concentrations were location specific, as seen by the range in R^2 values (0.03 to 0.29), whereby only 3 to 29 % of SO_2 could be explained by meteorology (Table 5.3). This suggests complexity in the factors governing SO_2 concentrations across the HPA. Low R^2 values, low significance values and high standard error values (10.55 and 17.32 ppb) suggest that meteorology was not the only factor governing SO_2 concentrations similar to Turaliğlu *et al.* (2005). Temperature and solar radiation were found to be positively related to SO_2, therefore as solar radiation and temperatures increased SO_2 concentrations increased (Table 5.3). Relative humidity, rainfall, wind speed and wind direction were all found to be negatively related to SO_2, therefore as each of these factors increased SO_2 concentrations as a result decreased, i.e. faster wind speeds diluted air, while higher levels of relative humidity promoted cloud cover as well as rainfall which removed SO_2.

Table 5.3: The relationship of SO_2 to meteorology. A statistically significant correlation is indicated by an asterisk. (T: Temperature; S: Solar radiation; RH: Relative humidity; WS: Wind speed; WD: Wind direction; R: Rainfall).

Monitoring station: Balfour		
$SO_2 = 9.045 - 0.287$ [R] $- 0.53$ [RH] $+ 0.307$ [T] $- 0.013$ [WD] $- 0.273$ [WS]		
Coefficient of determination (R^2)	Standard error (σ_{est})	Significance of correlation (p)
0.07	10.55	0.88
Monitoring station: Camden		
$SO_2 = 8.929 - 0.056$ [R] $- 0.150$ [RH] $+ 0.137$ [T] $- 0.028$ [WD] $- 0.583$ [WS]		
Coefficient of determination (R^2)	Standard error (σ_{est})	Significance of correlation (p)
*0.19	13.63	0.02

Monitoring station: Elandsfontein		
SO_2 = 8.772 - 0.375 [R] + 0.419 [T] - 0.035 [WD] - 1.287 [WS]		
Coefficient of determination (R^2)	Standard error (σ_{est})	Significance of correlation (p)
*0.10	16.94	0.004
Monitoring station: Ermelo		
SO_2 = 55.912 - 0.358 [RH] + 0.006 [S] + 0.945 [T]		
Coefficient of determination (R^2)	Standard error (σ_{est})	Significance of correlation (p)
0.29*	14.30	0.0001
Monitoring station: Grootvlei		
SO_2 = 8.409 + 0.313 [T] - 0.021 [WD] - 0.462 [WS]		
Coefficient of determination (R^2)	Standard error (σ_{est})	Significance of correlation (p)
0.04	15.43	0.70
Monitoring station: Komati		
SO_2 = -2.339 - 0.010 [RH] + 0.790 [T] - 0.016 [WD] - 0.482 [WS]		
Coefficient of determination (R^2)	Standard error (σ_{est})	Significance of correlation (p)
*0.10	17.32	0.01
Monitoring station: Leandra		
SO_2 = 14.840 - 0.189 [R] - 0.043 [RH] + 0.011 [S] + 0.175 [T] - 0.031 [WD] - 0.711 [WS]		
Coefficient of determination (R^2)	Standard error (σ_{est})	Significance of correlation (p)
0.15*	13.00	<0.001
Monitoring station: Middleburg		
SO_2 = 23.355 - 0.177 [RH] + 0.006 [S] + 0.375 [T] - 0.003 [WD] - 0.649 [WS]		
Coefficient of determination (R^2)	Standard error (σ_{est})	Significance of correlation (p)
0.17*	10.69	0.060
Monitoring station: Phola		
SO_2 = 18.574 + 0.054 [T] - 0.010 [WD] - 1.512 [WS]		
Coefficient of determination (R^2)	Standard error (σ_{est})	Significance of correlation (p)
0.03	15.39	0.02

5.3.2. NO_x

NO_x was found to be insignificantly and negatively related to most meteorological parameters similar to other studies (Table 5.4) (For example: Kuebler *et al.*, 2001; Pudasainee *et al.*, 2006; Lin *et al.*, 2011 Hassan *et al.*, 2013). The strength of relationships were location specific where only a few locations yielded significant relationships (Table 5.4).

Table 5.4: Strength of the relationship between NO_x and each meteorological variable. Statistically significant correlations are indicated by an asterisk; no data is represented by -.

Pollutant: NO_x							
		Monitoring station strength of relationship (r)					
Month	**Meteorological variable**	**Balfour**	**Camden**	**Grootvlei**	**Leandra**	**Middleburg**	**Phola**
January	Temperature (°C)	-0.11	-0.20	-0.03	-0.27	-0.06	*-0.35
	Solar radiation ($W.m^{-2}$)	-	-	-	-0.17	-0.08	-
	Relative humidity (%)	-0.10	-0.25	-	-0.01	-0.05	-
	Wind speed ($m.s^{-1}$)	-0.02	-0.28	-0.14	-0.04	-	-0.09
	Wind direction (°)	-0.24	-0.30	-0.24	-0.09	-	-0.03
	Rainfall (mm)	-0.02	-0.04	-	-0.12	-	-
February	Temperature (°C)	-0.20	-0.10	-0.12	*-0.32	-0.01	-0.14
	Solar radiation ($W.m^{-2}$)	-	-	-	-0.35	-0.10	-
	Relative humidity (%)	-0.18	-0.12	-	-0.02	-0.01	-
	Wind speed ($m.s^{-1}$)	-0.04	-0.26	-0.13	-0.11	-	-0.04
	Wind direction (°)	-0.18	-0.28	-0.20	-0.17	-	-0.07
	Rainfall (mm)	-0.01	-0.03	-	-0.05	-	-
March	Temperature (°C)	-0.01	-0.003	-0.03	-0.17	-0.09	-0.004
	Solar radiation ($W.m^{-2}$)	-	-	-	-0.23	-0.11	-
	Relative humidity (%)	-0.06	-0.02	-	-0.04	-0.05	-
	Wind speed ($m.s^{-1}$)	-0.28	-0.23	-0.26	-0.04	-	-0.01
	Wind direction (°)	-0.10	-0.26	-0.10	-0.01	-	-0.05
	Rainfall (mm)	-0.03	-0.02	-	-0.01	-	-
April	Temperature (°C)	*-0.46	-0.05	-0.0005	-0.004	-0.16	-0.19
	Solar radiation ($W.m^{-2}$)	-	-	-	-0.02	-0.11	-
	Relative humidity (%)	-0.15	-0.21	-	-0.07	-0.14	-
	Wind speed ($m.s^{-1}$)	*-0.43	-0.12	-0.26	-0.10	-	*-0.30
	Wind direction (°)	-0.29	-0.24	-0.26	-0.12	-	*-0.41
	Rainfall (mm)	-0.03	-0.04	-	-0.02	-	-
May	Temperature (°C)	-0.28	-0.0003	-0.20	-0.05	-0.23	*-0.47
	Solar radiation ($W.m^{-2}$)	-	-	-	-0.04	-0.22	-
	Relative humidity (%)	-0.10	-0.15	-	-0.17	-0.16	-
	Wind speed ($m.s^{-1}$)	*-0.34	-0.02	-0.27	-0.07	-	-0.23
	Wind direction (°)	-0.22	*-0.32	-0.18	-0.17	-	*-0.49
	Rainfall (mm)	-0.06	-0.01	-	-0.004	-	-
June	Temperature (°C)	-0.24	-0.09	-0.19	-0.05	*-0.36	*-0.46
	Solar radiation ($W.m^{-2}$)	-	-	-	-0.08	-0.26	-
	Relative humidity (%)	-0.16	-0.10	-	-0.05	*-0.46	-
	Wind speed ($m.s^{-1}$)	*-0.46	-0.15	-0.38	-0.01	-	-0.220
	Wind direction (°)	-0.26	-0.21	-0.11	-0.19	-	*-0.50
	Rainfall (mm)	-0.04	-0.05	-	-0.05	-	-
July	Temperature (°C)	-0.24	-0.18	-0.07	-0.004	-0.26	-0.27
	Solar radiation ($W.m^{-2}$)	-	-	-	-0.04	-0.10	-
	Relative humidity (%)	-0.02	-0.06	-	-0.08	-0.09	-

	Wind speed (m.s^{-1})	*-0.39	-0.18	-0.16	-0.11	-	-0.09
	Wind direction (°)	-0.0023	-0.36	-0.14	-0.23	-	*-0.49
	Rainfall (mm)	-0.02	-0.06	-	-0.04	-	-
August	Temperature (°C)	-0.17	-0.15	*-0.31	-0.13	-0.25	*-0.34
	Solar radiation (W.m^{-2})	-	-	-	-0.03	-0.16	-
	Relative humidity (%)	-0.02	-0.04	-	-0.13	-0.02	-
	Wind speed (m.s^{-1})	*-0.36	-0.21	*-0.31	-0.02	-	-0.10
	Wind direction (°)	-0.07	*-0.42	-0.15	-0.14	-	*-0.49
	Rainfall (mm)	-0.02	-0.04	-	-0.06	-	-
September	Temperature (°C)	-0.10	-0.23	-0.28	-0.11	-0.21	*-0.41
	Solar radiation (W.m^{-2})	-	-	-	-0.10	*-0.33	-
	Relative humidity (%)	-0.02	-0.28	-	-0.14	-0.18	-
	Wind speed (m.s^{-1})	*-0.33	-0.03	-0.36	-0.13	-	-0.18
	Wind direction (°)	-0.14	*-0.31	-0.12	-0.02	-	*-0.47
	Rainfall (mm)	-0.01	-0.03	-	-0.03	-	-
October	Temperature (°C)	-0.22	-0.17	-0.11	-0.13	*-0.32	-0.24
	Solar radiation (W.m^{-2})	-	-	-	-0.21	-0.01	-
	Relative humidity (%)	-0.10	-0.17	-	-0.06	-0.01	-
	Wind speed (m.s^{-1})	*-0.40	-0.08	-0.29	-0.01	-	-0.21
	Wind direction (°)	-0.09	*-0.31	-0.11	-0.03	-	*-0.52
	Rainfall (mm)	-0.09	-0.03	-	-0.06	-	-
November	Temperature (°C)	-0.09	-0.22	-0.05	-0.24	*-0.35	*-0.31
	Solar radiation (W.m^{-2})	-	-	-	-0.15	-0.28	-
	Relative humidity (%)	-0.05	-0.26	-	-0.19	-0.20	-
	Wind speed (m.s^{-1})	-0.26	-0.01	-0.24	-0.06	-	-0.26
	Wind direction (°)	-0.05	*-0.42	-0.10	-0.09	-	*-0.38
	Rainfall (mm)	-0.04	-0.04	-	-0.01	-	-
December	Temperature (°C)	-0.10	-0.16	-0.02	-0.28	-0.06	-0.09
	Solar radiation (W.m^{-2})	-	-	-	-0.14	-0.01	-
	Relative humidity (%)	-0.03	-0.19	-	-0.17	*-0.30	-
	Wind speed (m.s^{-1})	-0.11	-0.02	-0.17	-0.005	-	-0.06
	Wind direction (°)	-0.15	*-0.54	-0.10	-0.14	-	*-0.32
	Rainfall (mm)	-0.20	-0.09	-	-0.09	-	-

NO_x concentrations were significantly and positively related to atmospheric pressure (Table 5.5). Hence, as atmospheric pressure increased across the HPA, NO_x concentrations accumulated, similar to SO_2.

Table 5.5: Strength of the relationship between NO_x and atmospheric pressure. Statistically significant correlations are indicated by an asterisk.

Monitoring station	Strength of relationship (r)
Ermelo	*0.32
Secunda	*0.46

Meteorological governance of NO_x concentrations was typically location specific, whereby only 5 to 23 % of NO_x concentrations could be explained by meteorology (Table 5.6). The low R^2 values, low significance values and high standard error values (8.38 to 18.25 ppb) suggests that meteorology was not the only factor influencing NO_x concentrations (Table 5.6). Instead a number of other factors along with meteorology would have governed NO_x concentrations (For example: land use, atmospheric life time and previous day concentrations among other factors). All meteorological factors were negatively related to NO_x concentrations (Table 5.6). Hence, during the day when temperatures were high and solar radiation levels were high, conditions for photochemical reactions were set up and NO_x concentrations were scavenged to form surface O_3. Increasing wind speeds generally diluted NO_x concentrations and increasing relative humidity levels were often associated with rainfall which in turn scavenged NO_x through wet deposition processes.

Table 5.6: The relationship of NO_x to meteorology. A statistically significant correlation is indicated by an asterisk. (T: Temperature; S: Solar radiation; RH: Relative humidity; WS: Wind speed; WD: Wind direction; R: Rainfall).

Monitoring station: Balfour		
$NO_x = 41.542 - 4.844$ [R] $- 0.169$ [RH] $- 0.590$ [T] $- 0.013$ [WD] $- 2.452$ [WS]		
Coefficient of determination (R^2)	Standard error (σ_{est})	Significance of correlation (p)
*0.19	12.77	0.03
Monitoring station: Camden		
$NO_x = 17.575 - 0.299$ [R] $- 0.130$ [RH] $- 0.337$ [T] $- 0.028$ [WD] $- 0.554$ [WS]		
Coefficient of determination (R^2)	Standard error (σ_{est})	Significance of correlation (p)
*0.20	9.87	0.02
Monitoring station: Grootvlei		
$NO_x = 19.00 - 0.198$ [T] $- 0.006$ [WD] $- 0.882$ [WS]		
Coefficient of determination (R^2)	Standard error (σ_{est})	Significance of correlation (p)
0.06	11.14	0.50
Monitoring station: Leandra		
$NO_x = 17.410 - 0.150$ [R] $- 0.043$ [RH] $- 0.011$ [S] $- 0.175$ [T] $- 0.031$ [WD] $- 0.711$ [WS]		
Coefficient of determination (R^2)	Standard error (σ_{est})	Significance of correlation (p)
0.05	8.38	0.50
Monitoring station: Middleburg		
$NO_x = 17.481 - 0.038$ [RH] $- 0.002$ [S] $- 0.007$ [T] $- 0.003$ [WD] $- 1.688$ [WS]		
Coefficient of determination (R^2)	Standard error (σ_{est})	Significance of correlation (p)

0.06	9.72	0.01
Monitoring station: Phola		
NO_x = 36.539 - 0.736 [T] - 0.003 [WD] - 3.715 [WS]		
Coefficient of determination (R^2)	Standard error (σ_{est})	Significance of correlation (p)
0.23*	18.25	0.001

5.3.3. Surface O_3

As a secondary pollutant, surface O_3 is largely dependent on meteorology (Dueñas *et al.*, 2002). Generally surface O_3 displayed weak significant relationships to meteorology, whereby the relationship to temperature and solar radiation was positive and the relationship to relative humidity, wind speed and wind direction were negative similar to many studies (Table 5.7) (For example: Kuebler *et al.*, 2001; Dueñas *et al.*, 2002; Latini *et al.*, 2002; Elminir, 2005; Pudasainee *et al.*, 2006; Tu *et al.*, 2007; Elampari and Chithambarathanu, 2011; Lin *et al.*, 2011; Hassan *et al.*, 2013; Im *et al.*, 2013; Sharma *et al.*, 2013). Temperature, solar radiation and relative humidity were particularly significantly related to surface O_3 across the HPA similar to the studies previously mentioned (Table 5.7).

Table 5.7: Strength of the relationship between surface O_3 and each meteorological variable. Statistically significant correlations are indicated by an asterisk; relationships with a correlation coefficient greater than 0.7 highlighted by a double asterisk; no data is represented by -.

Pollutant: Surface O_3							
		Monitoring station strength of relationship (r)					
Month	**Meteorological variable**	**Balfour**	**Camden**	**Elandsfontein**	**Ermelo**	**Grootvlei**	**Standerton**
January	Temperature (°C)	*0.61	*0.66	*0.52	*0.47	*0.68	*0.54
	Solar radiation (W.m^{-2})	-	-	-	*0.44	-	
	Relative humidity (%)	*-0.54	*-0.56	-	*-0.56	-	*-0.54
	Wind speed (m.s^{-1})	-0.14	*-0.30	-0.14	-	-0.21	-0.19
	Wind direction (°)	-0.17	-0.03	-0.24	-	*-0.37	-0.26
	Rainfall (mm)	-0.04	-0.02	-0.02	-	-	-0.11
February	Temperature (°C)	*0.69	**0.75	**0.74	**0.74	**0.74	**0.73
	Solar radiation (W.m^{-2})	-	-	-	*0.58	-	
	Relative humidity (%)	*-0.65	*-0.68	-	*-0.66	-	**-0.76
	Wind speed (m.s^{-1})	-0.28	*-0.49	-0.26	-	*-0.34	*-0.47
	Wind direction (°)	-0.26	-0.03	*-0.35	-	*-0.38	-0.29
	Rainfall (mm)	-0.06	-0.04	-0.02	-	-	-0.05
March	Temperature (°C)	**0.79	**0.84	*0.62	**0.76	**0.78	*0.82
	Solar radiation (W.m^{-2})	-	-	-	*0.61	-	
	Relative humidity (%)	**-0.74	**-0.79	-	*-0.69	-	*-0.76

	Wind speed (m.s^{-1})	*-0.43	*-0.68	-0.14	-	*-0.33	*-0.56
	Wind direction (°)	-0.13	-0.09	-0.19	-	-0.16	-0.29
	Rainfall (mm)	-0.04	-0.06	-0.05	-	-	-0.06
April	Temperature (°C)	**0.78	*0.80	*0.34	*0.65	**0.77	**0.89
	Solar radiation (W.m^{-2})	-	-	-	*0.52	-	-
	Relative humidity (%)	**-0.72	*-0.65	-	*-0.59	-	**-0.86
	Wind speed (m.s^{-1})	*-0.48	*-0.49	-0.04	-	*-0.32	*-0.33
	Wind direction (°)	-0.17	-0.10	*-0.36	-	-0.20	*-0.33
	Rainfall (mm)	-0.0004	-0.01	-0.02	-	-	-0.07
May	Temperature (°C)	**0.86	*0.78	*0.37	*0.54	**0.81	*0.84
	Solar radiation (W.m^{-2})	-	-	-	*0.56	-	
	Relative humidity (%)	**-0.71	*-0.67	-	*-0.47	-	*-0.75
	Wind speed (m.s^{-1})	**-0.74	*-0.64	-0.23	-	*-0.55	*-0.70
	Wind direction (°)	*-0.47	-0.08	*-0.32	-	*-0.30	*-0.49
	Rainfall (mm)	-0.05	-0.02	-0.06	-	-	-0.03
June	Temperature (°C)	**0.73	*0.41	*0.41	*0.43	**0.76	**0.80
	Solar radiation (W.m^{-2})	-	-	-	*0.52	-	-
	Relative humidity (%)	*-0.66	*-0.33	-	*-0.36	-	*-0.63
	Wind speed (m.s^{-1})	*-0.64	-0.27	-0.03	-	*-0.46	**-0.70
	Wind direction (°)	*-0.38	-0.10	-0.26	-	-0.19	*-0.51
	Rainfall (mm)	-0.01	-0.01	-0.09	-	-	-0.01
July	Temperature (°C)	**0.80	**0.84	*0.61	*0.63	**0.76	**0.83
	Solar radiation (W.m^{-2})	-	-	-	*0.36	-	-
	Relative humidity (%)	*-0.53	*-0.62	-	*-0.43	-	*-0.61
	Wind speed (m.s^{-1})	*-0.44	*-0.64	-0.17	-	*-0.38	*-0.62
	Wind direction (°)	-0.25	-0.20	*-0.33	-	*-0.37	*-0.42
	Rainfall (mm)	-0.01	-0.03	-0.09	-	-	-0.04
August	Temperature (°C)	**0.82	**0.80	*0.51	*0.64	**0.84	**0.84
	Solar radiation (W.m^{-2})	-	-	-	*0.58	-	-
	Relative humidity (%)	*-0.59	*-0.63	-	*-0.32	-	**-0.72
	Wind speed (m.s^{-1})	*-0.45	*-0.58	-0.18	-	*-0.44	*-0.60
	Wind direction (°)	-0.28	-0.19	-0.12	-	-0.24	*-0.54
	Rainfall (mm)	-0.04	-0.05	-0.11	-	-	-0.02
September	Temperature (°C)	*0.65	**0.74	*0.82	*0.58	**0.72	**0.77
	Solar radiation (W.m^{-2})	-	-	-	*0.40	-	-
	Relative humidity (%)	*-0.46	*-0.60	-	*-0.53	-	*-0.59
	Wind speed (m.s^{-1})	*-0.38	*-0.36	-0.07	-	*-0.40	-0.21
	Wind direction (°)	*-0.32	-0.14	-0.21	-	-0.29	*-0.39
	Rainfall (mm)	-0.05	-0.07	-0.06	-	-	-0.04
October	Temperature (°C)	*0.51	**0.74	**0.75	0.23	*0.67	*0.63
	Solar radiation (W.m^{-2})	-	-	-	*0.34	-	-
	Relative humidity (%)	-0.15	*-0.58	-	-0.20	-	*-0.47
	Wind speed (m.s^{-1})	*-0.40	*-0.64	-0.18	-	*-0.41	*-0.69
	Wind direction (°)	-0.12	-0.19	-0.29	-	-0.25	*-0.58
	Rainfall (mm)	-0.13	-0.13	-0.05	-	-	-0.03

November	Temperature (°C)	**0.75	**0.80	*0.80	**0.74	**0.84	**0.77
	Solar radiation (W.m^{-2})	-	-	-	*0.47	-	-
	Relative humidity (%)	*-0.47	**-0.70	-	**-0.70	-	*-0.69
	Wind speed (m.s^{-1})	*-0.52	*-0.41	-0.16	-	*-0.52	-0.04
	Wind direction (°)	*-0.41	-0.23	*-0.40	-	*-0.45	*-0.62
	Rainfall (mm)	-0.07	-0.01	-0.03	-	-	-0.02
December	Temperature (°C)	*0.58	**0.78	0.67	0.24	**0.72	*0.59
	Solar radiation (W.m^{-2})	-	-	-	0.09	-	-
	Relative humidity (%)	*-0.58	**-0.73	-	-0.10	-	*-0.58
	Wind speed (m.s^{-1})	-0.25	*-0.41	-0.17	-	*-0.39	-0.15
	Wind direction (°)	-0.28	-0.03	-0.10	-	*-0.30	-0.06
	Rainfall (mm)	-0.10	-0.05	-0.003	-	-	-0.03

The relationship of atmospheric pressure to surface O_3 was insignificant and negative similar to other studies (For example: Dueñas *et al.*, 2002; Hassan *et al.*, 2013) (Table 5.8). Hence, increasing atmospheric pressure generally resulted in a decrease in surface O_3 concentrations.

Table 5.8: Strength of the relationship between Surface O_3 and atmospheric pressure. Statistically significant correlations are indicated by an asterisk.

Monitoring station	Strength of relationship (r)
Ermelo	-0.16
Secunda	-0.007

Meteorological governance of surface O_3 concentrations was weak and significant, as seen by the range in R^2 values (0.22 to 0.55), whereby about 22 to 55 % of surface O_3 concentrations could be explained by meteorology (Table 5.9). Only some of the surface O_3 concentrations across the HPA were explainable by meteorology suggesting complexity in the factors governing surface O_3 concentrations. Relatively high R^2 values coupled with low significance values and high standard error values (8.67 and 19.50 ppb) suggest that meteorology was not the only factor governing surface O_3 concentrations. Other factors may have governed the behaviour of surface O_3 concentrations, namely land use, atmospheric life time and previous day concentrations among other factors. Temperature and solar radiation were found to be positively related to surface O_3, therefore as solar radiation and temperatures increased surface O_3 concentrations increased (Table 5.9). Relative humidity, rainfall, wind speed and wind direction were all found to be negatively

related to surface O_3, therefore as each of these factors increased surface O_3 concentrations as a result decreased, i.e. faster wind speeds diluted air, while higher levels of relative humidity promoted cloud cover as well as rainfall, which removed surface O_3 (Table 5.9).

Table 5.9: The relationship of surface O_3 to meteorology. A statistically significant correlation is indicated by an asterisk. A relationship with a correlation coefficient greater than 0.7 highlighted by a double asterisk. (T: Temperature; S: Solar radiation; RH: Relative humidity; WS: Wind speed; WD: Wind direction; R: Rainfall).

Monitoring station: Balfour		
$O_3 = 11.481 - 8.359\ [R] - 0.136\ [RH] + 0.909\ [T] - 0.011\ [WD] - 1.188\ [WS]$		
Coefficient of determination (R^2)	Standard error (σ_{est})	Significance of correlation (p)
*0.46	10.31	<0.0001
Monitoring station: Camden		
$O_3 = 21.472 - 1.918\ [R] - 0.164\ [RH] + 0.806\ [T] - 0.008\ [WD] - 1.337\ [WS]$		
Coefficient of determination (R^2)	Standard error (σ_{est})	Significance of correlation (p)
**0.51	11.19	<0.0001
Monitoring station: Elandsfontein		
$O_3 = 13.378 - 1.232\ [R] + 1.410\ [T] - 0.033\ [WD] - 0.732\ [WS]$		
Coefficient of determination (R^2)	Standard error (σ_{est})	Significance of correlation (p)
*0.22	19.50	<0.0001
Monitoring station: Ermelo		
$O_3 = 29.996 - 0.192\ [R] + 0.005\ [S] + 0.030\ [T]$		
Coefficient of determination (R^2)	Standard error (σ_{est})	Significance of correlation (p)
*0.23	11.92	<0.0001
Monitoring station: Grootvlei		
$O_3 = 1.870 + 1.098\ [T] - 0.022\ [WD] - 2.207\ [WS]$		
Coefficient of determination (R^2)	Standard error (σ_{est})	Significance of correlation (p)
*0.46	12.03	<0.0001
Monitoring station: Standerton		
$O_3 = 17.364 - 3.504\ [R] - 0.188\ [RH] + 0.517\ [T] - 0.008\ [WD] - 1.691\ [WS]$		
Coefficient of determination (R^2)	Standard error (σ_{est})	Significance of correlation (p)
**0.53	8.67	<0.0001

5.4. Estimating ground-level pollutant concentrations using meteorological parameters and MODIS atmosphere products across the HPA

The following section is an investigation into estimating SO_2, NO_x and surface O_3 concentrations across the HPA using satellite-derived atmosphere products along with the

meteorological parameters to create spatio-temporal statistical pollution estimation models. Linear multiple regression were used. This is the first such attempt to model pollutants across the HPA and in South Africa using satellite-derived atmosphere products.

5.4.1. SO_2

Full year spatio-temporal models over a number of temporal (hourly, daily, 8-day and monthly) and spatial (10km to 1° grid cells) scales using meteorological parameters and satellite-derived AOD has been created for the purpose of estimating SO_2. Only 29 to 69 % of the SO_2 concentrations are explainable using this model (Table 5.10). A model predictive ability of 0.69 is relatively high and similar to recent studies, while lower has been considered to have a poor predictive ability (For example: Hu *et al.*, 2014a; Hu *et al.*, 2014b; Ma *et al.*, 2014; Sotoudeheian and Arhami, 2014; You *et al.*, 2015). Model performance may not fully explain the predictive ability of a model (Hu *et al.*, 2014a; Hu *et al.*, 2014b; Ma *et al.*, 2014; You *et al.*, 2015). Model performances of (R^2 is 0.0423 to 0.2252) and RMSE values (4.71 – 22.10 ppb) of error for each model was identified (Table 5.11). The model performance values were low compared to more recent multiple regression models with R^2 values typically larger than 0.62, possibly as all pollutant controlling factors across the HPA were not included in the model building process (For example: Hu *et al.*, 2014a; Hu *et al.*, 2014b; Ma *et al.*, 2014; Sotoudeheian and Arhami, 2014; You *et al.*, 2015). Multiple regression modelling for pollutant estimation for recent studies is typically associated with high RMSE values greater than 1 ppb (For example: Gupta and Christopher, 2009a; Gupta and Christopher, 2009b; Hu *et al.*, 2014a; Hu *et al.*, 2014b; Ma *et al.*, 2014; Sotoudeheian and Arhami, 2014; You *et al.*, 2015). The RMSE values for the SO_2 models was similar to recent studies (For example: Gupta and Christopher, 2009a; Gupta and Christopher, 2009b; Hu *et al.*, 2014a; Hu *et al.*, 2014b; Ma *et al.*, 2014; Sotoudeheian and Arhami, 2014; You *et al.*, 2015). Since the R^2 predictive performance values are lower for this study, the model performance ability is poor compared to other studies (For example: Gupta and Christopher, 2009a; Gupta and Christopher, 2009b; Hu *et al.*, 2014a; Hu *et al.*, 2014b; Ma *et al.*, 2014; Sotoudeheian and Arhami, 2014; You *et al.*, 2015). Hence, the four models produced are of poor quality and will not successfully estimate SO_2 concentrations.

Table 5.10: The relationship of SO_2 to level 2 and level 3 (daily, 8-day and monthly) satellite-derived AOD and meteorology. A statistically significant correlation is indicated by an asterisk. A relationship with a correlation coefficient greater than 0.7 highlighted by a double asterisk. AOD – Aerosol Optical Depth; T – Temperature; RH – Relative humidity; S – Solar radiation; R – Rainfall; WS – Wind speed; WD – Wind direction; A – Atmospheric pressure.

SO_2 Level 2 model	
Equation	SO_2 = 993.533 - 15.893 AOD + 0.178 T - 0.177 RH + 0.130 S - 0.023 R - 1.223 WS - 0.107 WD + 1.194 A
R^2	*0.27
SO_2 Level 3 Daily model	
Equation	SO_2 = 887.741 + 17.220 AOD + 0.043 T - 0.069 RH + 0.0106 S - 51.438 R - 0.336 WS - 0.136 WD + 1.060 A
R^2	**0.69
SO_2 Level 3 8-Day model	
Equation	SO_2 = 737.845 + 33.64 AOD + 0.049 T - 0.018 RH + 0.023 S - 0.039 R - 0.875 WS - 0.10 WD + 0.883 A
R^2	**0.60
SO_2 Level 3 Monthly model	
Equation	SO_2 = 482.164 + 97.317 AOD + 0.459 T - 0.032 RH + 0.042 S - 0.015 R - 0.183 WS - 0.054 WD + 0.566 A
R^2	**0.61

Table 5.11: Details of the RMSE and R^2 for the SO_2 level 2 and level 3 (daily, 8-day and monthly) model validation. A statistically significant correlation is indicated by an asterisk.

SO_2 Level 2 model validation	
RMSE (ppb)	4.71
R^2	0.0423
SO_2 Level 3 Daily model validation	
RMSE (ppb)	22.10
R^2	*0.2252
SO_2 Level 3 8-Day model validation	
RMSE (ppb)	9.01
R^2	0.0004
SO_2 Level 3 Monthly model validation	
RMSE (ppb)	8.67
R^2	0.0195

5.4.2. NO_x

Full year models to explain NO_x concentrations have been created over a number of temporal (hourly, daily, 8-day and monthly) and spatial (10km to 1° grid cells) scales (Table 5.12). These models performed better than the SO_2 models, where 67 to 74 % of NO_x concentrations can be explained by these models (Table 5.12). Compared to other studies,

with model predictive abilities greater than 0.40, the model predictive abilities are similar (For example: Gupta and Christopher, 2009a; Gupta and Christopher, 2009b; Hu *et al.*, 2014a; Hu *et al.*, 2014b; Ma *et al.*, 2014; Sotoudeheian and Arhami, 2014; You *et al.*, 2015). The high predicitive ability of the NO_x models is not enough to determine the predictive performance of the NO_x models. Compared to other studies, the model performance (R^2 is 0.0004 to 0.2252) were considerably low, while the error measurements of 7.02 up to 15.56 ppb were relatively similar (For example: Gupta and Christopher, 2009a; Gupta and Christopher, 2009b; Hu *et al.*, 2014a; Hu *et al.*, 2014b; Ma *et al.*, 2014; Sotoudeheian and Arhami, 2014; You *et al.*, 2015). Hence, the low performance values hinder the predictive ability of these models and as a result they are not suitable for NO_x concentration estimation.

Table 5.12: The relationship of NO_x to level 2 and level 3 (daily, 8-day and monthly) satellite-derived AOD and meteorology. A statistically significant correlation is indicated by an asterisk. A relationship with a correlation coefficient greater than 0.7 highlighted by a double asterisk. AOD – Aerosol Optical Depth; T – Temperature; RH – Relative humidity; S – Solar radiation; R – Rainfall; WS – Wind speed; WD – Wind direction; A – Atmospheric pressure.

NO_x Level 2 model	
Equation	NO_x = - 5206.268 + 36.430 AOD - 1.678 T - 0.793 RH - 0.046 S - 0.01 R - 15.801 WS - 0.277 WD + 6.514 A
R^2	**0.67
NO_x Level 3 Daily model	
Equation	NO_x = 226.214 + 3.059 AOD - 0.632 T - 0.384 RH - 0.017 S - 69.744 R - 5.001 WS - 0.020 WD + 0.186 A
R^2	**0.74
NO_x Level 3 8-Day model	
Equation	NO_x = 815.005 + 46.320 AOD - 0.437 T - 0.280 RH - 0.010 S - 0.042 R - 6.619 WS - 0.022 WD + 0.912 A
R^2	**0.68
NO_x Level 3 Monthly model	
Equation	NO_x = 331.293 + 5.647 AOD - 0.243 T - 0.364 RH - 0.0375 S - 1.635 R - 6.544 WS - 0.066 WD + 0.338 A
R^2	**0.70

Table 5.13: Details of the RMSE and R^2 for the NO_x level 2 and level 3 (daily, 8-day and monthly) model validation. A relationship with a correlation coefficient greater than 0.7 highlighted by a double asterisk.

NO_x Level 2 model validation	
RMSE (ppb)	7.02
R^2	**0.5057

NO_x Level 3 Daily model validation	
RMSE (ppb)	11.93
R^2	0.0151
NO_x Level 3 8-Day model validation	
RMSE (ppb)	15.56
R^2	*0.1547
NO_x Level 3 Monthly model validation	
RMSE (ppb)	10.69
R^2	0.1323

5.4.3. Surface O_3

The estimation ability of the level 2 and level 3 (daily, 8-day and monthly) surface O_3 models were 42 to 58 % which were similar to the SO_2 models but lower than the NO_x models (Table 5.14). Compared to recent studies, where model predictive ability is typically greater than 40 %, the surface O_3 models were similar (For example: Hu *et al.*, 2014a; Hu *et al.*, 2014b; Ma *et al.*, 2014; Sotoudeheian and Arhami, 2014; You *et al.*, 2015). Model predicitive performance cannot fully explain the predictive ability of the surface O_3 models. Upon validation of the models, it was seen that the performance of the level 3 models were considerably low and the level 2 model the performance was relatively high, 0.757 (Table 5.15). Compared to other studies, the level 2 model performance was similar and the level 3 model performances were lower (For example: Hu *et al.*, 2014a; Hu *et al.*, 2014b; Ma *et al.*, 2014; Sotoudeheian and Arhami, 2014; You *et al.*, 2015). High modelling errors, similar to recent studies, of 8.90 to 18.59 ppb were found (Table 5.15) (For example: Hu *et al.*, 2014a; Hu *et al.*, 2014b; Ma *et al.*, 2014; Sotoudeheian and Arhami, 2014; You *et al.*, 2015). Hence, the models produced will not successfully estimate surface O_3 concentrations.

Table 5.14: The relationship of surface O_3 to level 2 and level 3 (daily, 8-day and monthly) satellite-derived Ozone and meteorology. A statistically significant correlation is indicated by an asterisk. A relationship with a correlation coefficient greater than 0.7 highlighted by a double asterisk. DU – Dobson Units; T – Temperature; RH – Relative humidity; S – Solar radiation; R – Rainfall; WS – Wind speed; WD – Wind direction; A – Atmospheric pressure.

Surface O_3 Level 2 model	
Equation	Surface O_3 = 159.143 + 0.534 DU + 2.289 T - 0.219 RH + 0.089 S - 2.9 R - 2.899 WS - 0.013 WD - 0.292 A
R^2	**0.49
Surface O_3 Level 3 Daily model	

Equation	Surface O_3 = 30.605 + 0.319 DU + 3.413 T - 0.246 RH + 0.191 S - 5.458 R - 5.019 WS - 0.048 WS - 0.048 WD - 0.054 A
R^2	*0.42
SO_3 Level 3 8-Day model	
Equation	SurfaceO_3 = - 1009.597 + 2.718 DU + 6.5787 T - 1.862 RH + 0.153 S - 2.833 R - 0.514 WS - 0.246 WD - 0.177 A
R^2	**0.58
Surface O_3 Level 3 Monthly model	
Equation	Surface O_3 = - 500.655 + 0.711 DU + 1.629 T - 0.473 RH + 0.014 S - 1.712 R - 3.4 WS - 0.135 WD - 0.354 A
R^2	*0.43

Table 5.15: Details of the RMSE and R^2 for the surface O_3 level 2 and level 3 (daily, 8-day and monthly) model validation. A statistically significant correlation is indicated by an asterisk. A relationship with a correlation coefficient greater than 0.7 highlighted by a double asterisk.

Surface O_3 Level 2 model validation	
RMSE (ppb)	8.90
R^2	**0.7570
Surface O_3 Level 3 Daily model validation	
RMSE (ppb)	16.04
R^2	0.0117
Surface O_3 Level 3 8-Day model validation	
RMSE (ppb)	15.93
R^2	*0.1651
Surface O_3 Level 3 Monthly model validation	
RMSE (ppb)	18.59
R^2	0.0171

5.5. Air pollution 'hotspots'

Across the HPA a number of SO_2, NO_x and surface O_3 'hotspots' were identified based on the results below.

5.5.1. Exceedance of AQG's - SO_2

The South African 1 hour standard of 134 ppb was exceeded by each monitoring station, except for Hendrina and Secunda (Table 5.16). These two stations had concentrations of SO_2 above 100 ppb almost reaching the 134 ppb standard. Each monitoring station was considered a pollution 'hotspot' as the ambient air quality standards are/may be exceeded. The majority of exceedances for this standard were during May, June, July, August and September. No more than 88 exceedances of this standard are allowed during 1 year (DEA,

2009). The Witbank monitoring station exceeded the 1 hour standard 137 times, 49 times more than allowed (Table 5.16). Hence, the Witbank area is associated with a high level of risk to human health. Interpolation of the measure of exceedances shows that the highest proportion of exceedance of 1 hour SO_2 concentrations were observed in the small north western area of the HPA where the majority of the countries power stations occur (Figure 5.21d; Figure 3.1).

Ermelo, Grootvlei, Komati, Secunda and Witbank all exceeded the South African 24 hour 48 ppb standard (Table 5.16). Each monitoring station was again considered a 'hotspot' with regard to this standard as the standard was either exceeded or almost exceeded at each monitoring station. No more than 4 exceedances of this standard are allowed during a 1 year period (DEA, 2009). Both Ermelo and Witbank exceeded this amount, and are therefore considered high risk areas for human health (Table 5.16). When compared to the 8 ppb 24 hour guideline proposed by the WHO, all the monitoring stations exceeded this guideline (Table 5.16). Each station had more than 50 exceedances, while Elandsfontein, Ermelo, Hendrina, Phola and Witbank all exceeded this guideline more than 250 times (Table 5.16). According the WHO guideline, the SO_2 concentrations would have adversely affected the health of individuals living in this area.

Interpolation of both the 24 hour exceedances shows the "coolspot" and "hotspot" locations correspond to the measured values in Table 5.16. Both the north western and eastern areas of the HPA had high levels of exceedance of the WHO and South African 24 hour SO_2 standards (Figure 5.21 b and c). While, the rest of the HPA was typically represented as "coolspots" (Figure 5.21 b and c). The maxima and minima values, when interpolated using IDW, correspond to the measurements already captured (Emili *et al.*, 2011).

Witbank exceeded the 1 year standard of 19 ppb (Table 5.16). No exceedances of this standard are allowed (DEA, 2009). Ermelo and Hendrina were the only two stations that may have exceeded this limit. Interpolation of this exceedance shows that the north western area of the HPA was highly polluted (Figure 5.21 a).

Table 5.16: Frequency of exceedance SO_2 using the SANAAQS and the WHOAQG.

Frequency of exceedance for SO_2 for 2011				
	SANAAQS			WHOAQG
Station	1 hour - 134 ppb	24 hours - 48 ppb	1 year - 19 ppb	24 hours - 8 ppb
Balfour	1	0	No	119
Camden	11	0	No	122
Elandsfontein	17	0	No	268
Ermelo	21	14	No	284
Grootvlei	21	1	No	118
Hendrina	0	0	No	250
Komati	21	2	No	212
Leandra	1	0	No	234
Middleburg	3	0	No	96
Phola	15	0	No	274
Secunda	0	2	No	54
Wattville	1	0	No	167
Witbank	137	29	Yes	252

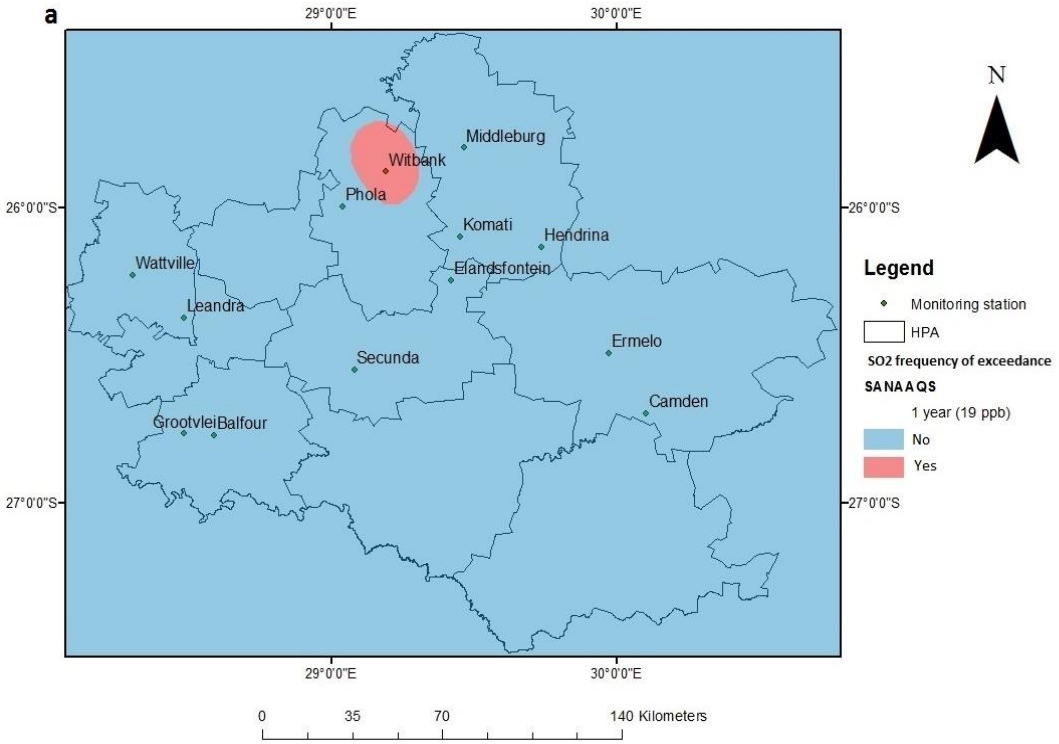

Figure 5.21: Spatial distribution of the exceedance of the a) 1 year SAAQIS SO_2 19 ppb standard, b) 24 hour SAAQIS SO_2 48 ppb, c) 24 hour WHOAQG SO_2 8 ppb and d) 1 hour SAAQIS SO_2 134 ppb.

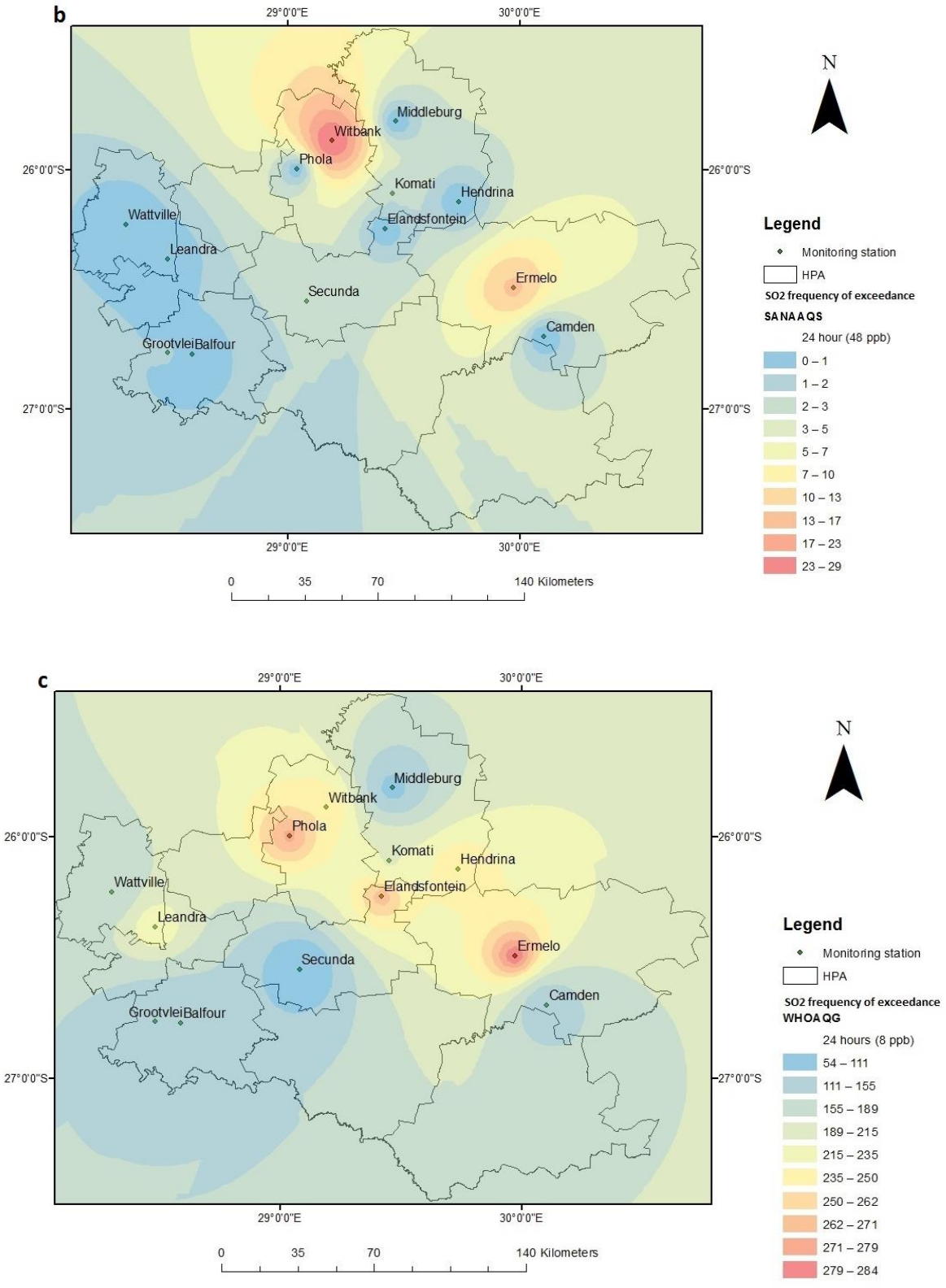

Figure 5.21 continued: Spatial distribution of the exceedance of the a) 1 year SAAQIS SO_2 19 ppb standard, b) 24 hour SAAQIS SO_2 48 ppb standard, c) 24 hour WHOAQG SO_2 8 ppb standard and d) 1 hour SAAQIS SO_2 134 ppb standard.

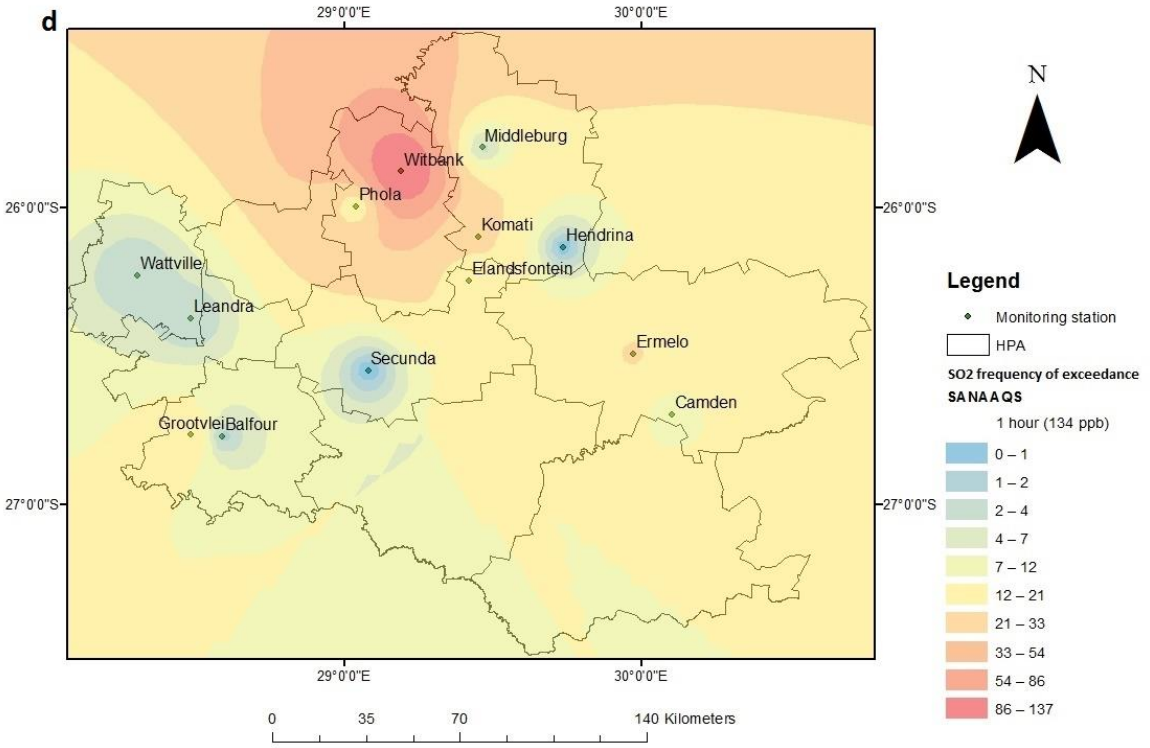

Figure 5.21 continued: Spatial distribution of the exceedance of the a) 1 year SAAQIS SO_2 19 ppb standard, b) 24 hour SAAQIS SO_2 48 ppb standard, c) 24 hour WHOAQG SO_2 8 ppb standard and d) 1 hour SAAQIS SO_2 134 ppb standard.

The probabilities of exceeding the South African ambient air 1 hour and 24 hour standards were low at each monitoring station (Table 5.17). Hence, there was little chance of exceedance of these standards. Witbank was the only station with a probability greater than 0.0001 to exceed to the 1 hour 134 ppb standard (Table 5.17). Elandsfontein, Ermelo and Witbank were the only stations with a probability greater than 0.0001 to exceed the 48 ppb 24 standard indicating that the north western and eastern areas of the HPA are particularly risky for human health (Table 5.17). Probabilities exceeding the 24 hour WHO guideline were all greater than 0.45 (Table 5.17).

Table 5.17: Probability of exceedance of the SANAAQS SO_2 1 hour 134 ppb, 24 hour 48 ppb and WHOAQG SO_2 24 hour 8 ppb standards.

Station	P (x > 134)	P (x > 48)	P (x > 8)
Balfour	P < 0.0001	P < 0.0001	0.4801
Camden	P < 0.0001	P < 0.0001	0.5160
Elandsfontein	P < 0.0001	0.0091	0.6700
Ermelo	P < 0.0001	0.0047	0.7734
Grootvlei	P < 0.0001	P < 0.0001	0.5000
Hendrina	P < 0.0001	P < 0.0001	0.9357
Komati	P < 0.0001	P < 0.0001	0.7157
Leandra	P < 0.0001	P < 0.0001	0.6844
Middleburg	P < 0.0001	P < 0.0001	0.5279
Phola	P < 0.0001	P < 0.0001	0.7852
Secunda	P < 0.0001	P < 0.0001	0.4880
Wattville	P < 0.0001	P < 0.0001	0.6591
Witbank	0.0011	0.0838	0.8461

5.5.2. Exceedance of AQG's - NO_x

The NO_x concentrations measured were compared to the NO_2 South African and WHO standards as no standards exist for NO_x. The 1 hour 106 ppb standard was exceeded by each monitoring station except for Camden and Leandra (Table 5.18). The hourly concentrations of NO_x at Camden and Leandra almost exceeded the 106 ppb limit. Hence, each monitoring station was a NO_x 'hotspot'. No more than 88 exceedances of the 106 ppb standard are allowed during a year (DEA, 2009). None of the stations exceeded this amount. Interpolation of the 1 hour exceedances shows the "coolspot" and "hotspot" locations typically correspond to the measured values in Table 5.18. Interpolation of the 1 hour exceedances showed that the north western area of the HPA had a particularly high level of exceedances similar to SO_2 (Figure 5.22b). The areas surrounding Witbank and Phola have been shown as relatively "coolspots" with a lower level of exceedances of the NO_2 standard (Figure 5.22b).

Similar to SO_2, only Witbank exceeded the 1 year 21 ppb standard (Table 5.18). No exceedances of this standard are allowed (DEA, 2009). Interpolation of this exceedance shows that the north western area of the HPA, similar to SO_2, was highly polluted (Figure 5.22 a). The NO_x concentrations would have adversely affected the health of individuals living in this area.

Table 5.18: Frequency of exceedance NO_2 using the SANAAQS and the WHOAQG.

Frequency of exceedance for NO_x for 2011		
	SANAAQS and WHOAQG	
Station	**NO_2 (106 ppb - 1 hour)**	**NO_2 (21 ppb - 1 year)**
Balfour	12	No
Camden	0	No
Grootvlei	16	No
Hendrina	11	No
Leandra	0	No
Middleburg	4	No
Phola	61	No
Witbank	80	Yes

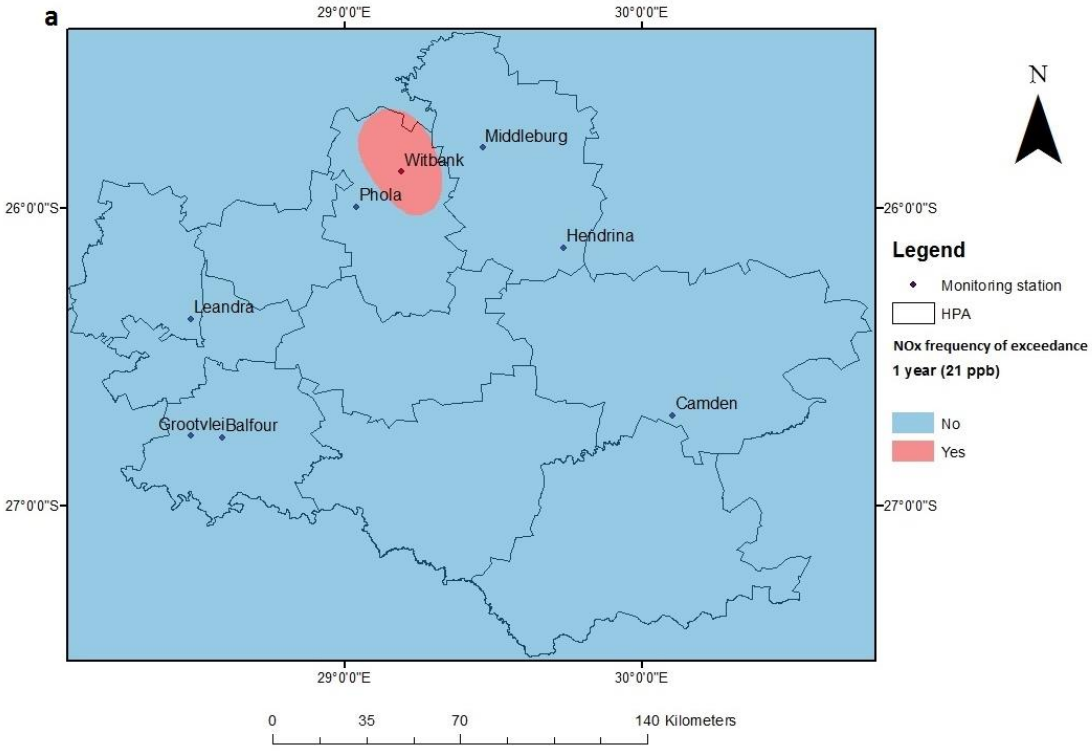

Figure 5.22: Spatial distribution of the exceedance of the a) 1 year SAAQIS NO_2 21 ppb standard and b) 1 hour SAAQIS NO_2 106 ppb standard.

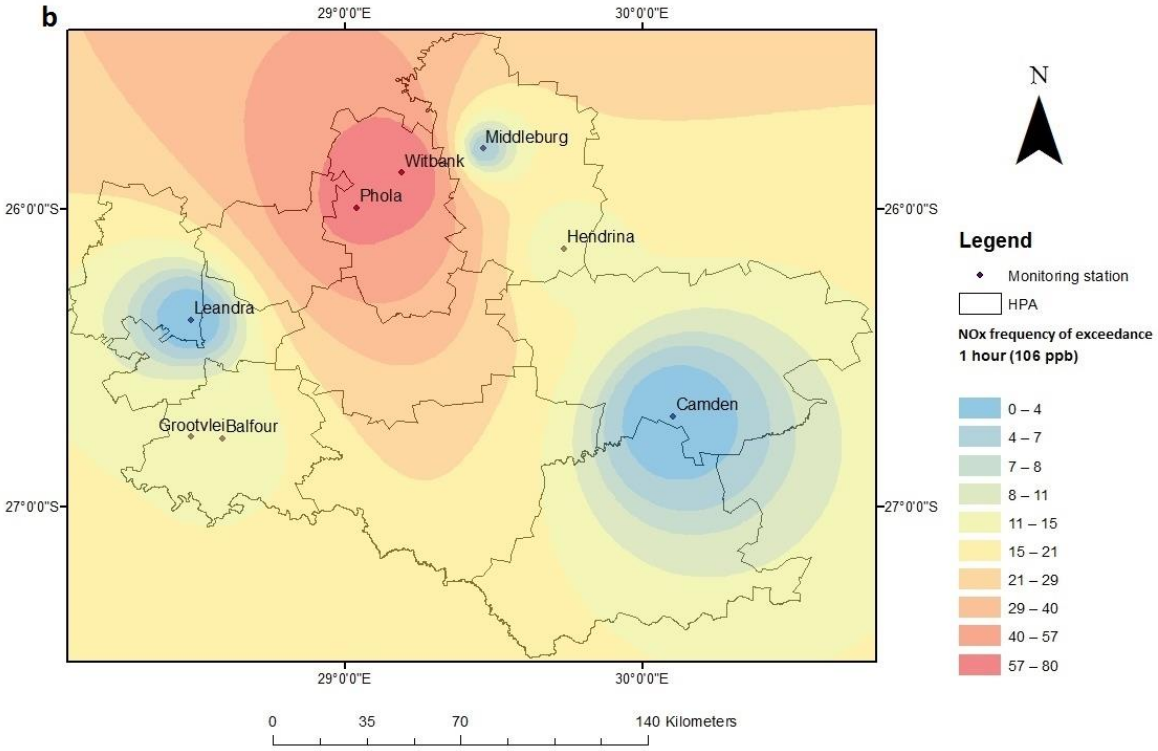

Figure 5.22: Spatial distribution of the exceedance of the a) 1 year SAAQIS NO_2 21 ppb standard and b) 1 hour SAAQIS NO_2 106 ppb standard.

The probabilities of exceeding the South African and WHO ambient air 1 hour standard were low at each monitoring station (Table 5.19). Hence, there was little chance of exceedance of this standard. Similarly to SO_2, Witbank was the only station with a probability of 0.0001 while the rest were less than 0.0001 (Table 5.19).

Table 5.19: Probability of exceedance of the SANAAQS and WHOAQG 1 hour NO_2 106 ppb standard.

Station	P (x > 106)
Balfour	P < 0.0001
Camden	P < 0.0001
Grootvlei	P < 0.0001
Hendrina	P < 0.0001
Leandra	P < 0.0001
Middleburg	P < 0.0001
Phola	P < 0.0001
Witbank	0.0001

5.5.3. Exceedance of AQG's - surface O_3

Both the South African 61 ppb 8 hour standard and the WHO 50 ppb 8 hour standard for surface O_3 were exceeded (Table 5.20). Elandsfontein, Hendrina and Secunda exceeded the South African standard more than 100 times, where Secunda exceeded this standard more than 200 times (Table 5.20). Only 11 exceedances are allowed per year (DEA, 2009). Elandsfontein, Hendrina and Secunda all exceeded the WHO standard more than 150 times, where Secunda exceeded this standard more than 350 times (Table 5.20). Hence, the entire HPA was a surface O_3 'hotspot'. Interpolation of both the 8 hour exceedances shows the "coolspot" and "hotspot" locations correspond to the measured values in Table 5.20 and no variation of these minima and maxima can be captured unless these values are captured in the measured data (Emili *et al.*, 2011). Interpolation of these two sets of exceedances shows that the central HPA has a considerably high level of surface O_3 pollution (Figure 5.23 a and b). The surface O_3 concentrations across would have adversely affected the health of individuals living in this area.

Table 5.20: Frequency of exceedance Surface O_3 using the SANAAQS and the WHOAQG.

Frequency of exceedance for surface O_3 for 2011		
	SANAAQS	**WHOAQG**
Station	**8 hours - 61 ppb**	**8 hours - 50 ppb**
Balfour	3	21
Camden	6	38
Elandsfontein	109	224
Ermelo	10	25
Grootvlei	25	97
Hendrina	104	183
Secunda	257	398
Standerton	3	10
Witbank	9	31

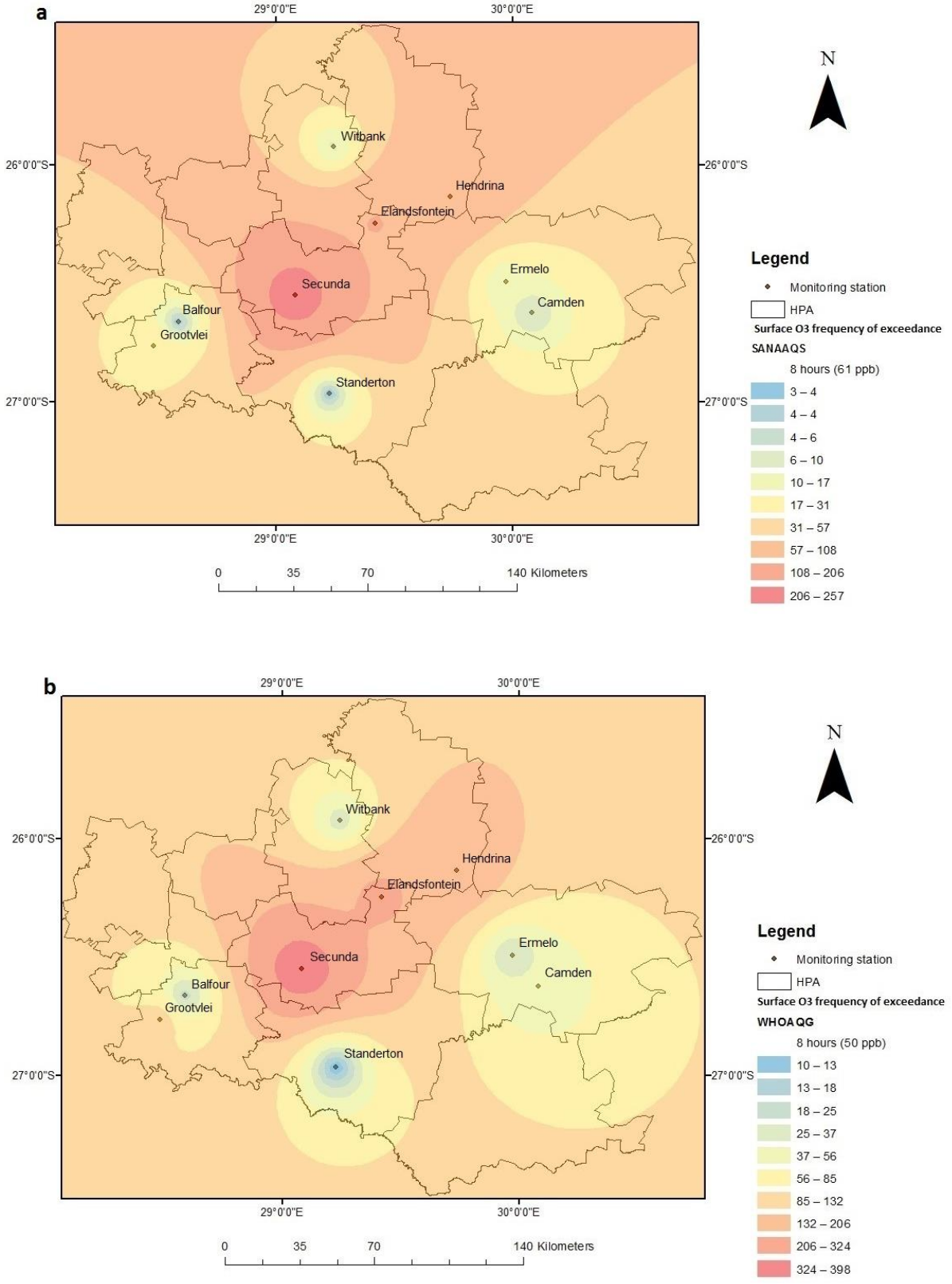

Figure 5.23: Spatial distribution of the exceedance of the a) 8 hour SAAQIS surface O_3 61 ppb standard and b) 8 hour WHOAQG surface O_3 50 ppb standard.

The probabilities of exceeding the South African ambient air 8 hour 61 ppb standard were low but they were considerably higher than the probabilities for exceedance of SO_2 and NO_x (Table 5.21). Each probability was higher than or equal to 0.0001, where Hendrina and Secunda were higher than 0.1 (Table 5.21). Probabilities exceeding the 8 hour 50 ppb WHO guideline were all greater than 0.001 (Table 5.21). This signifies the magnitude of surface O_3 pollution.

Table 5.21: Probability of exceedance of the SANAAQS and WHOAQG 8 hour surface O_3 standard.

Station	P (x > 61)	P (x > 50)
Balfour	0.005	0.0089
Camden	0.0021	0.0233
Elandsfontein	0.0968	0.2327
Ermelo	0.0002	0.0039
Grootvlei	0.0102	0.0655
Hendrina	0.1093	0.2236
Secunda	0.3707	0.4880
Standerton	0.0001	0.0015
Witbank	0.0024	0.0287

Chapter 6: Conclusion

(Wikimedia, 2016)

Despite knowledge of the serious air pollution problems across the HPA, detailed characterisation of pollutants is lacking. In an attempt to work towards improving air quality, this study aimed to investigate SO_2, NO_x and surface O_3 concentrations to develop a new pollution modelling technique which encompasses the full spatial array of the HPA. The intention is that this modelling technique promotes study into other modelling techniques and pollution management techniques to improve air quality to in turn work towards the government's main aim of improving air quality across the HPA and across South Africa. Measurements from the established SAAQIS network and MODIS satellite-derived atmosphere products were used in the first attempt to develop spatio-temporal statistical models for pollution estimation. It is deemed feasible to develop such modelling techniques knowing that the HPA is currently considered a pollution 'hotspot' area.

With this in mind, development of spatio-temporal modelling techniques to estimate pollutant levels required an understanding of the nature of pollutants across the HPA. It was also important to understand which factors contributed to the variation observed in these concentrations as previously studies creating models identified that a linear relationship between pollutants and satellite-derived atmospheric measurements is not sufficient enough to describe pollutants (Gupta *et al.*, 2009a). To create a model that accurately estimates pollutant concentrations, it was imperative that all factors causing variation of pollutants were included. The next sections highlight the main findings to get an understanding of: the nature of SO_2, NO_x and surface O_3, the meteorological factors causing variations in the concentrations of SO_2, NO_x and surface O_3, the outcome of the first statistical modelling attempt of SO_2, NO_x and surface O_3 across the HPA, and ways in which future model outcomes may be used for application with regard to national and international ambient air quality standards.

6.1. Variation of pollutants across the HPA

Systematic measurements of the criteria air pollutants over the HPA are continuously carried out. Measurements of SO_2, NO_x and surface O_3 during 2011 were used for this study, and these measurements ranged between 0.0008 to 474.3 ppb for SO_2, 0.004 and 261.8 ppb for NO_x and 0.001 and 495.5 for surface O_3. An analysis of the temporal variability of these pollutants was performed over seasonal, monthly and diurnal scales.

The variation of SO_2, NO_x and surface O_3 is typically influenced by changes in atmospheric conditions as well as from local emissions. Strong seasonal and monthly variations were exhibited in all pollutant concentrations. SO_2 and NO_x concentrations peaked during the winter months with average concentrations of 17.56 and 20.90 ppb potentially due to a combined effect of anthropogenic emissions and boundary layer processes (Gaur *et al.*, 2014). Minimum concentrations were experienced during the summer months with average measurements 9.73 of and 9.68 ppb perhaps due to higher solar intensity, stronger winds and wet depositional processes promoting lower emission levels (Gaur *et al.*, 2014).

During the spring months optimum conditions occurred for the formation and transport of surface O_3 concentrations where average concentrations were 32.82 ppb and during the autumn a seasonal average concentration of 23.88 ppb was found as during this time cleaner air would have travelled across the HPA diluting surface O_3 concentrations over the HPA for minimum concentrations (Adame *et al.*, 2008; Frieman and Piketh, 2002).

The diurnal variation of SO_2 and NO_x was most pronounced during winter and for surface O_3 it was most pronounced during spring. SO_2 and surface O_3 concentrations rose from a minimum during the night time and just before sunrise to a peak around midday (12h00 to 15h00) as an increase in the mixing layer height allowed for its accumulation, then decreasing again until the morning. NO_x levels were low and steady during the evening hours due to nocturnal inversion layers, and during traffic peak time hours (6h00 to 8h00; 17h00 to 19h00). NO_x levels peaked with a valley during the afternoon hours where NO_x was removed for the production of surface O_3. The variation patterns of these pollutants are indicative of rural or semi-rural sites.

6.2. Regional meteorological patterns and their influence on SO_2, NO_x and surface O_3 across the HPA

Continuous observations of meteorology across the HPA were used for this study. Ambient air temperature, solar radiation, wind speeds, relative humidity and rainfall levels peaked during summer. Atmospheric pressure was relatively stable throughout the year. Winds blew from N to E during January to April and during May to December they blew from S to NW.

The association between these meteorological variables and SO_2 and NO_x were found to be weak and insignificant, while the association to surface O_3 was found to be weak and moderately significant. SO_2 was positively related to atmospheric pressure, solar radiation and temperature, while it was negatively related relative humidity, wind speed, wind direction and rainfall. NO_x on the other hand was positively related to atmospheric pressure and negatively related to temperature, solar radiation, relative humidity, wind speed, wind direction and rainfall. Surface O_3 was positively related to solar radiation and temperature, while it was negatively related to atmospheric pressure, relative humidity, wind speed, wind direction and rainfall. Multiple regression analysis further reiterated that meteorology play a very small role in the variation of SO_2 and NO_x, where 3 to 29 % and 5 to 23 % of concentrations were explainable by meteorology. While still low and of weak significance, 22 to 55 % of surface O_3 variation was explainable by meteorology. These multiple regression analyses indicate that the variation in pollutants across the HPA may not only be explained by meteorology and rather is as a result of many factors, for example: source density, strength and distribution, atmospheric life time (previous day concentrations), transboundary air pollution, elevation, terrain and vegetation cover among other factors.

6.3. Estimating ground-level SO_2, NO_x and surface O_3 using MODIS atmosphere products and ground-based meteorological measurements over the HPA

Spatio-temporal modelling using multiple regression analysis for the purpose of SO_2, NO_x and surface O_3 concentration estimation has been performed for this study. This study is the first of its kind to be attempted in South Africa and essentially across the HPA. Theoretically many factors influence the concentrations of pollutants, and therefore including these factors into statistical models has been explored as a way to estimate pollutant concentrations across the HPA. The relationship of ground-level pollutant concentrations to satellite-derived MODIS AOD and total-ozone atmosphere products and ground-level meteorological parameters has been investigated. Several challenges were experienced regarding the coarse resolution of MODIS satellite-derived products and inclusion of all the factors that influence pollutant concentrations. As a result the final models, over the numerous temporal scales, exhibited poor performance. The resulting models were able to explain 27 to 69 % of SO_2, 67 to 74 % of NO_x and 42 to 58 % of surface O_3 concentrations.

The model validation process showed that these models had high error values and Low R^2 values of 4.71 to 22.10 ppb and 0.004 to 0.2252 for SO_2, 7.02 to 15.56 ppb and 0.0151 to 0.5057 for NO_x and 8.90 to 18.59 ppb and 0.117 to 0.7570 for surface O_3. It has been concluded that the HPA shows a need and the potential for spatio-temporal statistical modelling for pollutant concentration estimation and essentially modelling. Future work will need to be done for these models to be applicable for use in estimating pollutant concentrations across the HPA.

6.4. SO_2, NO_x and surface O_3 levels and national and international air quality guidelines

By comparing the results obtained across the HPA with the SANAAQS's and the WHOAQG's, it is evident that concentrations across many areas within the HPA during 2011 were not acceptable, as they exceeded the standards and above that the minimum number of exceedances allowed per year. Exceedances typically coincided with high population density (Figure 3.3).

Typically SO_2 concentrations were highest with higher probabilities of exceedance at the Elandsfontein, Ermelo, Grootvlei, Komati, Phola, Secunda and Witbank monitoring stations. Considering the high density of power stations across the HPA, this would have promoted high levels of SO_2 which were at levels possibly risky to human health (Figure 3.1). NO_x concentrations were compared to the NO_2 ambient air quality standards and these standards were exceeded at many locations. Typically NO_x concentrations were highest at the Camden, Leandra, Phola and Witbank monitoring stations. Considering the high population density across the HPA, it is no surprise that fossil fuel burning and vehicle emissions among others have contributed to the high NO_x concentrations. Surface O_3 ambient air quality standards were exceeded at the Elandsfontein, Hendrina and Secunda monitoring stations. Considering the high density of precursor emission sources, this was no surprise. The high level of exceedances of the ambient air quality standards clearly signifies the magnitude of SO_2, NO_x and surface O_3 pollution across the HPA.

6.5. Future work, recommendations and implications for the HPA

As a pilot study future work can come out of this study. This study was the first of its kind with regard to spatio-temporal monitoring of pollutants within South Africa and across the HPA. The HPA, being a pollutant 'hotspot' and a priority area demands work on ambient air pollution. To address the ambient air pollution issues across the HPA monitoring is essential. Hence, this work should be used to promote further innovations in modelling techniques to promote the management of air pollution across the HPA.

In South Africa, seven criteria air pollutant exist. Across the surface of the HPA exceedances in all seven of these pollutants have been recorded (DEA, 2011). Future work will benefit from creating spatio-temporal models of all the criteria air pollutants. These future models should incorporate all factors that influence the concentration of pollutants, from land cover/use to meteorology, to improve model accuracy and predictive ability. These models should also incorporate season specific models as influential factors may differ from season to season (You *et al.*, 2015). Efforts regarding the multiple regression models were not particularly successful. To create models that may perform better to accurately estimate concentrations should be considered. Other statistical modelling methods may be useful to model these complex spatio-temporal patterns. Before this may be done more work into improving the multiple regression models is needed. Once this option is exhausted other statistical methods should be used. These methods include, but are not limited to, GWR and multivariate non-linear modelling.

Satellite imagery plays an important role in the model building process. Most available satellite imagery, especially the MODIS imagery used in this study, provide imagery of the atmosphere over coarse spatial resolutions not suitable to detect local scale pollution episodes. Future models should incorporate satellite-derived measurements with a high spatial resolution to capture these episodes. An improved spatial scale may mean that daily coverage of an area may not be possible and more limitations may be introduced into the model. Hence, possible options for this include MAIAC 1km AOD, where AOD measurements have the potential to detect most ambient air pollutants. AOD measurements may prove suitable to estimate all criteria air pollutants across the HPA.

Models may benefit from improvements in ground-level monitoring networks and addition of longer data records. Improvements in the SAAQIS monitoring network are always possible through maintenance, calibration and addition of new monitoring stations to better represent pollution across South Africa and the HPA.

The South African national ambient air quality standards provide measurements to track air pollution and identify pollution 'hotspot' areas. These standards were reviewed in 2009. It is currently 2017. A review of these standards is in order. Other possible pollutants may be added to this list, for example NO_x. Compliance with these standards should also be checked more often, especially within industry to reduce industrial emissions.

The HPA is a highly populated area. The option to move away from the HPA is only available for a select few. Mitigation strategies should be developed and put in place to reduce the risk of ambient air pollution among those living in the HPA. Possible mitigation strategies may only be put in place, especially within households, if there is socio-economic upliftment of low-income groups (Venter *et al.*, 2012). A main air pollution issue across the HPA is domestic fossil fuel burning as this is the only option for heating, cooking and lighting for many low-income groups. Additionally, methods to reduce industrial emissions should be developed and put in place as this is a more realistic option to reduce ambient pollution across the HPA.

7. References

Abdul-Wahab, S.A. and Al-Alwai, S.M., 2002: Assessment and prediction of tropospheric ozone concentration levels using artificial neural networks, *Environmental Modelling Software*, 17, 219 – 228.

Abdul-Wahab, S.A. and Bouhamra, W.S., 2004: Diurnal variations of air pollution from motor vehicles in residential area, *International Journal of Environmental Studies*, 61, 73 – 98.

Abiodun, B.J., Ojumu, A.M., Jenner, S. and Ojumu, T.V., 2014: The transport of atmospheric NO_x and HNO_3 over Cape Town, *Atmospheric Chemistry and Physics*, 14, 559 – 575.

Ahammed, Y.N., Reddy, R.R., Gopal, K.R., Narasimhulu, K., Basha, D.B., Reddy, L.S.S. and Rao, T.V.R., 2006: Seasonal variation of the surface ozone and its precursor gases during 2001–2003, measured at Anantapur (14.628N), a semi-arid site in India, *Atmospheric Research*, 80, 151 – 164.

Ahrens, C.D., 2009: *Meteorology Today: An Introduction to Weather, Climate, and the Environment*, Brooks/Cole, Cengage Learning, USA.

Akpinar, S., Oztop, H.F. and Akpinar, E.K., 2008: Evaluation of relationship between meteorological parameters and air pollutant concentrations during winter season in Elazığ, Turkey, *Environmental Monitoring and Assessment*, 146, 211 – 224.

Akpinar, E.K., Akpinar, S. and Öztop, H.F., 2009: Statistical analysis of meteorological factors and air pollution at winter months in Elaziğ, Turkey, *Journal of Environmental Engineering*, 7 – 16.

Al-Saadi, J., Szykman, J., Pierce, R.B., Kittaka, C., Neil, D., Chu, D.A., Remer, L., Gumley, L., Prins, E., Weinstock, L., MacDonald, C., Wayland, R., Dimmick, F. and Fishman, J., 2005: Improving national air quality forecasts with satellite aerosol observations, American Meteorological Society, DOI:10.1175/BAMS-86-9-1249

Alston, E.J., Sokolik, I.N. and Kalashnikova, O.V., 2012: Characterization of atmospheric aerosol in the US Southeast from ground- and space-based measurements over the past decade, *Atmospheric measurements techniques*, 5, 1667 – 1682.

An, X., Wang, Z., Li, C. and Wang, Y., 2007: A modeling analysis of a heavy air pollution episode occurred in Beijing, *Atmospheric Chemistry and Physics*, 7, 3103 – 3114.

Australian Government., 2002: Ambient Air Quality Standards. Available from: http://www.environment.gov.au/protection/air-quality/air-quality-standards#air (Accessed 30 January 2017).

Avnery, S., Mauzerall, D.L., Liu, J. and Horowitz, L.W., 2011: Global crop yield reductions due to surface ozone exposure: 1. Year 2000 crop production losses and economic damage, *Atmospheric Environment*, 45, 2284 – 2296.

Balashov, N.V., Thompson, A.M., Piketh, S.J. and Langerman, K.E., 2014: Surface ozone variability and trends over the South African Highveld from 1990 to 2007, *Journal of Geophysical Research: Atmosphere*, 119, 4323 – 4342.

Barnaba, F., Putaud, J.P., Gruening, C., dell'Acqua, A. and Dos Santos, S., 2010: Annual cycle in co-located in situ, total-column, and height-resolved aerosol observations in the Po Valley (Italy): Implications for ground-level particulate matter mass concentration estimation from remote sensing, *Journal of Geophysical Research*, 115, 1 – 22.

Beig, G., Gunthe, S. and Jadhav, D.B., 2007: Simultaneous measurements of ozone and its precursors on a diurnal scale at a semi urban site in India, *Journal of Atmospheric Chemistry*, 57, 239 – 253.

Betts, A.K., Gatti, L.V., Cordova, A.M., Dias, M.A.F.S. and Fuentes, J.D., 2002: Transport of ozone to the surface by convective downdrafts at night, *Journal of Geophysical Research*, 107, 1 – 7.

Burt, J.E., Barber, G.M. and Rigby, D.L., 2009: *Elementary Statistics for Geographers*, The Guilford Press, London.

Carmichael, G.R., Ferm, M., Thongboonchoo, N., Woo, J., Kentaro, C., Pham, M., Viet, P.H., Mossberg, C., Bala, R., Boonjawat, J., Upatum, P., Mohan, M., Adhikary, S.P., Shrestha, A.B., Pienaar, J.J., Brunke, E.B., Chen, T., Jie, T., Guoan, D., Peng, L.C., Dhiharto, S., Harjanto, H., Jose, A.M., Kimani, W., Kirouane, A., Lacaux, J., Richard, S., Barturen, O., Cerda, J.C., Athayde, A., Tavares, T., Cotrina, J.S. and Bilici, E., 2003: Measurements of sulfur dioxide, ozone and ammonia concentrations in Asia, Africa and South America using passive samplers, *Atmospheric Environment*, 37, 1293 – 1308.

Chelani, A.B., 2012: Persistence analysis of extreme CO, NO_2 and O_3 concentrations in ambient air of Delhi, *Atmospheric Research*, 108, 128 – 134.

Chen, L.W.A., Doddridge, B.G., Dickerson, R.R., Chow, J.C., Mueller, P.K., Quinn, J. and Butler, W.A., 2001: Seasonal variations in elemental carbon aerosol, carbon monoxide and sulfur dioxide: Implications for sources, *Geophysical Research Letters*, 28, 1711 – 1714.

Chen, B.B., Sverdlik, L.G., Imashey, S.A., Solomon, P.A., Lantz, J., Schauer, J.J., Shafer, M.M., Artamonova, M.S. and Carmichael., 2013: Empirical relationship between particulate matter and aerosol optical depth over Northern Tien-Shan, Central Asia, *Atmospheric Quality and Atmospheric Health*, 6, 385 – 396.

Chio, W., Paulson, S.E., Casmassi, J. and Winer, A.M., 2013: Evaluating meteorological comparability in air quality studies: Classification and regression trees for primary pollutants in California's South Coast Air Basin, *Atmospheric Environment*, 64, 150 – 159.

Chu, D.A., Kaufman, Y.J., Zibordi, G., Chern, J.D., Mao, J., Li, C. and Holben, B.N., 2003: Global monitoring of air pollution over land from the Earth Observing System-Terra Moderate Resolution Imaging Spectroradiometer (MODIS), *Journal of Geophysical Research*, 108, 1 – 18.

Chu, D.A., Ferrare, R., Szykman, J., Lewis, J., Scarino, A., Hains, J., Burton, S., Chen, G., Tsai, T., Hostetler, C., Hair, J., Holben, B. Crawford, J., 2015: Regional characteristics of the

relationship between columnar AOD and surface $PM_{2.5}$: Application of lidar aerosol extinction profiles over Baltimore-Washington Corridor during DISCOVER-AQ, *Atmospheric Environment*, 101, 338 – 349.

Colls, J., 1999: *Air Pollution: an introduction*, London: E & FN Spon.

Collett, K. S., Piketh, S.J. and Ross, K.E., 2010: An assessment of the atmospheric nitrogen budget on the South African Highveld, *South African Journal of Science*, 106, 1 – 9.

Comrie, A., 1994: A synoptic climatology of rural ozone pollution at three forest sites in Pennsylvania, *Atmospheric Environment*, 28, 1601 – 1614.

Cosjin, C. and Tyson, P.D., 1996: Stable discontinuities in the atmosphere over South Africa, *South African Journal of Science*, 92, 381 – 386.

Crompton, R., 2016: SA needs to get out of its petrochemicals cul-de-sac. Available from: http://www.moneyweb.co.za/moneyweb-opinion/soapbox/sa-needs-to-get-out-of-its-petrochemicals-cul-de-sac/ (Accessed 16 January 2017).

Crutzen, P.J., Lawrence, M.G. and Pöschl, U., 1999: On the background photochemistry of tropospheric ozone, *Tellus*, 51, 123 – 146.

CSIR., 2012: *Best practices guide to consider air-related human health in your area: for South African air quality officers and environmental health practitioners*, Pretoria.

Cuhadaroglu, B. and Demirci, E., 1997: Influence of some meteorological factors on air pollution in Trabzon city, *Energy and Buildings*, 25, 179 – 184.

Datta, A., Saud, T., Goel, A., Tiwari, S., Sharma, S.K., Saxena, M. and Mandal, T.K., 2010: Variation of ambient SO_2 over Delhi, 65, 127 – 143.

David, L.M. and Nair, P.R., 2011: Diurnal and seasonal variability of surface ozone and NOx at a tropical coastal site: Association with mesoscale and synoptic meteorological conditions, *Journal of Geophysical Research*, 116, 1 – 16.

DEA., 2004: *Environmental Management: Air Quality Act, 2004 (Act No. 39 of 2004)*, Government Gazette, Cape Town.

DEA., 2009: *National Environmental Management: Air Quality Act, 2004 (Act No. 39 of 2004): National Ambient Air Quality Standards*, Government Gazette, Cape Town.

DEA., 2011: *Highveld Priority Area Air Quality Management Plan*, Department of Environmental Affairs, report NO. GG 34250, GNR270, government printer, Pretoria.

DEA., 2017: Priority Areas. Available from: http://www.saaqis.org.za/Priority%20Areas.aspx (Accessed 4 January 2017).

Debaje, S.B. and Kakade, A.D., 2009: Surface ozone variability over western Maharashtra, India, *Journal of Hazardous Materials*, 161, 686 – 700.

Demirci, E. and Cuhadaroglu, B., 2000: Statistical analysis of wind circulation and air pollution in urban Trabzon, *Energy and Buildings*, 31, 49 – 53.

DNP., 2012: Monitoring stations. Available from: http://www.dnpinternational.net/Products.aspx?Group=32 (Accessed 18 May 2017).

Dueñas, C., Fernàndez, M.C., Cañete, S., Carretero, J. and Liger, E., 2002: Assessment of ozone variations and meteorological effects in an urban area in the Mediterranean Coast, *The Science of the Total Environment*, 299, 97 – 113.

Eder, B.K., Davis, J.M. and Bloomfield, P., 1994: An automated classification scheme designed to better elucidate the dependence of ozone on meteorology, *Journal of Applied Meteorology*, 33, 1182 – 1199.

Edwards, D.P., 2006: Air Quality Remote Sensing from space, *EOS*, 87, 327 – 328.

Elampari, K. and Chithambarathanu, T., 2011: Diurnal and seasonal variations in surface ozone levels at tropical semi-urban site, Nagercoil, India, and relationships with meteorological conditions, *International Journal of Science and Technology*, 1, 80 – 88.

Elminir, H.K., 2005: Dependence of urban air pollutants on meteorology, *Science of the Total Environment*, 350, 225 – 237.

Emili, E., Popp, C., Wunderle, S., Zebisch, M. and Petittia, M., 2011: Mapping particulate matter in alpine regions with satellite and ground-based measurements: an exploratory study for data assimilation, *Atmospheric Environment*, 45, 4344 – 4353.

Engel-Cox, J.A., Holloman, C.H., Coutant, B.W. and Hoff, R.M., 2004: Qualitative and quantitative evaluation of MODIS satellite sensor data for regional and urban scale air quality, *Atmospheric Environment*, 38, 2495 – 2509.

Engel-Cox, J.A., Hoff, R.M., Rogers, R., Dimmick, F., Rush, A., Szykman, J.J., Al-Saadi, J., Chu, D.A. Zell, E.R., 2006: Integrating lidar and satellite optical depth with ambient monitoring for 3-dimensional particulate characterization, *Atmospheric Environment*, 40, 8056 – 8067.

EPA, 2016: NAAQS Table. Available from: https://www.epa.gov/criteria-air-pollutants/naaqs-table (Accessed 6 February 2017).

Esau, I., Luhunga, P., Djolov, G., Rautenbach, C.J.W. and Zilitinkevich, S., 2012: Links between observed micro-meteorological variability and land-use patterns in the Highveld priority area of South Africa, *Meteorology and Atmospheric Physics*, 118, 129 – 142.

Eskom., 2017a: Camden Power Station. Available from: http://www.eskom.co.za/Whatweredoing/ElectricityGeneration/PowerStations/Pages/Camden_Power_Station.aspx (Accessed 16 January 2017).

Eskom., 2017b: Komati Power Station. Available from: http://www.eskom.co.za/Whatweredoing/ElectricityGeneration/PowerStations/Pages/Komati_Power_Station.aspx (Accessed 16 January 2017).

European Commission., 2015: Air Quality Standards. Available from: http://ec.europa.eu/environment/air/quality/standards.htm (Accessed 6 February 2017).

Fishman, J., Fakhruzzaman, K., Cros, B. and Nganga, D., 1991: Identification of widespread pollution in the southern hemisphere deduced from satellite analyses, *Science*, 252, 1693 – 1696.

Fishman, J., Creilson, J.K., Parker, P.A., Ainsworth, E.A., Vinning, G.G., Szarka, J., Booker, F. and Xu, X., 2010: An investigation of widespread ozone damage to the soybean crop in the upper Midwest determined from ground-based and satellite measurements, *Atmospheric Environment*, 44, 2248 – 2256.

Fisshea, R., Dommen, L., Gutzwiller, E., Weingartner, M., Gysel, M., Emmenegger, C., Kalberer, M. and Baltensperger, U., 2006: Seasonal and diurnal characteristics of water soluble inorganic compounds in the gas and aerosol phase in the Zurich area, *Atmospheric Chemistry and Physics*, 6, 1895 – 1904.

Flaum, J.B., Rao, S.T. and Zurbenko, I.G., 1996: Moderating the influence of meteorological conditions on ambient ozone concentrations, *Air and Waste Management Association*, 46, 35 – 46.

Freiman, M.T. and Piketh, S.J., 2002: Air Transport into and out of the Industrial Highveld Region of South Africa, *Journal of Applied Meteorology*, 42, 994 – 1002.

Gartsang, M., Tyson, P.D., Swap, R., Edwards, M., Kållberg, P. and Lindesay, J.A., 1996: Horizontal and vertical transport of air over southern Africa, *Journal of Geophysical Research*, 101, 721 – 736.

Gaur, A., Tripathi, S.N., Kanawade, V.P., Tare, V. and Shukla, S.P., 2014: Four-year measurements of trace gases (SO_2, NO_x and surface O_3) at an urban location, Kanpur, in Northern India, *Journal of Atmospheric Chemistry*, 71, 283 – 301.

Giri, D., Krishna, M.V. and Adhikary, P.R., 2008: The influence of meteorological conditions on PM_{10} concentrations in Kathmandu Valley, *Journal of Environmental Research*, 2, 49 – 60.

Guicherit, R. and Roemer, M., 2000: Tropospheric ozone trends, *Chemosphere – Global Change Science*, 2, 167 – 183.

Gupta, P., Christopher, S.A., Wang, J., Gehrig, R., Lee, Y. and Kumar, N., 2006: Satellite remote sensing of particulate matter and air quality assessment over global cities, *Atmospheric Environment*, 40, 5580 – 5892.

Gupta, P. and Christopher, S.A., 2008: Seven year particulate matter air quality assessment from surface and satellite measurements, *Atmospheric Chemistry and Physics*, 8, 3311 – 3324.

Gupta, P. and Christopher, S.A., 2009a: Particulate matter air quality assessment using integrated surface, satellite, and meteorological products: Multiple regression approach, *Journal of Geophysical Research*, 114, 1 – 13.

Gupta, P. and Christopher, S.A., 2009b: Particulate matter air quality assessment using integrated surface, satellite, and meteorological products: 2. A neural network approach, *Journal of Geophysical Research*, 114, 1 – 14.

Gvozdić, V., Kovač-Andrić, E. and Brana, J., 2011: Influence of meteorological factors, NO_2, SO_2, CO and PM_{10} on the concentration of O_3 in the urban atmosphere of eastern Croatia, *Environmental Modelling and Assessment*, 16, 491 – 501.

Harrison, R.M., Pope, F.D. and Shi, Z., 2014: Air pollution, *Earth Systems and Environmental Sciences*, 1 – 17.

Hassan, I.A., Basahi, J.M., Ismail, I.M. and Habeebullah, T., 2013: Spatial distribution and temporal variation in ambient ozone and its associated NO_x in the atmosphere of Jeddah City, Saudi Arabia, *Aerosol and Air Quality Research*, 13. 1712 – 1722.

Hoff, R.M. and Christopher, S.A., 2009: Remote Sensing of Particulate Pollution from Space: Have We Reached the Promised Land?, *Journal of the Air & Waste Management Association*, 49, 645 – 675.

Hu, X., Waller, L.A., Lyapustin, A., Wang, Y., Al-Hamdan, M.Z., Crosson, W.L., Estes Jr, M.G., Estes, S.M., Quattrochi, D.A., Puttaswamya, S.J. and Liua, Y., 2014a: Estimating ground-level PM2.5 concentrations in the Southeastern United States using MAIAC AOD retrievals and a two-stage model, *Remote Sensing of Environment*, 140, 220 – 232.

Hu, X., Waller, L.A., Lyapustin, A., Wang, Y. and Liu, Y., 2014b: 10-year spatial and temporal trends of $PM_{2.5}$ concentrations in the southeastern US estimated using high-resolution satellite data, *Atmospheric Chemistry and Physics*, 14, 6301 – 6314.

Hutchinson, K.D., 2003: Applications of MODIS satellite data and products for monitoring air quality in the state of Texas, *Atmospheric Environment*, 37, 2403 – 2412.

Hutchinson, K.D., Pekker, T. and Smith, S., 2006: Improved Retrievals of Cloud Boundaries from MODIS for Use in Air Quality Modeling; *Atmospheric Environment*, *40*, 5798-5806.

Ilten, N. and Selici, A.T., 2008: Investigating the impacts of some meteorological parameters on air pollution in Balikesir, Turkey, *Environmental Monitoring and Assessment*, 140, 267 – 277.

IPCC, 2001: *Climate Change 2001: The Scientific Basis, Contribution of Working Group I to the Third Assessment Report of Intergovernmental Panel on Climate Change (IPCC),* Cambridge: University Press.

Jaffe, D. and Ray., 2007: Increase in surface ozone at rural sites in western US, *Atmospheric Environment*, 41, 5452 – 5463.

Jain, S.L., Arya, B.C., Kumar, A., Ghude, S.D. and Kulkarni, P.S., 2005: Observational study of surface ozone at New Delhi, India, *International Journal of Remote Sensing*, 26, 3515 – 3524.

Josipovic, M., Annegarn, H.J., Knee, M.A., Pienaar, J.J. and Piketh, S.J., 2010: Concentrations, distributions and critical level exceedance assessment of SO_2, NO_2 and O_3 in South Africa, *Environmental Monitoring and Assessment*, 171, 181 – 196.

Jourdain, B. and Legrand, M., 2001: Seasonal variations of atmospheric dimethylsulfide, dimethylsulfoxides, sulfur dioxide, methanesulfonate, and non-sea-salt sulfate aerosols at Dumont d'Urville (coastal Antarctic) (December 1998 to July 1999), *Journal of Geophysical Research*, 106, 391 – 408.

Kartal, S. and Özer, U., 1998: Determination and parameterization of some air pollutants as a function of meteorological parameters in Kayseri, Turkey, *Journal of Air and Waste Management*, 48, 853 – 859.

Khemani, L.T., Momin, G.A., Rao, P.S.P., Vijayakumar, R. and Safai, P.D., 1995: Study of surface ozone behaviour at urban and forested sites, *Atmospheric Environment*, 29, 2021 – 2024.

Khoder, M.I., 2009: Diurnal, seasonal and weekdays–weekends variations of ground level ozone concentrations in an urban area in greater Cairo, *Environmental Monitoring and Assessment*, 149, 349 – 362.

Kirkman, G.A., Piketh, S.J., Andreae, M.O., Annegarn, H.J. and Helas., 2000: Distribution of aerosols, ozone and carbon monoxide over southern Africa, *South African Journal of Science*, 96, 423 – 421.

Koelemeijer, R.B.A., Homan, C.D. and Matthijsen, J., 2006: Comparison of spatial and temporal variations of aerosol optical thickness and particulate matter over Europe, *Atmospheric Environment*, 40, 5304 – 5315.

Kouvarakis, G., Tsigaridis, K., Kanakidou, M. and Mihalopoulos, N., 2000: Temporal variations of surface regional background ozone over Crete Island in the southeast Mediterranean, *Journal of Geophysical Research*, 105, 4399 – 4407.

Kumar, R., Naja, M., Venkataramani, S. and Wild, O., 2010: Variations in surface ozone at Nainital: a high-altitude site in central Himalayas, *Journal of Geophysical Research*, 115, 1 – 12.

Lal, S., Naja, M. and Subbaraya, B.H., 2000: Seasonal variations in surface ozone and its precursors over an urban site in India, *Atmospheric Environment*, 34, 2713 – 2724.

Laakso, L., Laakso, H., Aalto, P.P., Keronen, P., Petäjä, T., Nieminen, T., Pohja, T., Siivola, E., Kumala, M., Kgabi, N., Molefe, M., Mabaso, D., Phalatse, D., Pienaar, K. and Kerminen, M., 2008: Basic characteristics of atmospheric particles, trace gases and meteorology in a relatively clean Southern African Savannah environment, *Atmospheric Chemistry and Physics Discussions*, 8, 6313 – 6353.

Laasko, L., Vakkari, V., Virkkula, A., Laakso, H., Backman, J., Kulmala, M., Beukes, J.P., van Zyl, P.G., Tiitta, P., Josipovic, M., Pienaar, J.J., Chiloane, K., Gilardoni, S., Vignati, E., Wiedensohler, A., Tuch, T., Birmili, W., Piketh, S., Collett, K., Fourie, G.D., Komppula, M., Lihavainene, H., de Leeuw, G. and Kerminen, V.M., 2012: South Africa EUCAARI

measurements: seasonal variation of trace gases and aerosol optical properties, *Atmospheric Chemistry and Physics*, 12, 1847 – 1864.

Lamasal, L.N., Martin, R.V., van Donkelaar, A., Steinbacher, M., Celarier, E.A., Bucsela, E., Dunlea, E.J. and Pinto, J.P., 2008: Ground-level nitrogen dioxide concentrations inferred from the satellite-borne Ozone Monitoring Instrument, *Journal of Geophysical Research*, 113, 1 – 15.

Latini, G., Grifoni, R.C. and Passerini, G., 2002: Influence of meteorological parameters on urban and suburban air pollution, in *Air Pollution*, Wit Press, Southampton, UK, 753 – 762.

Laurinavičienė, D., 2008: Nitrogen Dioxide concentrations and their relation with meteorological conditions and some environmental factors in Kaunas, *Environmental Research, Engineering and* Management, 43, 21 – 27.

Lee, H.J., Liu, Y., Coull, B.A., Schwartz, J. and Koutrakis, P., 2011: A novel calibration approach of MODIS AOD data to predict $PM_{2.5}$ concentrations, *Atmospheric Chemistry and Physics*, 11, 9769 – 9795.

Li, C., Lau, A.K., Mao, J. and Chu, D.A., 2005: Retrieval, Validation, and Application of the 1-km Aerosol Optical Depth from MODIS measurements over Hong Kong*, Transactions on Geoscience and Remote Sensing*, 43, 2650 – 2658.

Li, C., Hsu, N.C. and Tsay, S., 2011: A study on the potential applications of satellite data in air quality monitoring and forecasting, *Atmospheric Environment*, 45, 3663 – 3675.

Lin, W., Xu, X., Zhang, X. and Tang, J., 2008: Contributions of pollutants from North China Plain to surface ozone at the Shangdianzi GAW station, *Atmospheric Chemistry and Physics*, 8, 5889 – 5898.

Lin, C., Li, Y., Yuan, Z., Lau, A.K.H., Li, C. and Fung, J.C.H., 2015: Using satellite remote sensing data to estimate the high-resolution distribution of ground-level $PM_{2.5}$, *Remote Sensing of the Environment*, 156, 117 – 128.

Lourens, A.S., Beukes, J.P., van Zyl, P.G., Fourie, G.D., Burger, J.W., Pienaar, J.J., Read, C.E. and Jordaan, J.H., 2011: Spatial and temporal assessment of gaseous pollutants in the Highveld of South Africa, South African Journal of Science, 1 – 8.

Luvsan, M., Shiea, R., Purevdroid, T, Badarche, L., Baldorje, B. and Chana, C., 2012: The influence of emission sources and meteorological conditions on SO_2 pollution in Mongolia, *Atmospheric Environment*, 61, 542 – 549.

Lyubovtseva, Y.S., Maso, M.D., Bonn, B., Keronen, P. and Kulmala, M., 2005: Seasonal variations of trace gases, meteorological parameters, and formation of aerosols in Boreal forests, *Boreal Environment Research*, 10, 493 – 510.

Ma, Z., Hu, X., Huang, L., Bi, J. and Liu, Y., 2014: Estimating Ground-Level $PM_{2.5}$ in China using satellite remote sensing, *Environmental Science and Technology*, 48, 7436 – 7444.

Martin, R.V., 2008: Satellite remote sensing of surface air quality, *Atmospheric Environment*, 42, 7823 – 7843.

Mendenhall, W., 2009: *Introduction to Probability and Statistics*, Brooks/Cole Cenegage Learning, Belmont.

Meng, Z.Y., Xu, X.B., Yan, P., Ding, G.A., Tang, J., Lin, W.L., Xu, X.D. and Wang, S.F., 2009: Characteristics of trace gaseous pollutants at a regional background station in Northern China, *Atmospheric Chemistry and Physics*, 9, 927 – 936.

Montgomery, D.C., Peak, E.A. and Vinning, G.G., 2012: Introduction to Linear Regression Analysis, Wiley, Hoboken.

Naja, M. and Lal, S., 2002: Surface ozone and precursor gases at Gadanki (13.5°N, 79.2°E), a tropical rural site in India, *Journal of Geophysical Research*, 107, 8 – 13.

Naja, M., Lal, S. and Chand, D., 2003: Diurnal and seasonal variabilities in surface ozone at a high altitude site Mt Abu (24.6°N, 72.7°E, 1680m asl) in India, *Atmospheric Environment*, 37, 4205 – 4215.

NASA., 2016: MODIS: Moderate Resolution Imaging Spectroradiometer. Available from: https://modis.gsfc.nasa.gov/about/ (Accessed 9 February 2017).

Nguyen, T.T.N., Bui, H.Q., Pham, H.V., Luu, H.V., Man, C.D., Pham, H.N., Le, H.T. and Nguyen, T.T., 2015: Particulate matter concentration mapping from MODIS satellite data: a Vietnamese case study, *Environmental Research Letters*, 10, 1 – 13.

Nicolantonio, W.D., Cacciari, A. and Tomasi, C., 2009: Particulate Matter at Surface: Northern Italy Monitoring Based on Satellite Remote Sensing, Meteorological Fields, and in-situ Samplings, *Journal of selected Topics in Applied Earth Observations and Remote Sensing*, 2, 284 – 292.

Nishanth, T., Kumar, S.M.K. and Valsarai, K.T., 2012: Variations in surface ozone and NO_x at Kannur: a tropical coastal site in India, *Journal of Atmospheric Chemistry*, 69, 101 – 126.

Outdoorphoto., 2007: Grootvlei Power Station. Available from: http://www.outdoorphoto.community/gallery/showphoto.php?photo=201971 (Accessed 16 January 2017).

Pandey, S.K., Kima, K., Chunga, S., Chob, S., Kimb, M. and Shonc, Z., 2008: Long-term study of NOx behavior at urban roadside and background locations in Seoul, Korea, *Atmospheric Environment*, 42, 607 – 622.

Piketh, S.J., Annegain, H.J. Tyson, P.D., 1999: Lower tropospheric aerosol loadings over South Africa: the relative contribution of Aeolian dust, industrial emissions and biomass burning, *Journal of Geophysical Research*, 104, 1597 – 1607.

Pochanart, P., Hirokawa, J., Kajii., Akimoto, H. and Nakao, M., 1999: Influence of regional-scale anthropogenic activity in northeast Asia on seasonal variations of surface ozone

and carbon monoxide observed at Oki, Japan, *Journal of Geophysical Research*, 104, 3621 – 3631.

Prasad, A.K and Singh, R.P., 2007: Comparison of MISR-MODIS aerosol optical depth over the Indo-Gangetic basin during the winter and summer seasons (2000 – 2005).

Pudasainee, D., Sapkota, B., Shrestha, M.L., Kaga, A., Kondo, A. and Inoue, Y., 2006: Ground level ozone concentrations and its association with NO_x and meteorological parameters in Kathmadu valley, Nepal, *Atmospheric Environment*, 40, 8081 – 8087.

Reddy, B.S.K., Kumar, K.R., Balakrishnaiah, G., Gopal, K.R., Reddy, R.R., Sivakumar, V., Lingaswamy, A.P., Arafath, S.M., Umadevi, K., Kumari, S.P., Ahammed, Y.N. and Lal, S., 2012: Analysis of diurnal and seasonal behaviour of surface ozone and its precursors (NO_x) at a semi-arid rural site in southern India, *Aerosol and Air Quality Research*, 12: 1081 – 1094.

Romieu, I. and Herndandez-Avila, M., 2002: Air pollution and Health in Developing countries: a review of epidemiological evidence, in G. McGranahan and F. Murray (eds), *Air Pollution and Health in Developing Countries*, Earthscan: London, 49 – 62.

Saliba, N.A., Moussa, S., Salame, H. and El-Fadel, M., 2006: Variation of selected air quality indicators over the city of Beirut, Lebanon: assessment of emission sources, *Atmospheric Environment*, 40, 3263 – 3268.

Satsangi, G.S., Lakhani, A., Kulshrestha, P.R. and Taneja, A., 2004: Seasonal and diurnal variation of surface ozone and a preliminary analysis of exceedance of its critical levels at a semi-arid site in India, *Journal of Atmospheric Chemistry*, 47, 271 – 286.

Sahu, L.K. and Lal, S., 2006: Distributions of $C_2 – C_5$ NMHC's and related trace gases at a tropical urban site in India, *Atmospheric Environment*, 40, 880 – 891.

SAWS, 2017: How are the dates of the four seasons worked out?. Available from: http://www.weathersa.co.za/learning/weather-questions/82-how-are-the-dates-of-the-four-seasons-worked-out (Accessed 9 February 2017).

Schaap, M., Apituley, A., Timmermans, R.M.A., Koelemeijer, R.B.A. and de Leeuw, G., 2009: Exploring the relation between aerosol optical depth and $PM_{2.5}$ at Cabauw, the Netherlands, *Atmospheric Chemistry and Physics*, 9, 909 – 925.

Seeman, S.W., Borbas, E.E., Li, J., Menzel, W.P. and Gumley, L.E., 2006: *MODIS atmospheric profile retrieval algorithm theoretical basis*, Cooperative Institue for meteorological satellite studies, Davyton, Madison.

Sharma, P., Kuniyal, J.C., Chand, K., Guleria, R.P., Dhyani, P.P. and Chauhan, C., 2013: Surface ozone concentration and its behaviour with aerosols in the northwestern Himalaya, India, *Atmospheric Environment*, 71, 44 – 53.

Sinha, P.R., Gupta, P., Kaskaoutis, D.G., Sahu, L.K., Nagendra, N., Manchanda, R.K., Kumar, Y.B. and Sreenivasan, S., 2015: Estimation of particulate matter from satellite and ground-based observations over Hyderabad, India, *International Journal of Remote Sensing,* 36, 6192 – 6213.

Sotoudeheian, S. and Arhami, M., 2014: Estimating ground-level PM_{10} using satellite remote sensing and ground-based meteorological measurements over Tehran, *Journal of Environmental Health Science and Engineering*, 12, 1 – 13.

Staehelin, J., Thudium, J., Buehler, R., Volz-Thomas, A. and Graber, W., 2001: Trends in surface O_3 concnetrations at Arosa (Switzerland), *Atmospheric Environment*, 28, 75 – 87.

Statistics South Africa., 2012: *Census 2011 Statistical release*, Pretoria.

Stehr, J.W., Dickerson, R.R., Hallock-Waters, K.A., Doddridge, B.G. and Kirk, D., 2000: Observations of NO_y, CO and SO_2 and the origin of reactive Nitrogen in the eastern United States, *Journal of Geophysical Research*, 105, 3553 – 3563.

Steyn, H., 2013: Kriel Power Station. Available from: https://www.flickr.com/photos/hannes_steyn/10007120103 (Accessed 16 January 2017).

The Royal Society., 2008: *Ground-level ozone in the 21st century: future trends, impacts and policy implications*, Carlton House Terrace, London.

Thompson, M.L., Reynolds, J., Cox, L.H., Guttorp, P. and Sampson, P.D., 2001: A review of statistical methods for the meteorological adjustment of tropospheric ozone, *Atmospheric Environment*, 35, 617 – 630.

Turalioğlu, F., Nuhoğlu, A. and Bayraktar, H., 2005: Impacts of some meteorological parameters on SO_2 and TSP concentrations in Erzurum, Turkey, *Chemosphere*, 59, 1633 – 1642.

Tiwari, S., Rai, R. and Agrawal, M., 2008: Annual and seasonal variations in tropospheric ozone concentrations around Varanasi, *International Journal of Remote Sensing*, 29, 4499 – 4514.

Toth, T.D., Zhang, J., Campbell, J.R., Hyer, E.J., Reid, J.S., Shi, Y. and Westphal, D.L., 2014: Impact of data quality and surface-to-column representativeness on the $PM_{2.5}$/satellite AOD relationship for the contiguous United States, *Atmospheric Chemistry and Physics*, 14, 6049 – 6062.

Tsai, T., Jeng, Y., Chu, D.A., Chen, J. and Chang, S., 2011: Analysis of the relationship between MODIS aerosol optical depth and particulate matter from 2006 to 2008, *Atmospheric Environment*, 45, 4777 – 4788.

Tu, J., Xia, Z., Wang, H. and Li, W., 2007: Temporal variations in surface ozone and its precursors and meteorological effects at an urban site in China, *Atmospheric Research*, 85, 310 – 337.

Turalioğlu, F.S., Nuhoğlu, A. and Bayraktar, H., 2005: Impacts of some meteorological parameters on SO_2 and TSP concentrations in Erzurum, Turkey, *Chemosphere*, 59, 1633 – 1642.

Tyson, P.D., Kruger, F.J. and Louw, C.W., 1988: *Atmospheric pollution and its implications in the Eastern Traansvaal Highveld*, Council for Scientific and Industrial Research, Pretoria.

Tyson, P.D., Gartsang, M. and Swap, R., 1996a: Large-scale recirculation of air over South Africa, *Journal of Applied Meteorology*, 2218 – 2236.

Tyson, P.D., Gartsang, M., Swap, R., Kallberg, P. and Edwards, M., 1996b: An air transport climatology for subtropical southern Africa, *International Journal of Climatology*, 16, 265 – 291.

Tyson, P.D., Gartsang, M., Thompson, A.M., D'Abreton., Diab, D. and Browell, E.V., 1997: Atmospheric transport and photochemistry of ozone over central southern Africa during the Southern Africa Fire-Atmosphere Research Initiative, *Journal of Geophysical Research*, 102, 623 – 635.

Tyson, P.D. and D'Abreton, P.C., 1998: Transport and recirculation of aerosols off southern Africa-Macroscale plume structure, *Atmospheric Environment*, 32, 1511 – 1524.

Tyson, P.D. and Preston-Whyte, R.A., 2000: *The Weather and Climate of Southern Africa Second Edition*, Oxford University Press, Cape Town.

Tyson, P.D. and Gatebe, C.K., 2001: The atmosphere, aerosols, trace gases and biochemical change in southern Africa: a regional integration, *South African Journal of Science*, 97, 106 – 118.

Underhill, L. and Bradfield., 2009: *Introstat*, Juta and Co. Ltd, Cape Town.

Vallero, D., 2008: *Fundamentals of Air Pollution, Fourth Edition*, Elsevier, Amsterdam.

van Donkelaar, A., Martin, R.V. and Park, R.J., 2006: Estimating ground-level PM2.5 using aerosol optical depth determined from satellite remote sensing, *Journal of Geophysical Research*, 111, 1 – 10.

van Donkelaar, A., Martin, R.V., Brauer, M., Kahn, R., Levy, R., Verduzco, C. and Villeneuve, P.J., 2010: Global Estimates of Ambient Fine Particulate Matter Concentrations from Satellite-Based Aerosol Optical Depth: Development and Application, *Environmental Health Perspectives*, 118, 847 – 855.

van Emden, H., 2009: *Statistics for the terrified biologists*, Blackwell Publishing, UK.

Varotsos, C., Kondratyev, K.Y. and Efstathiou, M., 2001: On the seasonal variation of the surface ozone in Athens, Greece, *Atmospheric Environment*, 35, 315 – 320.

Venter, A.D., Vakkari, V., Beukes, J.P., van Zyl, P.G., Laakso, H., Mabaso, D., Josipovic, D., Tiitta, P., Josipovic, M., Kulmala, M., Pienaar, J.J. and Laakso, L., 2012: An air quality assessment in the industrialised western Bushveld Igneous Complex, South Africa, *South African Journal of Science*, 108, 1 – 10.

Vingarzan, R., 2004: A review of surface ozone background levels and trends, *Atmospheric Environment*, 38, 3431 – 3442.

Wang, J. and Christopher, S.A., 2003: Intercomparison between satellite-derived aerosol optical thickness and PM2.5 mass: Implications for air quality studies, *Journal of Geophysical Research*, 30, 1 – 4.

Wang, X. and Mauzerall, D.L., 2004: Characterizing distributions of surface ozone and its impact on grain production in China, Japan and South Korea: 1990 and 2020, *Atmospheric Environment*, 38, 4383 – 4402.

WHO., 2005: *WHO air quality guidelines for particulate matter, ozone, nitrogen dioxide and sulfur dioxide: global update 2005, summary of risk assessment*, WHO Press, Switzerland.

Wikimedia., 2016: Arnot Power Station. Available from: https://commons.wikimedia.org/wiki/File:South_Africa-Mpumalanga-Middelburg-Arnot_Power_Station_(cropped).jpg (accessed 16 January 2017).

Wong, D., Yuan, L. and Perlin, S., 2004: Comparison of spatial interpolation methods for the estimation of air quality data, Journal of Exposure Science and Environmental Epidemiology, 14, 404 - 415.

Xin, J., Zhang, Q., Wang, L., Gonga, C., Wanga, Y., Liua, Z., Gaoa, W., 2014: The empirical relationship between the PM2.5 concentration and aerosol optical depth over the background of North China from 2009 to 2011, *Atmospheric Research*, 138, 179 – 188.

Xu, X., Lin, W., Wang, T., Yan, P., Tang, J., Meng, Z. and Wang, Y., 2008: Long-term trend of surface ozone at a regional background station in eastern China 1991 – 2006: enhanced variability, *Atmospheric Chemistry and Physics*, 8, 2595 – 2607.

Yamanji, K., Ohara, T., Uno, I., Tanimoto, H., Kurokawa, J. and Akimoto, H., 2006: Analysis of the seasonal variation of ozone in the boundary layer in East Asia using community multi-scale air quality model: What controls surface ozone levels over Japan?, *Atmospheric Environment*, 40, 1856 – 1868.

You, W., Zanga, Z., Zhana, L., Lib, Z., Chenc, D. and Zhanga, G., 2015: Estimating ground-level PM10 concentration in northwestern China using geographically weighted regression based on satellite AOD combined with CALIPSO and MODIS fire count, *Remote Sensing of the Environment*, 168, 276 – 285.

Zhang, H., Hoff, R.M. and Engel-Cox, J.A., 2009: The Relation between Moderate Resolution Imaging Spectroradiometer (MODIS) Aerosol Optical Depth and PM2.5 over the United States: A Geographical Comparison by U.S. Environmental Protection Agency Regions, *Journal of Air and Waste Management*, 59, 1358 – 1369.

Zheng, J., Zhong, L., Wang, T., Louie, P.K.K. and Li, Z., 2010: Ground-level ozone in the Pearl River Delta region: Analysis of data from a recently established regional air quality monitoring network, *Atmospheric Environment*, 44, 814 – 823.

Zunckel, M., Turner, C.R. and Wells, R.B., 1996: Dry deposition of Sulphur on the Mpumalanga Highveld: a pilot study using the inferential method, *South African Journal of Science*, 92, 485 – 491.

Zunckel, M., Robertson, L., Tyson, P.D. and Rodhe, H., 2000: Modelled transport and deposition of Sulphur over Southern Africa, *Atmospheric Environment*, 34, 2797 – 2808.

Zunckel, M., Venjonoka, K., Pienaar, J.J., Brunke, E.G., Pretorius, O., Koosialee, A., Raghunandan, A. and van Tienhoven, A.M., 2004: Surface ozone over southern Africa: synthesis of monitoring results during the cross border air pollution impact assessment study: *Atmospheric Environment*, 38, 6139 – 6147.

8. Appendix

Appendix 8.1.

Table 8.1: Details of the MODIS – level 2 and level 3 – satellite imagery used.

Satellite sensor and data level	File name (dataset used)	Data used (dates)	Temporal resolution	Spatial resolution
Terra MODIS Level 2	MOD04_L2.A2011015.0730.051.2011015180140	15/01/2011	07h30	10 x 10 km
Terra MODIS Level 2	MOD07_L2.A2011105.0810.005.2011105181309	15/04/2011	7h30	5 x 5 km
Terra MODIS Level 2	MOD04_L2.A2011166.0740.051.2011168155934	15/06/2011	7h40	10 x 10 km
Terra MODIS Level 2	MOD07_L2.A2011258.0810.005.2011258154611	15/09/2011	7h40	5 x 5 km
Terra MODIS Level 3	MOD08_D3.A2011015.051.2011016122533	15/01/2011	Daily average	1°x1°
Terra MODIS Level 3	MOD08_E3.A2011017.051.2011028232815	12/01/2011 – 19/01/2011	8-Day	1°x1°
Terra MODIS Level 3	MOD08_M3.A2011001.051.2011036104003	1/01/2011 – 31/01/2011	Monthly	1°x1°
Terra MODIS Level 3	MOD08_D3.A2011105.051.201110612925	15/04/2011	Daily	1°x1°

Terra MODIS Level 3	MOD08_E3.A2011105.051.2011116232206	12/04/2011 – 19/04/2011	8-Day	1°x1°
Terra MODIS Level 3	MOD08_M3.A2011091.051.2011124012012	1/04/2011 – 30/04/2011	Monthly	1°x1°
Terra MODIS Level 3	MOD08_D3.A2011166.051.2011169060522	15/06/2011	Daily	1°x1°
Terra MODIS Level 3	MOD08_E3.A2011169.051.2011188150332	12/06/2011 – 19/06/2011	8-Day	1°x1°
Terra MODIS Level 3	MOD08_M3.A2011152.051.2011201174823	1/06/2011 – 30/06/2011	Monthly	1°x1°
Terra MODIS Level 3	MOD08_D3.A20111258.051.2011259082708	15/09/2011	Daily	1°x1°
Terra MODIS Level 3	MOD08_E3.A2011257.051.2011265084732	12/09/2011 – 19/09/2011	8-Day	1°x1°
Terra MODIS Level 3	MOD08_M3.A2011244.051.2011276124808	1/09/2011 – 30/09/2011	Monthly	1°x1°
Terra MODIS Level 2	MOD04_L2.A2016228.0740.051.2016228142511	15/08/2011	7h40	10 x 10 km
Terra MODIS Level 2	MOD07_L2.A2016228.0740.005.2016228141641	15/08/2011	7h40	5 x 5 km

Terra MODIS Level 3	MOD08_D3.A2011227.051.2011228235633	15/08/2011	Daily	1°x1°
Terra MODIS Level 3	MOD08_E3.A2011225.051.2011234011559	12/08/2011 – 19/08/2011	8-Day	1°x1°
Terra MODIS Level 3	MOD08_M3.A2011213.006.2015055211024	1/08/2011 – 30/08/2011	Monthly	1°x1°

Appendix 8.2.

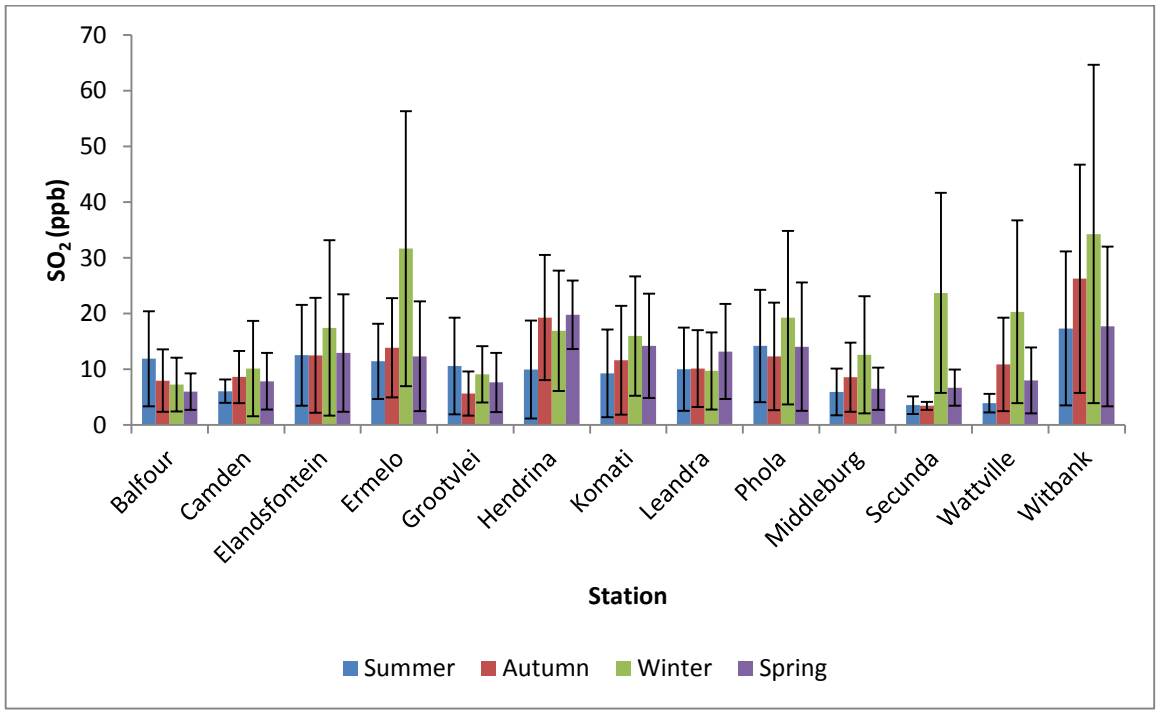

Figure 8.1: Seasonal variation of SO_2.

Appendix 8.3.

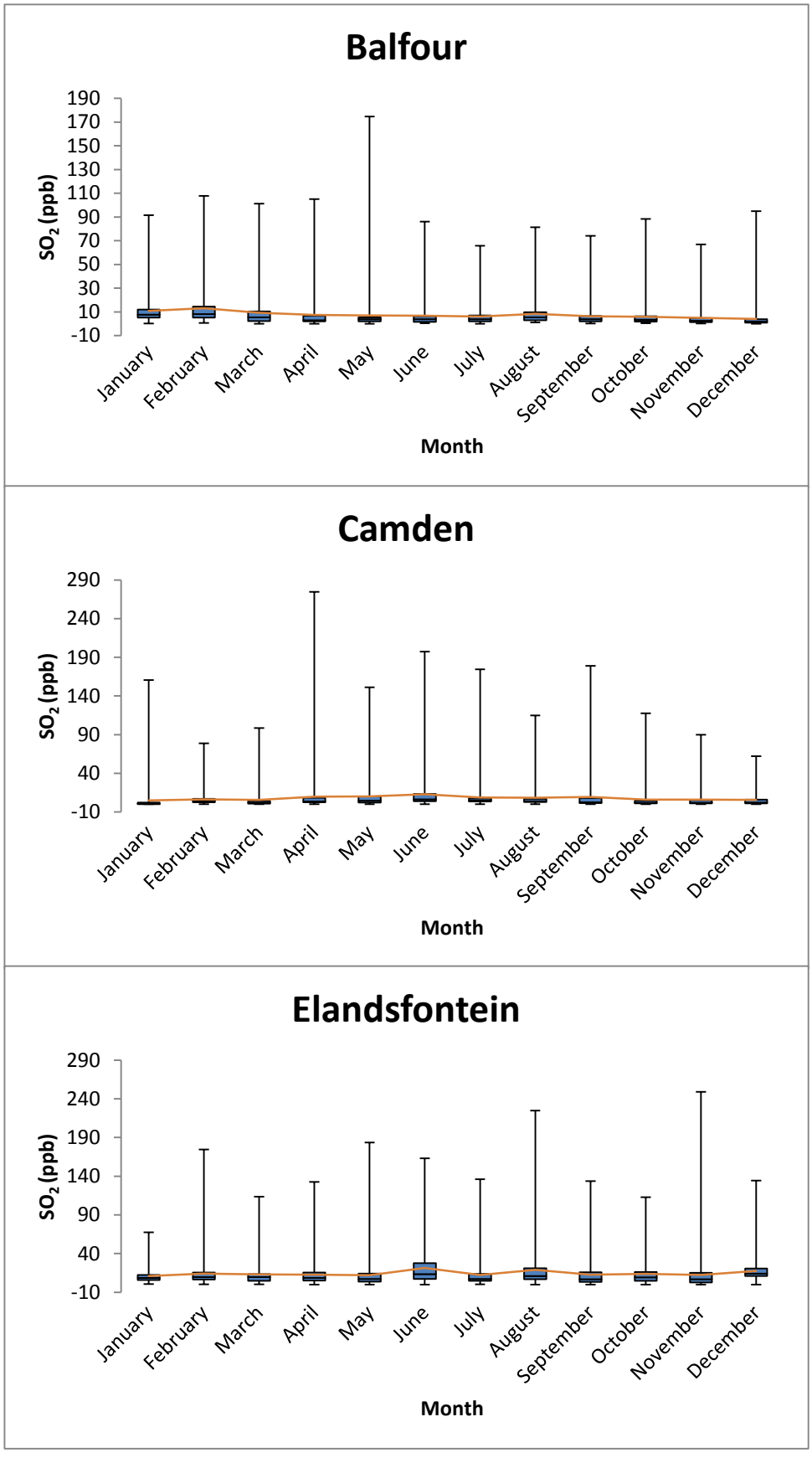

Figure 8.2: Monthly variation of SO_2

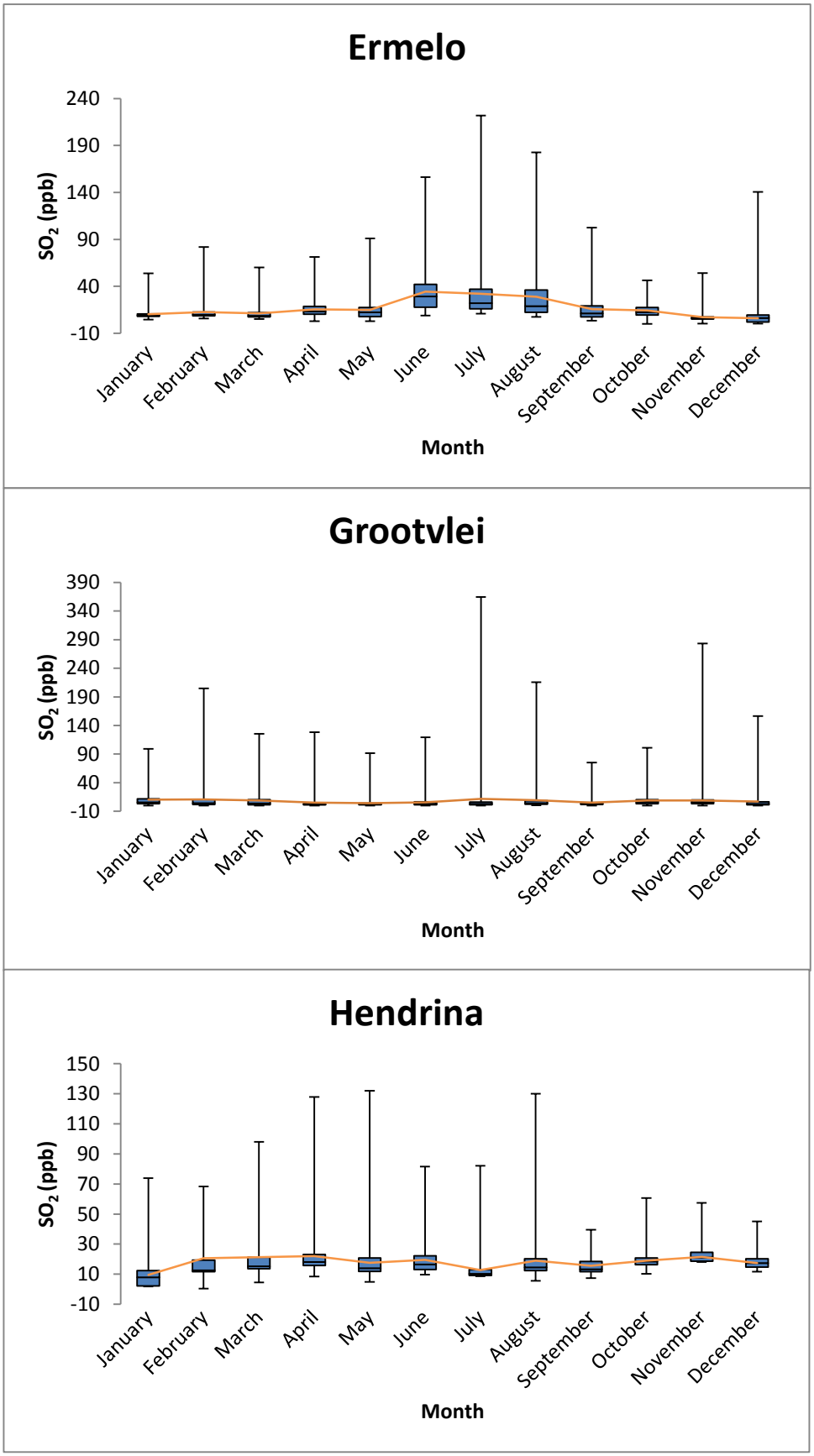

Figure 8.2 continued: Monthly variation of SO_2.

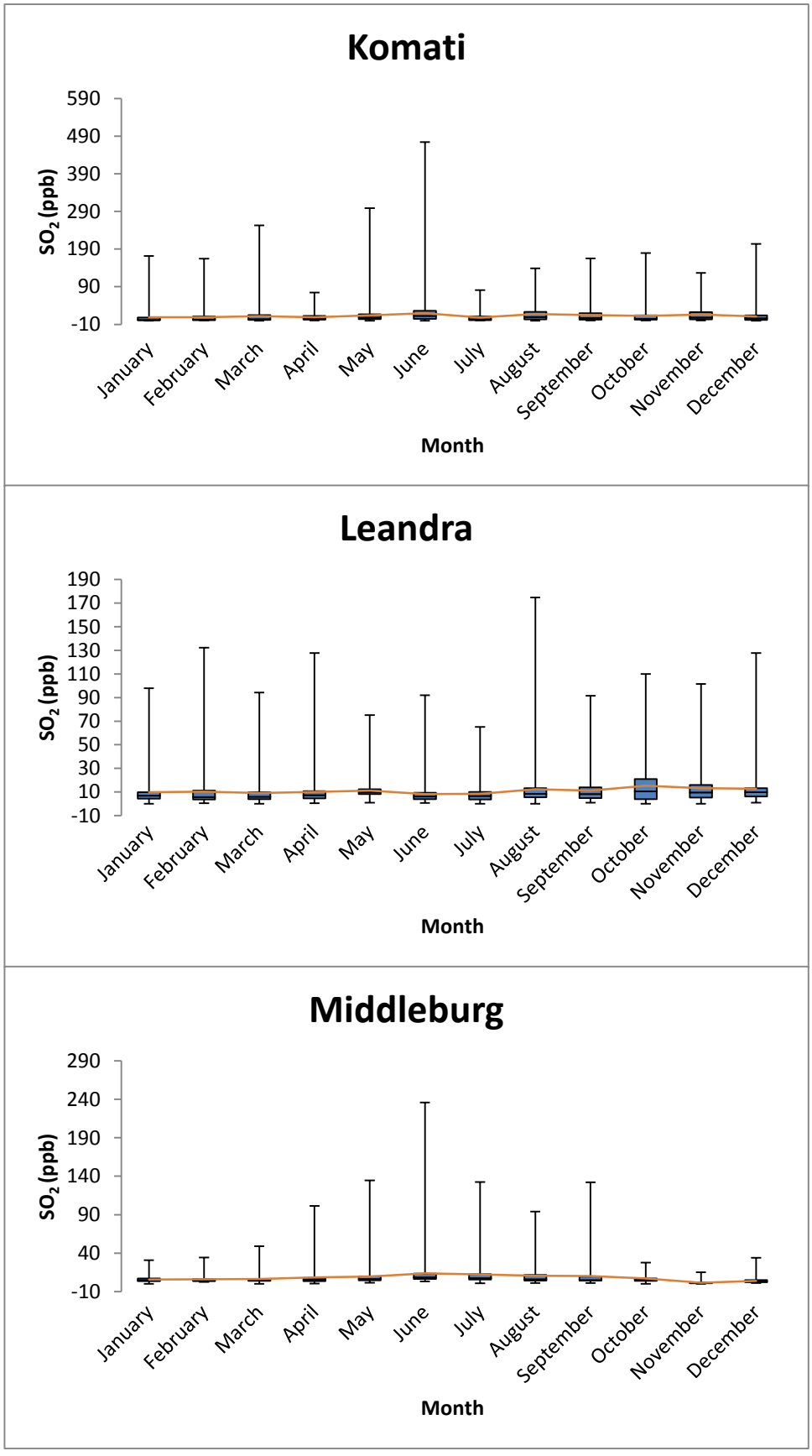

Figure 8.2 continued: Monthly variation of SO_2.

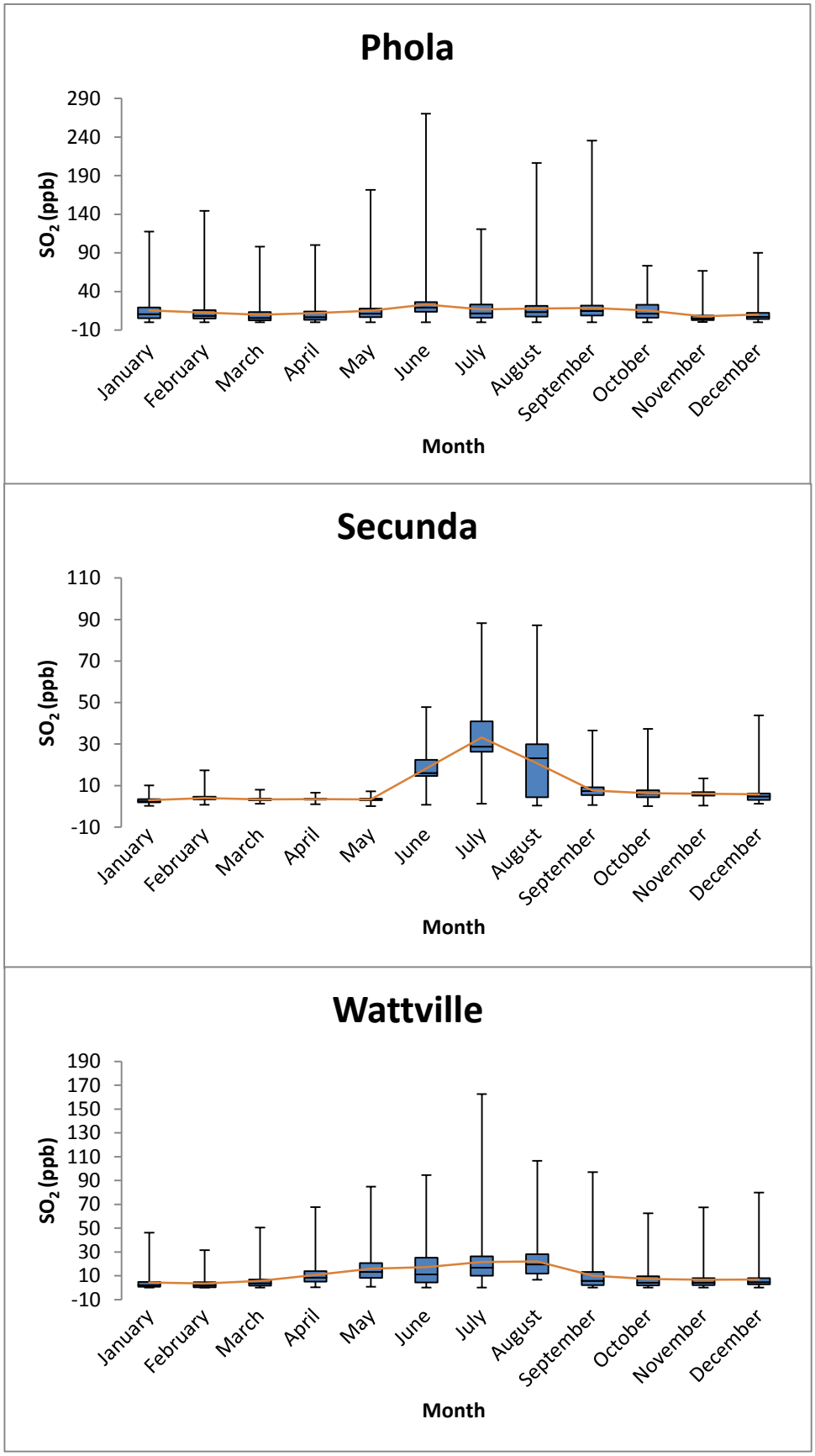

Figure 8.2 continued: Monthly variation of SO_2

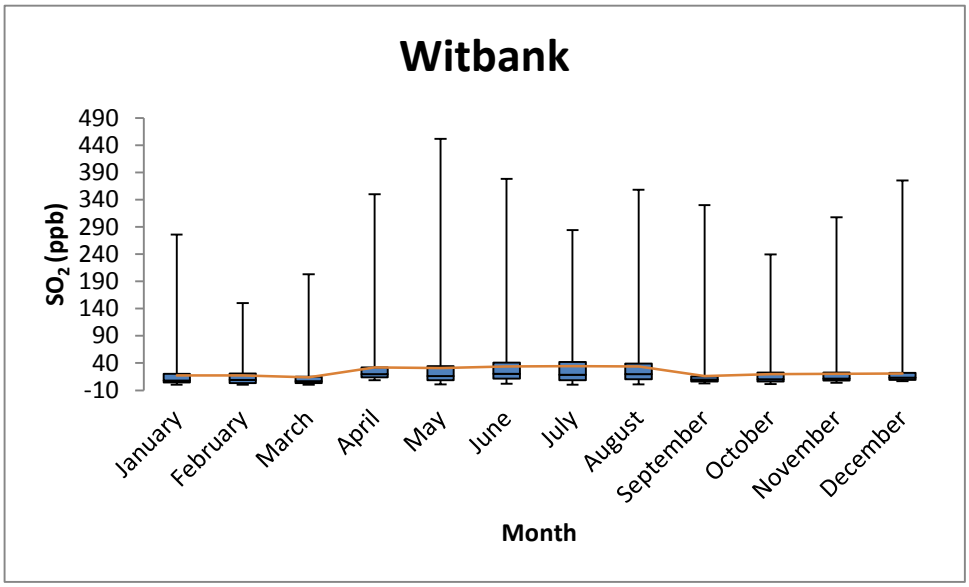

Figure 8.2 continued: Monthly variation of SO_2.

Appendix 8.4.

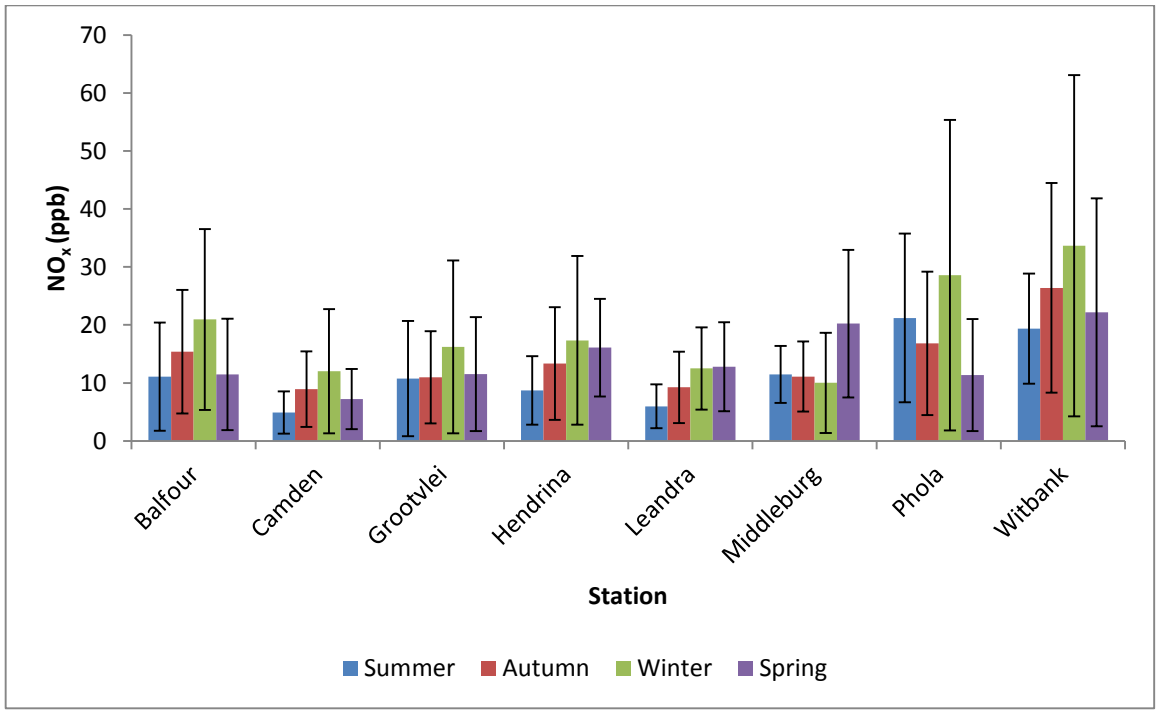

Figure 8.3: Seasonal variation of NO_x.

Appendix 8.5.

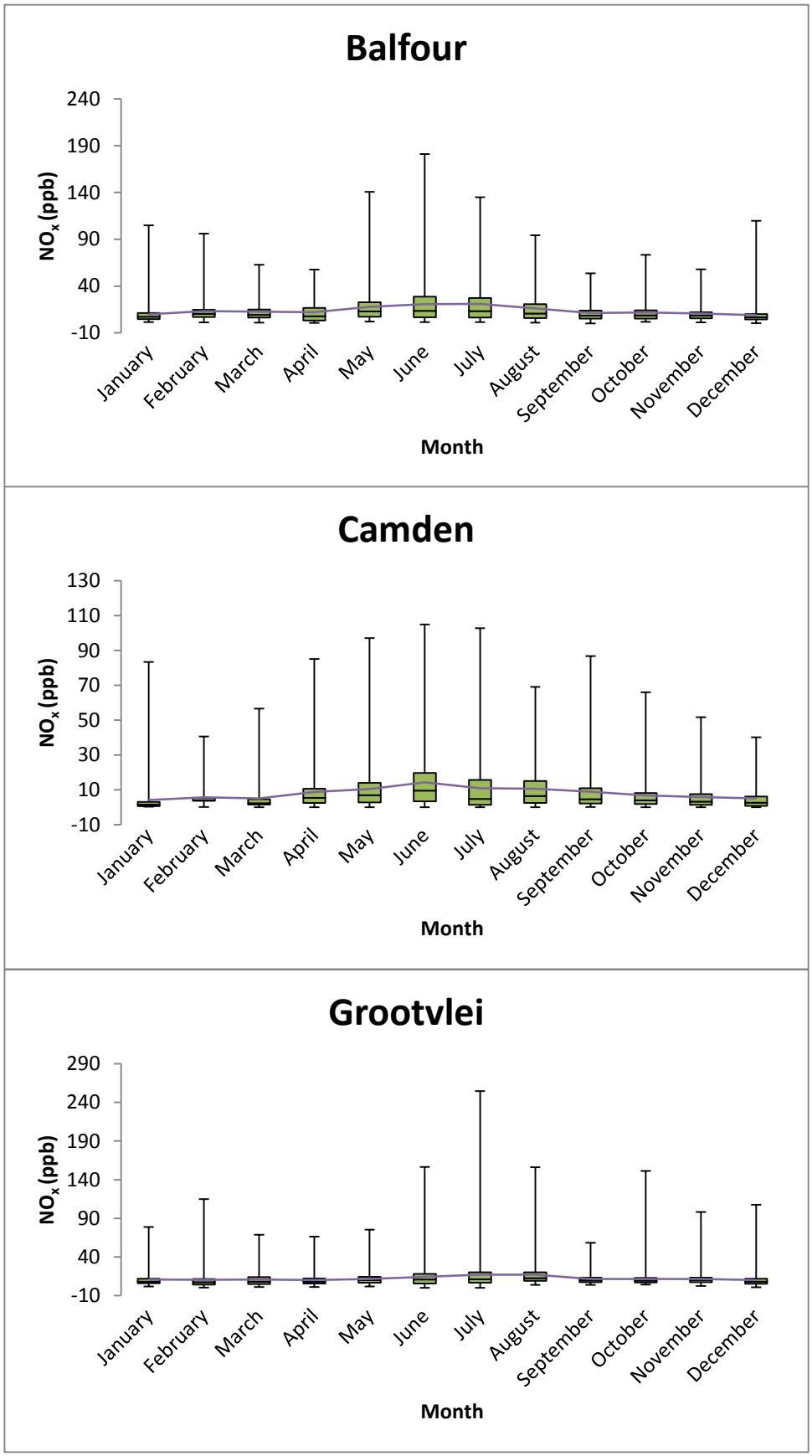

Figure 8.4: Monthly variation of NO_x.

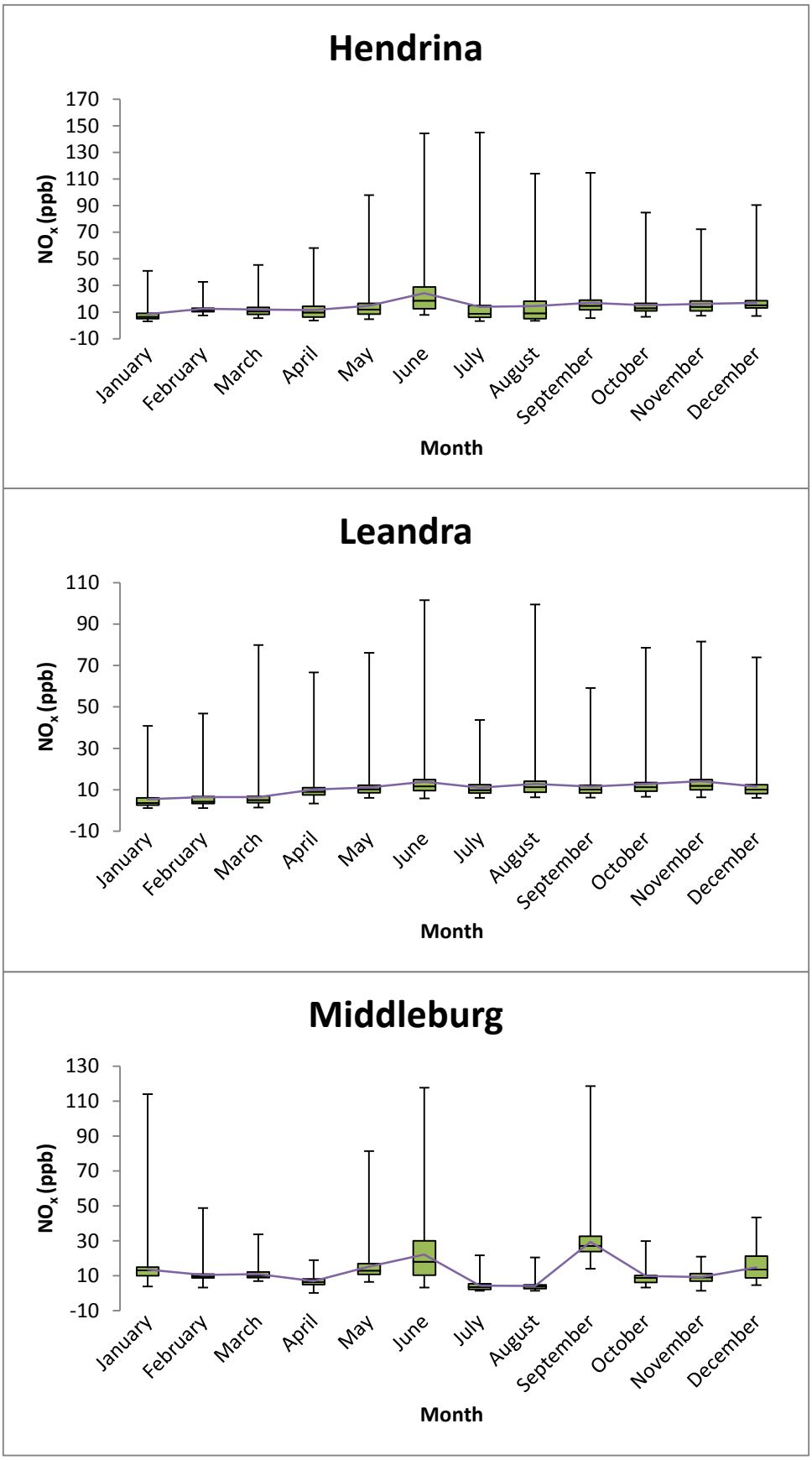

Figure 8.4 continued: Monthly variation of NO_x.

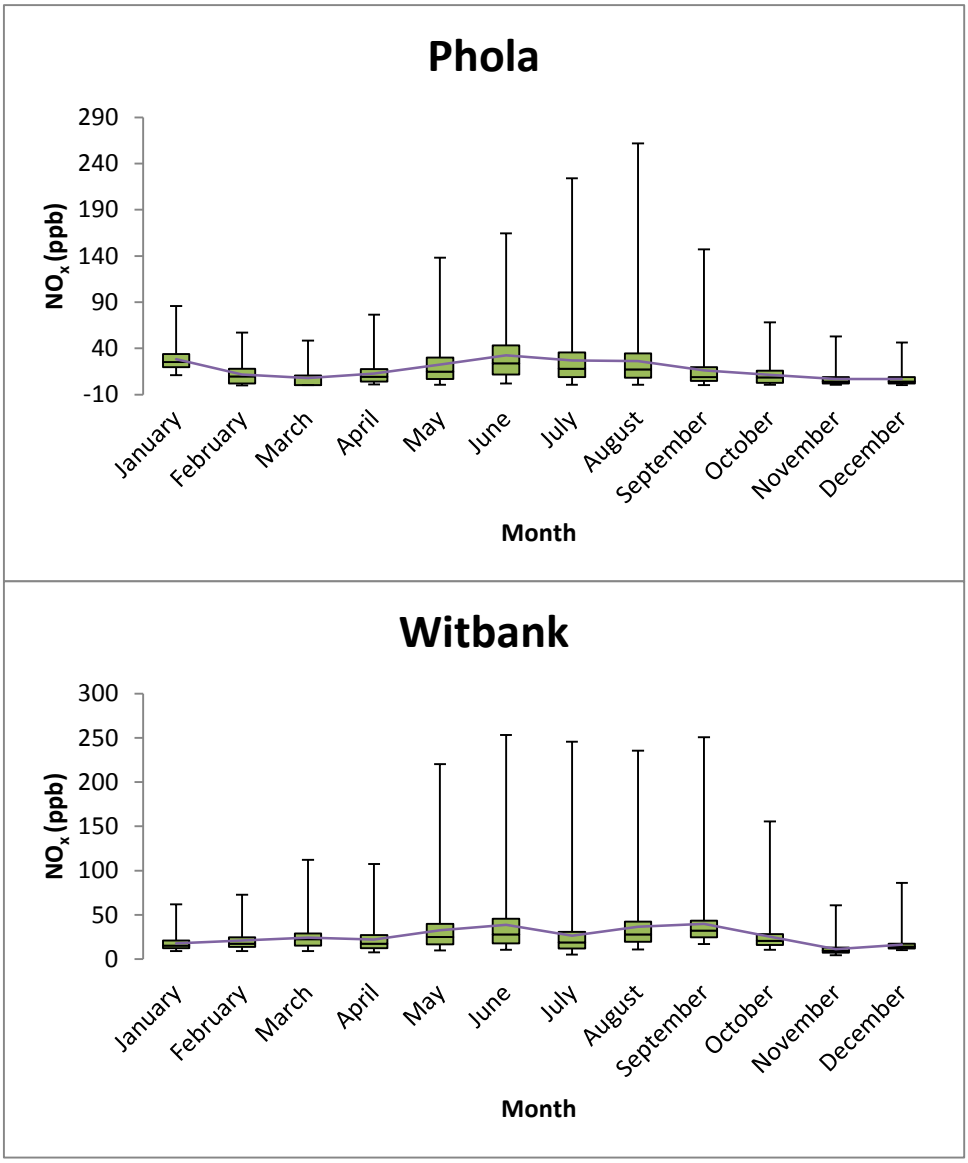

Figure 8.4 continued: Monthly variation of NO_x.

Appendix 8.6.

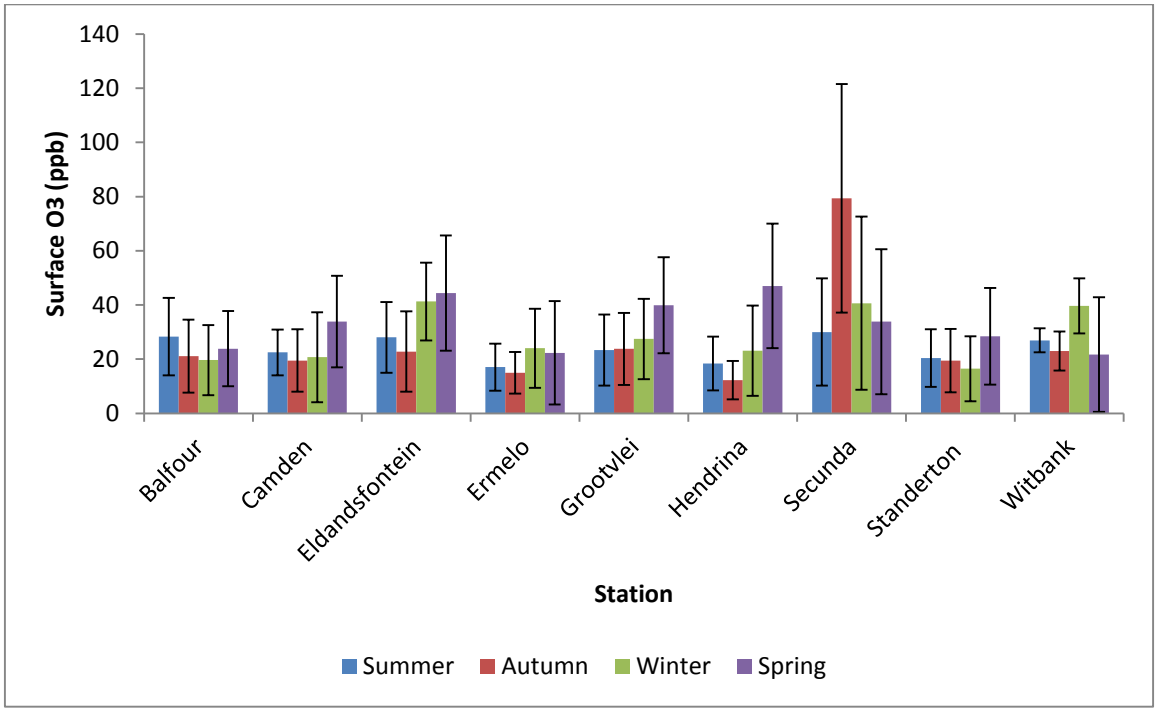

Figure 8.5: Seasonal variation of surface O_3.

Appendix 8.7.

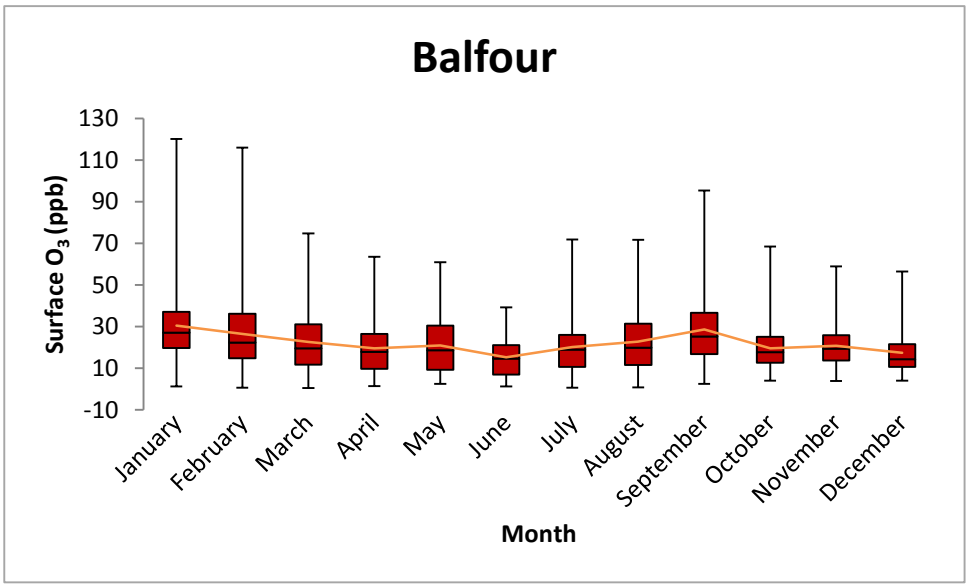

Figure 8.6: Monthly variation of surface O_3.

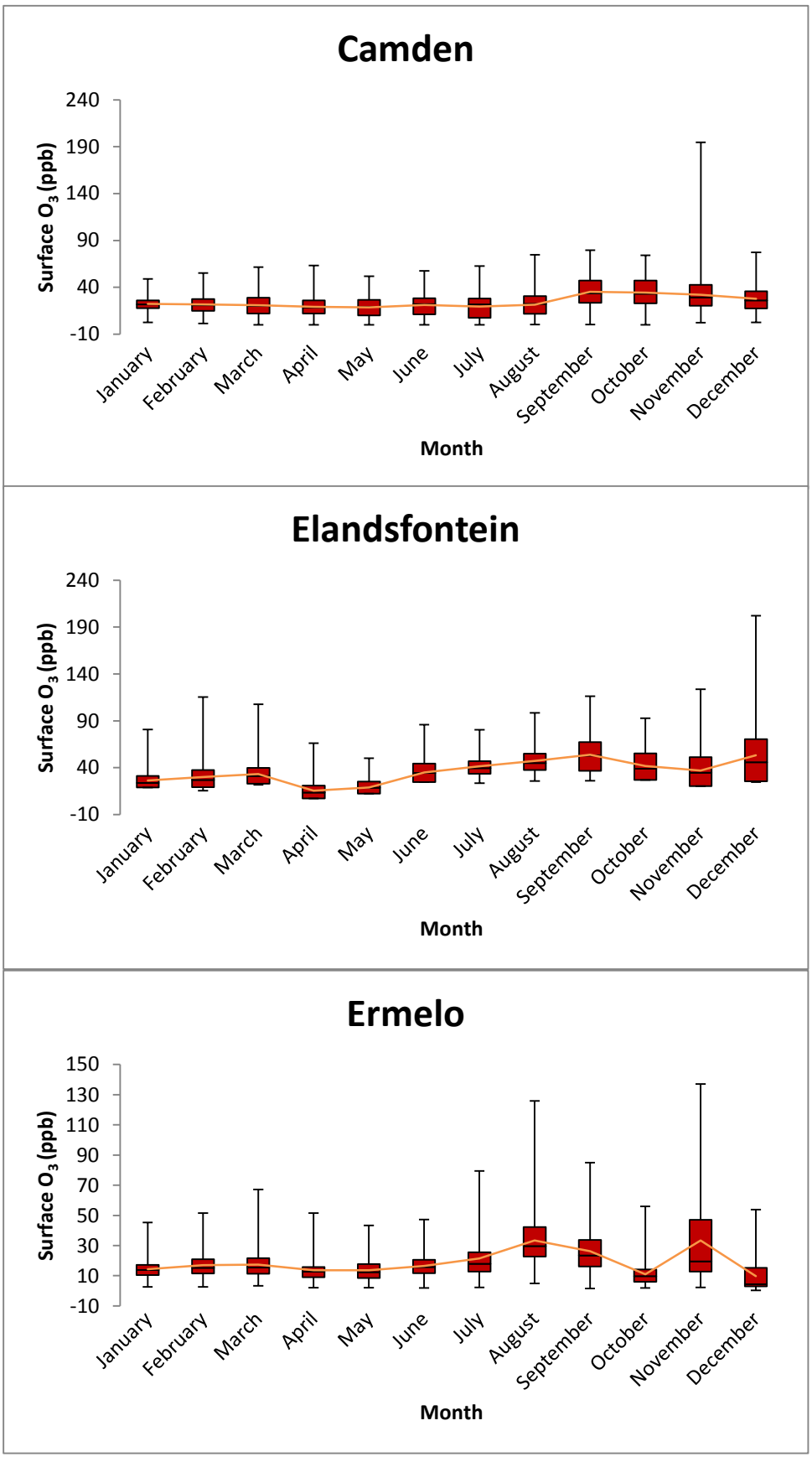

Figure 8.6 continued: Monthly variation of surface O_3

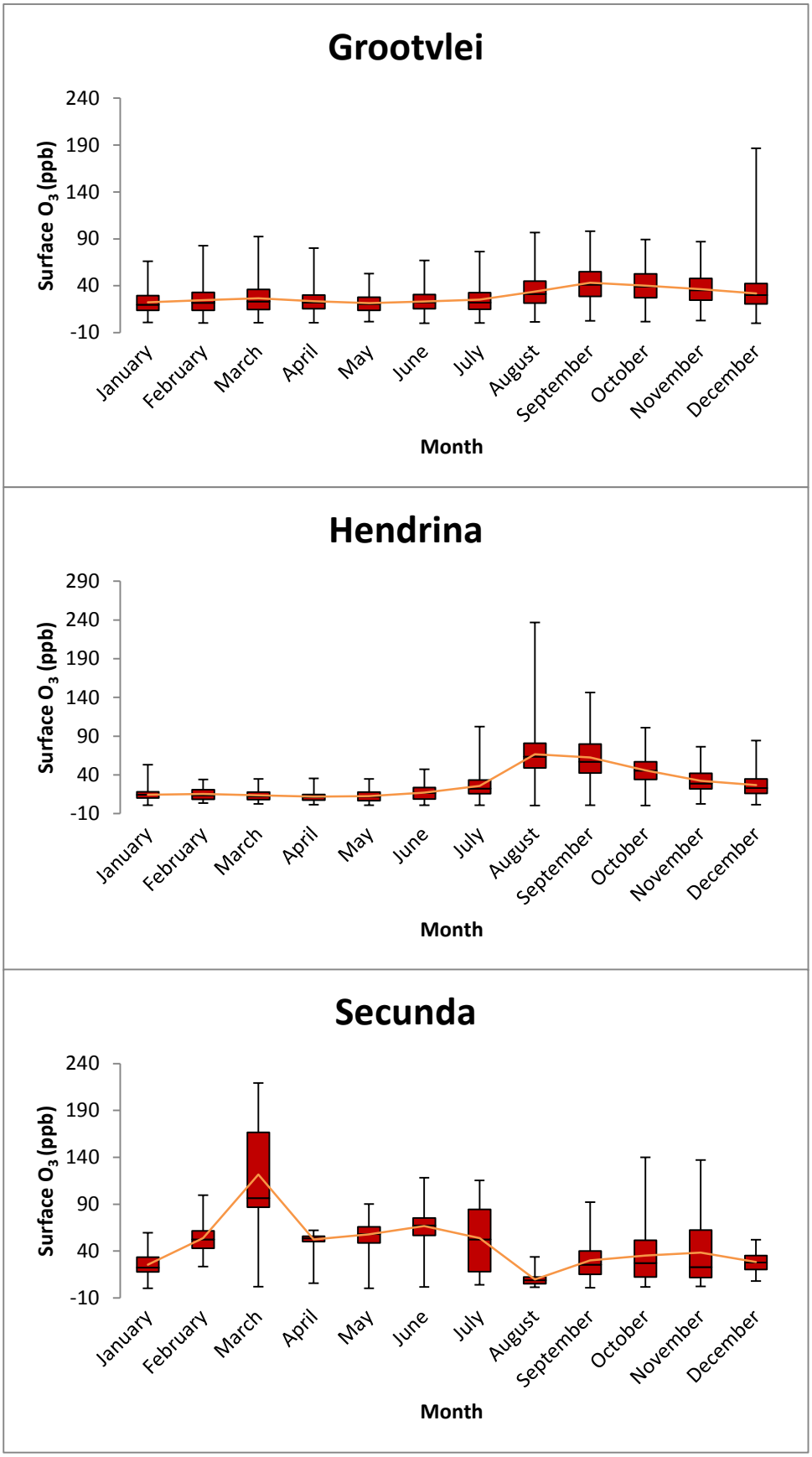

Figure 8.6 continued: Monthly variation of surface O_3.

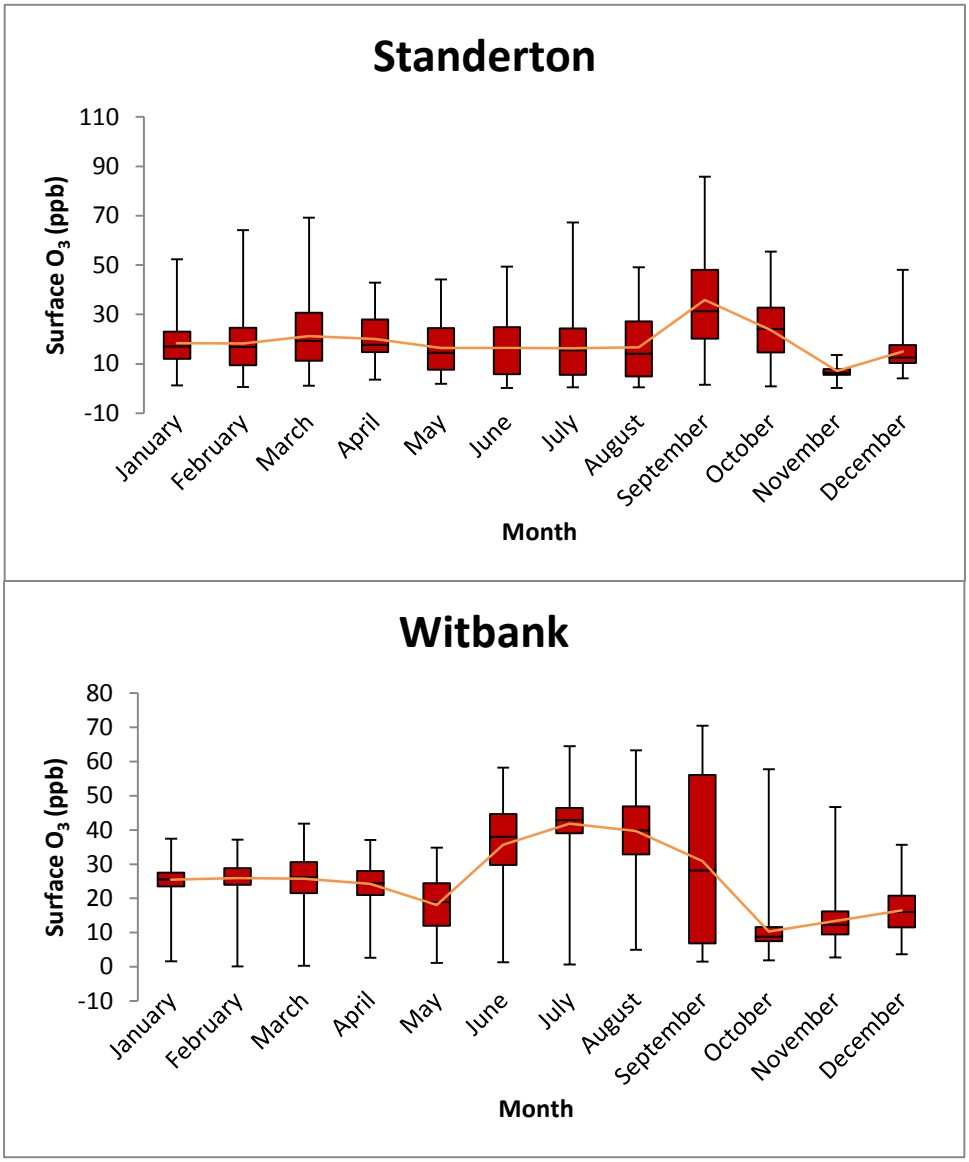

Figure 8.6 continued: Monthly variation of surface O_3.

Appendix 8.8.

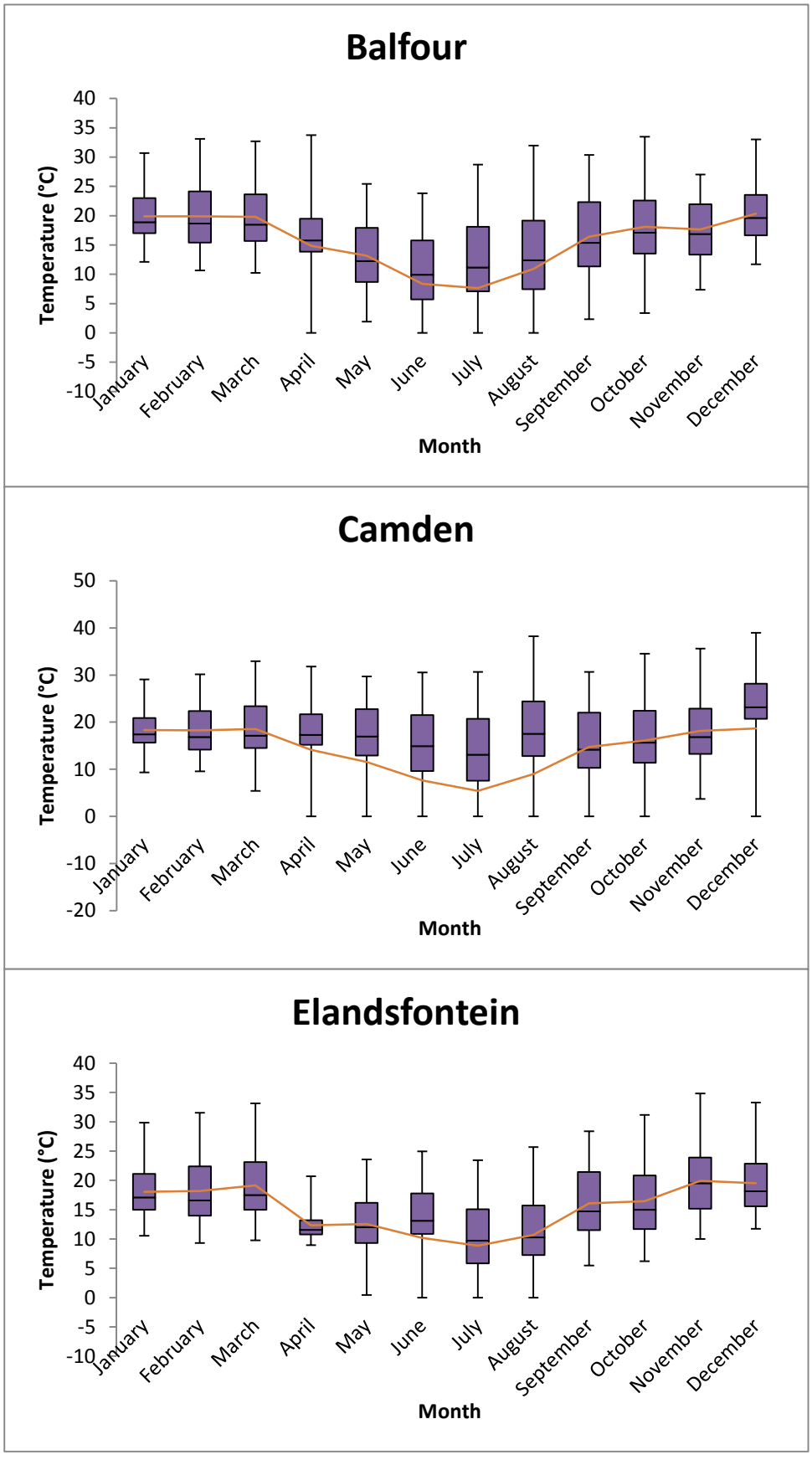

Figure 8.7: Monthly variation of temperature.

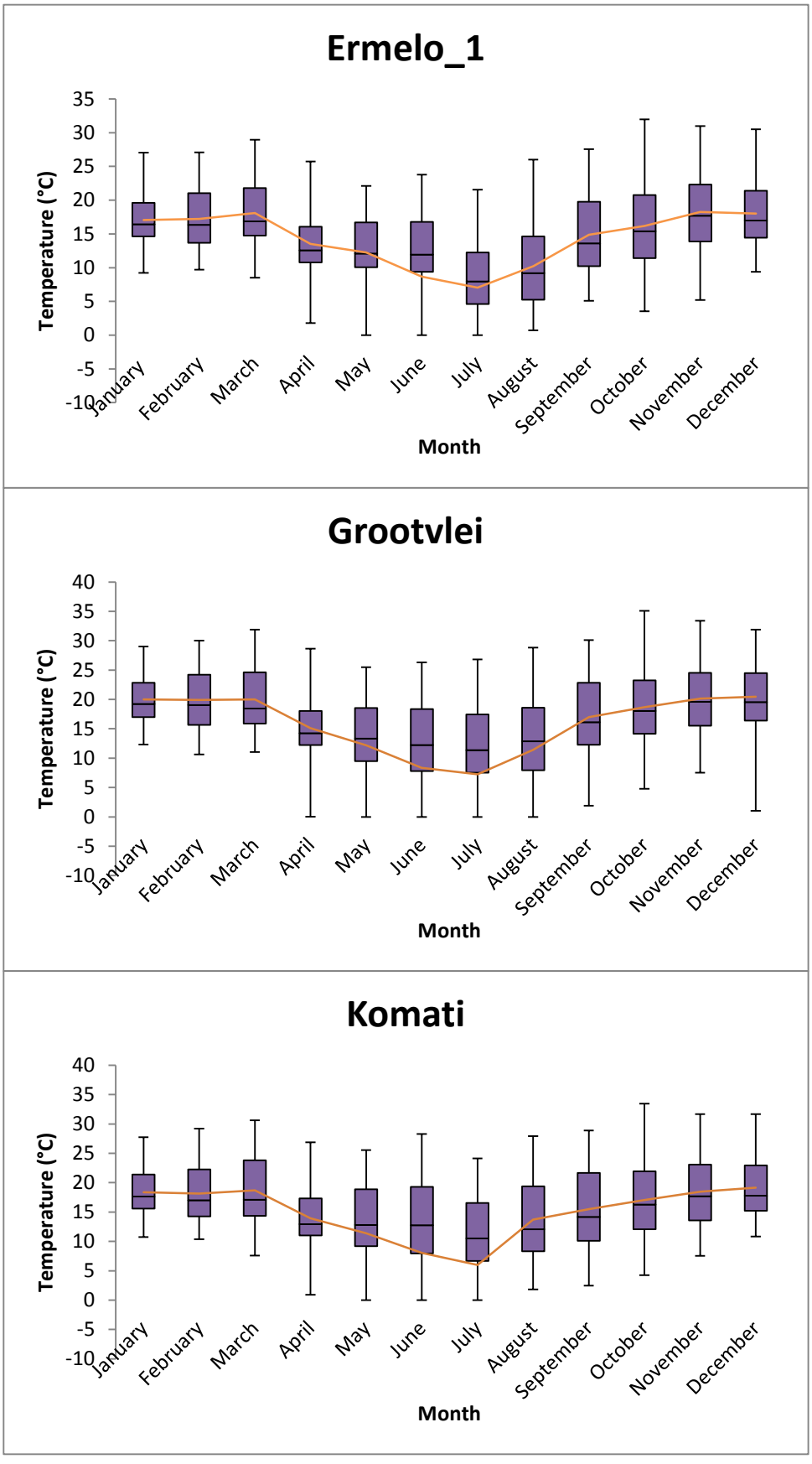

Figure 8.7 continued: Monthly variation of temperature.

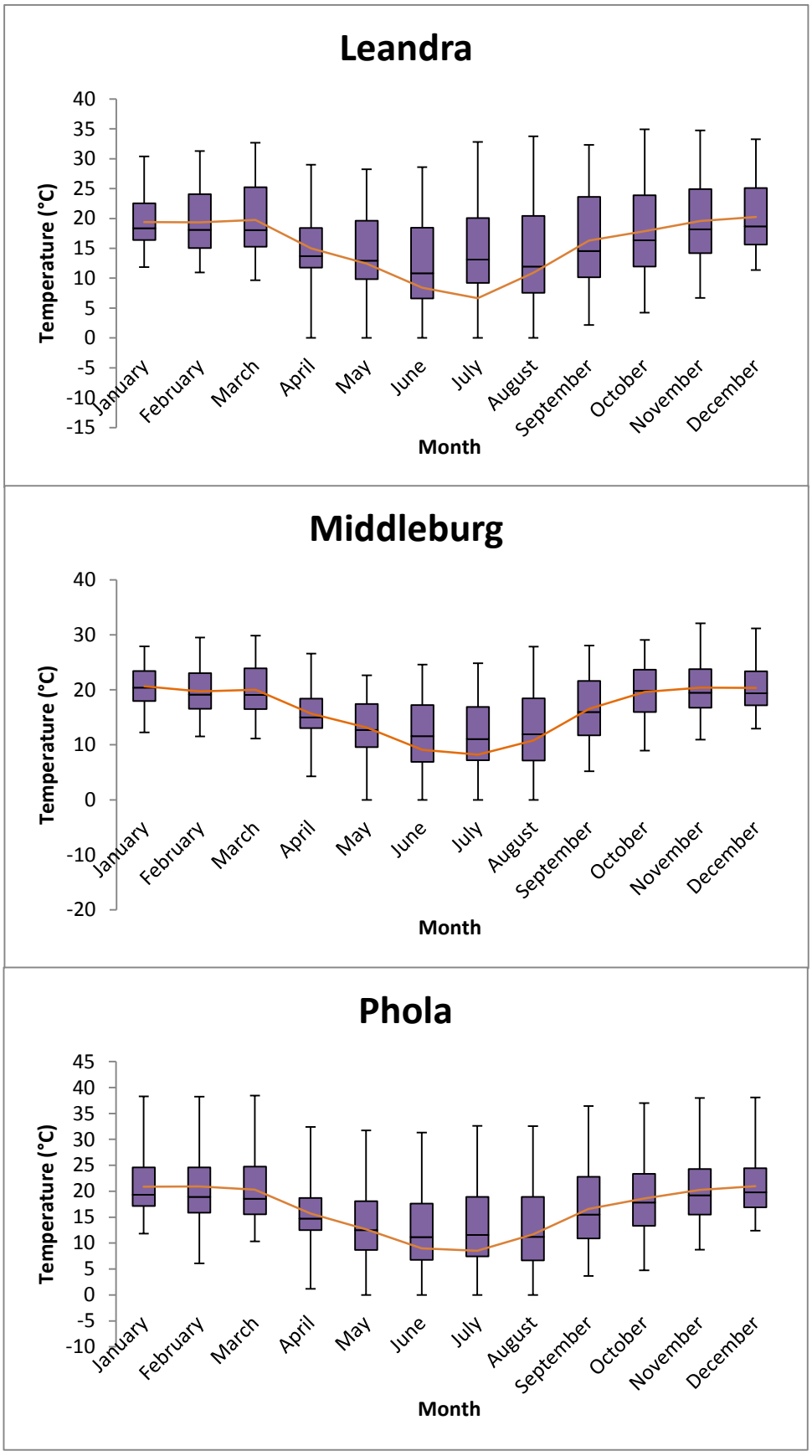

Figure 8.7 continued: Monthly variation of temperature.

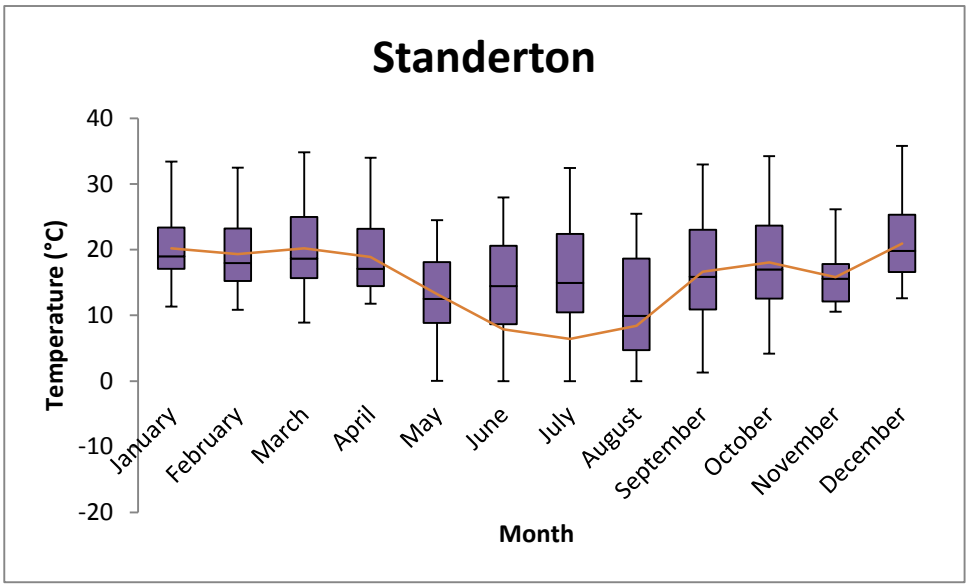

Figure 8.7 continued: Monthly variation of temperature.

Appendix 8.9.

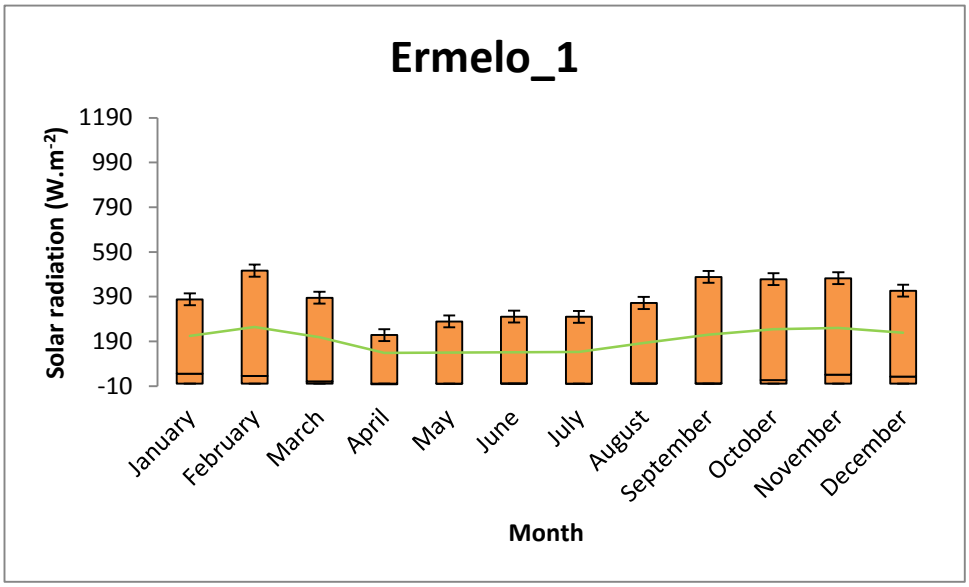

Figure 8.8: Monthly variation of solar radiation.

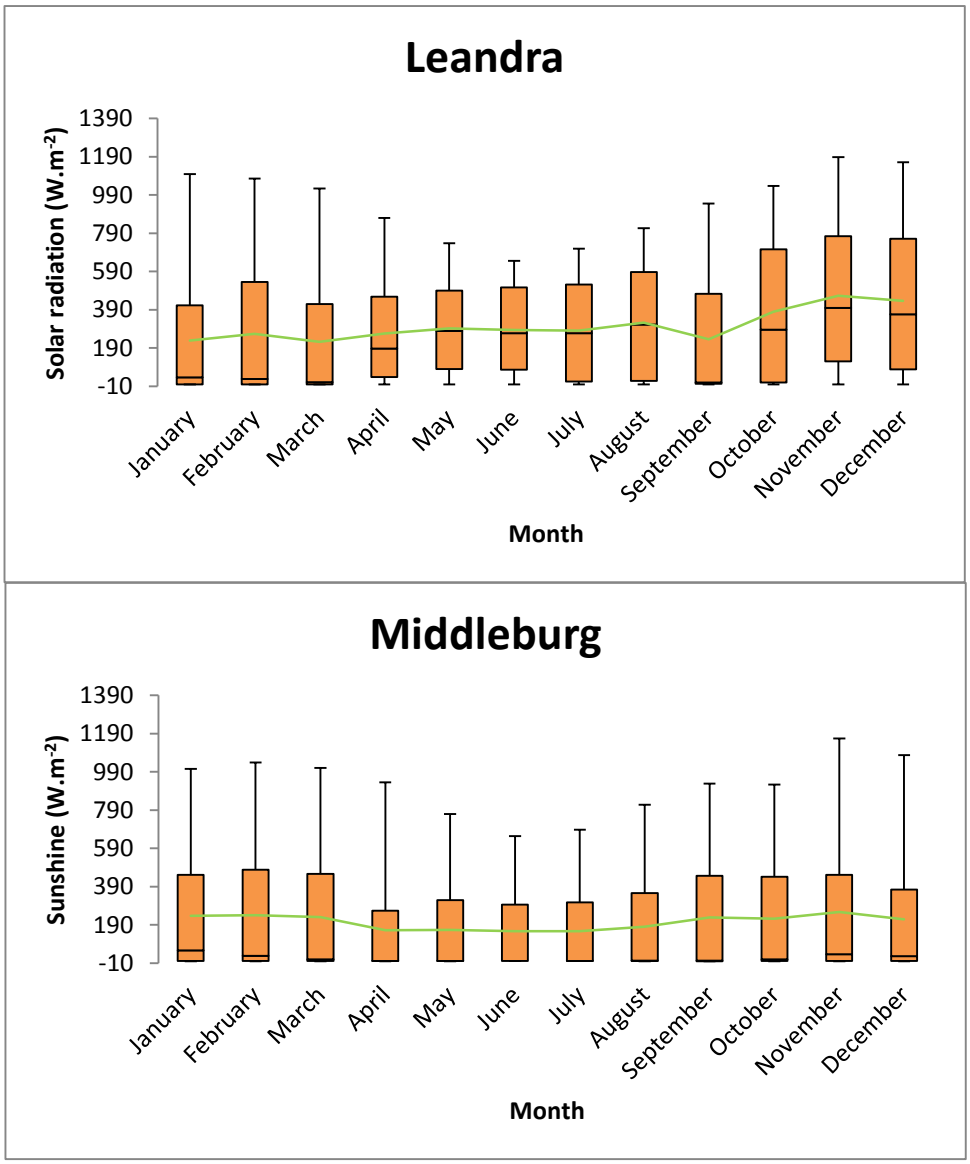

Figure 8.8 continued: Monthly variation of solar radiation.

Appendix 8.10.

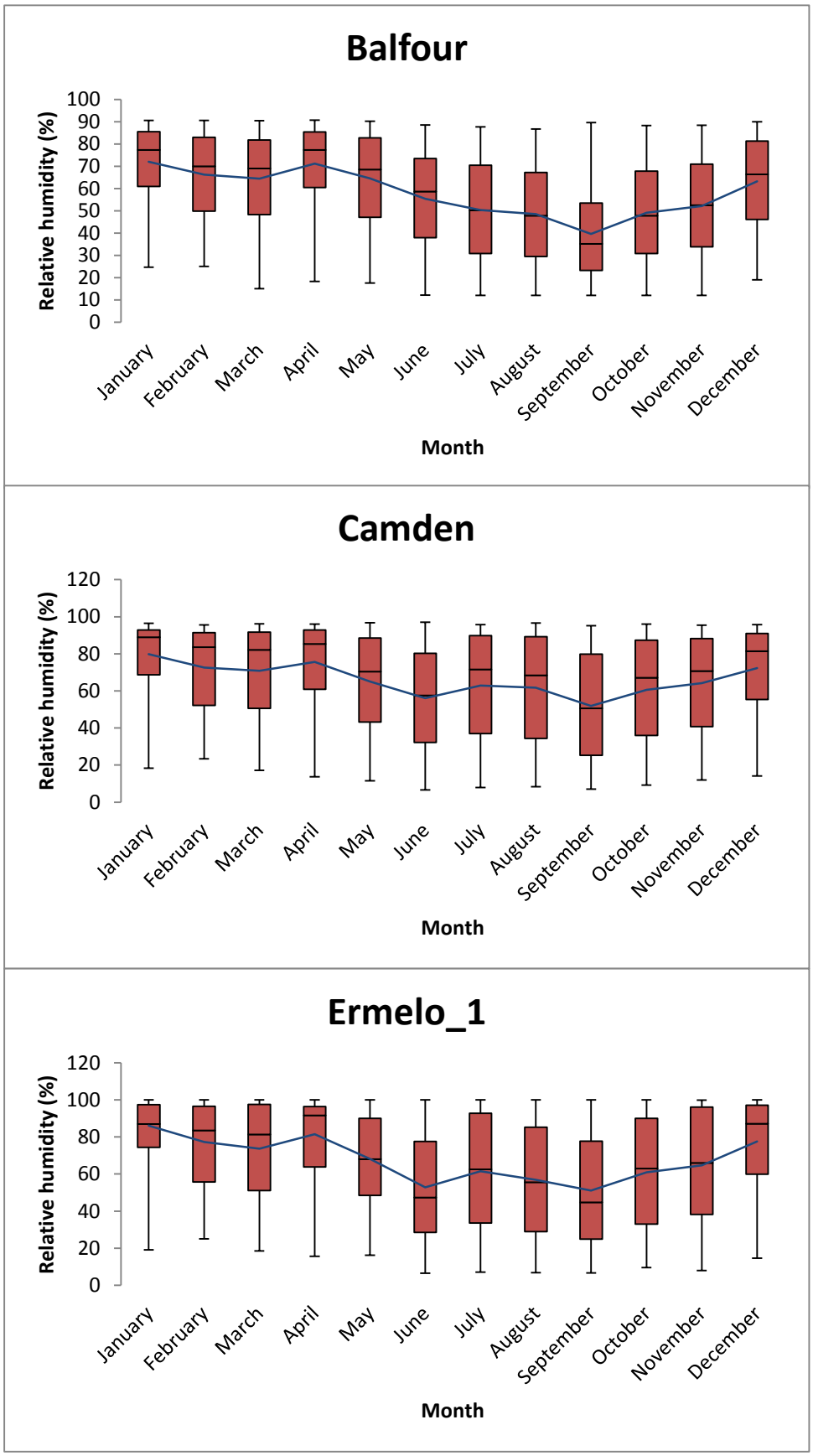

Figure 8.9: Monthly variation of relative humidity.

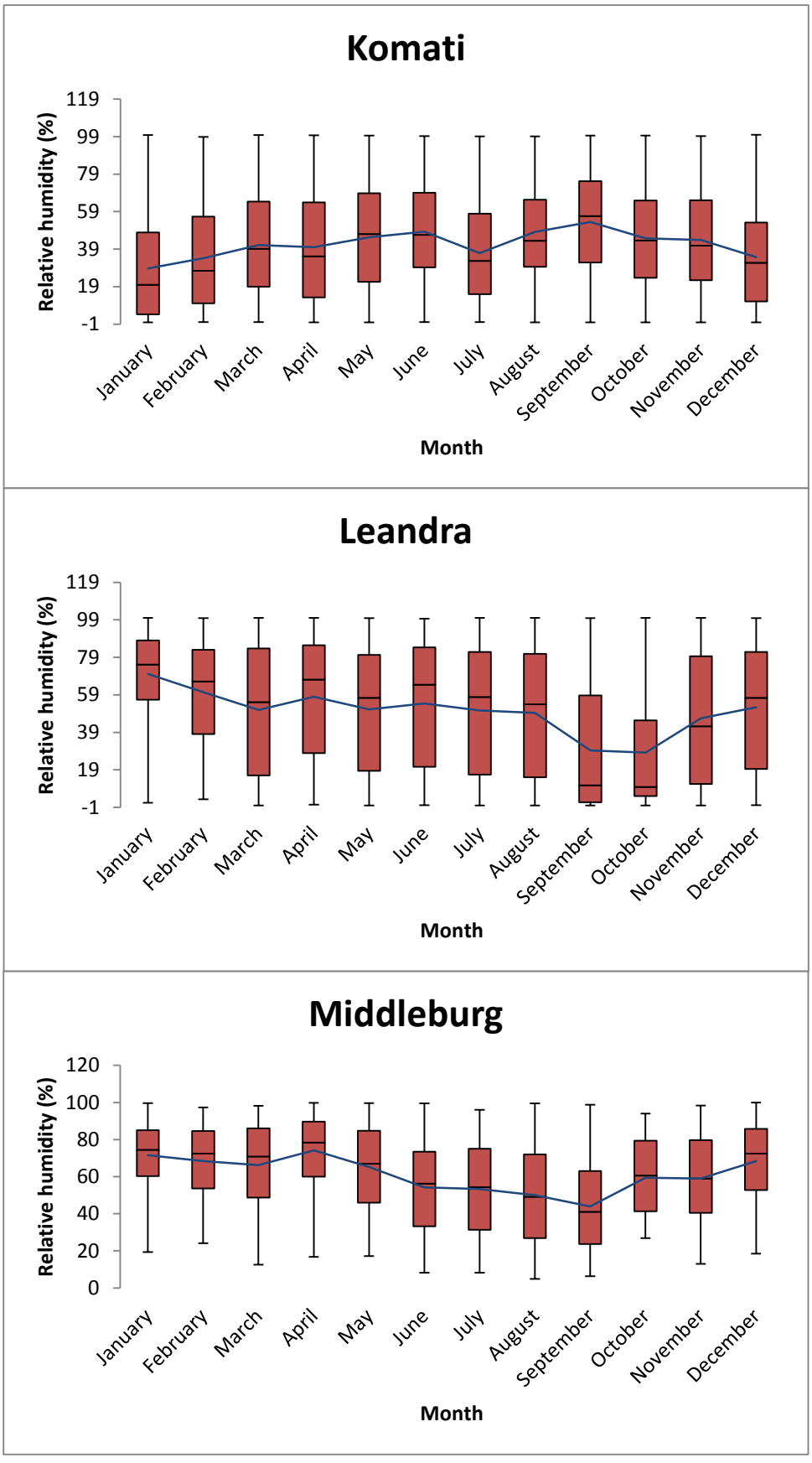

Figure 8.9 continued: Monthly variation of relative humidity.

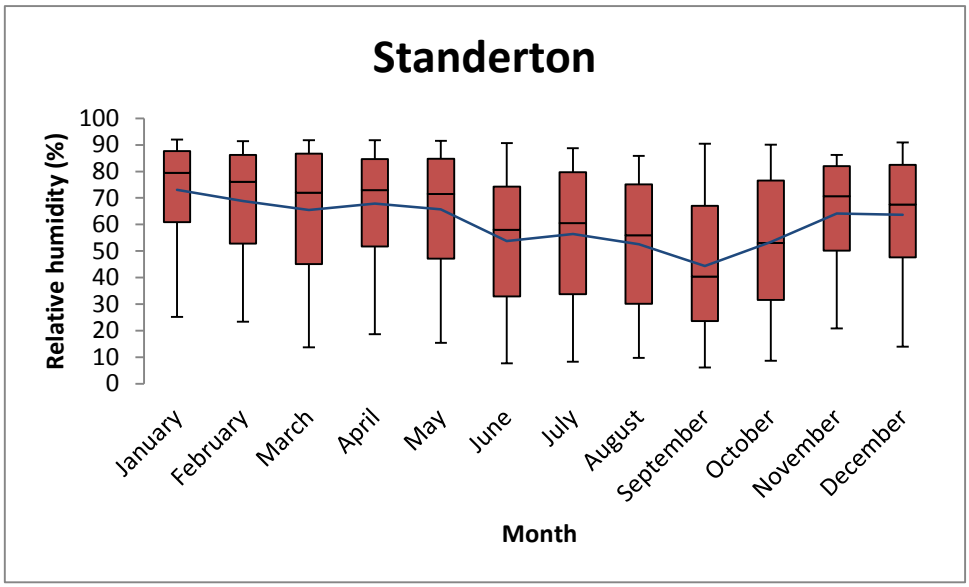

Figure 8.9 continued: Monthly variation of relative humidity.

Appendix 8.11.

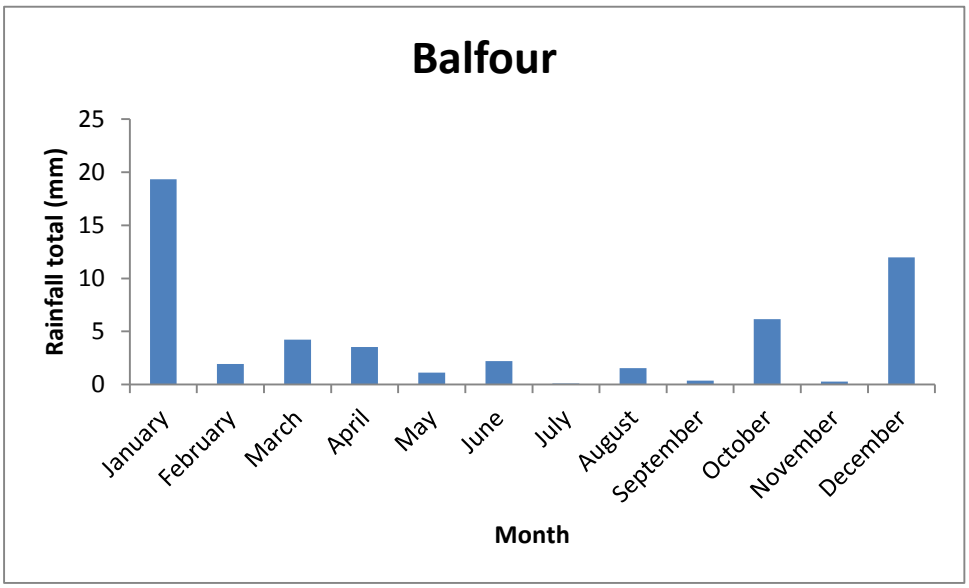

Figure 8.10: Monthly levels of rainfall.

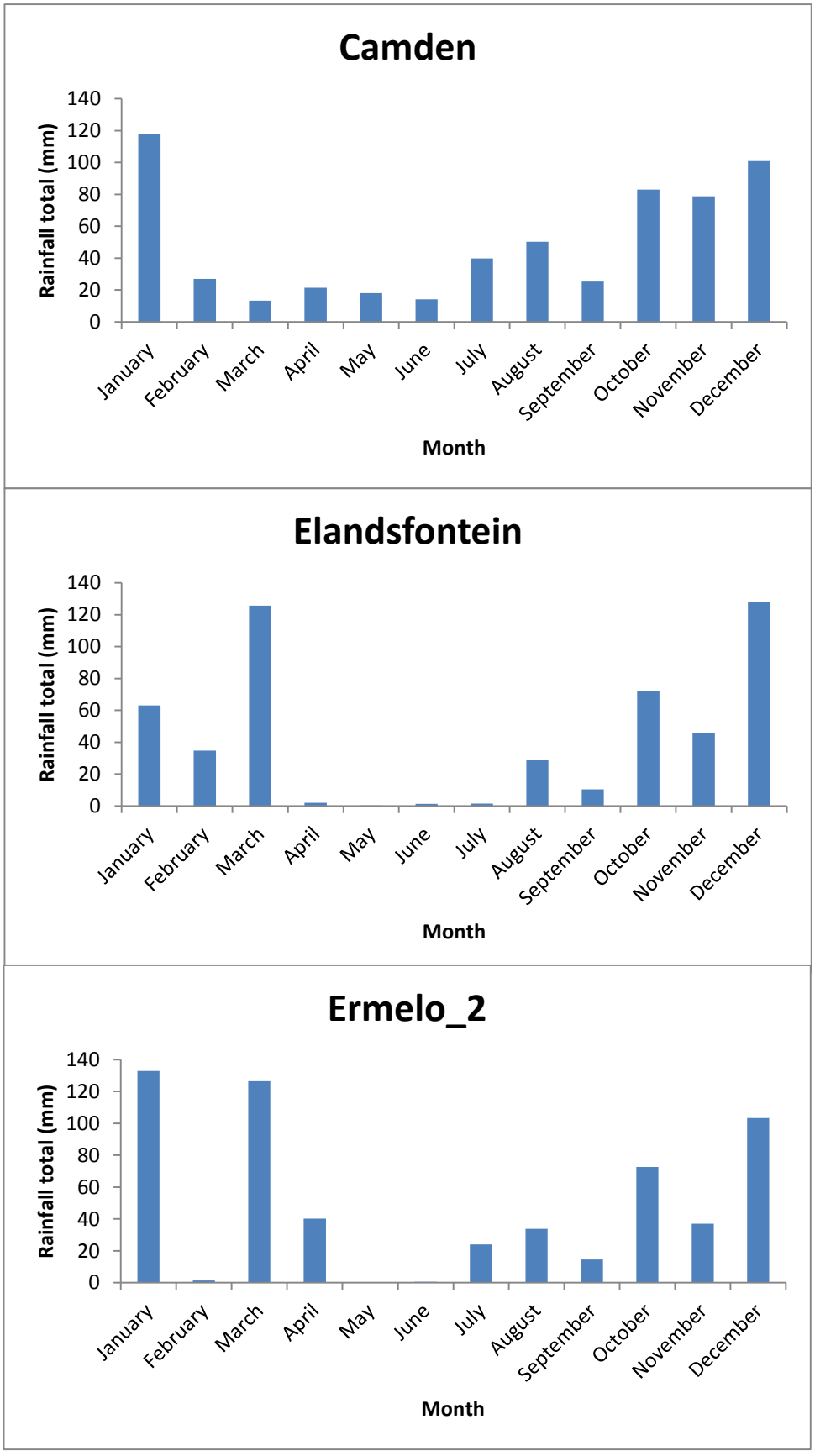

Figure 8.10 continued: Monthly levels of rainfall.

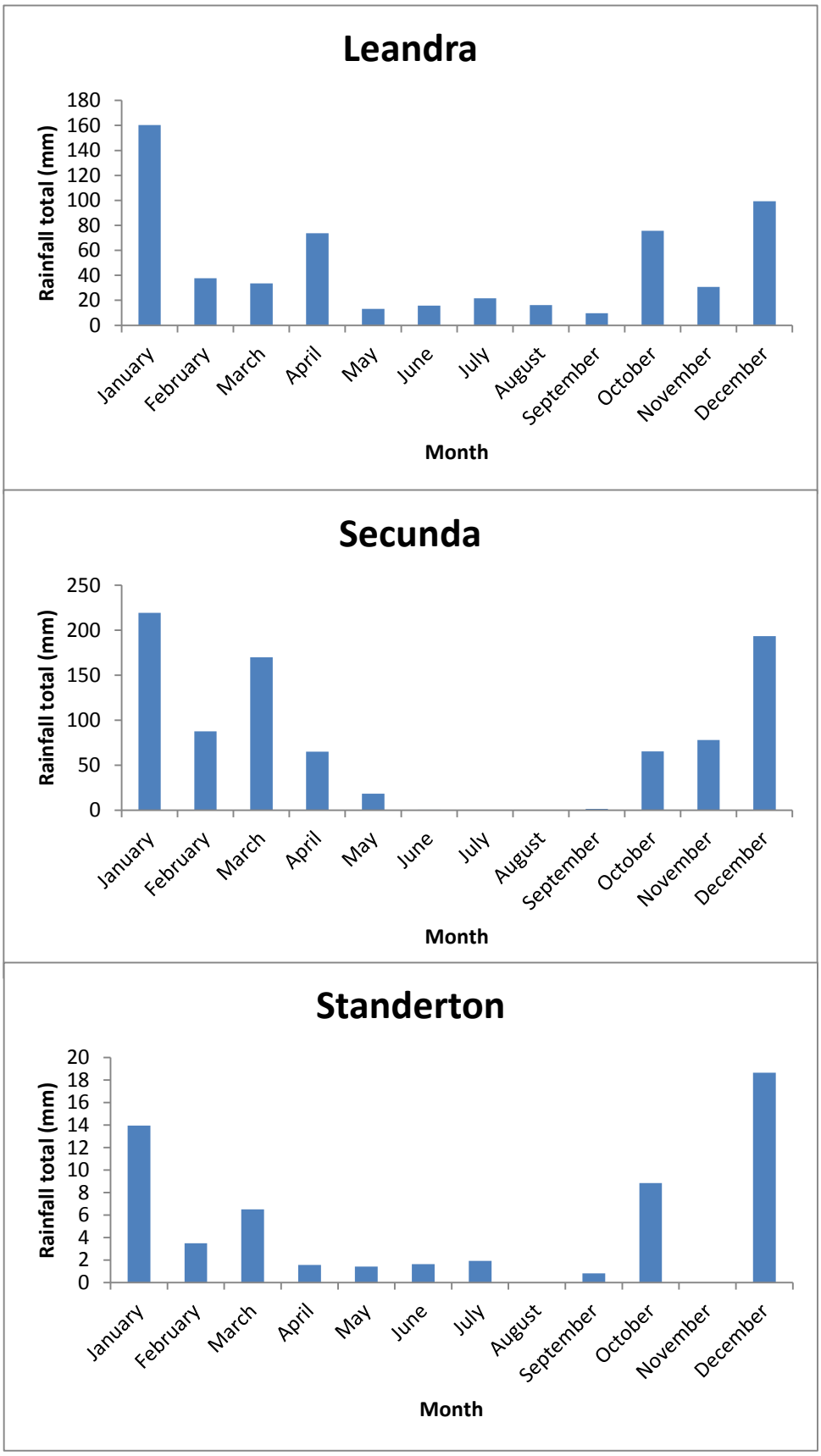

Figure 8.10 continued: Monthly levels of rainfall.

Appendix 8.12.

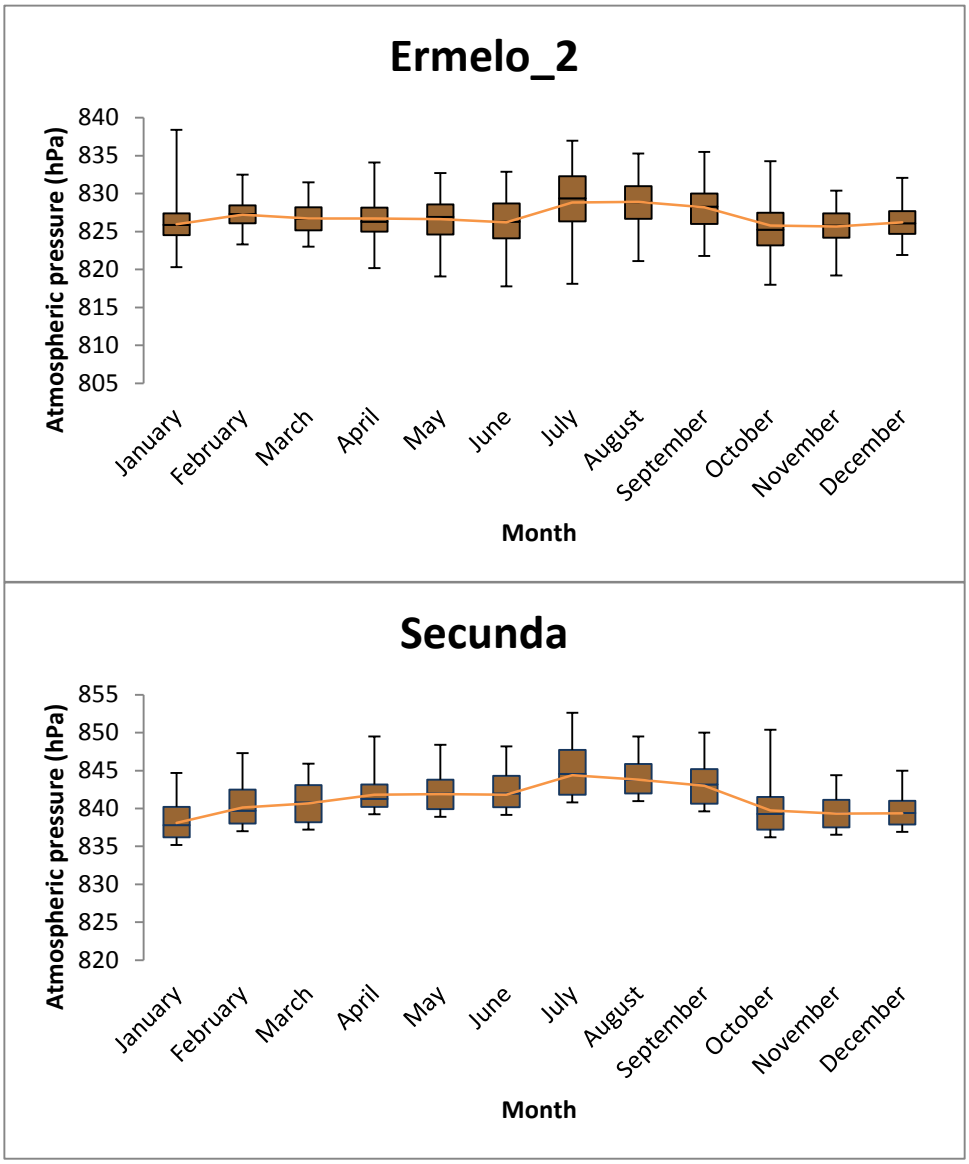

Figure 8.11: Monthly variation of atmospheric pressure.

Appendix 8.13.

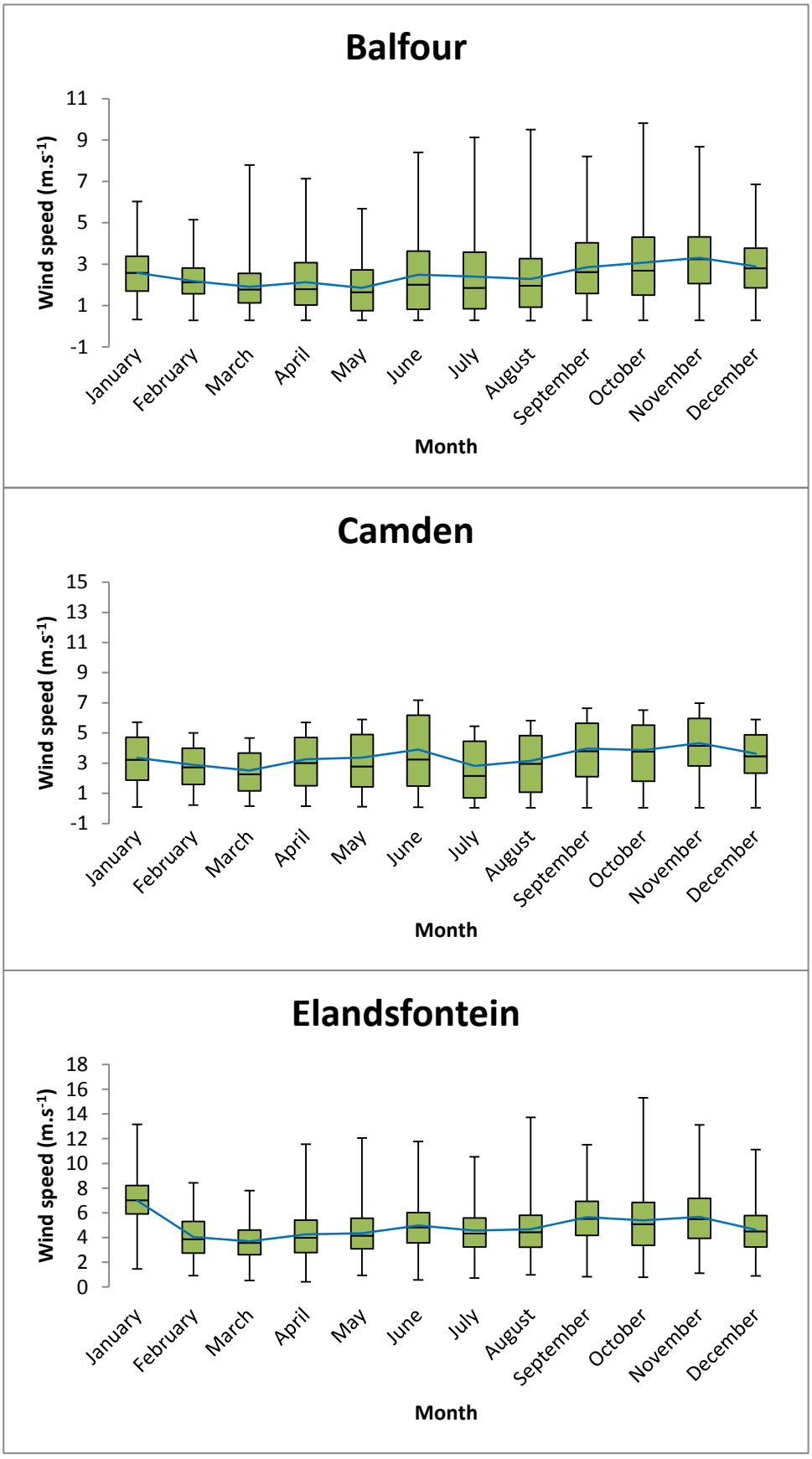

Figure 8.12: Monthly variation of wind speed.

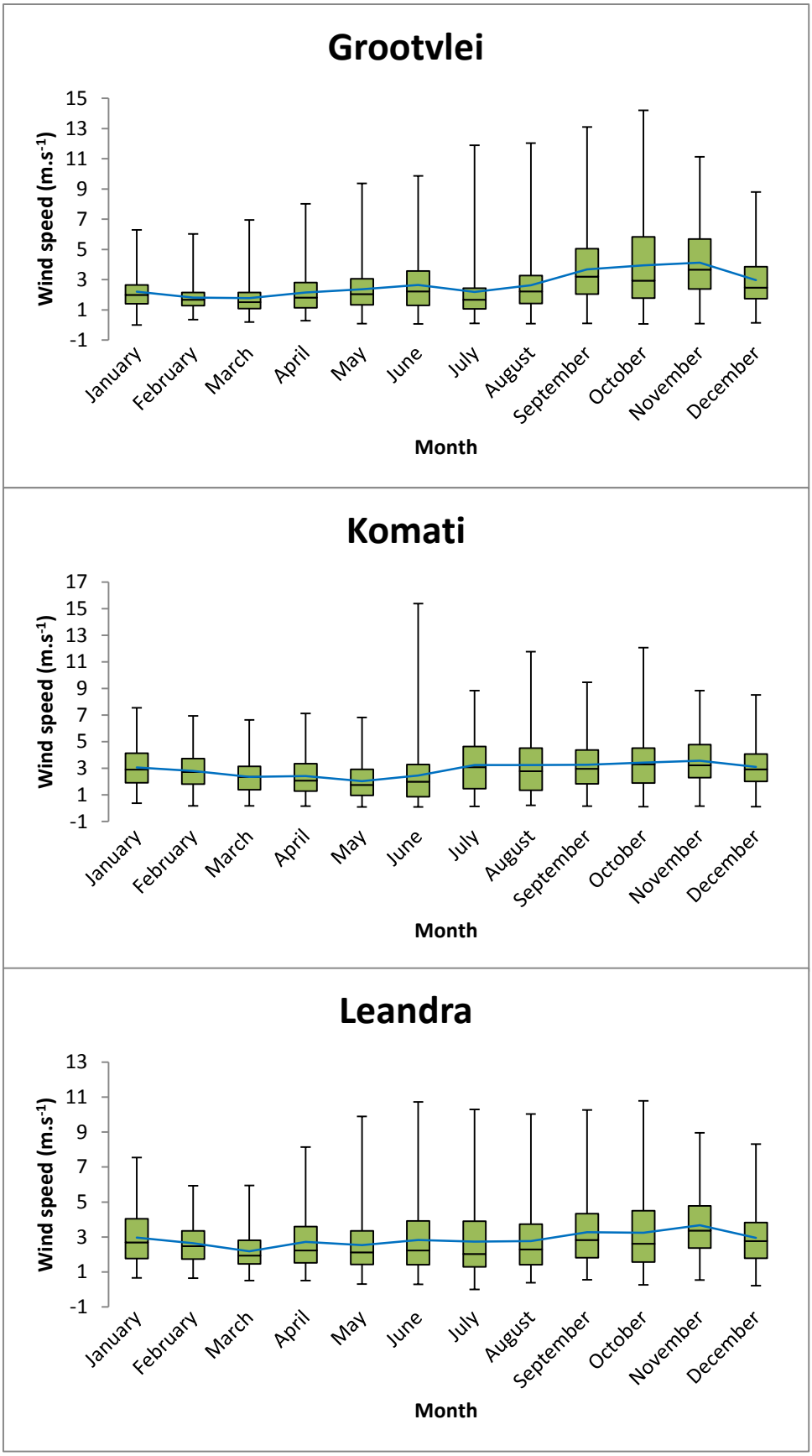

Figure 8.12 continued: Monthly variation of wind speed.

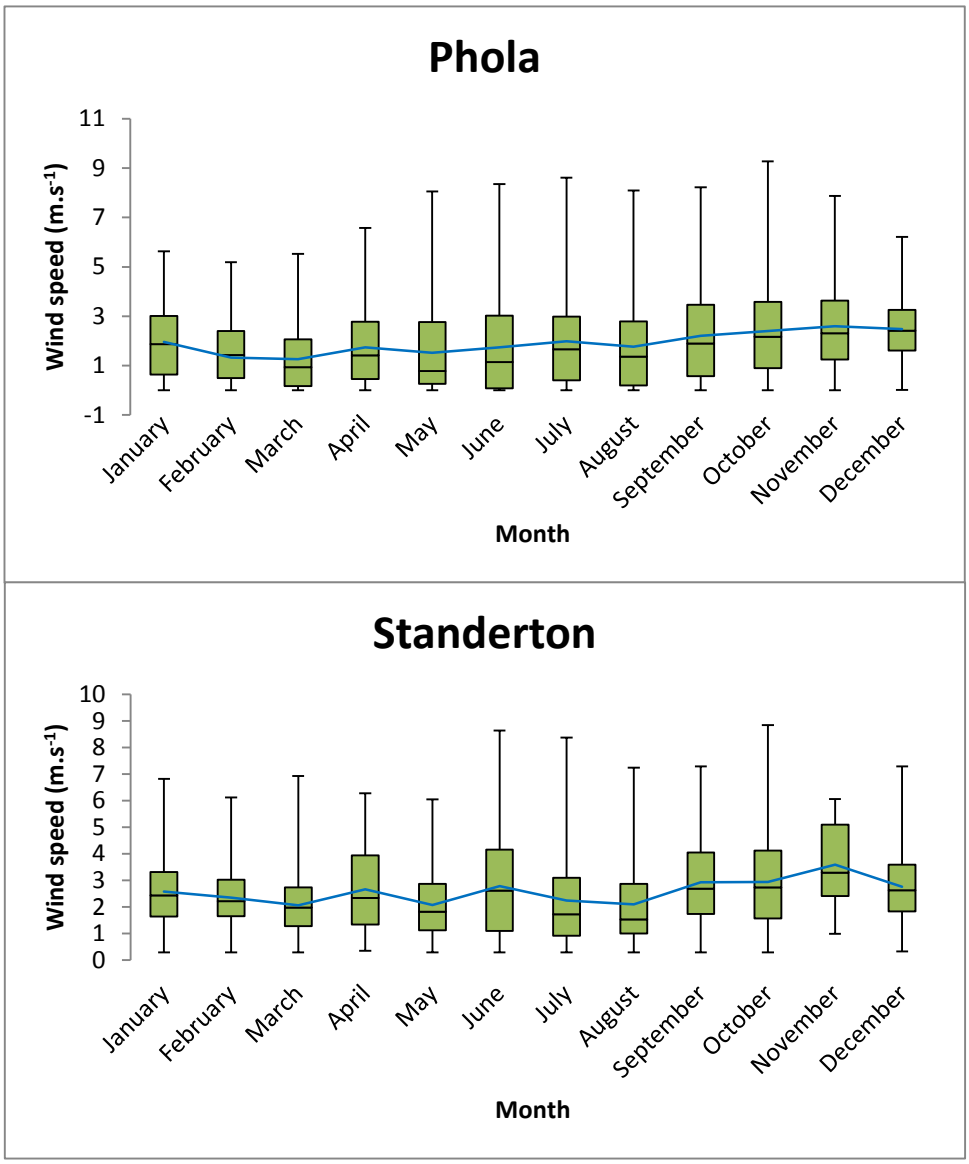

Figure 8.12 continued: Monthly variation of wind speed.